Ministero dell'Istruzione,
dell'Università e della Ricerca

Università degli studi di
Palermo

Principles and method for H_2 and CO_2 monitoring in volcanic areas: preliminary results for Stromboli and Etna volcanoes

PhD thesis by
Roberto M. R. Di Martino

Tutor
Prof. Mariano Valenza

Co-Tutor
Dr Marco Camarda

Coordinator
Prof. Francesco Parello

DOTTORATO DI RICERCA IN GEOCHIMICA XXII CICLO (GEO/08)
(January 2008 – December 2010)

Dipartimento di Chimica e Fisica della Terra ed
Applicazioni alle Georisorse ed ai Rischi Naturali (C.F.T.A.)

Ministero dell'Istruzione,
dell'Università e della Ricerca

Università degli studi di
Palermo

Principles and method for H_2 and CO_2 monitoring in volcanic areas: preliminary results for Stromboli and Etna volcanoes

PhD thesis by
Roberto M. R. Di Martino

Tutor
Prof. Mariano Valenza

Co-Tutor
Dr Marco Camarda

Coordinator
Prof. Francesco Parello

Reviewers

Prof. Dario Luzio
Dipartimento C.F.T.A.
Università degli Studi di Palermo

Dr Anthony Finizola
Laboratoire GéoSciences Réunion,
Université de la Réunion

DOTTORATO DI RICERCA IN GEOCHIMICA XXII CICLO (GEO/08)
(January 2008 – December 2010)

Dipartimento di Chimica e Fisica della Terra ed

Applicazioni alle Georisorse ed ai Rischi Naturali (C.F.T.A.)

Table of contents

ABSTRACT

Geochemical investigation of fumarolic and soil gases is a powerful tool for volcanic surveillance, for investigating the subsurface magma dynamics and for hazard assessment in volcanic areas. The development of theoretical models that describe in a consistent way the observed volcanic phenomena, as well as the design of pioneering analytical instruments for measuring the geochemical parameters sensitive to the magmatic processes occurring in the Earth interior, are of primary importance for identifying the precursor signals of future volcanic activities.

In order to improve the tools for geochemical monitoring of the volcanoes, an automated system has been designed for measuring the H_2 concentration and CO_2 flux from both fumaroles and soils. The detection equipment of the H_2-CO_2 system consisted of the RewPower fuel cell and the Gascard II for measuring the H_2 concentration and the CO_2 flux respectively.

The H_2-CO_2 system underwent the rigorous qualification procedure in laboratory and some preliminary in field-testing aimed to check the reliability, the accuracy and the efficiency for its effective application in volcanic areas.

The promising results obtained from the tests supported the use of the automated system for H_2 and CO_2 continuous monitoring at two active italian volcanoes, Mount Etna and Stromboli. The measurements performed at both volcanoes have been focused to investigate the relationships between the time-changing fumarolic degassing and the variations of the volcanic activity.

The results of the continuous monitoring carried out at Mount Etna showed that the main variations of both the H_2 concentration and the CO_2 flux preceded the changes of Etna's volcanic activity that took place during the period of observation. The direct comparison of the data acquired by the H_2 and CO_2 continuous monitoring and the eruptive activity indicated that the H_2 concentration peaks were correlated with the explosions occurred at Bocca Nuova crater throughout august 2010. The correlation suggested also the progressive approach of the gas-richer magma source to the point of measurement.

The analysis of the data collected at Stromboli volcano, which has been made by using reliable models for describing the degassing process, provided a better understanding of the relationships between the variations of the fumarolic emissions and the volcanic activity. The high frequency variations exhibited by both parameters seem well correlated with Stromboli's eruptive activity, typically time-changing on time scale of hours or days. Moreover, the investigations of the reciprocal relationships between both parameters allowed the evaluation

that the upper surface of the degassing source, from which the gas mixture containing H_2 and CO_2 begins to move through the porous medium, ranges between 2 and 4 Km within the volcano plumbing system, where a magma storage zone has been found by geochemical, volcanological, petrological and geophysical investigations.

Furthermore, for both the monitored volcanoes, the results showed that the main changes of H_2 concentration preceded systematically the CO_2 flux ones, by exhibiting the typical sound of the H_2 and CO_2 continuous monitoring. This specific behavior has been described by formulating the theoretical model of the chemical composition transients of the gases emitted from fumaroles and soils.

The model has been developed in this thesis for describing the compositional changes of the emitted gases according to the transport processes of advection and diffusion through the porous media. The hypothesis of the model is that the compositional variation of the mixture released from the underground reservoir causes the compositional changes of the surface emissions.

The model provides the relationship between the depth of the gas reservoir, the flux rate of the gas mixture, the properties of the medium (porosity and permeability), the diffusivity of the considered gas species and the time between the beginning of the compositional disturbance at the bottom surface, that separates the medium from the reservoir, and his detection on the top surface. The results of this model assess that keeping constant the gas flux rate and the depth of the gas reservoir, the delay among the different concentration disturbances mainly depends from the different diffusivities of the considered gas species.

In order to check the reliability of the theoretical model, several laboratory tests have been performed using the gas flux simulator, consisting of a column filled with volcanic sand. The tests have been performed with pure gases (CO_2 and He) as well as with multicomponent mixtures ($He – H_2 – O_2 – N_2 – CO – CH_4 - CO_2$), by setting the flux rate in a range far greater than the typical of soils and fumaroles. The tests results provided the time between the beginning of the compositional disturbance entering the bottom base and his detection at the top surface of the flux simulator, according to the flux rate of the gas mixture. Finally, the test results and the theoretical predictions have been compared in order to check the reliability of the model for describing the chemical composition transients of the gases emitted from fumaroles and soils of volcanic, geothermal and seismic areas.

Based on the results achieved through the field experiences as well as from the formulation, the development and the experimental testing of the theoretical model of the chemical composition transients, this study provides the accurate description of a separation process,

made by porous medium, of the gas mixtures originally released from a deep gas reservoir. The investigation of this separation process, equivalent to a sort of natural chromatographic effect, enables better understanding the relationships between the variations of the soils degassing activity and the changes of the degassing dynamics occurring within the underground reservoirs.

Chapter 1

Introduction

Since decades, geochemical monitoring of soil gases have been widely used as powerful tools for geothermal exploration (Badalamenti et al., 1984; Badalamenti et al., 1988; Bertrami et al., 1990; Finlayson 1992; Chiodini et al., 1998), oil and gas reserve exploitation (Gregory et al., 1985; McCarthy and Reimer 1986) and other applications such as volcanic surveillance (Sato and McGee, 1981; Baubron et al., 1991; Badalamenti et al., 1991; Valenza, 1994; Barberi and Carapezza, 1994; Giammanco et al., 1995; Giammanco et al., 1996; Diliberto et al., 2002; Granieri et al., 2009) and earthquakes prediction (Irwin and Barnes 1980; King, 1980; Oskarsonn, 1984; Wakita et al 1980; Satake et al., 1984; Wakita, 1996; Kameda et al., 2003; Salazar et al., 2002; Giammanco et al., 2006; Sugisaki et al., 1983; Sato et al., 1984).

The gas produced or accumulated within a subsurface reservoir can escape toward the Earth surface, along preferential pathways such as fractures and faults of the Earth crust. Large amounts of gases are emitted through distinctive manifestations as volcanic plumes, fumarole emissions, geysers and thermal springs. Nonetheless, noticeably amounts of deep-seated gases enter the atmosphere through the soils surface by the process known as diffuse degassing (Valenza M., 1993; Giammanco et al., 1995 a, b; Diliberto et al., 1996; Aiuppa et al., 2004; Giammanco et al., 2007). Diffuse degassing received great attention in several applications as environmental science, geothermal and gas exploration and volcanological research, using the variations of the soil degassing anomalies to monitor the volcanic activity, namely throughout the transition from quiescent to eruptive conditions at dormant volcanoes (Badalamenti et al., 1994; Giammanco et al., 1995; Giammanco et al., 1996; Barberi and Carapezza, 1994).

Several gas species, as helium (He), radon (Rn), carbon dioxide (CO_2) and molecular hydrogen (H_2), have been studied and the relations with the reservoirs have been used to identify each species as best pathfinder of geochemical processes occurring in the Earth interior. In particular, several study results established that the focused CO_2 emissions can reveal the occurrence of active fault system (Sugisaki et al., 1983; D'Alessandro et al., 1992; Klusman, 1993; Boubron et al., 1996; Giammanco et al., 1998). The spatial analysis of CO_2 flux distribution has been successfully used to identify the presence of tectonic structures buried by clastic or epiclastic sediments hided for the typical geological investigation (Giammanco et al., 1995; Lombardi et al., 1996; Azzaro et al., 1997; Giammanco et al., 1997; Ciotoli et al., 1998; De Gregorio et al., 2002; Giammanco et al., 2007). In regions where earthquakes are historically rare or potentially unknown, anomalous soil degassing may be used as a tool to identify the areas having higher potential seismic hazard. In particular, the

spatial distribution of both the H_2 anomalies, produced by mechanochemical reaction between water and tectonically-induced fractures in rocks (Kita et al., 1982; Ito et al., 1999; Kameda et al., 2003), and CO_2, produced by organic decomposition, has been used as powerful tool to mark the historically most active fault systems (Sugisaki et al., 1983).

In volcanic and geothermal areas (Diliberto et al., 2002; Giammanco et al., 2000; Diliberto et al., 2000; Chiodini et al., 1998; Giammanco et al., 1998; Gerlach and Graeber, 1985; Gerlach et al., 2001), diffuse CO_2 degassing shows wide spatial variability and time-changing fluctuations. Several authors focused their interest on CO_2 since it is the most abundant gas species in volatile magmatic phase, after water. Moreover, carbon dioxide is the less soluble gas species in silicate magmas, attaining CO_2 saturation at mantle to deep crustal level (Symonds et al., 1994; Giggenbach, 1996). As a consequence, large amount of CO_2 are released from the magma bodies upon their ascent toward the surface, producing large soil gas anomalies that can be broadly acknowledged.

Starting from the pioneering studies of Sato and McGee (1980), several researches on the geochemical monitoring of volcanic gases have been focused on the hydrogen species and its relationships with volcanic activity (Sato and McGee, 1980; Carapezza et al., 1980; Carapezza et al., 1983; Badalamenti et al., 1991; Giammanco et al., 1997; Melián et al., 2002). H_2 has low solubility in groundwater and both low and constant concentration in air (about 0.5 ppm vol.) resulting less affected by atmospheric contamination (Melián et al., 2007).

The researches in the field of geochemical monitoring of volcanic gases applied to the volcanic surveillance have been developed following two main branches. The first research line made progress on the development of theoretical models needed to better understand the connections between gas emissions and volcanic activity. The second one has been focused on thoroughly-researched and field-tested pioneering techniques for detecting, near the surface, the geochemical expressions of subsurface time-changing magmatic activity. Both the research lines converge into the achievement of the same goal: the development of accurate models needed to build cutting-edge geochemical monitoring systems, which enable the collection of accurate measurements. In turn, the reliable measurements allow the checking, the verifying and the perfecting of the model itself.

In this thesis has been proposed a new device for continuous measurements of H_2 concentrations and CO_2 flux from soils and low temperature fumaroles, aimed to monitor the volcanic activity. The hydrogen concentration has been measured through hydrogen fuel cell-based H_2-detector carefully prepared to perform the measurements in volcanic areas. The

hydrogen fuel cell operation has been checked through laboratory tests, allowing the investigations of the technical features of the H_2 sensor. The results of this laboratory activity, preliminary to the measurements performed in volcanic areas, are shown in Chapter 2. The reliability of the sensor for the H_2 concentration measurements in field applications has been checked at Solfatara di Pozzuoli area. The CO_2 flux has been measured according to the dynamic concentration method (Gurrieri and Valenza, 1988; Camarda et al., 2006) using an I.R. spectrometer.

The measurements of H_2 concentration and CO_2 flux have been performed through two different H_2-CO_2 continuous monitoring devices installed on Mount Etna and Stromboli volcanoes.

Two different periods of measurements have been performed on Mount Etna: at Torre del Filosofo fumarolic field from the month of July to the October 2008 and at Belvedere fumarolic field from the month of April 2010 to September 2010. These field experiences can be considered really fruitful since allowed the qualification of the facility and the testing of the system efficiency. Moreover, it allowed the collection of preliminary and very promising results to understand the connection between the degassing activity from the fumarolic fields close to the top area of the volcanic pile and the volcanic activity of Mount Etna.

The second field experience has been performed at the Pizzo sopra la Fossa, a fumarolic field on the top area of Stromboli volcano, using a new H_2-CO_2 system specially designed and tuned to perform the measurements in this area. In this thesis have been shown the measurements performed from the month of May 2009 to the October 2010 aimed to investigate the relationships between the degassing from the fumarolic field and the typical time-changing Stromboli's volcanic activity.

The results of these measurements have been shown and discussed in comparison with volcanic activity. Data acquisition on different volcanoes represents an initial step forward the development of reliable and innovative techniques dedicated to the study of volcanic systems as well as ultimately allowing the volcanic surveillance.

The understanding of the connection between the gases emitted from the fumarolic fields and the volcanic activity, based on continuous and high frequency geochemical monitoring techniques, requires the investigation of the transport dynamics of a multicomponent mixture in multiphase system. One of the achievements of this thesis has been the development of a theoretical model of the chemical composition transients in the gases emitted from the fumarolic field. The model, based on the solution of the convective-diffusive gas transport equation, has been developed in order to describe the relationships among the chemical

composition of the surface gas emissions, the subsurface gas flow regime, the physical features of the porous medium and the depth of the gas reservoir.

Finally, a set of dedicated laboratory tests has been performed to check the reliability of the proposed model, studying the limits of its validity by the comparison of the experimental results with the theoretical prediction.

Chapter 2
Experimental detectors for H_2 and CO_2 monitoring

Introduction

One of the main goals of this thesis is the improvement of the detector and the techniques suitable for the monitoring the volcanic activity.

Well performing detectors should be reliable in making the chemical composition analysis of the gas emissions, and moreover innovative techniques with high efficiency should be experienced.

In order to achieve the goals proposed in this thesis, we associate the measurement of CO_2 flux from the soils and low temperature fumaroles with the measurement of H_2 concentration.

The association of the monitoring of an extensive parameter, such as the CO_2 flux, with an intensive parameter, such as the H_2 concentration, could greatly improve the understanding on the process correlating the surface fluid emissions, the chemistry of the fluid released from the magmas upon their ascent toward the surface and the volcanic activity.

Among the ordinary monitoring techniques, the CO_2 soil flux measurements are currently used in several fields of applications as in agronomy, in hydrocarbon exploration and volcanology. In volcanological research, the CO_2 flux is one of the most promising tools for the monitoring of the volcanic activity, since the CO_2 is one of the main not-condensable magmatic gas species. Furthermore, since the CO_2 is the less soluble gas specie in silicate magmas, it is among the first gas released during the magma ascent toward the earth surface.

In past years, several authors proposed the use of the monitoring of the reducing gas species concentration as well as the H_2 one in order to monitor volcanic activity (Carapezza et al., 1980; Sato et al., 1985; Sato and McGee, 1982; Wakita et al., 1980). The H_2 molecular specie has noteworthy geochemical features such as the fast movement capability, both low and constant atmospheric concentration (0.5 ppm vol.) and low water solubility. Moreover, since its earth sources are exactly recognizable, for example the H_2O-C mantle reactions, the H_2O-(Fe-bearing mineral) reactions in the eruptive magmas and the reactions involving the water and the active shear surfaces in the active fault systems, the H_2 is considered a promising geochemical indicator of the process working into the earth crust.

In this chapter we describe features of the H_2-CO_2 measurement system. In the first part, we illustrate the technical features of the fuel cell. The main part is dedicated to the description of the results attained through laboratory experiments suitably designed and performed in order to use the fuel cell as H_2 sensor. Moreover, we describe the working principles and the

measurement methods of the experimental automatic permanent system used for the measurement of the H_2 concentration and the CO_2 flux in field applications.
In order to design a device to monitor the hydrogen concentration in the gases emitted from the low temperature fumaroles as well as from the soils, we use a hydrogen RewPower fuel cell as the H_2 sensor.

Basic structure of the fuel cell

The fuel cells are electrochemical devices commonly used to convert the energy associated to the chemical reaction of hydrogen in electric energy.
Some details about the historical development of the fuel cell technologies are listed in Appendix 1.
The three main components of a single fuel cell are:

- the membrane-electrode assemblage (MEA);
- the bipolar plates;
- the seals.

The MEA consists of the two gas diffusion layers (GDL), the two dispersed catalyst layers and the proton exchange membrane.
The GDL allows the appropriate amounts of the reactants to reach uniformly the catalyst layers and the water produced by the cell reaction to leave the cathode, keeping anyway humidified the fuel cell membrane, preventing the electrode flooding.
Often, the GDLs have carbon-based structure associated to PolyTetraFluoroEthylene (PTFE). The PTFE wet-proofing properties ensure that at least some of the pores of the carbon-based GDL are not blocked by water molecules that could prevent the rapid diffusion of the reactants toward the electrodes.
Into the Proton Exchange Membrane fuel cells, the catalyst layer is the essential component enhancing the rate of the electrode reactions. Several fuel cells have catalyst layer made of Platinum or Platinum-precious metal alloys supported by carbon. The use of platinum or platinum-alloy decreases the poisoning of the active layers by the reactants. The carbon-based supports present several advantages such as the chemical stability, the electrical conductivity and the high porosity. The latter, enhances the rate of mobility of the reactant at the electrode-electrolyte-reactant interface, named triple-phase boundary. Furthermore, the electrical

conductivity of the carbon enables the electrons produced by the hydrogen oxidation reaction to flow toward the bipolar plate.

The bipolar plate accomplishes several functions into the fuel cells (Mehta and Cooper, 2003):

- represents the link between the inner side of the cell and the external one,
- carries away the electric current from the half-cell toward the external circuit,
- helps in the water balance management,
- cools the half-cell and
- distributes uniformly the reactants on the active catalyzed area.

In order to accomplish these important functions, both the materials and the topologies of the plates become crucial features. The materials must satisfy:

- chemical compatibility and resistance,
- mechanical resistance,
- electric conductivity,
- low cost and
- good gas conductivity.

Also the device geometry is designed to improve the performance, i.e. the serpentine or interdigitated paths are used to improve the gas conductivity and as a consequence improves the catalyst efficiency.

The innermost part of a single PEM fuel cell is the solid electrolyte membrane. According to Sakthivel and Weppner (2006) solid electrolytes present several advantages such as the direct use as half cells separator. Moreover, they do not dissolve the impurities of the gas mixtures and allow the manufacturing of miniaturized devices.

In order to obtain the better features of proton conductivity and robustness, the industries proposed a variety of materials and manufacturing alternatives (Mehta and Cooper, 2003). The most popular material and commonly employed solid electrolyte into the fuel cell applications is the Nafion® membrane, the Dupont Co. trade mark of the perfluorosulfonic acid.

The Perfluorosulfonic acid ($CF_2CFOCF_2CFOCF_2CF_2SO_3H$) is a copolymer having elongated molecular structure made of three main parts (monomers). The first one is the backbone PTFE chain ensuring both the physical and the chemical resistance properties of the solid electrolyte membrane in both oxidative and reductive environments. The second one is the -O-CF_2-CFO-CF_2-CF_2- side chain linking the PTFE-like backbone to the third part which is the sulfonic acid ion cluster -SO_3H.

Depending on the chemical features of the monomers, the molecular structure of the perfluorosulfonic acid is made by one hydrophobic part, represented by the PTFE-like backbone, and by one hydrophilic part represented by the sulfonic radical. When the solid electrolyte membrane becomes hydrated, the sulfonic radicals tend to cluster forming a sort of channels framework. Through the channels, the protons linked to the water molecules are moving from one to one another sulfonic site. The moving process among the sulfonic sites gives rise to the proton conduction between the two electrodes of the cell.

The chemistry of a fuel cell

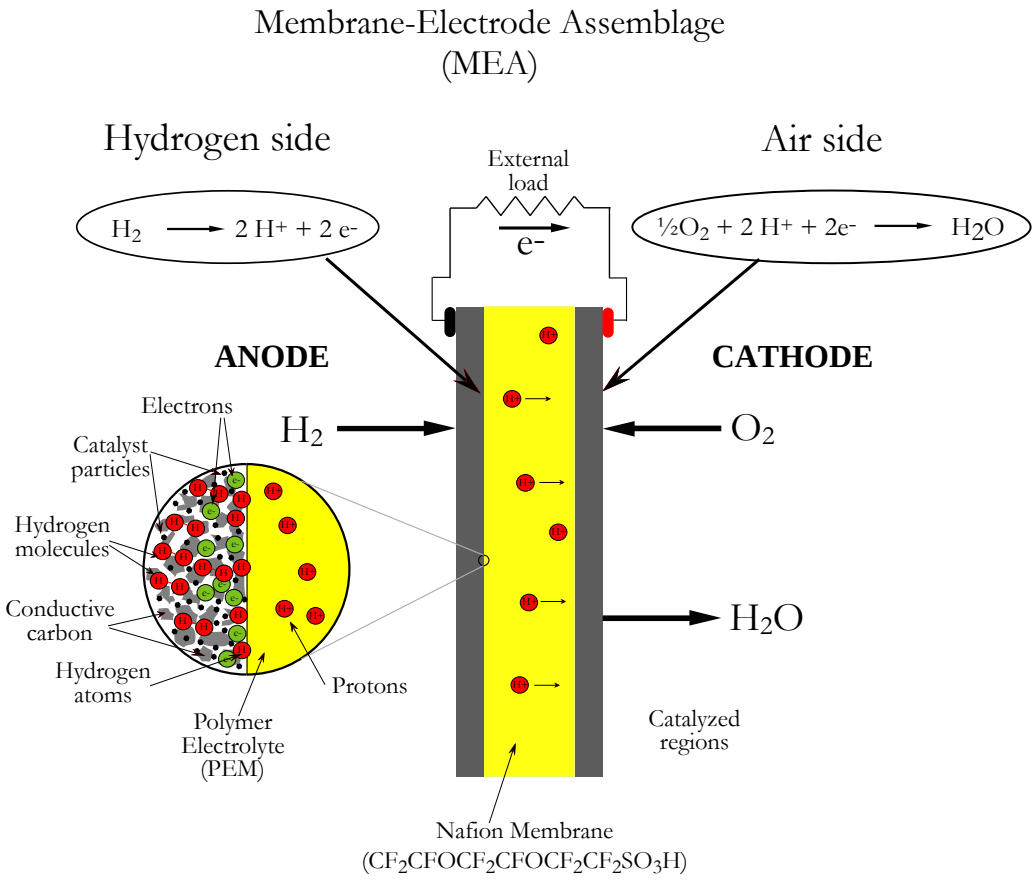

Figure 1 The Single Proton Exchange Membrane Fuel Cell (PEMFC). The figure shows the main elements of a PEMFC and the chemical reactions occurring at the cathode side and at the anode side of

the cell. The circle box shows the triple phase boundary (see text) and the designs not in scale of the proton exchange mechanism of the solid electrolyte membrane. The conductive carbone particles, the catalyst particles, the H_2 molecules and the electrons are also pictured.

The main chemical process in a fuel cell is represented by a redox reaction. In detail, two simultaneous half-reactions take place at the electrodes of the cell. An oxidation reaction (loss of electrons) occurs at the anode side while its counterpart, the reduction reaction (gain of electrons), takes place at the cathode side of the cell.

Figure 1 shows a schematic view of a single hydrogen fuel cell. The anode and the cathode side of the cell are separated by the Nafion® solid electrolyte membrane allowing the protons ions linked to H_2O molecules to be transferred from one electrode to the other. At the anode side of the cell, the H_2 molecules come in contact with the thin platinum particles dispersed on the carbon-based electrode surface.

At the anode side, the oxidation reaction do not occurs as far as the H atoms are linked in the H_2 molecules. Therefore, the platinum particles form weak H-Pt bonds keeping apart the hydrogen atoms. Moreover, they catalyze the H oxidation occurring on the anode electrode surface according to the half-cell reaction:

$$H_2 \rightarrow 2H^+ + 2e^- \qquad [1]$$

The two electrons produced by the reaction [1] flow through the external circuit of the cell generating an electric current. At the same time, at the triple-phase boundary the H^+ ions link the H_2O molecules and move through the solid electrolyte membrane toward the cathode as H_3O^+ ions. In so doing, the protons leaved the platinum particles of the anode side free to catalyze the reaction of the next H_2 molecule.

Similarly, at the cathode side of the cell the platinum particles fix the weak bonds with the O_2 molecules, allowing the reduction of the oxygen atoms to take place. The half-reaction occurring at the cathode side is

$$\frac{1}{2}O_2 + 2e^- \rightarrow O^{2-} \qquad [2]$$

Each oxygen ion combines with the two protons reaching the cathode through the solid electrolyte membrane and forms one H_2O molecule. The reaction occurs by producing heat. Therefore, the overall redox process occurring into the cell is the inverse water electrolysis reaction

$$H_2 + \frac{1}{2}O_2 \rightarrow H_2O \qquad [3]$$

Summarizing, the working principle of the sensor is the oxidation reaction of the hydrogen contained into the gas mixture entering the anode side of the fuel cell (sensing electrode). The electrons produced by the reaction flow through the external circuit from the anode toward the cathode (counter electrode) generating an electric signal.

In order to use the hydrogen fuel cell as an H_2 sensor, we use the sensing electrode where the reaction [1] take place, meanwhile the cathode as the counter electrode, where the reaction [2] take places.

Characterization of the H_2 Sensor.

The intensity of electric current, *I*, flowing through the external circuit of the fuel cell represents the signal of interest in our measurement, produced by the sensor and proportional to the hydrogen entering the anode.

The electric *I* is measured by the voltage drop across the known electric resistor (*R*), according to the Ohm's law

$$V = R \times I \qquad [4]$$

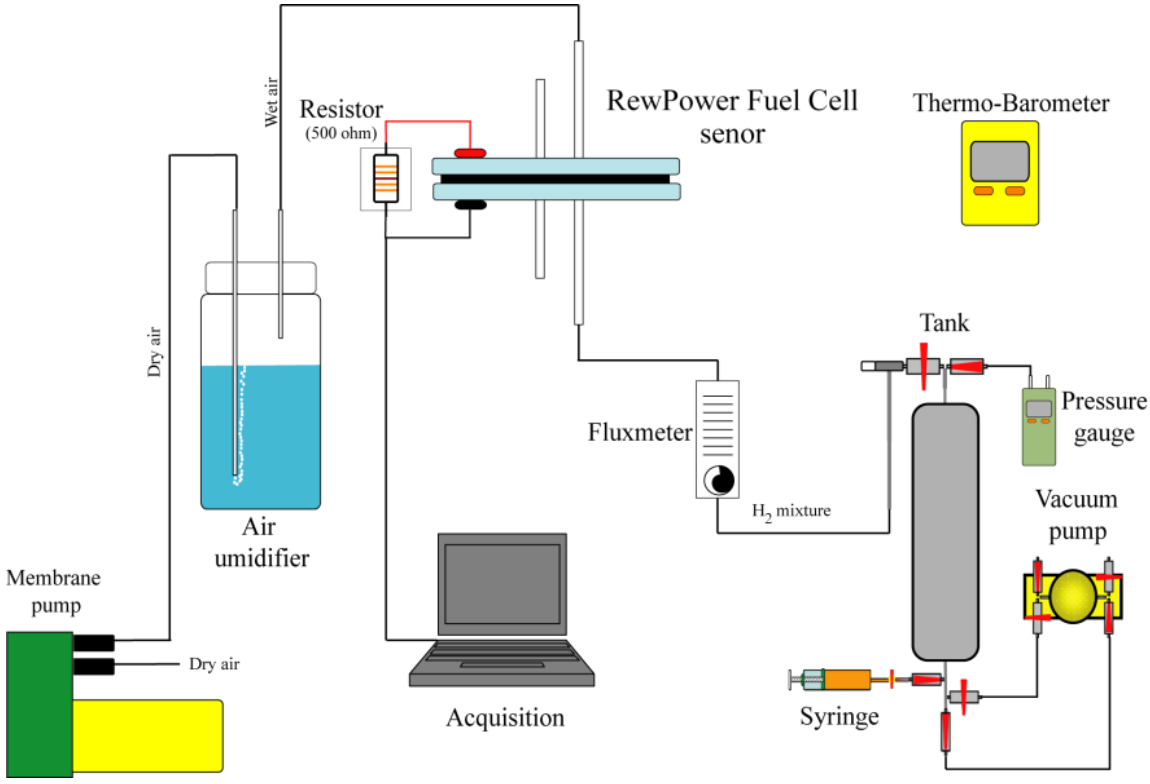

Figure 2 Schematic picture of the system used to perform the laboratory tests during the characterization of the RewPower Fuel Cell as H_2 sensor for the concentration measurements. The figure shows the connection among the H_2-containing tank entering the hydrogen fuel cell, the computer acquisition system and the air humidifier. The arrows point to the flux directions of both gas mixture and air.

The potential difference (*V*) is measured through the voltmeter connected in parallel to the resistor *R*. The electric signal was sampled at 1 Hz and recorded through the ADC-12 Picolog data logger connected to a computer and straight stored.

Figure 2 shows the system used during the laboratory tests performed with the RewPower Fuel Cell. In the picture are shown the main hydraulic and electronic components. In order to optimize the water management of the sensor and to keep constant the water content of the air entering the fuel cell, the cathode side was connected to an air-humidifier.

The gaseous mixtures with different hydrogen concentrations was produced into a tank by dilution of a standard laboratory mixture containing H_2 (200 ppm vol.) and N_2 (99.98% vol.) with air. The flux of the mixtures entering the anode of the fuel cell was known and maintained constant setting the fluxmeter at 0.25 l min^{-1}.

The optimization of the various parts was made by performing a set of complete tests and calibrations. The tests were performed at controlled temperature and pressure conditions with the aim to optimize both the performance of the fuel cell and the electronic equipments needed to transform the electric output produced by the cell into a sensitive and robust electric output signal.

The figure 3 shows a typical measurement result of the concentration-signal tests.

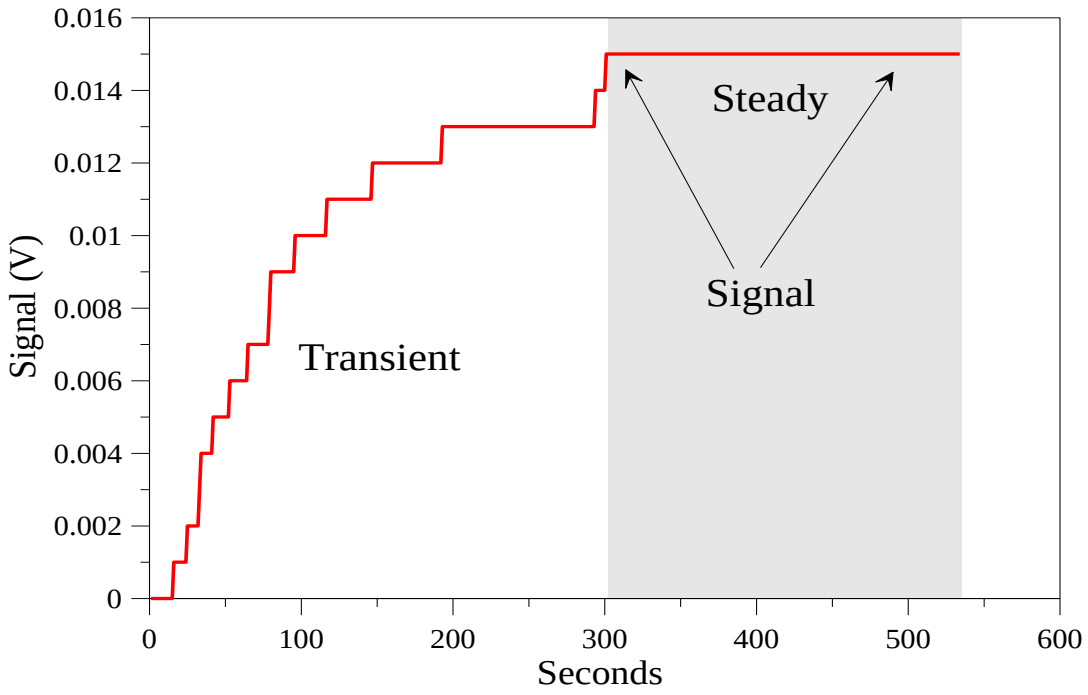

Figure 3 The H_2 concentration-signal tests**.** The record of a typical measurement result shows the transient state during which the differential potential increase until the attainement of the stationary maximum value. Since then, the differential potential remains constant. The maximum value attained in stationary state conditions is assumed as the signal of the sensor related to the H_2 concentration into the gas mixtures.

The time zero represents the instant at which the mixture starts to enter the anode side of the cell by the opening of the tank stopcock. As can be seen, a few second later the potential difference measured at the ends of the resistor start to increase (transient state) until it reach a maximum stationary value. Each test was considered completed when the potential difference reaches the maximum stable stationary value within a few tenths of mV for several minutes.

The achievement of the stationary value of the potential difference represents a dynamic equilibrium condition among the kinetic of the reduction reaction occurring at the cathode side, the protons flux through the solid electrolyte membrane and the kinetic of the oxidation reaction occurring at the anode side of the fuel cell.

This maximum stationary value achieved by the potential difference (shown in the picture for times larger than 300 sec) is the signal of the RewPower fuel cell sensor proportional to the H_2 concentration in the mixture.

Several tests were performed in order to study the repeatability of the measurements, the resolution, the accuracy and the response time of the H_2 sensor.

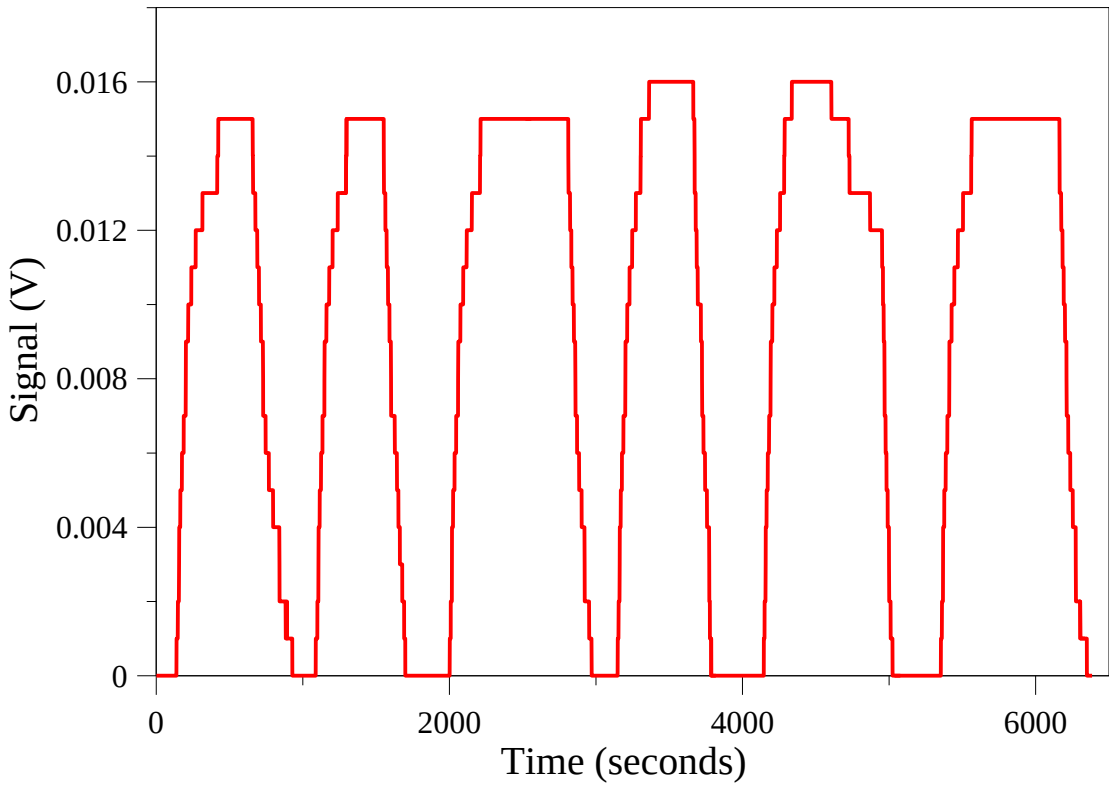

Figure 4 Six sequential repetitions of the concentration-signal measurement tests. The figure shows that maintaining constant the H_2 concentration into the gas mixture entering the anode side of the cell, the maximum stationary value attained from the sensor remain constant. Between two subsequent tests, the anode side of the cell was flushed with air in order to eliminate the residual hydrogen on the catalyst layer.

Moreover a few tests have been designed to tune the best resistor value at the external circuit of the fuel cell. The test results obtained by changing the impedance of the circuit suggest that the best setting among resolution, response time and linearity of the signal is obtained with a 500 ohm resistor.

Figure 4 summarizes six repetitions of the test performed with the H_2 (100 ppm vol)-air mixture. Between two subsequent tests with the H_2-containing mixture, the sensor was flushed with air for several minutes to set the zero of the measurements corresponding to the absence of the hydrogen.

Throughout the tests, the maximum stationary values remain stable due to the reproducibility of the redox process occurring at the electrodes: the largest difference recorded in the signal is of 1 mV on top of 16 mV suggesting that the performance error in the repeatability of the measurement ($\sigma = 0.267$) is within 3.4%.

Figure 5 shows the time need for the sensor to achieve the 90% of the maximum stationary signal (T90) vs the H_2 concentration in the mixture. The results achieved by all the tests reported into the figure show that the T90 is independent from the H_2 concentration.

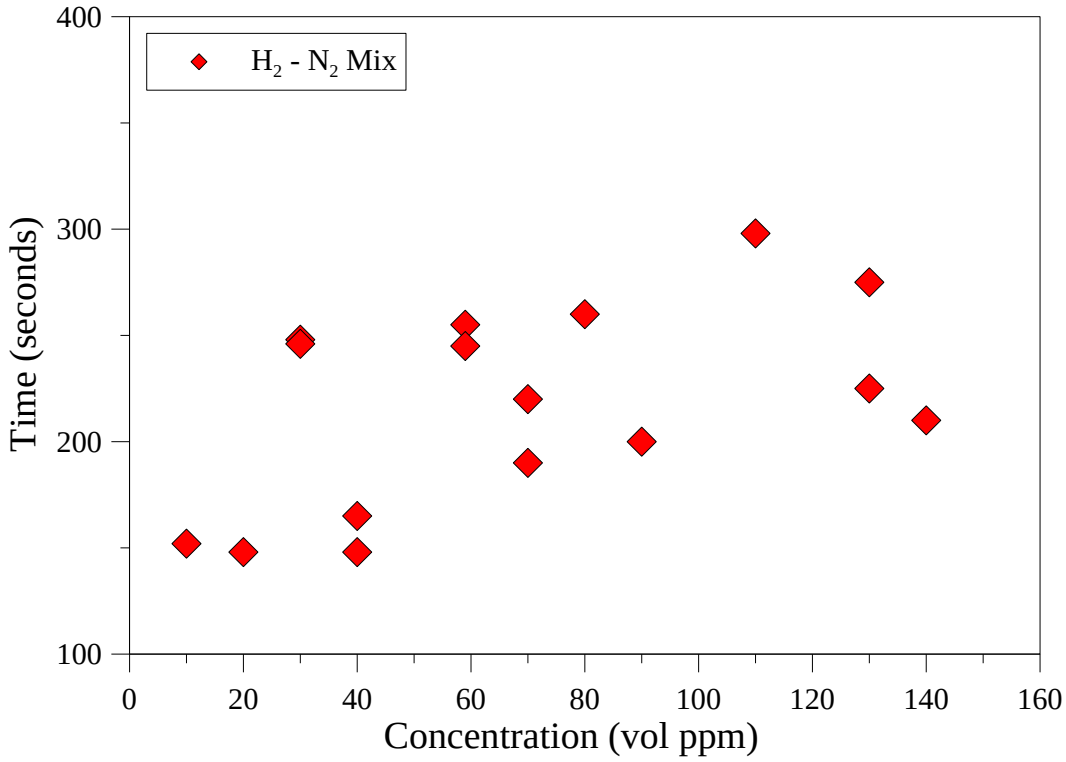

Figure 5 Relation between the H_2 concentration into the mixtures and the T90. T90 is the time need for the sensor to achieve the 90% of the maximum stationary value. The T90 of the H_2 sensor is independent from the hydrogen concentration in the mixtures and below 300 seconds. In almost all the cases reported, the T90 have high frequency in the range between 150 and 300 seconds.

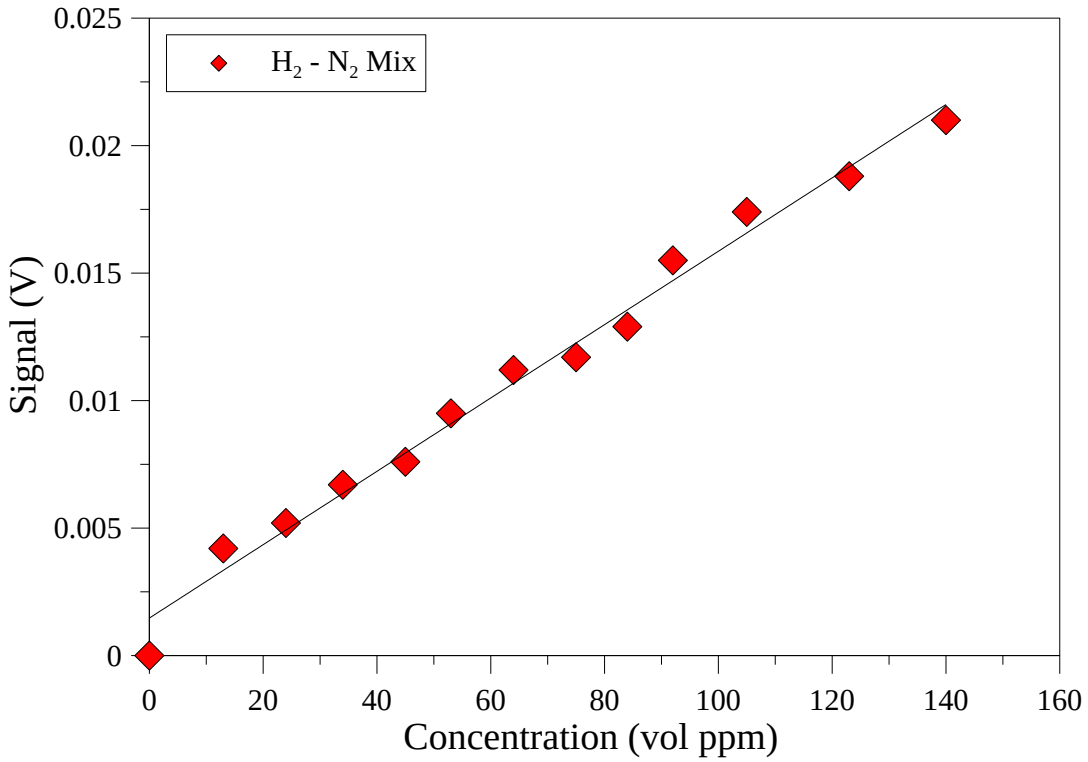

Figure 6 Relation between the signal of the fuel cell vs the H_2 concentrations into the gas mixtures. The gas mixture has been prepared by dilution of a laboratory gas mixture with H_2 200 ppm vol in N_2 matrix with air. The figure also reports the fitting line of the tests investigating the H_2 concentration range from 0 to 100 ppm vol. All the tests are performed at controlled temperature and pressure conditions.

Moreover, it is also showed that the T90 of the H_2 sensor was below 300 seconds and comprised in the range between 150 and 300 seconds in almost all the cases. Since the time to obtain the concentration measurement is longer than the T90, this result suggests that the reliability of the measurement performed with our fuel cell is achieved provided that the H_2-containing mixture enters the anode of the cell for a time longer than 300 seconds.

A calibration of the H_2-sensor has been performed to study the relation between the stationary sensor signal and the H_2 concentration in the mixtures. Figure 6 shows the results of the tests in the operative conditions established by setting to 500 ohm the electric impedance of the circuit. In these conditions, a linear relation was found between the stationary sensor signal and the H_2 concentration in the full range investigated. From the fitting line of all the tests we estimate that the sensitivity is 0.2 mV per ppm vol. of H_2.

In order to study the repeatability of the H_2 concentration measurements relative to the variations of the environmental conditions, we repeated the tests in fairly the same temperature conditions, with a variation of the atmospheric pressure on the order of tenth of mbar. The signal values reported into the table 1 refer to the tests performed in the H_2 concentration range from 0 (air) to about 100 ppm vol..

Table 1 Stationary maximum signal value. The maximum stationary signal of the sensor recorded through the test performed with H_2-containing mixtures in the concentration range from 0 ppm vol. to 100 ppm vol. The H_2 concentration has been investigated with chromatographic analysis.

H_2 Concentration (ppm vol)	**Signal first test (Volt)**	**Signal 1-day after (Volt)**	**Signal 5-day after (Volt)**
13	0.0041	0.0040	0.0044
24	0.0050	0.0054	0.0061
34	0.0067	0.0065	0.0071
45	0.0076	0.0075	0.0100
53	0.0095	0.0092	0.0102
64	0.0112	0.0114	0.0130
75	0.0117	0.0118	0.0135
84	0.0130	0.0130	0.0161
92	0.0155	0.0155	0.0166
105	0.0171	0.0172	0.0176

The difference among the value recorded was less than a few hundredth of mV between the first two tests, while the signal difference between the first tests and the one performed 5-day later was about 10%. The measurements show a standard deviation of about 0.0010 V corresponding to the accuracy of the sensor in H_2 concentration of ± 5ppm vol.

The effect of the H_2 flux value was evaluated through dedicated tests. The results reported into the table 2 show that the sensor signal obtained setting the flux of the mixture at 0.5 l min^{-1} is the same of the one recorded setting the flux at 0.25 l min^{-1}. This flux values corresponds to the foreseen operational condition of the sensor in the field applications.

The results show that the measurement is independent from the flux. This fulfilled condition is necessary to correctly evaluate the H_2 concentration into the mixture.

Table 2 Stationary maximum signal value. The table reports the stationary signal value obtained by changing the flux value with which the H_2-containing mixture enters the anode of the cell. As reported in the table 1, the H_2 concentration has been investigated with chromatographic analysis.

H_2 Concentration (ppm vol)	**Signal first test – flux 0.25 l min^{-1} (Volt)**	**Signal first test – flux 0.5 l min^{-1} (Volt)**
13	0.0041	0.0041
24	0.0050	0.0050
34	0.0060	0.0061
45	0.0072	0.0073
53	0.0090	0.0090
64	0.0114	0.0115
75	0.0118	0.0118
84	0.0130	0.0130
92	0.0155	0.0154
105	0.0171	0.0172
123	0.0188	0.0188

Cross-sensitivities: influences of the H_2 dilution matrix

A relevant part of the characterization of the fuel cell as been done with the gas mixtures prepared by dilution of H_2-N_2 laboratory gas standard, using the air as dilution matrix. To verify the bias on the stationary signal value of the sensor, we performed some tests changing the dilution matrix of the H_2-N_2 standard.

We carried out dedicated tests using H_2-containing mixtures diluted with pure oxygen (O_2 = 99.99) and the results of the tests are showed in figure 7.

The results of the test suggest that the stationary signal of the sensor shows a decrease of about 30% when the gas entering the anode of the cell is a mixture of H_2 diluted with pure oxygen. We believe that this drop of the sensor signal is produced by the reduction of the O_2 molecules at the anode of the cell and by the consequently uncontrolled water-forming reaction between H_2 and O_2 at the anode of the sensor.

Several tests were performed in order to study the reliability of the measurements of the H_2 concentration in the volcanic environmental conditions exposing the sensor to H_2-containing mixtures diluted with carbon dioxide (CO_2) matrix, since the CO_2 is one of the main components of volcanic emissions.

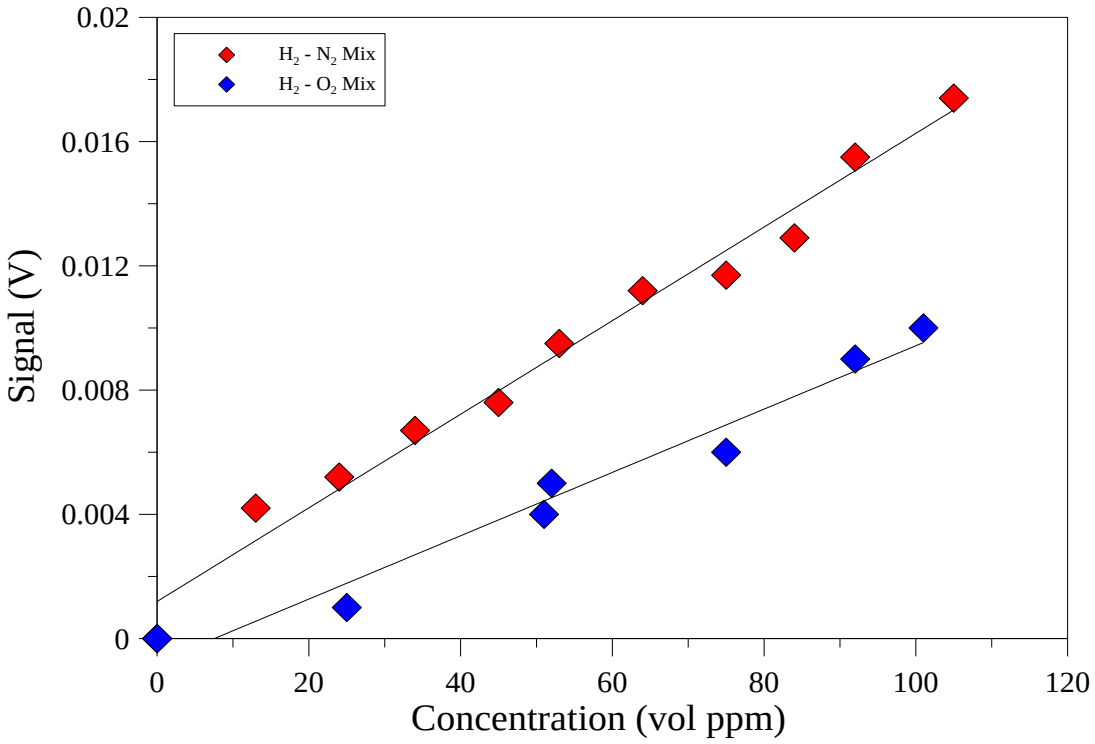

Figure 7 Relation between the signal of the fuel cell vs the H_2 concentrations into the gas mixtures. Blue diamonds refers to the test series performed with the mixture prepared by dilution of the H_2-N_2 laboratory standard gas mixture (H_2 = 200 ppm vol; N_2 = 99.98 %vol) with pure oxygen (O_2 = 99.99). For comparison, Red diamonds refers to the test series performed with the mixtures obtained by dilution of the same laboratory standard with air.

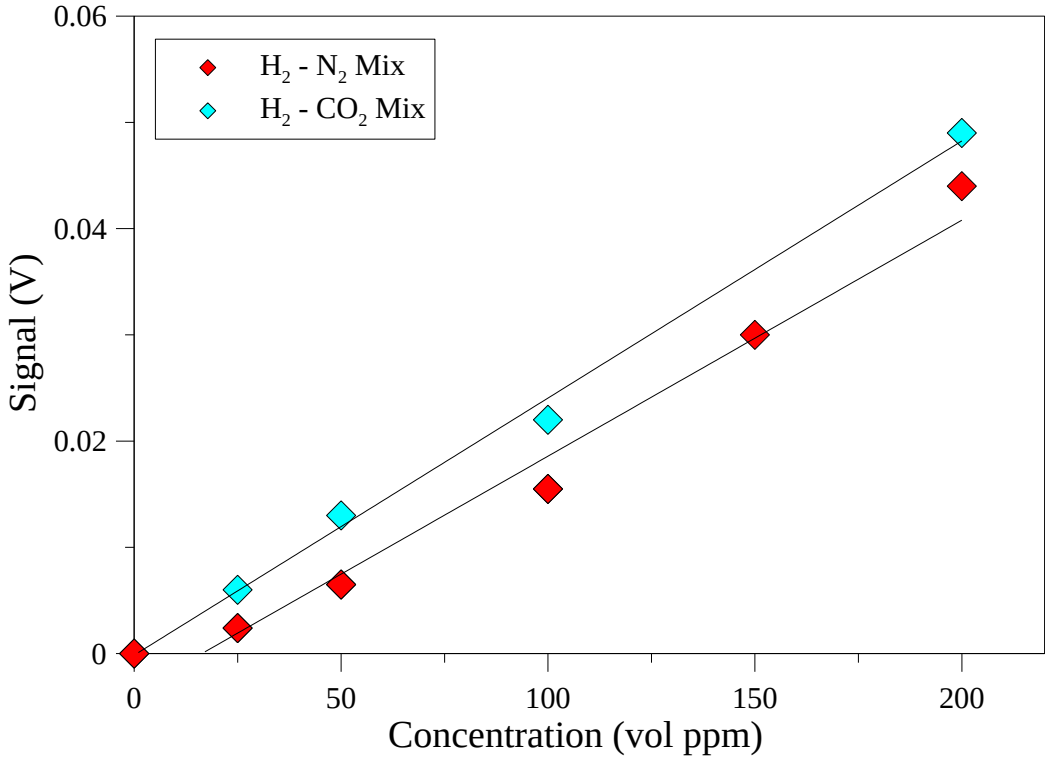

Figure 8 Relation between the signal of the fuel cell vs the H_2 concentrations into the gas mixtures. Light blue diamonds refers to the test series performed with the mixture prepared by dilution of the H_2-N_2 laboratory standard gas mixture (H_2 = 200 ppm vol; N_2 = 99.98 %vol) with pure carbon dioxide (CO_2 = 99.99). For comparison, Red diamonds refers to the test series performed through H_2 mixture obtained by dilution of the same laboratory standard with air.

Figure 8 shows the result of the five tests performed with the H_2-CO_2 mixtures compared to the six tests performed with the H_2-air ones. Each test refers to the H_2 concentration ranging between 0 (air) and 200 ppm vol. The results of the tests show an increase in the stationary signal of the sensor of about 10% by introducing the H_2-CO_2 mixtures. This bias as expected is smaller compared the oxygen effect. Moreover, as will be shown in the follow, a dedicated detector will be used to evaluate the CO_2 amounts in field measurements.

Cross-sensitivities: influences of other reducing gas species

The chemical gas composition of low temperature fumaroles includes CO_2 as dominant component together with other species as the methane (CH_4), carbon monoxide (CO) and hydrogen sulphide (H_2S) showing reduction capabilities. Since the fuel cell sensor may exhibit a response to the above mentioned reducing species, we performed several dedicated tests in order to evaluate their cross sensitivities on the stationary value of the H_2-sensor signal.

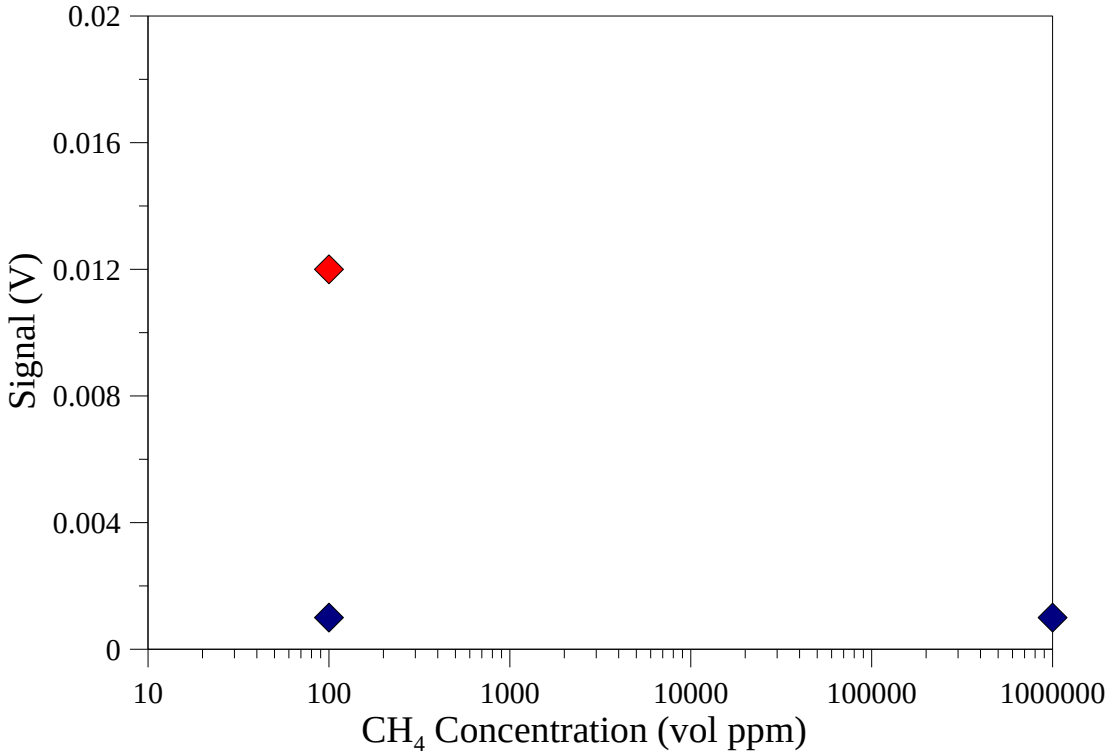

Figure 9 Relation between the reducing specie concentrations into the gas mixtures vs the signal of the fuel cell. Yellow diamonds refers to the tests performed with pure methane (CH_4 = 99.99 % vol.) and the mixture CH_4-Air (CH_4 = 100 ppm vol.). For comparison, the Red diamond refers to the test performed through H_2 (100 ppm vol) mixture obtained by dilution of the same laboratory standard with air. The CH_4 concentration of the mixture can be read on the left axis, while the H_2 concentration on the right axis.

Figure 9 shows the results of the tests performed using two mixtures containing respectively pure CH_4 (CH_4 = 99.99 % vol) and CH_4-air (CH_4 = 100 ppm vol). Into the same plot is also showed the sensor signal obtained using the H_2-air mixture (H_2 = 100 ppm vol). The results show that the sensor signal produced by the CH_4-containing mixture is near 1mV, independently from the CH_4 concentration. This effect is within the measurement error of the sensor. We believe that the absence of cross sensitivities respect the CH_4 is due to the slow kinetic of the oxidation reaction of the methane at low temperature, even in the presence of the catalytic particles.

The figure 10 shows the results of the tests performed using mixtures containing both the H_2 and the CO reducing species. The concentration ratio between CO and H_2 was set equal to 1 (CO/H_2 =1) in all the test series. In the same plot, the sensor signal was compared to the results obtained using the H_2-air mixtures. The tests show that the presence of CO introduces a 20% error on the H_2 measurement.

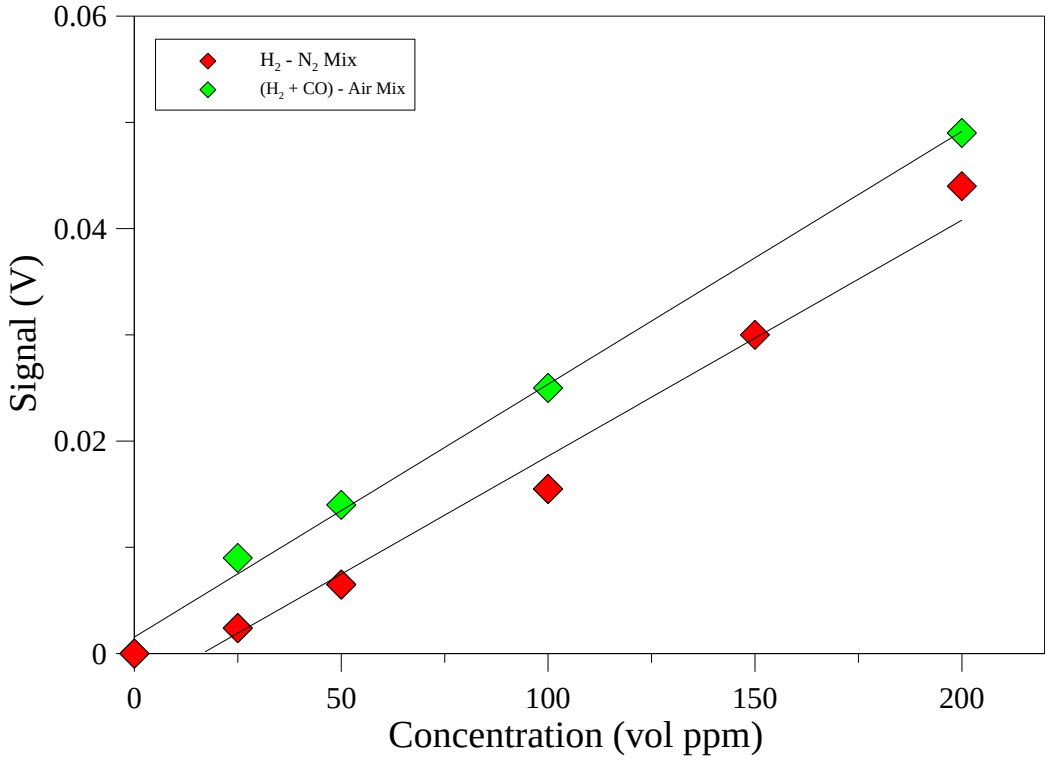

Figure 10 Relation between the signal of the fuel cell vs the reducing species concentration into the gas mixtures. Green diamonds refers to the test series performed with (H_2 + CO) reducing species in the concentration range 0-200 ppm vol. The concentration ratio CO/H_2 =1. For comparison, the Red diamonds refer to the test series performed by using gas mixture containing only the H_2 as reducing specie.

For instance, by inserting the mixture containing 100 ppm vol. of both H_2 and CO, we recorded a signal like to that produced by a mixture containing 120 ppm vol of only H_2. However, in the volcanic emissions the typical concentration ratio between CO and H_2 is of order of 1/100. Therefore, we believe that the error produced by the presence of CO into the gas mixture could be about 0.2%, a value within the error range affecting the H_2 measurement. Furthermore, the figure 10 shows that the slope of the trend line representing the five tests performed with the (H_2+CO)-containing mixtures is fairly similar to the one representing the H_2-containing mixture suggesting that the cross sensitivity remains constant in all concentration range investigated.

The cross sensitivity effect can be produced by CO poisoning affecting the fuel cell systems and specifically through the coverage of reactive sites onto the catalyst layer. According to the studies on the poisoning produced by hydrocarbons-derived H_2-dominant gas mixtures (Cheng et al., 2007 and reference therein; Schmittinger and Vahidi, 2008 and reference therein), the effect of CO on the Pt catalyst is reversible because the water vapour counteracts the coverage of CO supporting the oxidation of the CO to CO_2.

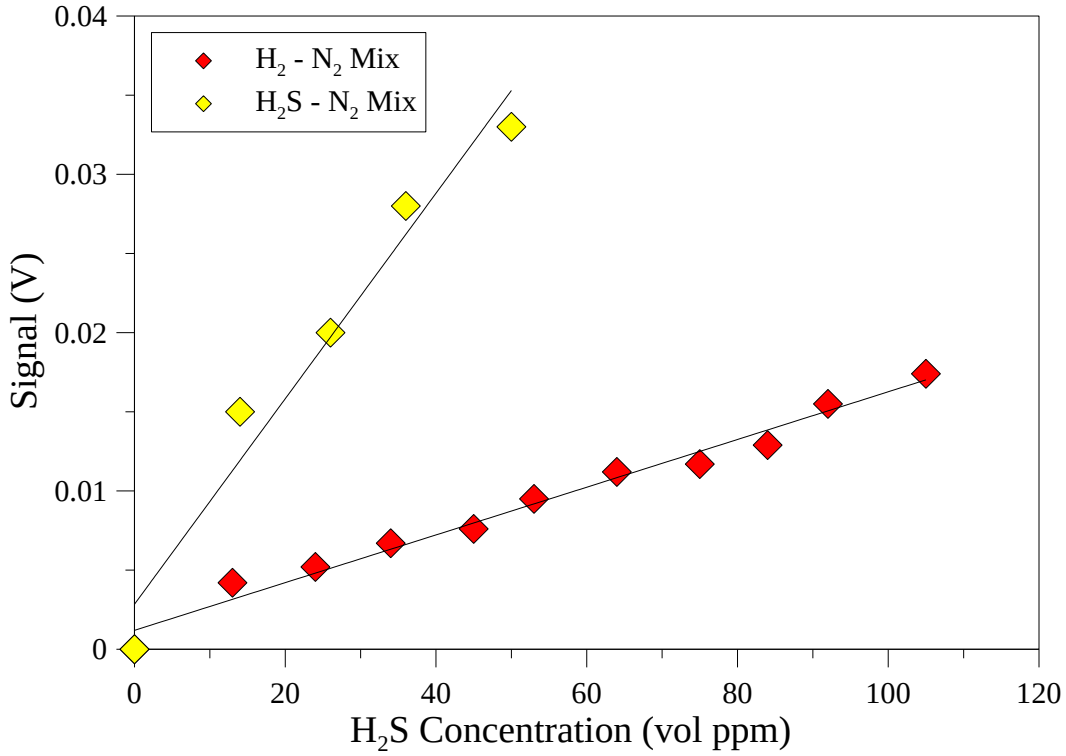

Figure 11 Relation between the signals of the fuel cell vs the reducing specie concentration into the gas mixtures. Yellow diamonds refers to the test series performed with H_2S in the concentration range 0-50 ppm vol. Red diamonds refer to the test series performed using gas mixture containing only H_2 as reducing specie in the concentration range 0-100 ppm vol.

Therefore, we infer that the slight increase in the sensor signal recorded with the (H_2+CO)-containing mixtures was the result of the oxidation reaction of carbon monoxide molecules to CO_2.

The H_2S is the main sulphur specie of the gaseous mixtures emitted from the low temperature fumaroles. The effect of cross sensitivity produced by the presence of H_2S into the mixture entering the hydrogen sensor has been evaluated. The figure 11 shows the results of both the five tests performed with the H_2S-containing mixtures in the range of the H_2S concentration from 0 (air) to 50 ppm vol. as well as the tests performed with H_2-containing mixtures in the H_2 concentration range from 0 (air) to 110 ppm vol. The slope of the trend line is four times larger than the slope of trend line representing the test results of H_2-air. The sensitivity of the H_2 sensor to the H_2S is evaluable in about 0.8 mV ppm^{-1} vol^{-1} suggesting, for example, that the presence of only 25 ppm vol of H_2S produces a signal output of the same intensity of that produced by a mixture containing 100 ppm vol of H_2 in air.

In almost similar way to CO, the H_2S prevents the oxidative reaction of the H_2 molecules on the catalyst layer. Nevertheless, the reverse water electrolysis involves the sharing of two electrons, while the redox reaction affecting the S-containing species involves eight electrons,

providing an electric current of greater intensity for equal concentrations of the reducing species. Therefore, having the same electrical impedance of the external circuit, the sensor has four times sensitivity to H_2S-mixtures larger than the H_2 one, providing an account of the greater slope of the trend line showed in figure 11.

During the laboratory experiments the original performance of the sensor can be recovered by air flushing.

In field applications, to get read of this poisoning effect produced by the H_2S on the catalyst layer and the cross sensitivity with the hydrogen sensor, the gas was sampled through a lead acetate trap. The trap was interposed between the probe and the sensor. Indeed, according to the reaction

$$Pb(CH_3COO)_2 + H_2S \rightarrow PbS + 2CH_3COOH$$

the lead acetate allowed to cut the H_2S concentration into the mixture.

Summarizing the results of the laboratory tests showed above, we identify that among the reducing species investigated, the H_2 fuel cell sensor has the main effect of cross sensitivity in the signal produced by the presence of H_2S into the fumarolic emissions.

The first prototype of a portable H_2 measuring device

In order to tests the performance of the H_2-sensor in the volcanic areas and compare the reliability of the field measurements with the laboratory test results, a prototype of H_2 detector Rew Power fuel cell-based has been designed. Besides the H_2 sensor, an external circuit containing the 500 ohm resistor as well as one air-humidifier system and one lead battery were onboard the device.

The air-humidifier system was connected to the cathode of the fuel cell with the aim to prevent the drying of the membrane (Figure 12) and to improve the water management of the cell. The lead battery feeds the membrane pump of the air-humidifier system.

The measurements have been performed at Solfatara di Pozzuoli area. The measuring method was tuned to the field effectiveness conditions. The main difference compared to the laboratory test consists on the measurement of a fixed gas volume of 100 cc. The gas mixture was sampled with a syringe through a probe inserted up to 50 cm deep into the soil.

The figure 13 show the straight calibration of the H_2 portable device obtained by progressive dilutions of the H_2-N_2 standard mixture with air in the operative conditions mentioned above.

Figure 12 The H_2-measuring portable device. The picture shows the RewPower Fuel Cell H_2 sensor, the external circuit with 500 ohm resistor, the air-humidifier, the membrane pump and the power supply.

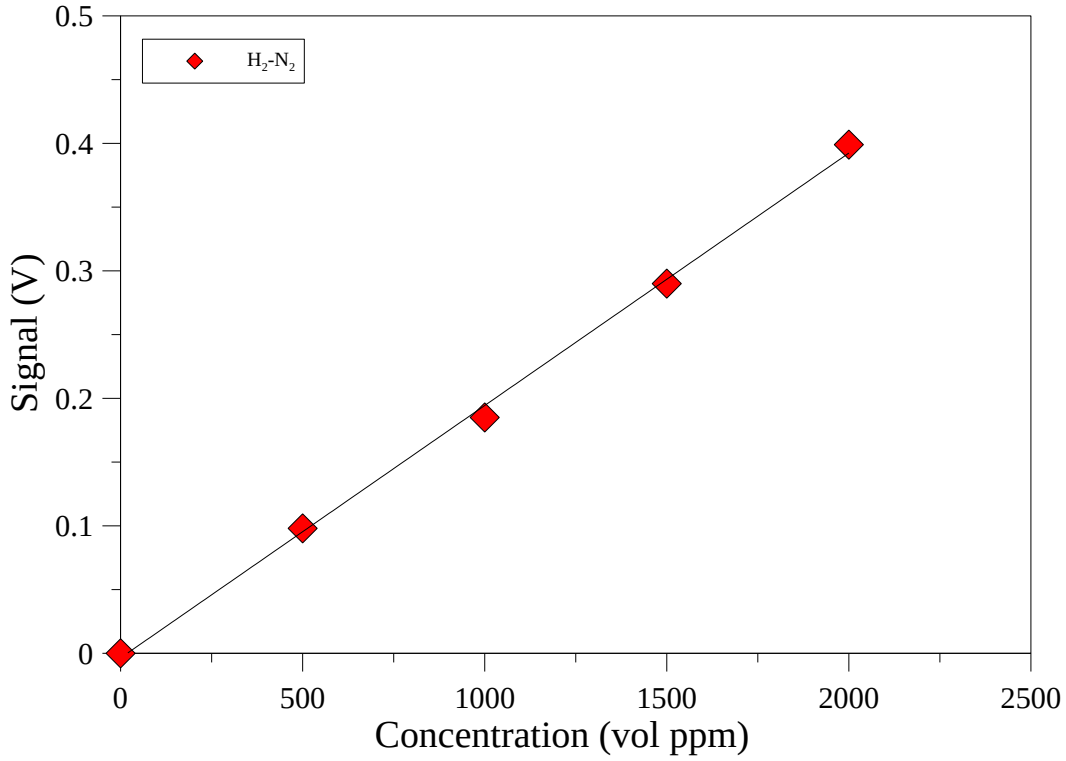

Figure 13 Relation among the signal of the sensor onboard the H_2 portable device vs the H_2 concentration in the mixture. The last ones have been prepared by dilution of H_2-N_2 laboratory gas standard (H_2 = 2000 ppm vol.; N_2 = 99.8 % vol). It is also showed the equation of the fitting line used to change the voltage output recorded during the field measurements in H_2 concentration of the mixtures.

One H_2S-proper electrochemical sensor allowed measuring the H_2S concentration in the sampled gases. The H_2S concentrations spanned in the range between 1600 and 2000 ppm vol. In order to avoid both the poisoning effect produced by the H_2S on the catalyst layer and the effect of the cross sensitivity with the hydrogen sensor, the gas was sampled through a lead acetate trap that allows cutting the H_2 S concentration from about 2000 ppm to 4-6 ppm by the formation of the solid lead sulphide.

The table 3 summarizes the measurements performed with the H_2 sensor and the H_2 equivalent concentration evaluated in the field through the equation of the fitting line showed in the figure 13.

Table 3 Summarization of the measurements performed at the Solfatara di Pozzuoli. The table reports the differential potentials recorded during the measurements and the equivalent concentrations calculated from the calibration line reported in Figure 13.

Site	Signal (mV)	Concentration
P4	5.3	27.16
P4	9.4	48.19
P4	7.5	38.45
P2	64	328.19
P2	62	317.93

Table 4 The table summarizes the chemical analysis of the gas sampled at the Solfatara di Pozzuoli sites.

Sito	**He ppm**	**H_2 ppm**	**O_2 %**	**N_2 %**	**CO ppm**	**CH_4 ppm**	**CO_2 %**	**TOT**
P-4	8	27	3,5	18,01	1,3	50	78,02	99,53
P2Rif H2S	9	308	3,48	13,96	1,9	86	82,65	100,09
P2 2H2S	8	273	5,53	21,98	3	79	72,74	100,25
2P2	8	273	4,26	17,23	1,1	66	78,7	100,19

In order to evaluate the reliability of the performed measurements, we collected several samples from the same sites of the field measurements. The Table 4 summarizes the chemical composition analysis obtained through the laboratory gas-chromatographic technique.

The comparison between the evaluated H_2 concentrations in the field (see third column in Table 4) and the chemical analysis suggests a good agreement of the measurements performed in the field with the hydrogen fuel cell sensor and the true concentration of H_2 in the mixtures analysed.

The automatic permanent device

In order to improve the techniques of continuous geochemical monitoring of the volcanic activity, we combined both the continuous measurement of the H_2 concentration with the CO_2 soil flux. Therefore, we developed a system that integrates one Gascard II spectrophotometer and the hydrogen RewPower fuel cell. The last component has been accurately characterized through rigorous laboratory experiments as H_2-sensor. The association of both sensors allows the monitoring of a massive parameter, such as the CO_2 flux, with an intensive parameter, such as the H_2 concentration.

The Gascard II spectrophotometer measures the CO_2 concentration into the gas mixtures, while the fuel cell measures the H_2 concentrations according to the detection features mentioned in the previous sections. In order to increase its H_2-sensitivity, the device has been equipped with one linear amplifier of the electric signal of the H_2 fuel cell sensor. Figure 15 shows the result of the calibration procedure of the H_2 sensor onboard the automatic monitoring device.

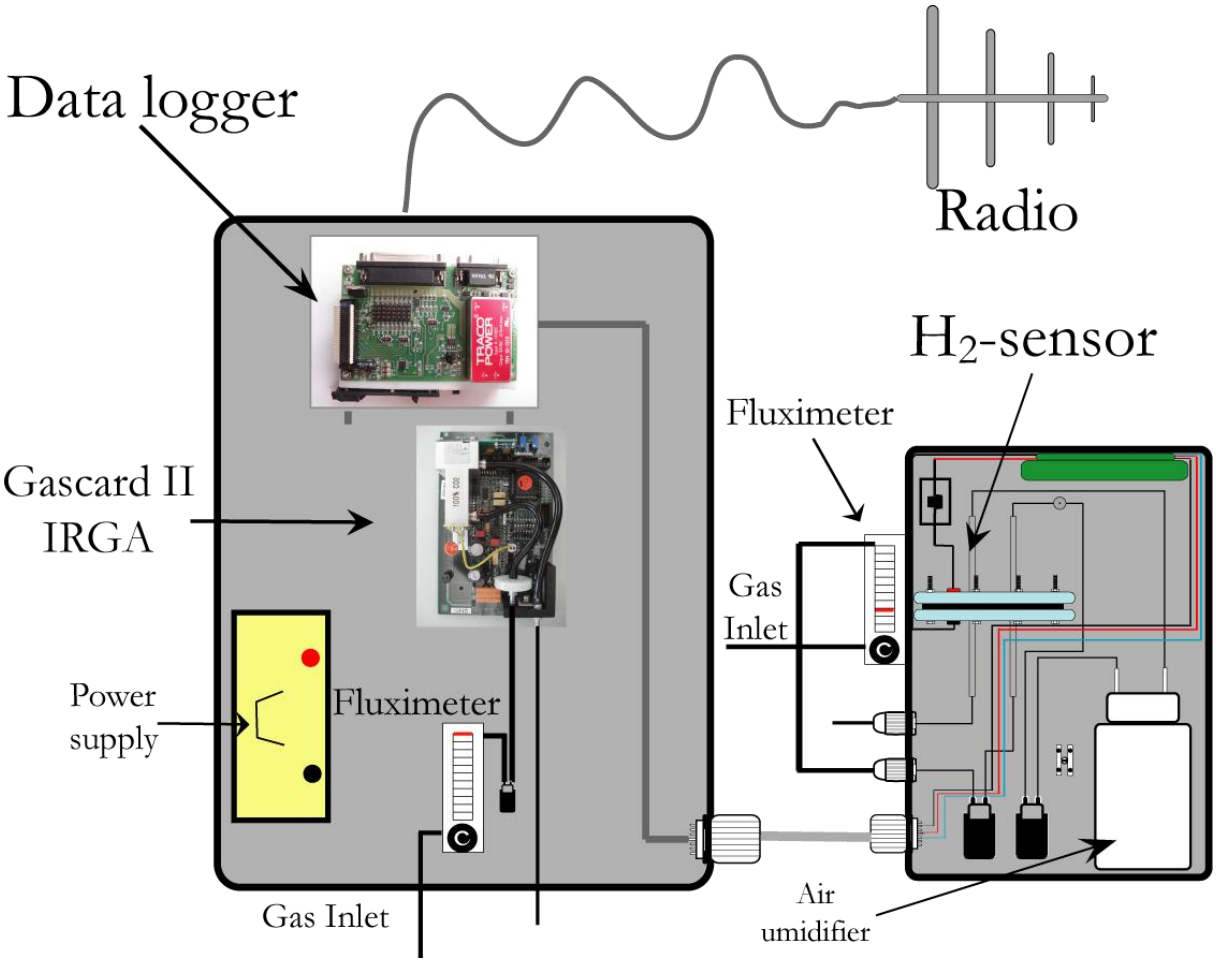

Figura 14 Schematic view of the main components of the permanent H_2-CO_2 monitoring device.

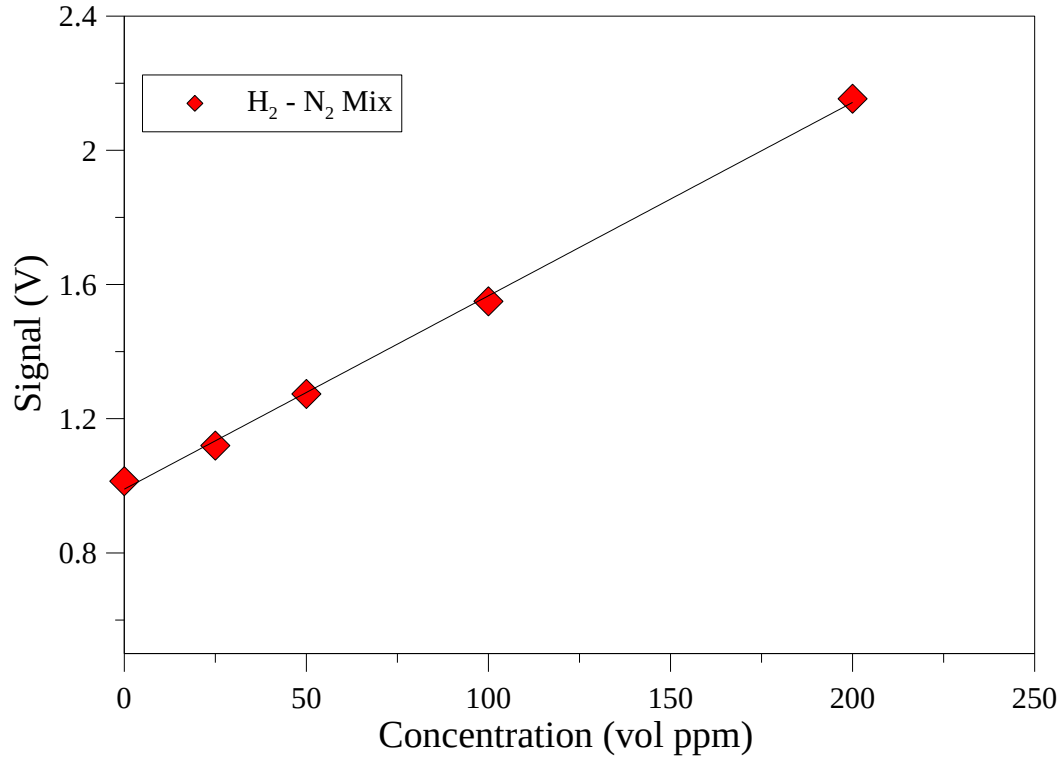

Figura 15 Calibration line of the H_2-sensor onboard the automatic device used to perform the measurements in the field. The standard mixtures are made by dilution of a H_2-N_2 mixture (H_2 = 200 ppm vol.) with air. The H_2 signal is amplified and the concentration H_2 = 0 ppm vol. give about 1 V signal.

All the sensors onboard the automatic system were put into a proof-case together with the fluxmeter, T and P atmospheric sensors and one 100 A lead battery power supply. The latter attends to the electrical power required by

- the Gascard II operation,
- the H_2-sensor amplifier operation,
- the data logger
- the membrane pump of the air-humidifier system of the H_2 sensor and
- the membrane pumps necessary for the automatic sampling of the soil gases.

The Gascard II is an infrared spectrophotometer designed for the accurate and reliable measurement of the CO_2 concentration. The sensor head is based on a technique that provides true, dual wavelength infra-red sensing with no moving parts. The result is a low drift, high accuracy sensor with fast response time and low power consumption.

The working principle of the sensor is based on the property of the molecules to adsorb the electromagnetic energy. The adsorption occurs at the specific frequencies corresponding to the resonant frequencies of bond vibrations within the molecule itself. Therefore, measuring

at characteristic adsorption wavelength enables the detection of the target molecular specie and the strength of the adsorption gives a measure of the gas specie concentration.

Since the CO_2 has a strong adsorption frequency in the infrared range of the electromagnetic spectrum, the radiation source is a tungsten lamp emitting a broad band of radiation in that wavelength range. The radiation directs toward the gas in the sensing cell and then passes through two filters. The filters are selected so that one is coincident with the target gas specie, while the other one is independent of any gas likely to be present in the cell. In absence of target gas specie, the energy reaching both filters is equal and at maximum. As the target gas concentration increases into the detection cell, the amount of infrared radiation reaching the two detectors differs due to adsorption of one wavelength only. The microprocessor onboard the Gascard II provides the conversion of the energy difference recorded at the two detectors and the target gas concentration.

The Gascard II onboard the H_2-CO_2 device has range of CO_2 concentration measurement 0-100 % vol. Its sensitivity is 16mV $\%vol^{-1}$, while the accuracy of the measurement of the CO_2 concentration is ± 2% of range. The repeatability at zero is ± 0.3%, while the repeatability at span is ± 1.5 %. Finally, the input voltage requirement is 24V dc and warm-up time is 1 minute.

Measurement methods

The CO_2 flux measurements were performed applying the dynamic concentration method proposed by Gurrieri and Valenza (1988) and accurately calibrated through a series of laboratory experiments by Camarda et al. (2006a). According to the authors, the measurements were performed by inserting a special probe up to 50 cm deep into the soil. Since the suction pump of the measuring device is set in action, the soil gases start to mix with the air entering through a calibrated opening made on the top of the probe. After a few seconds, the system attains a stationary state and the CO_2 concentration into the mixture begins constant. In steady state conditions, pumping the gases at both known and constant suction flux rate, the CO_2 concentration into the mixture made of soil gases and air (named *CO_2 dynamic concentration*) is right dependent from the CO_2 flux from the soil toward the mixing environment.

According to Camarda et al. (2006a), the empirical relationship between the CO_2 dynamic concentration and the CO_2 flux is

$$\varphi_{CO_2} = (32 - 5.8 \cdot k^{0.24}) C_d + 6.3 \cdot k^{0.6} C_d^{\,3}$$

where C_d is the CO_2 dynamic concentration (% vol), φ_{CO2} is the CO_2 soil flux (kg $m^{-2}d^{-1}$) and k is the permeability (Darcy) of the soil. The permeability is measured in the field according to the method proposed by Camarda et al. (2006b). In order to obtain short response time and to limit the error made by the permeability of the soil, the best setting of the suction flux was obtained pumping the soil gases at 0.8 l min^{-1} (Camarda et al., 2006a).

The H_2 concentration measurements were performed inserting a special probe up to 50 cm deep into the soil, similarly to those of the CO_2 flux measurement. Nevertheless, they differ since the probe for the measurement of the H_2 concentration is atmosphere-proof at the summit. The probe is inserted in close vicinity of the CO_2 flux measurement one. The soil gases entering the probe from the openings of its bottom are sucked by the membrane pump at 0.5 l min^{-1}. According to this sampling method, the soil gases are then analysed by the hydrogen fuel cell sensor.

In order to perform the measurement with our automatic permanent device in low temperature fumarolic fields, some adjustments of the sampling method for the CO_2 flux measurement has been done. In detail, we interpose a steam-condenser between the sampling probe and the spectrophotometer in order to prevent the water entering into the CO_2 analyzing cell. Moreover, in order to prevent the cross sensitivity with the H_2 concentration, a sulphur lead trap has been interposed between the sampling probe and the Fuel Cell H_2 sensor. Figure 16 shows the permanent H_2-CO_2 monitoring device and the sampling probe inserted into the soil.

-

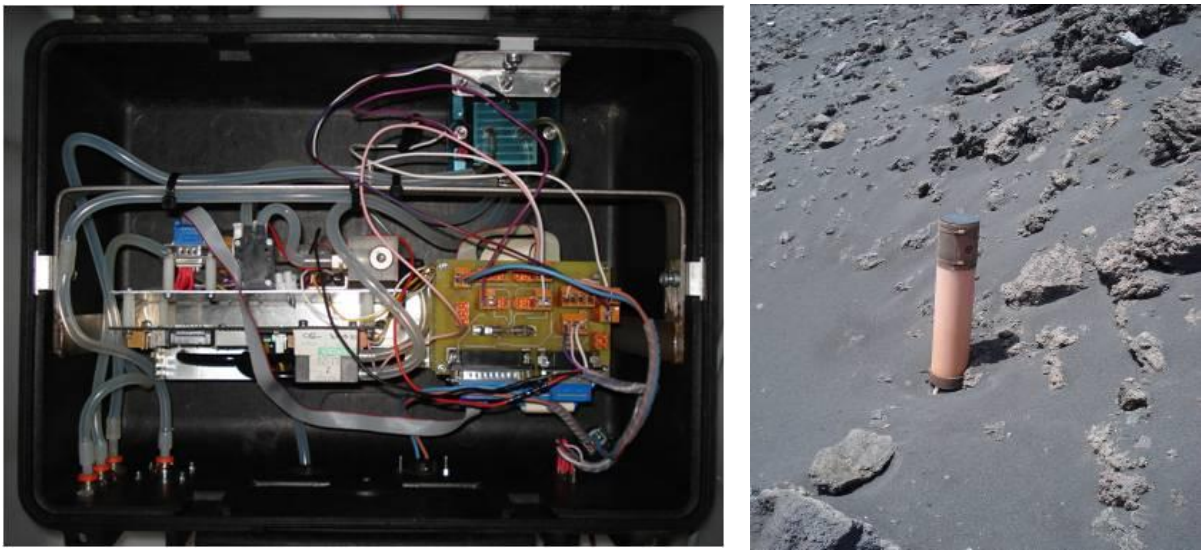

Figura 16 The automatic H_2-CO_2 monitoring device. The picture on the left shows the proof case containing the Gascard II spectrophotometer, the H_2 sensor and the data logger. The hydraulic system need to sample the gas is also showed. The picture on the right shows the sampling probe inserted into the soil.

In order to obtain the H_2 concentration and CO_2 soil flux, the device performs a measurement cycle comprising three main time-intervals:

- the warm up
- the measurement
- the purge

The total time required for each measurement cycle is about seven minute. In field applications, the measurements were performed once per hour and straight stored on the solid memory of the data logger onboard the device. Once a day, the data pass toward the operative-room of the Istituto Nazionale di Geofisica e Vulcanologia (INGV-PA) trough scheduled radio or internet connection. Moreover, at any time of the day, it is possible the manual download of the data. In so doing, we have the possibility to process the data in near-real time.

Chapter 3

The applications of the H_2-CO_2 permanent device in volcanic areas

Introduction

Two H_2-CO_2 automatic permanent systems have been installed on Mount Etna and Stromboli volcano in order to study the relationship between the variation of the H_2 concentration, the CO_2 flux and the volcanic activity.

The first part of the chapter is dedicated to the field applications performed on Mount Etna volcano. We summarize the main structural and volcanological features of the studied area through the existing literature. The data collected during last two years by the permanent H_2-CO_2 monitoring device are shown and discussed. The recent volcanic activity summarized on the basis of the Istituto Nazionale di Geofisica e Vulcanologia (INGV) daily- and week-bulletins and from direct observations performed by the authors has been reported in Appendix 2.

The second part of the chapter is dedicated to the field experience performed at the island of Stromboli volcano. The data collected by the permanent system in this area has been performed for longer time compared to the experience made at the Etna volcano. As in the latter case the Stromboli data are shown and analyzed.

The continuous monitoring of the gas chemistry and gaseous mass releases from volcanic areas allows improving our understanding on the magmatic degassing processes. Furthermore, the data analysis of the fluid dynamic can be helpful to match model interpretation with the volcanic activity in a consistent way.

The H_2-CO_2 measurements performed in both volcanoes allow emphasizing the difference in the degassing features associated to the volcanic activity of two different basaltic volcanoes. Moreover, the acquisition of H_2-CO_2 measurements allows the validation of the theoretical model in different volcanological conditions.

In this chapter we present and discuss the data acquired in the field throughout the last two years.

Continuous monitoring of the H_2-CO_2 on Mount Etna

Geological aspect

The first field application of the H_2-CO_2 continuous monitoring device has been performed on the summit areas of the Mount Etna volcano.

Mount Etna is a complex strato-volcano which growth started about 500 ky ago with the sparse effusions of mainly tholeiitic products (Tanguy et al., 1997) inside a lifting sedimentary basin mostly filled with clay of Messinian age. Today, the mountain summit is at about 3300 m a.s.l. and Mount Etna results the highest European emerged volcano. Mount Etna is also the biggest volcano since covers an area wide more than 1200 km^2 in the eastern side of Sicily Island (Italy) bounded between the Calabro-Peloritan arc at the north, the hybleian foreland at the south and the Ionian Sea at the east. From the geodynamics point of view, these areas represent the European and African convergent margin, the little deformed margin of African plate and the oceanic Ionian lithosphere respectively (Cannata et al., 2008; Giammanco et al., 1997; Patanè et al., 2006 and reference therein; Viccaro et al., 2010 and reference therein; Alparone et al., 2004).

Two main structural regional trends affect the tectonic setting of the Etna area. The first one is the NNW-SSE trending structure dividing the western part of the volcanic edifice from the eastern one. This structure represents the northern extension of the Hiblean-Maltese scarp, reaching the fault systems of the Aeolian archipelago through the system of the Tindari-Letojanni faults, having the same orientation NNW-SSE. The second regional structure is the NNE-SSW trending fault system of the Fiumefreddo-Messina line.

Moreover, two locally important fault systems are the Pernicana fault, in the north-eastern sector of the volcanic edifice, and the Ragalna fault in the south one.

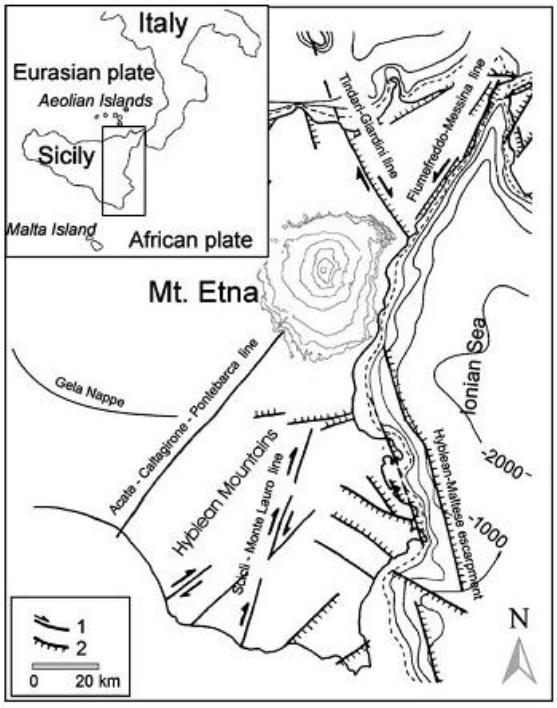

Figure 1 Structural sketch map of the eastern Sicily. From Patanè et al., 2006

The Pernicana is among the longest fault systems of Etnean area trending WNW-ESE 10 Km long. In its outcropping area, take place high seismicity as well as high diffuse CO_2 degassing (Azzaro et al., 1998; Giammanco et al., 1997). The Ragalna fault is a NNE-SSW trending fault system outcropping between Ragalna and Paternò towns. Both systems, but overall the Pernicana fault zone, showed strong seismic swarms before the onset of the past volcanic eruption of Mount Etna.

The Volcanological framework of Etna volcano

During the last 5000 years, Etna has been experienced persistent volcanic activity displaying a wide range of energetic as well as eruptive scenarios. The main part of the volcanic activity involved the summit areas of the volcano having four active summit craters whose altitudes range from about 3200 to above 3300. The Voragine (VOR) crater and Bocca Nuova (BN) crater are located in the central part of the summit area and are named terminal craters. The North-East Crater (NEC) is located on the north-eastern flank of the volcano and named subterminal crater (Alparone et al., 2004). The fourth is the South-East Crater (SEC) located on the southern flank of the volcano. The SEC is the youngest crater formed during the 1971 eruption (Alparone et al., 2004).

The different types of Etna's volcanic activities should be summarized in:

- Passive degassing,
- Summit eruptions,
- Flank eruptions and
- "Eccentric" eruptions.

The passive degassing indicates the fairly continuous emission of a voluminous gaseous plume from the summit craters of the volcano. The fairly quiet activity of passive degassing has great importance from both geochemical and environmental point of views. Through the passive degassing activity, Etna volcano emits a huge amount of volatile from the Earth's interior into the atmosphere (Allard et al 2004.). According to Aiuppa et al. (2008), the total volatile flux emitted through the passive degassing activity from Etna's summit craters is of order ~ 21.000 t d^{-1} and the study of the plume chemistry provides insight into the magma degassing processes (Aiuppa et al., 2007; Aiuppa et al., 2004; Aiuppa et al., 2002). The volcanic plume is mainly composed by H_2O, CO_2, SO_2 and only to a limited extent even of H_2S (Aiuppa et al 2005), changing from H_2O-dominated to CO_2-dominated before the eruptive periods (Aiuppa et al., 2008).

The emission of volatile compounds through the summit craters play a key role on the impact that the volcanic activity drives on the vegetation, the water resources and people living around the volcano edifices (Bellomo et al 2007; Bagnato et al., 2007; Martin et al., 2007).

During the past, the summit eruptions of Etna volcano showed an extraordinary diversity of eruptive styles spanning from moderately quiet lava effusions and lava fountains through middle strombolian activity up to rare and more violent explosive sub-plinian eruptions.

The summit eruptions involved all the craters allowing to the development of large cones. According to Allard et al. (2006), they occur simultaneously to the magma supply into a shallow magma storage volume located ~ 5 km b.s.l. beneath the volcano.

Though the Etna is among the best known volcanoes on earth and among the intensively monitored, some key questions about its plumbing system remains still a matter of debate.

Nevertheless, the occurrence of a shallow storage body at about ~ 5 km b.s.l. has been revealed by geophysical investigations (Murru et al., 1999) and allows explaining the petrological features of the volcanic products (Viccaro et al., 2010; Métrich et al., 2004; Tanguy et al., 1997).

Figure 2 Mount Etna volcano view. The picture was taken near the Paternò town during the survey performed the April 2010.

Flank eruptions occur at Mount Etna volcano with time interval from a few months to several decades during which passive degassing activity or summit eruptions prevail. Most of the flank eruptions involved eruptive fractures developed in different sectors of the edifice, focusing mainly along the tectonic-volcanic structures propagating from the summit area toward NNW-SSE and NNE-SSW directions. According to Behnckle and Neri (2003), from the 1866 to the 2001 Etna volcano showed a progressively increase in the lava volumes emitted through the flank eruptions. The enhancing trend in the rate of energy release has been evident in the past century since a sharp increase in the comprehensive volcanic activity occurred after the 1950.

Besides the eruptions of the XXI century, since 1669 one of the most voluminous flank eruptions (Calvari et al. 1994), emptying the shallow plumbing system below the volcano through flank eruptive fractures connected to their central conduit (Behncke and Neri 2003), occurred in 1991-1993 years.

Several studies has been dedicated to the understanding of the flank eruptions of the Etna volcano, since both the large amounts of lava emitted as well as the likelihood opening of the eruptive fracture at relatively low altitude make this activity among the hazardous ones for thousands people living the slopes of the volcano.

Several triggering mechanisms have been suggested for the flank eruptions, the main questions arising from the role played by the movement of the tectonic structures along which open the eruptive fractures. One of the plausible triggering mechanism, proposed on the base of seismic data acquired during the 2001 eruptions, consider a feedback process between magma intrusion and flank instability which result in a lateral draining of the magma from the central conduit system (Neri et al., 2005; Acocella and Neri, 2003; Behnckle and Neri, 2003).

According to Rittmann, the term “eccentric” indicates a specific group of very rare eruptions of the Etna volcano fed by the conduits that are essentially different from the central ones. According to several authors (Behncke and Neri 2003; Neri et al., 2005), the volcanological and eruptive processes of the 2001 flank eruption differed from the previously ones, because it has been triggered by the upraising of an eccentric dike.

Moreover, also during the 2002-2003 Etna showed several features similar to those of the 2001 eruption. According to Behncke and Neri (2003) and Allard et al. (2006) the happening of such a wide range of volcanic activities does not occur randomly, but following cyclic sequences lasting from several decades to a few centuries.

Several authors (Badalamenti et al. 2004; Giammanco et al., 1998 a-b; Azzaro et al., 1998; Giammanco et al., 1996 Giammanco et al., 1995; Valenza, 1994, 1993; D’Alessandro et al.,

1992) reported high level of diffuse CO_2 degassing throughout the peripheral areas of the volcanic edifice as well as the focused emissions of CO_2 associated with other components such as CH_4, H_2 and He. Those emissions have been connected to the release of a gas phase CO_2–rich from the deep feeding system of the volcano and have been used for monitoring the volcanic activity.

The amounts of the gas released through the volcanic edifice could represent the remarkable part of the total gas phase released during the magma persistence within the plumbing system. According to Allard et al. (1991) the diffuse emission of CO_2 from upper flanks of the Etna volcano are magma-derived and, at least during periods of lava effusions or during shallow magma ponding, the amount of the gases emitted are of comparable magnitude of those emitted from the crater plume.

Figure 3 Gas emission from the peripheral areas of the Etna volcano edifice. The picture was taken near the Paternò town. The gaseous emissions water-bubbling are CO_2-dominated and containing high concentration of CH_4 and He. The monitoring of such emissions provide insight on the magma degassing process and helps in the forecasting the Etna's eruptions.

Sampling sites of the permanent H_2-CO_2 monitoring device

Throughout our observation period, we performed two prolonged experiences in order to collect the measurements with the permanent H_2-CO_2 monitoring system. According to Giammanco et al. (1998), during the 1994 - 1995 years the low temperature fumarolic fields located at the summit areas of the Mount Etna showed sharp variations of the H_2 concentration and CO_2 flux preceding the beginning of strong volcanic activity at the summit craters of the volcano.

We have choose to perform the H_2-CO_2 measurements of the gas emitted from the low temperature fumarolic fields located close to the SEC cone, which showed the strongest activity during the last Etna's eruptions.

The first long-lasting experience has been performed at Torre Del Filosofo. The measurement site is close to the SEC cone at about 2900 meters a.s.l. showing a low temperature fumarolic field. In that area were several eruptive fractures activated during the XX century eruptions (Alparone et al., 2004) and buried below recent pyroclastic deposits. The Figure 4 shows the map of the summit area of Mount Etna and the sampling point of the permanent H_2-CO_2 device.

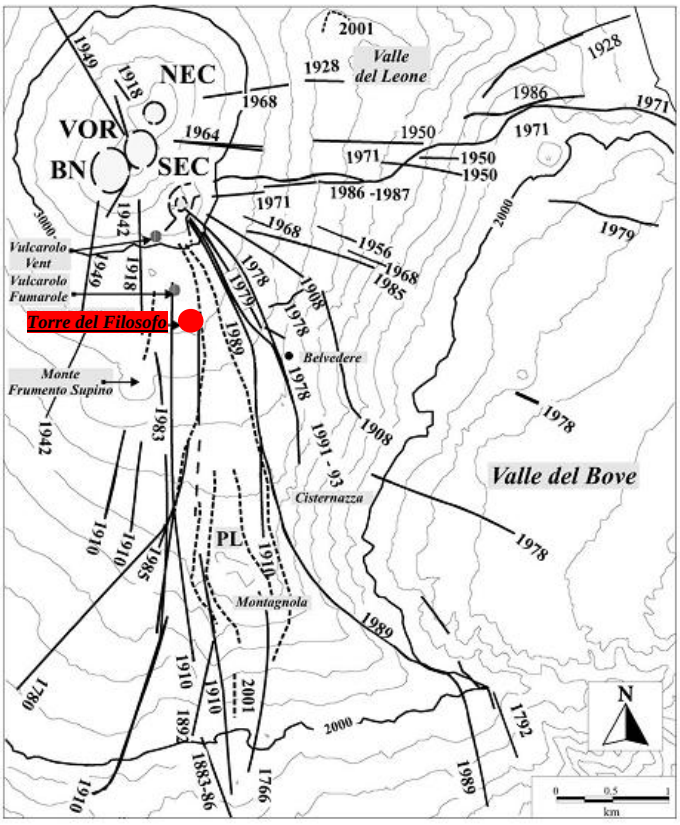

Figura 4 Sketch map of south-eastern sector of Mount Etna Volcano showing the eruptive fractures activated during the XX century eruptions. From Alparone et al. (2004).

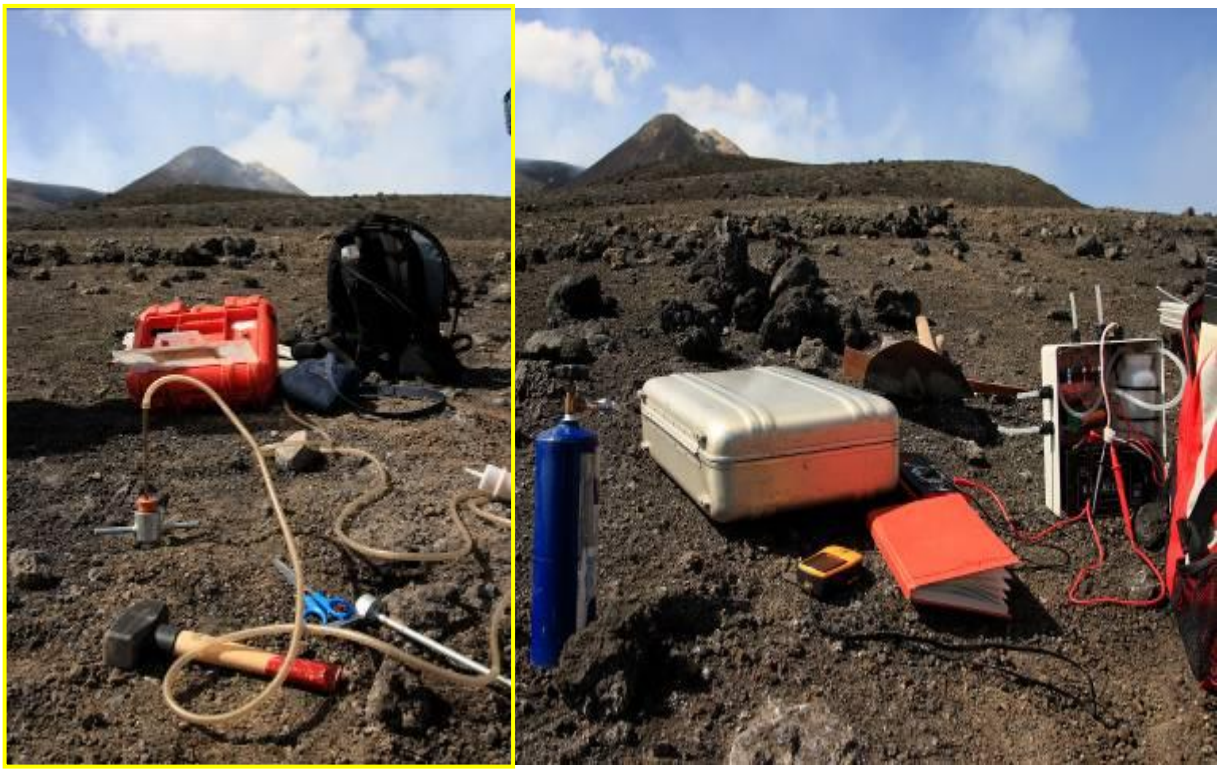

Figure 5 Torre del Filosofo measurements site. The picture was took during the preliminary survey performed in order to find the sampling point of the H_2-CO_2 permanent monitoring device. The picture shows the portable devices to measure the H_2 concentration (on the right) and the CO_2 flux according to the dynamic concentration method (Gurrieri and Valenza, 1980; Camarda et al., 2006). The picture shows the sampling site chosen to perform the H_2-CO_2 measurements close to the road used by tourists to climb around the Torre Del Filosofo Crater. On the background the picture shows the SEC cone undergoing degassing activity.

The sampling site of the gas of the fumarolic field was chosen after a short survey performed around the Torre del Filosofo area with the portable H_2 device RewPower fuel cell-based showed in the previous chapter and the Infra Red Gas Analyzer (IRGA) Gascard II-based portable spectrophotometer. The survey has been performed in order to identify the best locations having:

- from moderate to high amount of CO_2 flux,
- from moderate to high amount of H_2 concentration and
- low to moderate temperature of the subsoil.

The last feature of the site is required to hold underground the case containing the permanent monitoring system, since high temperature could have detrimental effects on the electronic equipments.

The Figure 5 shows the operations performed during the preliminary survey need for the installation of the permanent device at Torre Del Filosofo site.

The acquisition period of the H_2-CO_2 measurements began the 21 July and finished the 8 October 2008 because the typical weather conditions on Mount Etna during the winter season prevented to climb on the summit areas of the volcano with the sufficient frequency need to perform the maintenance operations of the experimental H_2-CO_2 measurement system.

The device battery lifetime and the non efficient GSM coverage of the site implied a periodical maintenance to recovery failing parts and to download the recorded data.

Several efforts are planned in order to improve the system energy and power together with the wireless connection.

One of the main goals of the field experiment performed a Torre del Filosofo site was to check the reliability of the measurements performed with the H_2-CO_2 system in the really long lasting conditions existing in the fumarolic environments.

Since the 8 October 2008 the H_2-CO_2 system has brought back to the INGV-PA laboratories where re-validation tests of the sensors efficiency have been performed with laboratory gas standard containing H_2 or CO_2 and the results are reported into the table 1. The agreement between the concentrations of the H_2 and CO_2 species in the laboratory gas standard with the concentration readings made by both the sensors (H_2 and CO_2) suggest the goodness of the continuous measurement at Torre del Filosofo site.

Table 1 Data of the laboratory tests performed after dismantle from TDF site of the H_2-CO_2 device aimed to verify the proper operations of both the sensors.

H_2 concentration Standard (ppm vol)	**H_2-Sensor measured value (ppm vol)**	**CO_2 concentration Standard (% vol)**	**CO_2-Sensor measured value (% vol)**
0	0	0.045	0
200	198	3	2.98
546	561	30	30.05
1000	982	100	100.09

Results and discussion I

The main goal of the field experiments carried out at Torre Del Filosofo was to study the relationships between the variations of the degassing features of the fumarolic field and the volcanic activity occurring at Mount Etna.

The variations of both the H_2 concentration and the CO_2 flux measured by the permanent H_2-CO_2 monitoring system have been used to produce the data time series. Data analysis was performed by sorting the data in background and anomalous populations based on the cumulative probability plot (Sinclair, 1974) designed for CO_2 flux and H_2 concentration

values and comparing the variations in the range of anomalous values with the volcanic activity occurring at Mount Etna. At the same time, the correlation analyses were performed to verify the reciprocal relations among the monitored parameters.

Table 2 collects the chemical analysis of the gas mixtures sampled from the fumarolic field during the periodical surveys carried out at Torre del Filosofo (TDF) site. A set of survey samples has been collected from the sampling site of the H_2-CO_2 system and inserted into the sample-holders to be analyzed through laboratory chromatographic techniques. Both the H_2 and CO_2 concentration values were used to check the accuracy of the continuous measurements.

The data acquired by the H_2-CO_2 system have been used to study the temporal variations of the chemical composition and the gas output from the TDF site and all the measurements of the H_2 concentration, CO_2 flux, case temperature and atmospheric pressure are reported in Figure 6. The Figure 6c and 6d shows the time series of the case temperature (T-Case) and the atmospheric pressure respectively, the last one beginning from the 16 September 2008. These parameters have been measured in order to evaluate the working conditions of the system.

During the preliminary survey, the soil temperature of the TDF site was 42°C directly measured with a thermometer. As reported in the left side of the diagram, the starting T-Case was about 35°C showing sharp increase up to about 80°C during the weeks following the installation. The relatively high soil temperature (>80°C) has affected the battery lifetime producing an acquisition gap since the 14 August until to the 16 September when the H_2-CO_2 device functionality was restored.

Table 2 Chemical analysis obtained by chromatographic techniques of the gas sampled from the TDF fumarolic field during the surveys carried out to download the measurement performed with the H_2-CO_2 permanent device. The gas samples were collected through the same probe inserted into the soil and used to perform the measurement with the automatic device and transported toward the INGV-Pa laboratory for the analysis. Each sample consists of ~ 20 cc of fumarolic gases. Zero indicates that the gas species concentration was below the detection limit (b. d. l.) of the chromatographic detectors.

Date	**He ppm vol**	**H_2 ppm vol**	**O_2 % vol**	**N_2 % vol**	**CH_4 ppm vol**	**CO_2 % vol**
21.07.2008	7	23	14.37	66.22	50	19.07
22.07.2008	5	7	18.29	75.24	9	4.64
09.08.2008	7	4	19.74	76.04	7	3.14
26.08.2008	9	0 (b. d. l.)	15.06	65.29	44	19.15
16.09.2008	6	6	18.92	75.89	43	4.95
06.10.2008	6	8	16.31	76.54	38	7.08

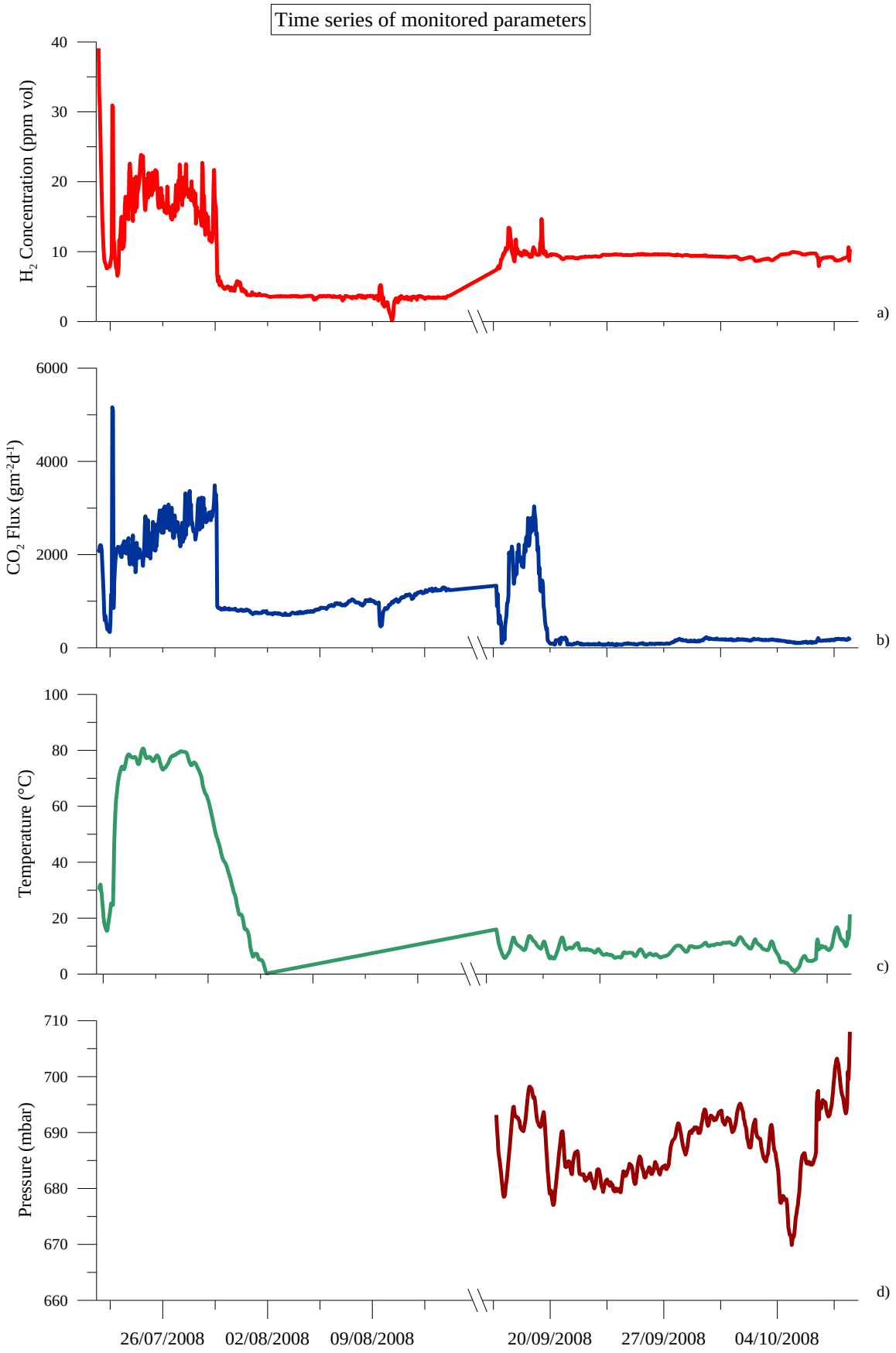

Figure 6 Time series of the measurements performed by the permanent H_2-CO_2 device at Torre Del Filosofo (TDF) site. a) H_2 concentration; b) CO_2 flux; c) Case temperature; d) Atmospheric pressure.

The time series, in figure 6d, shows that the main changes of the atmospheric pressure affecting the monitoring system are in the range of a few tens of mbar.

Beside the direct interferences on the measurement H_2-CO_2 device, these variations may produce pumping barometric effects on the soil gases in agreement with the variations of the weather conditions. The amplitude of these effects could be evaluated trough the correlation analysis between the atmospheric pressure and both the H_2 concentration and CO_2 flux data as will be shown later in this chapter.

H_2 concentration at Torre del Filosofo – Mt. Etna

The figure 7 shows in detail the time series of the H_2 concentration measurements. Within the plot are also superimposed with black diamonds the H_2 concentrations measured, with chromatographic analysis, in the gas samples collected from the same sampling site of the automated system. The agreement between the concentrations measured with the two methods is a further validation of the H_2-CO_2 system performances.

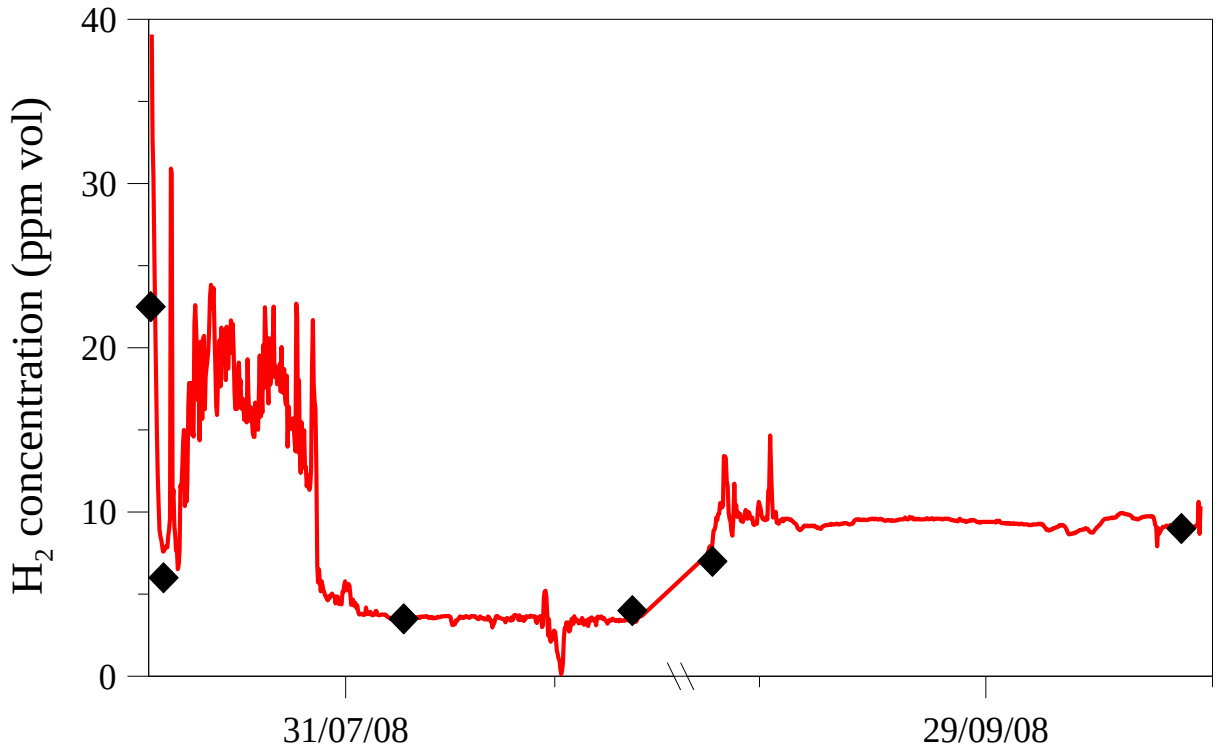

Figure 7 Time series showing the H_2 concentration measurement performed at Torre Del Filosofo since the 21 July 2008 until the 8 October 2008. During our observation period, the H_2 concentration was below 40 ppm vol showing appreciable variations during the last weeks of July 2008.

The data indicate that the H_2 concentration reached the maximum value of 39 ppm vol staying above the average value of 16 ppm vol. (standard deviation 5.3 ppm vol.) at least during all the two weeks following the installation of the H_2-CO_2 system. The figure also shows two secondary peaks in the H_2 concentration, lasting several hours, included into a wider variability period beginning the 22 July until the end of July 2008.

Small variations in the H_2 concentrations have been recorded also during the second half of the September 2008, although their amplitudes changed into the error measurement of the H_2 sensor.

In order to identify the anomalous values of the H_2 concentrations, the data have been reported into the cumulative probability plot showed in figure 8.

According to Sinclair (1974) any data set having polymodal distribution could be classified with their appropriate density distribution, each group showing straight line distribution on the probability plot.

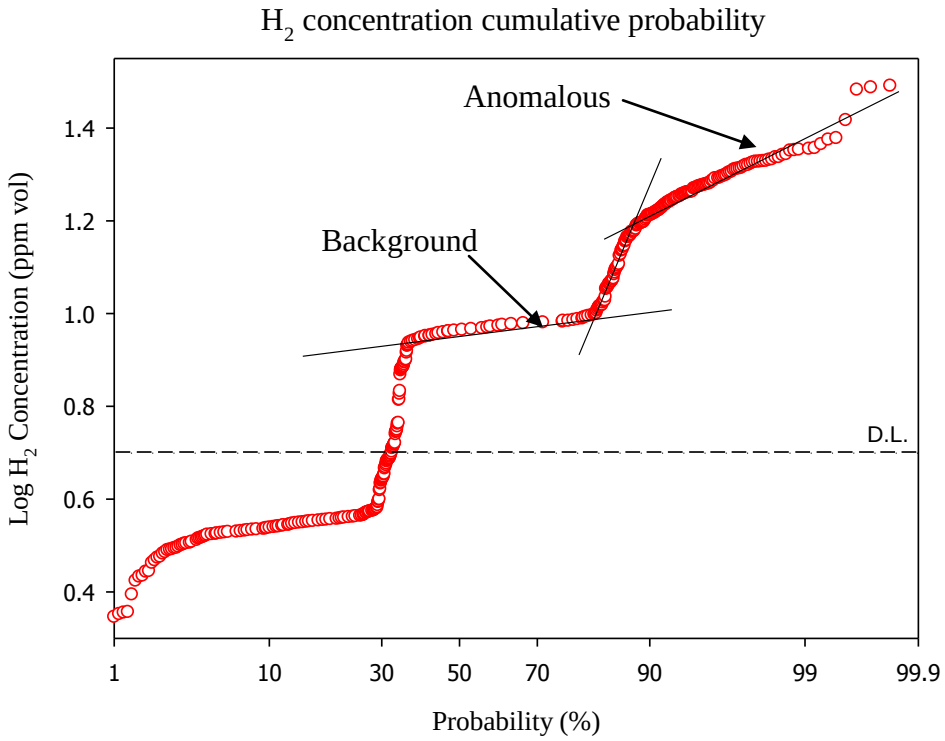

Figure 8 Lognormal probability plot of the H_2 concentration data measured at TDF site. The Ordinate axis shows the logarithm of the H_2 concentration value, while the horizontal axis has probability scale type. Above the detection limit of the H_2 sensor, the H_2 concentration data have bimodal distribution. The higher group (anomalous population) having concentration values above 15 ppm vol represent the 10% of all the measurement, while the lower group (background population) has concentration below 10 ppm vol representing about 60% of the measurements. About the 30% of the measurements show concentration value below the detection limit of the H_2 sensor. D.L. indicates the detection limit of the H_2 sensor.

Two populations of H_2 concentration values representing about 70% of all the measurements could be identified above the typical detection limit of the RewPower Fuel Cell-based H_2 sensor (~ 5 ppm vol), while the residual 30% has values below the detection limit.

The group of highest concentration values (anomalous population) represents about the 10% of all the data set having H_2 concentration above 15 ppm vol., while the lowest group (background population) has H_2 concentration values below 10 ppm vol and represents about the 60% of all the measurements data set.

A comparison between the data classification showed on the probability plot and the time series of the H_2 concentration suggests that anomalous H_2 release occurred during the second half of July 2008 from the TDF fumarolic field. The others variations recorded until the 8 October are included in the range of H_2 concentrations typical of the background population of the gas emitted during the period of observation.

The classification obtained from the probability plot allows doing an initial selection of the measurements before the correlation analysis with the others measured parameters.

The comparison of the H_2 concentrations with the T-Case and atmospheric pressure data allows the evaluation of the effects produced by the variations of the working and meteorological conditions on the measurements performed with the RewPower fuel cell sensor. Taking into account the detection limit of the H_2 sensor, in the comparison are considered only the H_2 concentration values above ~ 5 ppm vol.

Figure 9 contains the correlation diagram between the H_2 concentration values and the T-Case. The analysis of the whole data set indicates moderate positive correlation with the case temperature having Pearson's coefficient[1] value of 0.748.

[1] The Pearson correlation coefficient is widely used as a measure of the correlation between two variables giving a value between 1 or -1 corresponding to data points lying exactly on a line, while value of 0 implies that there is no linear correlation between the variables. Other specifications regarding the Pearson's coefficient are listed in Appendix 3.

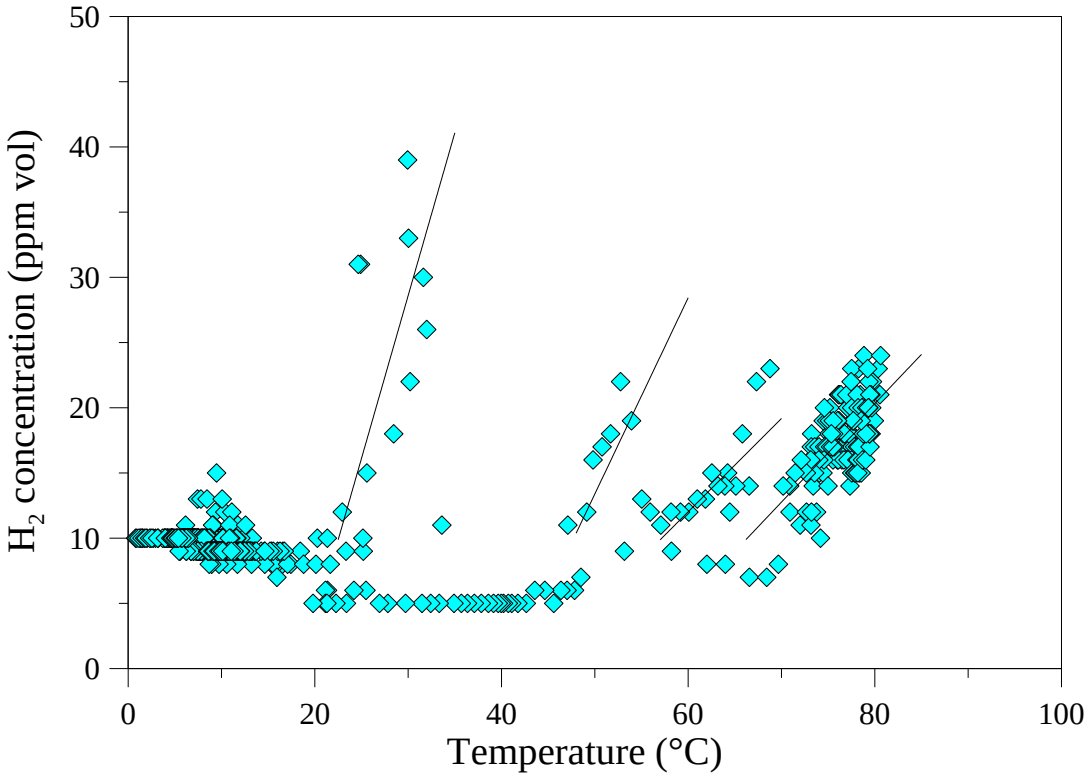

Figure 9 Correlation diagram of H_2 concentration measurements vs. the case temperature (T-Case). Considering the H_2 concentration values above the detection limit of the sensor, a slight positive correlation is showed with the T-Case. Some groups of the data show larger dependence from the temperature, while the data below 10 ppm vol show independency from the T-Case.

The selection of the measurements classified from the probability plot allows a more detailed analysis of the distribution of the H_2 concentration values in comparison to the T-Case.

As shown in the figure 9, the H_2 concentration data below 10 ppm vol change independently from the T-Case showing sub-horizontal distribution parallel to the temperature axis.

Above the threshold values of 10 ppm vol., can be identified four groups of concentration values having larger dependency from the T-Case. Each group forms concentrations trends ranging from the background toward the anomalous populations in the temperature intervals of about 10°C.

As shown in the chapter dedicated to the technical features of the system, the characterization tests of the H_2 sensor indicate that temperature variations of the order of 10 °C may produce 10% error in the measurement of H_2 concentration. Since the concentration measured there are larger than the 10% sensor error, can be hardly attributed to the temperature variations.

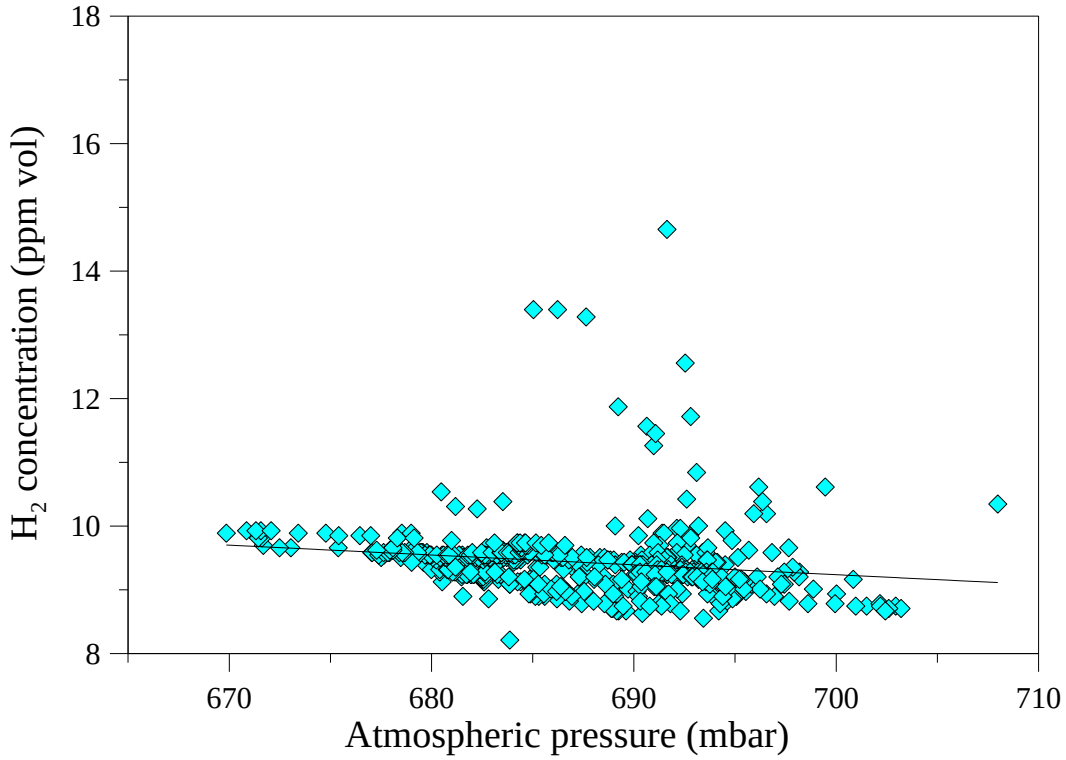

Figure 10 Correlation diagram of H_2 concentration measurements vs the atmospheric pressure. The latter parameter has been monitored since the 16 September 2008. Considering the whole dataset, the measurements show a slight negative correlation described by the fitting line with the atmospheric pressure.

Figure 10 contains the correlation diagram between the atmospheric pressure and the H_2 concentration. The figure shows that a large fraction of the measurements has sub-parallel distribution in comparison to the pressure axis and data fitting line shows negative slope and low value of the coefficient of correlation[2] ($R^2 = 0.029$).

This distribution together with the negative Pearson's coefficient of ($r = - 0.1705$) suggests that the whole data set of H_2 concentration values have a slight inverse relation to the atmospheric pressure. A few other measurements scattering away from the fitting line are within the range of the typical measurement error of the sensor.

The analysis of the data collected with the H_2-CO_2 device at TDF site suggests that the H_2 concentrations data may show in a limited extent dependency from both the temperature and the atmospheric pressure. However, the variations of the H_2 concentration are wider than the

[2] In the case of linear regression, R^2 is the square of the sample correlation coefficient between the outcome and the values being used for prediction, changing between 0 and 1. Other specifications regarding the coefficient of correlation are listed in Appendix 3.

typical errors affecting the H_2 sensor and can be hardly attributed to the effects of both the working and meteorological conditions.

CO_2 Flux at Torre del Filosofo – Mt. Etna

The Figure 11 shows the time series of the CO_2 flux measurements. The data show that the average CO_2 flux value measured until the 30 July 2008 was about 2269 $gm^{-2}d^{-1}$ having the standard deviations of 649 $gm^{-2}d^{-1}$ and range changing from the minimum flux value of about 335 $gm^{-2}d^{-1}$ to the maximum of 5160 $gm^{-2}d^{-1}$.

Starting from the 22 July, the CO_2 flux showed well defined enhancing trend characterized by secondary peaks lasting several hours (from 20 to 50 hours). During the second half of September 2008 an increase in the CO_2 flux attaining about 2727 $gm^{-2}d^{-1}$, has been also observed. Since the following week the CO_2 flux sharply decreased, keeping the mean value at about 129 $gm^{-2}d^{-1}$ and slightly changing up to the maximum value of 211 $gm^{-2}d^{-1}$.

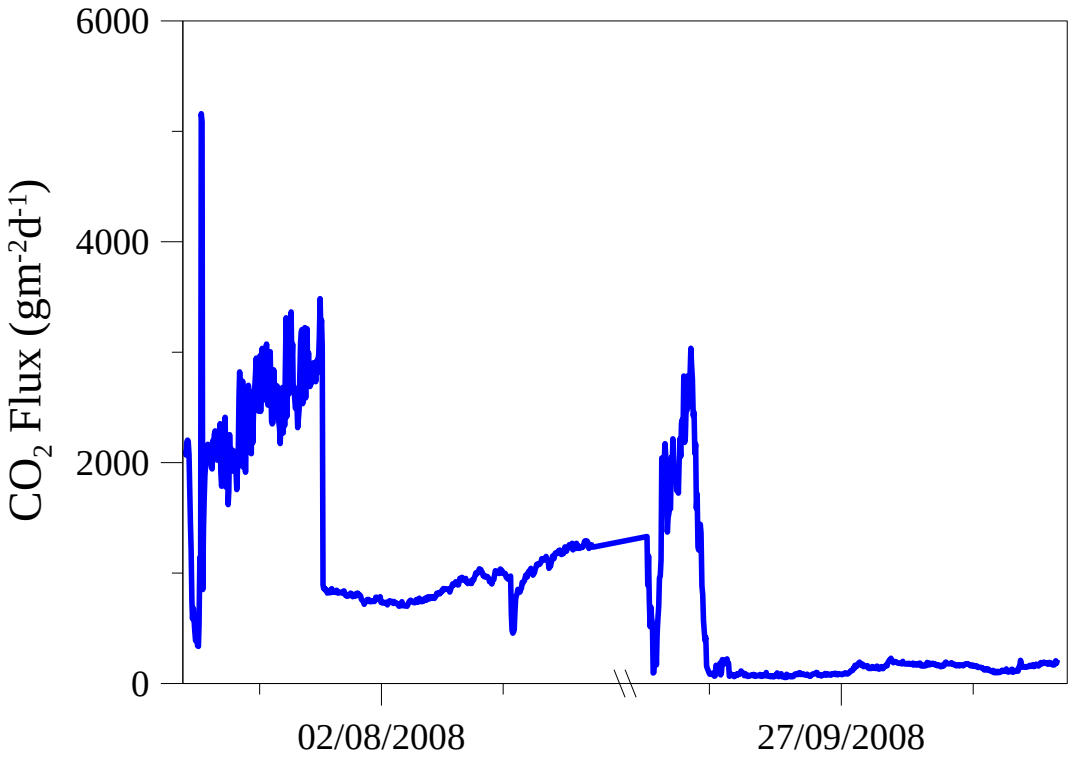

Figure 11 Time series showing the CO_2 flux measurement performed at Torre del Filosofo since the 21 July 2008 until the 8 October 2008. The CO_2 flux values are given in g m^{-2} d^{-1}. During our observation period, the CO_2 flux was below 4000 $gm^{-2}d^{-1}$ showing appreciable increase during the last week of July 2008. The CO_2 flux increase is also recorded during the second half of September 2008.

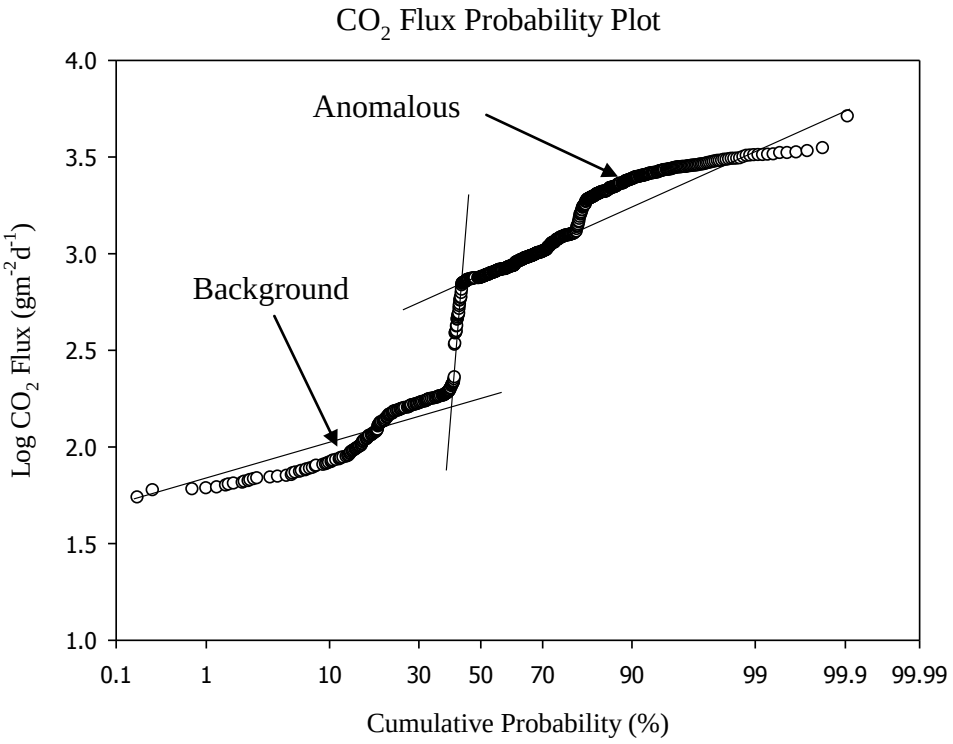

Figure 12 Lognormal probability plot of the CO_2 flux data measured at TDF site. The Ordinate axis shows the logarithm of the CO_2 flux value, while the horizontal axis has probability scale type. The whole data set shows three main groupings of the flux values, the higher one (anomalous population) having values above 650 $gm^{-2}d^{-1}$ represents the 60% of all the measurement. The anomalous flux values contain two sub-populations showing the highest values above 1500 $gm^{-2}d^{-1}$. The background population shows flux value below 150 $gm^{-2}d^{-1}$ representing about 35% of the measurements. A third population of intermediate flux values represents the residual 5% of the whole data set.

In order to classify the measurements and separate the anomalous from the background values, the CO_2 flux data have been reported into the cumulative probability plot showed in figure 12.

The whole CO_2 flux data set splits in three main groups. The highest CO_2 flux population (anomalous) contains flux values above 650 $gm^{-2}d^{-1}$ representing about the 60% of all the measurements performed throughout the observation period. In each turn, the anomalous group contains two sub-populations showing the highest values above 1500 $gm^{-2}d^{-1}$ and representing about the 30% of all the recorded values. The background population shows flux value below 150 $gm^{-2}d^{-1}$ representing about 35% of the measurements, while the third population contains the residual 5% of the whole data set being characterized by intermediate flux values.

A comparison between the distribution showed on the probability plot and the time series of the CO_2 flux measurements suggests that the highest CO_2 flux from the TDF fumarolic field have been recorded during the second half of July 2008 and only in a limited extent during the

second half of September 2008. The comparison of the CO_2 flux values with the T-Case and atmospheric pressure measurements allows the evaluation of the effects produced by the variations of the working and weather conditions on the sensor and the amplitude of the pumping effects that may be produced on the soil gases in agreement with the variations of the weather conditions.

The figure 13 shows the correlation diagram between the flux values and the temperature. The analysis of the whole data set of the measurements suggests that the CO_2 flux data shows positive correlation with the T-Case, since the fitting line has positive slope, the coefficient of correlation has intermediate value ($R^2 = 0.666$) and the Pearson's coefficient $r = 0.816$. Some groups of data make vertical trend that shows variations larger than three orders of magnitude, independently from the temperature variations. Such variations, which are larger than expected for temperature variations of about 10°C even in the areas where the organic decompositions occurs, can be hardly attributed to the temperature variations in the environmental conditions found at TDF site.

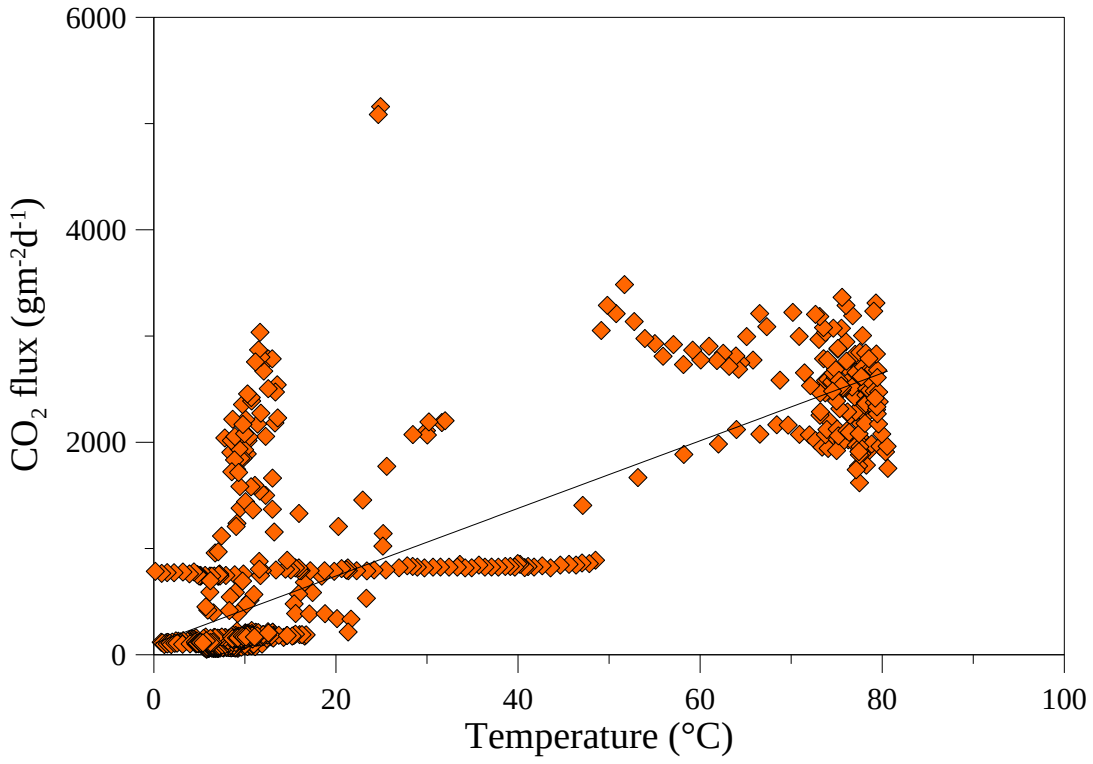

Figure 13 Correlation diagram between the CO_2 flux measurements vs the case temperature (T-Case). The figure also shows that the CO_2 flux value scatter away from the fitting line of the data suggesting larger variation independently from the T-Case. It is worth nothing that the CO_2 flux shows variations of three order magnitude. Considering the whole dataset of the measurements, about the 20% shows a slight positive correlation according to the fitting line with the T-Case.

Moreover, two measurement groups having constant values of 100 $gm^{-2}d^{-1}$ and 900 $gm^{-2}d^{-1}$ of the CO_2 flux are also reported, showing smaller variation despite temperature variations larger than 40°C.

The comparison of the variations occurred in both the H_2 concentration and the CO_2 flux allows analyzing the degassing activity occurred at TDF site.

The figure 14 shows the correlation diagram between the CO_2 flux and the H_2 concentration values. Taking into account the sensibility of the sensor, the figure contains the data above the H_2 concentration value of ~ 5ppm vol.

Within the dotted area reported in figure 14 are included the anomalous data of both H_2 concentration and CO_2 flux in agreement with the classification resulting from the probability plot. The values of both H_2 concentration and CO_2 flux peaks are removed from the selected data, because the singularity of the maximum values may underestimate the average relation between the two parameters.

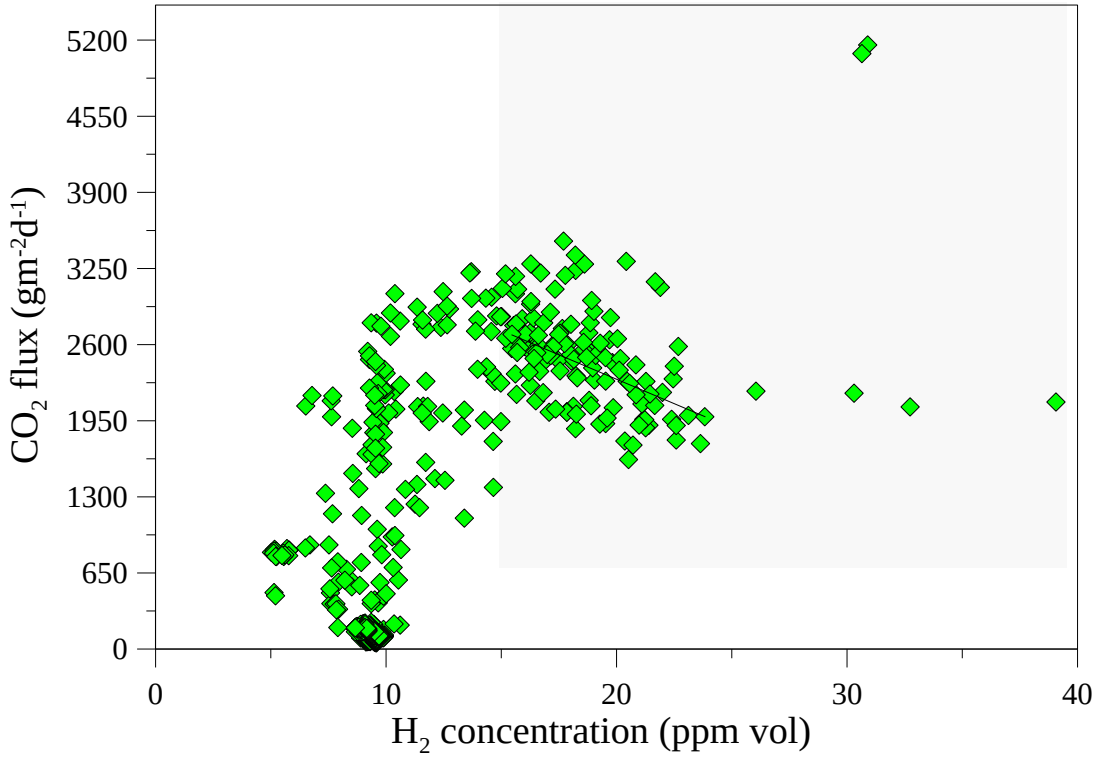

Figure 14 Correlation diagram between the CO_2 flux and the H_2 concentration measurements performed at TDF site. The whole dataset suggest low correlation between the two parameters. The data set values shows one main clustering areas in the H_2 concentration range 10-25 ppm vol and CO_2 flux range 1500-3250 $gm^{-2}d^{-1}$ while the average value are $H_{2\,a}$ = 11 ppm vol and $CO_{2\,f\,a}$ = 872 $gm^{-2}d^{-1}$ respectively.

The selected data have low negative Pearson's correlation coefficient (r = -0.484) and intermediate coefficient of correlation (R^2 = 0.234) with the fitting line. Such distribution of the data suggests that when the H_2 concentration reached anomalous values, two distinct behaviours have been showed by the CO_2 flux.

Peaks values (unselected data) show agreement between the H_2 concentration and CO_2 flux, while the other ones (selected data) show negative dependence suggesting that the geochemical signal obtained by the monitoring of the H_2 concentration could be not standard correlated to the CO_2 flux one.

In order to identify the relation between the variations of the H_2 concentration and those of the CO_2 flux, the data have been processed and filtered from the interferences of environmental conditions according to the results obtained through their own comparison. The data processing has been done in MatLab environment using the Signal Processing tool (SPtool), considering the unprocessed data of the time series as digital signals and identifying the frequency variations through the Fast Fourier Transform (FFT) analysis.

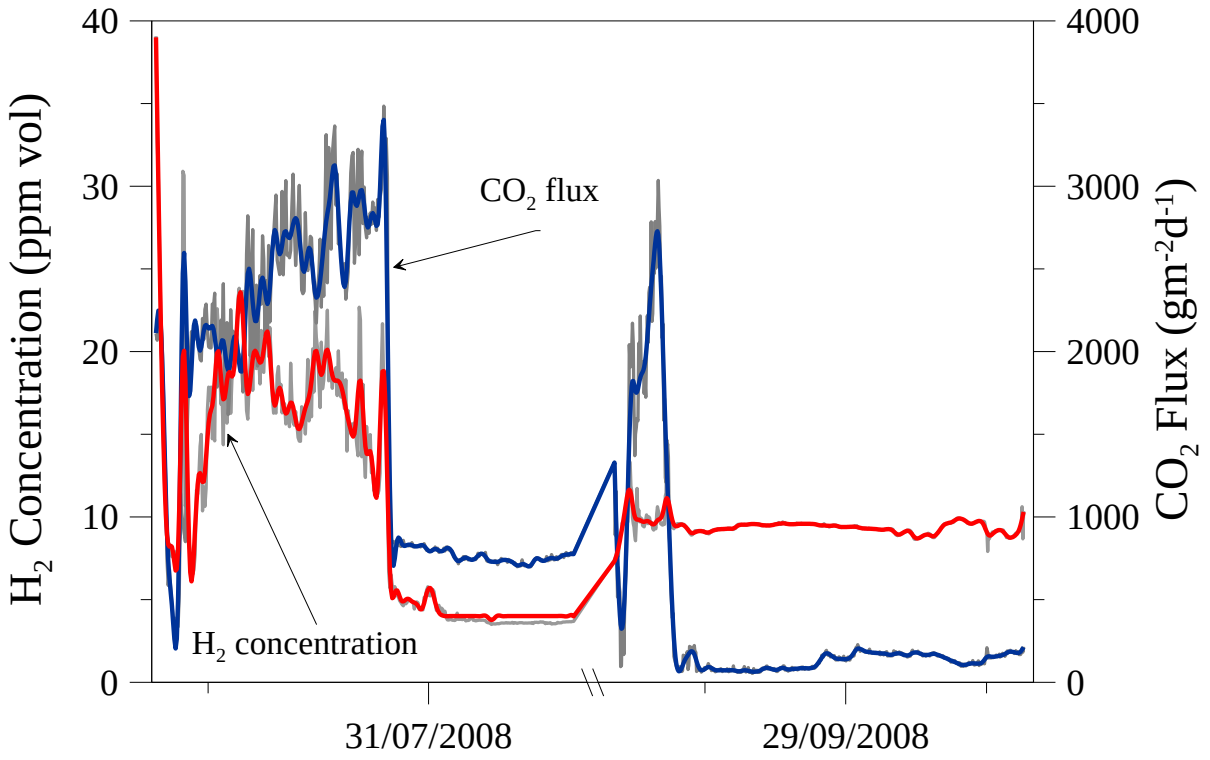

Figure 15 Time series of the H_2 concentration (red line) and CO_2 flux measurements (blue line) performed at Torre del Filosofo site (Mount Etna volcano) since the 21 July 2008 until the 8 October 2008. The figure contains the unprocessed data on the background while the relative processed data are superimposed. The data processing has been performed using the Signal Processing tool (SPtool) in MatLab environment.

The frequency bands identified in the H_2 concentration and CO_2 flux signals have been compared with the frequencies spectrum of the Case Temperature and the Atmospheric Pressure.

The figure 15 shows the results of the data processing obtained from the time series of H_2 concentration and CO_2 flux through lowpass four order stable filter using the zero phases IIR Butterworth designing method of the SPtool in MatLab environment. The results show that the general trends are unmodified, pointing out important differences in the time series of the H_2 and the CO_2 species, mainly throughout the second half of July 2008. In the left part of the diagram, the H_2 concentration shows a wider climax containing two secondary peaks of amplitude larger than the sensor error in a general decreasing trend. The secondary peaks, lasting a few tens of hours, attain the culminations the 24 and the 27 July 2008 respectively.

In a different way from the H_2 concentration, the CO_2 flux time series shows a general increasing trend, though two secondary peaks having amplitude of a few hundreds of grams up to squared meters per day are also recognizable.

The climax of CO_2 fluxes have been attained during the first hours of the 25 July and the 28 July 2008, occurring a few hours later the H_2 concentration ones.

The data of the H_2 concentration and CO_2 flux recorded with the H_2-CO_2 system throughout the first experiment on Mount Etna volcano makes time series fairly narrow for correlating directly the degassing variations observed at Torre Del Filosofo site with the magmatic process occurring into the volcanic feeding system. Therefore, conclusions could be draft by comparing the variations observed on the monitored parameters with the volcanic activity occurred on Mount Etna throughout the period of observation. According to the INGV bulletins (31 July 2008 INGV-PA bulletin – see Appendix XX for more details), increases in both the CO_2 concentration dissolved in ground-water and in the C/S ratio of the plume emissions have been recorded since the 25 until the 28 July 2008 suggesting a modest refilling process of the central conduits of the volcano during the ongoing 2008-2009 eruption.

Throughout the same period, remarkable variations of both the chemical composition and the mass output of the fluid emitted from fumarolic field occurred at Torre Del Filosofo, showing measurable variations of the H_2 concentrations and the CO_2 flux. The variations are identified by the peaks in the time series and according to their climax, the change in the chemical composition occurred a few hours before the increasing of the CO_2 flux.

The INGV-CT week-bulletins (7-13 September and 14-20 September) reports the enhancement of the passive degassing activity from the pit-crater opened at the base of the

SEC cone since the first days of September. In the second half of the month a variation of three orders of magnitude in the CO_2 flux have been recorded at the TDF site during a phase of increasing degassing activity from the SEC cone.

Belvedere site

The second H_2-CO_2 system has been installed at Belvedere site (BLV) on the south-eastern flank of Mount Etna volcano. This is a low temperature fumarolic field close to the SEC cone formed after the 1991-93 eruption where the eruptive fissure crossed the edge of the Valle del Bove (Pecoraino and Giammanco, 2005). The schematic map showing the south-eastern sector of Mount Etna volcano and the eruptive fractures activated during the XX century eruptions has been reported in figure 5 from Alparone et al. (2004).

The H_2-CO_2 permanent monitoring system has been installed at Belvedere site since the 27 May 2010 and the measurements reported here cover the period until the 8 September 2010. The sampling site of the gas released from the fumarolic field was chosen after a short survey performed around the Belvedere area with the portable H_2 device RewPower fuel cell-based and the Infra Red Gas Analyzer (IRGA) Gascard II-based portable spectrophotometer, both showed in figure 12. As in the TDF site experiment, the survey has been aimed to identify the best locations showing:

- intermediate CO_2 flux,
- from moderate to high H_2 concentration.

The overall aim of the experiment performed at Belvedere site was to study the relationships between the variations of the degassing features from the fumarolic field and the volcanic activity of Mount Etna. The variations of both the H_2 concentration and the CO_2 flux measured by the permanent H_2-CO_2 monitoring system have been used to produce the data time series.

The cumulative probability plots (Sinclair, 1974) have been designed for both the CO_2 flux and the H_2 concentration measurements in order to sort the data in background and anomalous populations. The data analysis allowed the comparison of the variations of both parameters in the respective ranges of anomalous values with the volcanic activity occurred at Mount Etna throughout the period of observation.

The data acquired by the H_2-CO_2 system have been used to study the temporal variations of both the chemical composition and the mass output from the BLV fumarolic field. The measurements of the H_2 concentration and CO_2 flux are reported in figure 16.

The atmospheric pressure data for the observation period, reported in figure 16a), were obtained from the ECMWF (European Centre for Medium-Range Weather Forecasts) MARS archive under license from the Italian Air Force Meteorological Service and kindly provided by Dr. Liotta M.

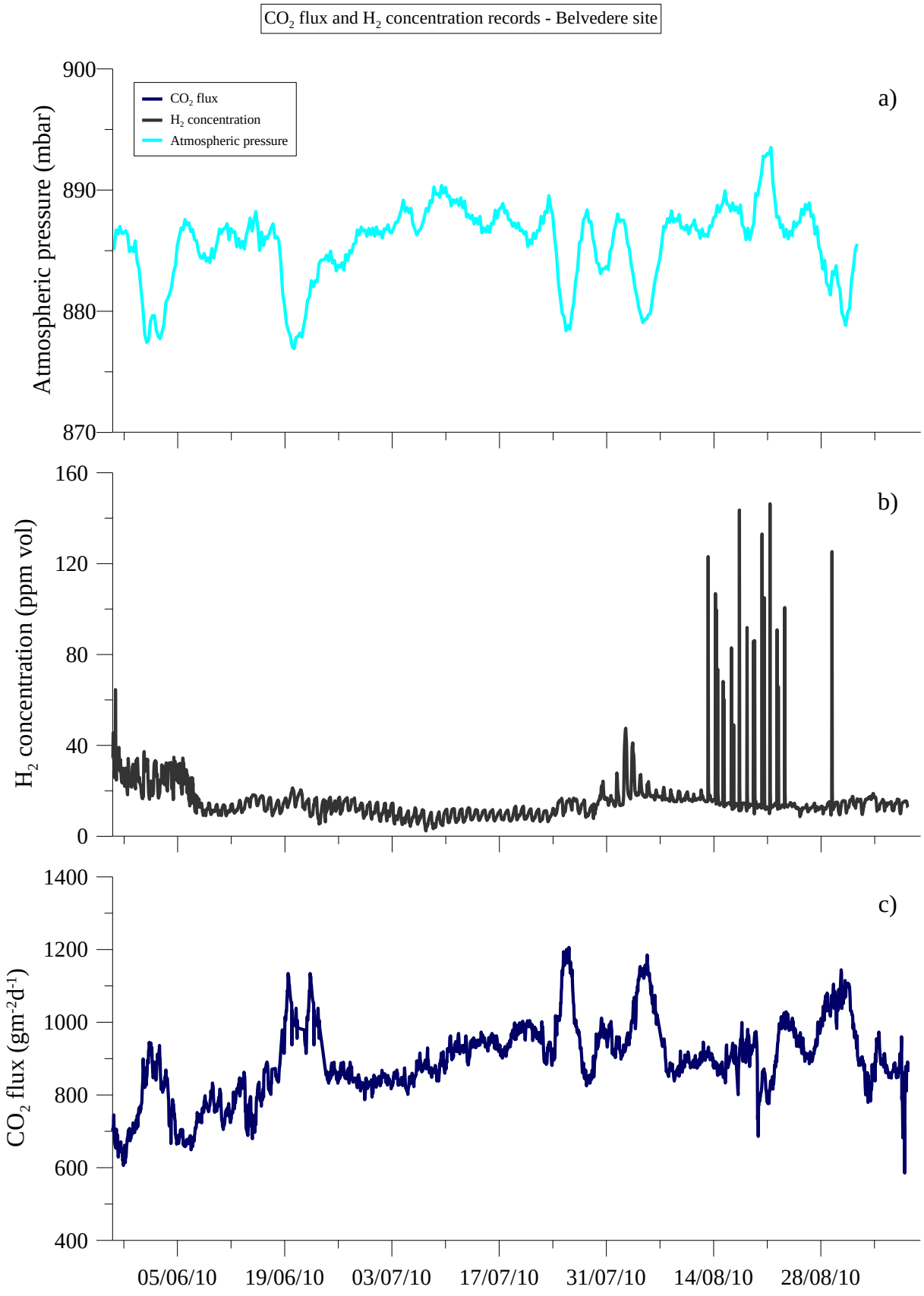

Figure 16 Time series of the measurements performed by the permanent H_2-CO_2 device at Belvedere site (henceforth BLV). The data have been acquired since the 27 May until the 8 September 2010. a) Atmospheric pressure. b) H_2 concentration. c) CO_2 flux.

H_2 concentration at Belvedere – Mt. Etna

The figure 17 shows in detail the time series of the H_2 concentration measured in the gases released from BLV fumarolic field. The average value of 15 ppm vol. has been recorded since the first week of June until the late July 2010, slightly changing within the range of 10 ppm vol. with daily frequency. The H_2 diurnal variations show typically the lower values in the morning and the highest in the evening.

Larger variations occurred since the late July 2010, when the relative maximum concentration of 50 ppm vol. has been measured. Moreover, several increases of the H_2 concentration occurred throughout the second half of August 2010. In different way from the first increase, which persists about three days, the other increases observed since the 13 August 2010 have spike-like shape within the time series, resulting from rises of the H_2 concentration that persist a few hours. The rises produce peaks of the H_2 concentration reaching the maximum value of 146 ppm vol., one order of magnitude larger than the average concentration of BLV emissions. It is worth noting that differently from the diurnal changes, these irregular increases occurred in the morning or in the afternoon, without any comparable peaks recorded in the evening.

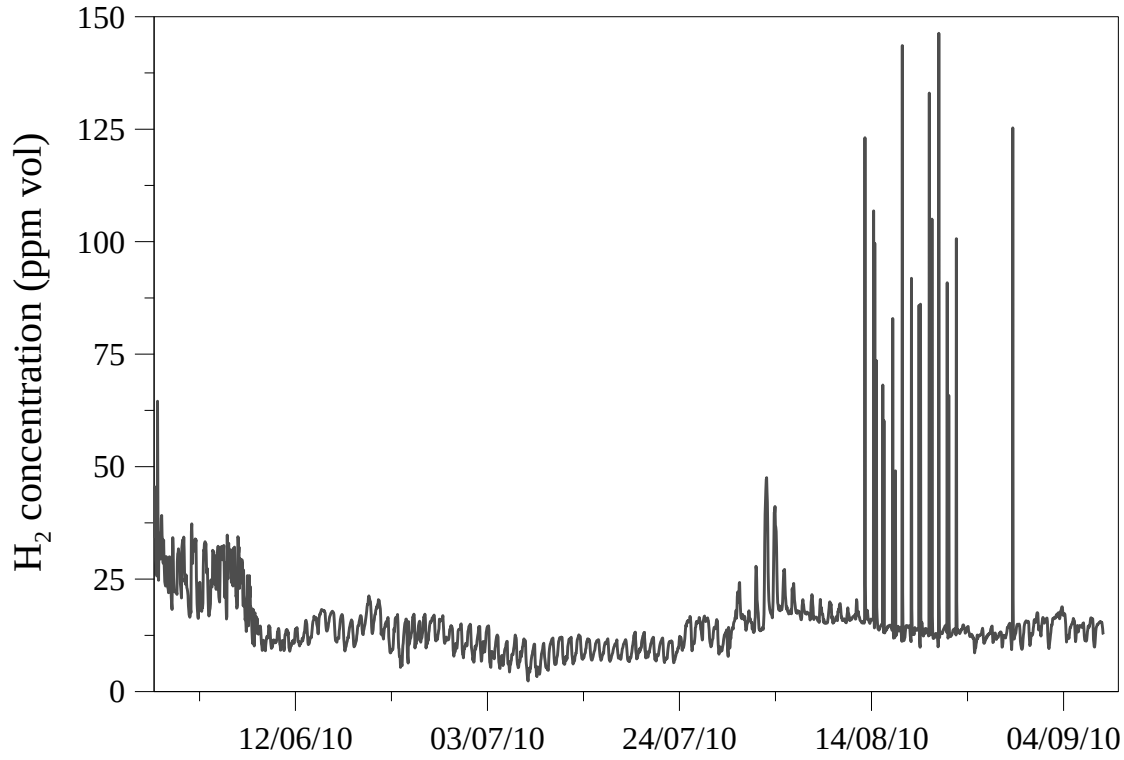

Figure 17 Time series showing the H_2 concentration measurements performed at Belvedere since the 27 May 2010 until the 8 September 2010. During the large part of the observation period, the H_2 concentration was below 40 ppm vol showing large variations since the last week of July 2010.

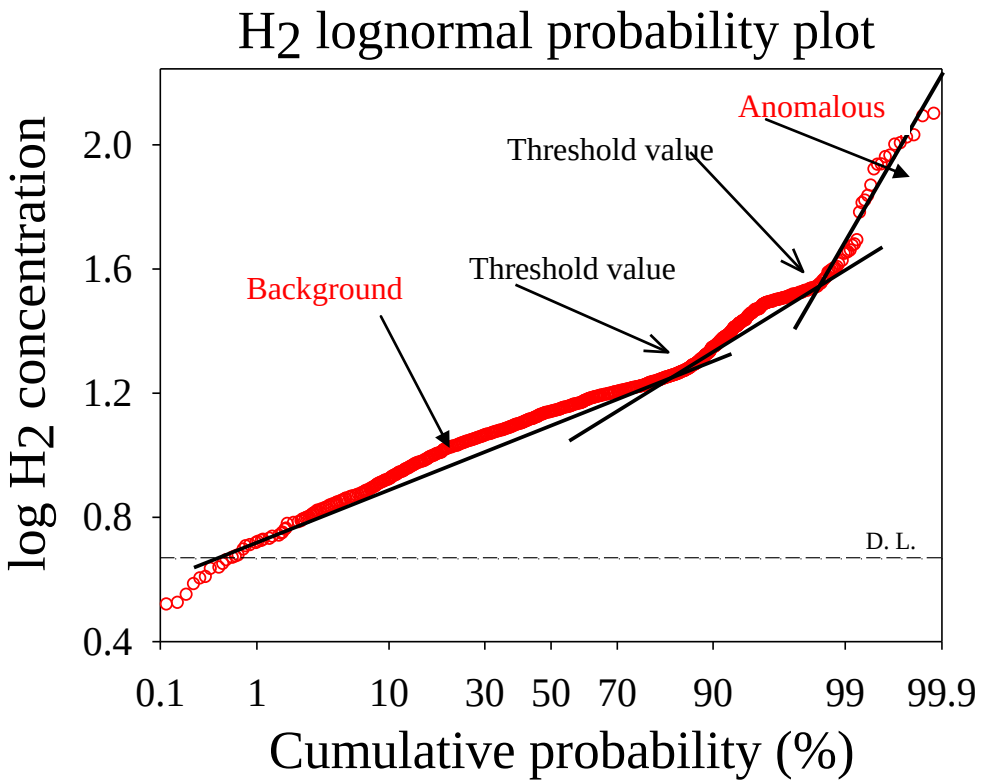

Figure 18 Lognormal probability plot of the H_2 concentration data measured at BLV site. The Ordinate axis shows the logarithm of the H_2 concentration value, while the horizontal axis has probability scale type. Above the detection limit of the H_2 sensor, the H_2 concentration data have polymodal distribution. The highest group (anomalous population) having concentration values above 40 ppm vol. represents the 1% of all the measurement, while the lower group (background population) has concentration below 15 ppm vol. representing about 89% of the measurements. The third group represents the 9% of the measurements data set having intermediate value between anomalous and background populations. About the 1% of the measurements show concentration value below the detection limit of the H_2 sensor. D.L. indicates the detection limit of the H_2 sensor.

In order to distinguish the anomalous values of the H_2 concentrations, the statistical-graphical analysis has been performed by reporting the data into the cumulative probability plot (Figure 18). As mentioned before, according to Sinclair (1974) the data sets having polymodal distributions can be sorted according to their appropriate density distribution, since each group exhibits straight line distribution on the probability plot.

Three populations of H_2 concentration values representing about 99% of all the measurements data set can be identified above the typical detection limit of the Rew Power Fuel Cell-based H_2 sensor, while the residual 1% represents values below the detection limit (~ 5 ppm vol).

The group of highest values (anomalous population) represents about 1% of all the data set having H_2 concentration above 40 ppm vol. The large part of the measurements (about the 89 %) represents the background population having the average value of 15 ppm vol.

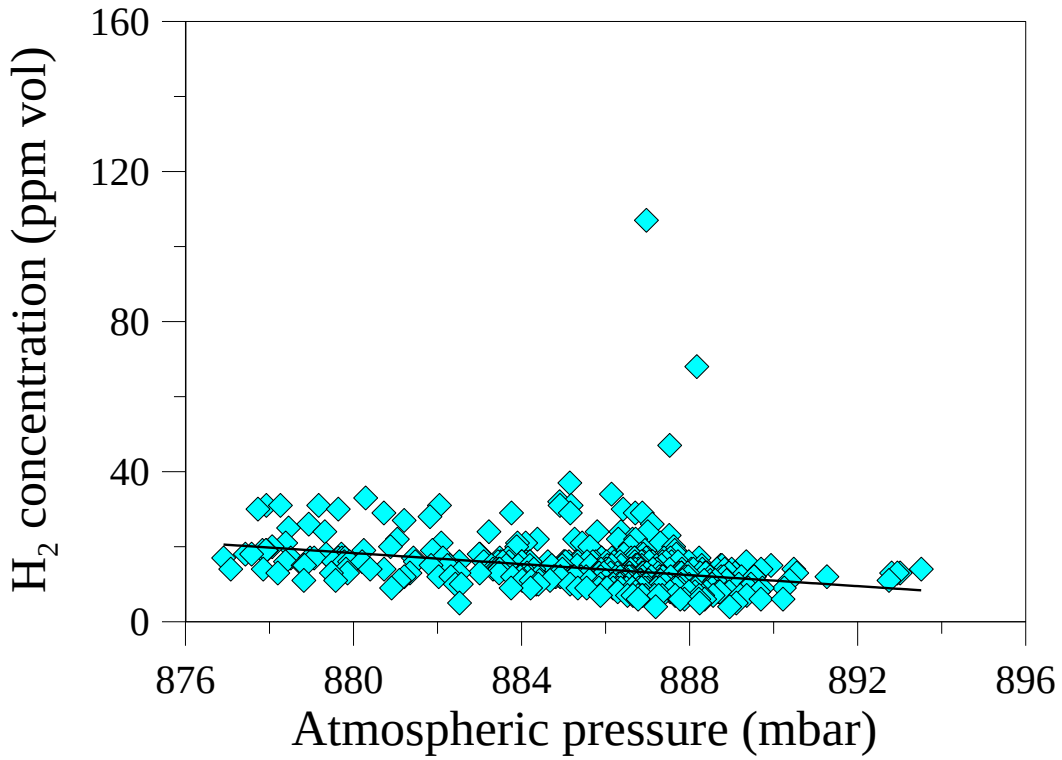

Figure 19 Correlation diagram of H_2 concentration measurements vs. the atmospheric pressure (obtained from the European Centre for Medium-Range Weather Forecasts MARS archive under license from the Italian Air Force Meteorological Service).

A third group of measurements having intermediate "threshold" values between the anomalous and background populations, represents about the 9% of the measurements. The comparison between the data classification obtained from the probability plot and the time series of the H_2 concentration (Figure 18) suggests that anomalous H_2 release occurred mainly during the second half of August 2010 from the BLV fumarolic field.

The probability plot allows a detailed analysis of the distribution of the H_2 concentration data. According to the acquisition frequency of the atmospheric pressure data, the H_2 concentration measurements have been resampled with 6 hour frequency. Both parameters have been compared in the correlation diagram showed in Figure 19. The figure shows that a large part of the background values has sub-parallel distribution in comparison to the pressure axis and negative slope of the fitting line. This distribution, which has low value of the coefficient of correlation (R^2 = 0.179) together with the negative Pearson's coefficient (r = - 0.416), suggests that the H_2 concentration measurements have a slight inverse relationship with the atmospheric pressure.

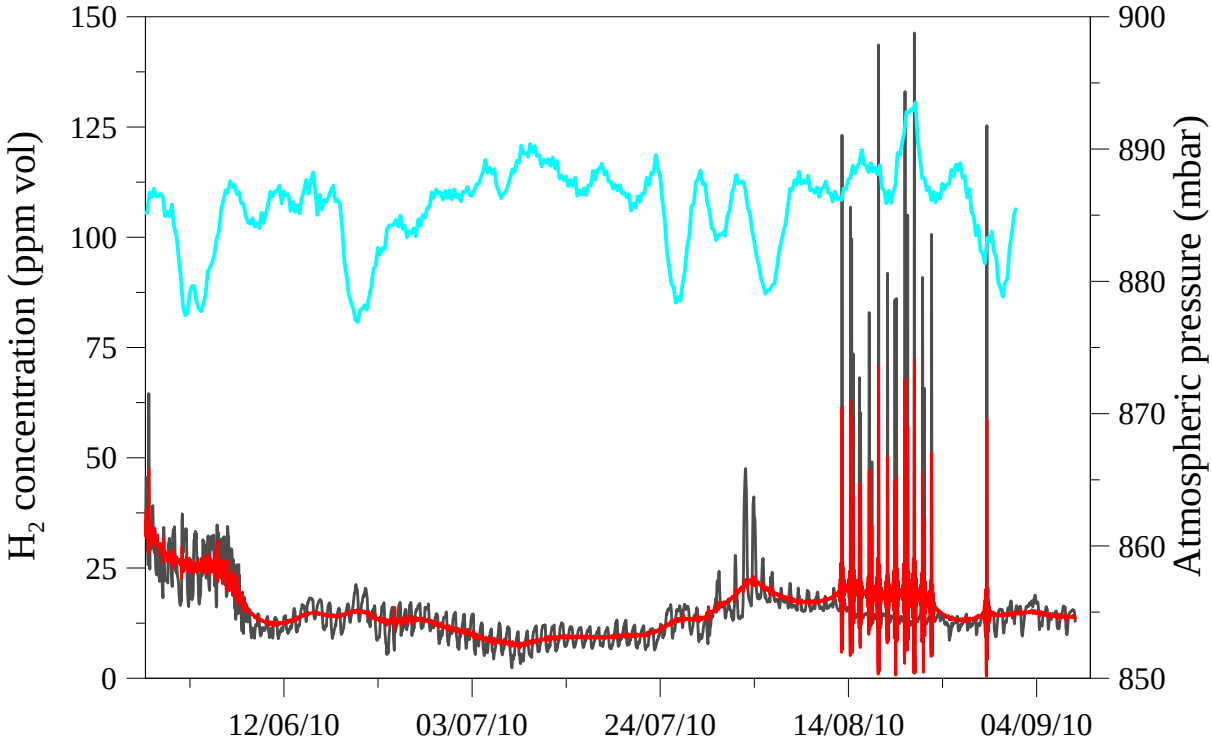

Figure 20 Time series of H_2 concentration (red line – filtered data) and atmospheric pressure (light blue line). The grey line shows the H_2 concentration unprocessed data.

The H_2 concentration measurements hourly acquired by the H_2-CO_2 system have been processed according to the results obtained by the comparison with the atmospheric pressure and filtered from the interferences of working conditions. The data processing has been done in MatLab environment using the Signal Processing tool (SPtool), by considering the unprocessed data of the time series as digital signals and identifying the frequency variations through the Fast Fourier Transform (FFT) analysis. Two distinct digital filter (Bandstop direct form II filter structure, second order sections stable filter, IIR Butterworth designing method and Lowpass direct form II filter structure, first order section stable filter, IIR Butterworth designing method) have been designed and applied to the unprocessed data in order to remove the variations of the H_2 concentration having daily frequency and the variations having frequencies higher than 3 hours. In this way the non-periodic variations are better detectable and could be more directly correlated with the changes of the volcanic activity.

The time series reported in Figure 20 shows the temporal comparison between the filtered H_2 concentration measurements and the atmospheric pressure data. The monitored parameter (the H_2 concentration) shows small variations around the average values of 15 ppm vol., despite the changes occurring in the atmospheric pressure, until the end of July. Pressure variations of comparable amplitude (about 10 mbar) occurred also throughout the following period, when

several variations of the concentration have been measured. Since the amplitude of the H_2 variations were larger than the typical error affecting the sensor, they can be hardly attributed to the cross sensitivities effects of the atmospheric pressure variations.

CO_2 flux at Belvedere – Mt. Etna

The Figure 21 shows in detail the time series of the CO_2 flux measurements. The data shows that the average CO_2 flux measured until the 8 September 2010 was about 900 $gm^{-2}d^{-1}$ with standard deviations of 104 $gm^{-2}d^{-1}$ and ranging from 585 to 1200 $gm^{-2}d^{-1}$.

Since the installation of the H_2-CO_2 system, the CO_2 flux showed a general enhancing trend interrupted by several flux rate peaks persisting a few days on average. The trend of increase persisted until the late week of July, reaching the value of 1000 $gm^{-2}d^{-1}$. The following period has been characterized by moderate variations close to the average value of 900 $gm^{-2}d^{-1}$.

The selection of the measurements aimed to distinguish the anomalous and background values of the CO_2 flux emitted from the BLV fumarolic field has been performed through the statistical-graphical analysis reported in Figure 22.

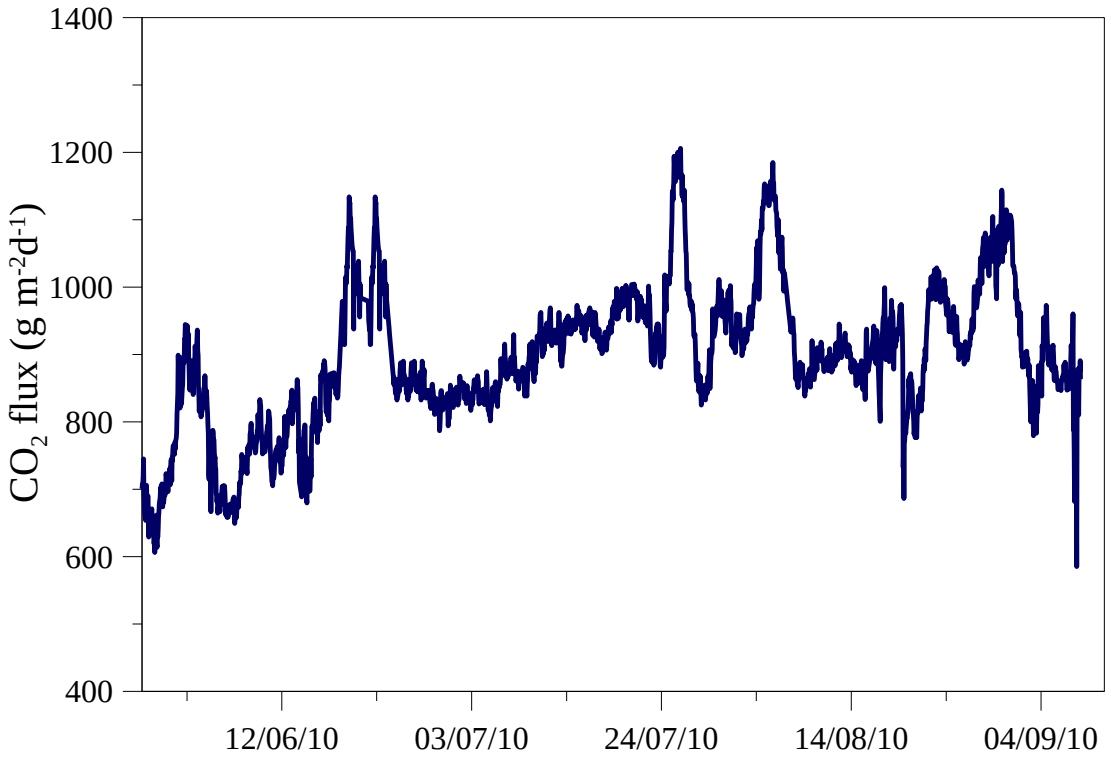

Figure 21 Time series showing the CO_2 flux measurements performed at Belvedere since the 27 May 2010 until the 8 September 2010.

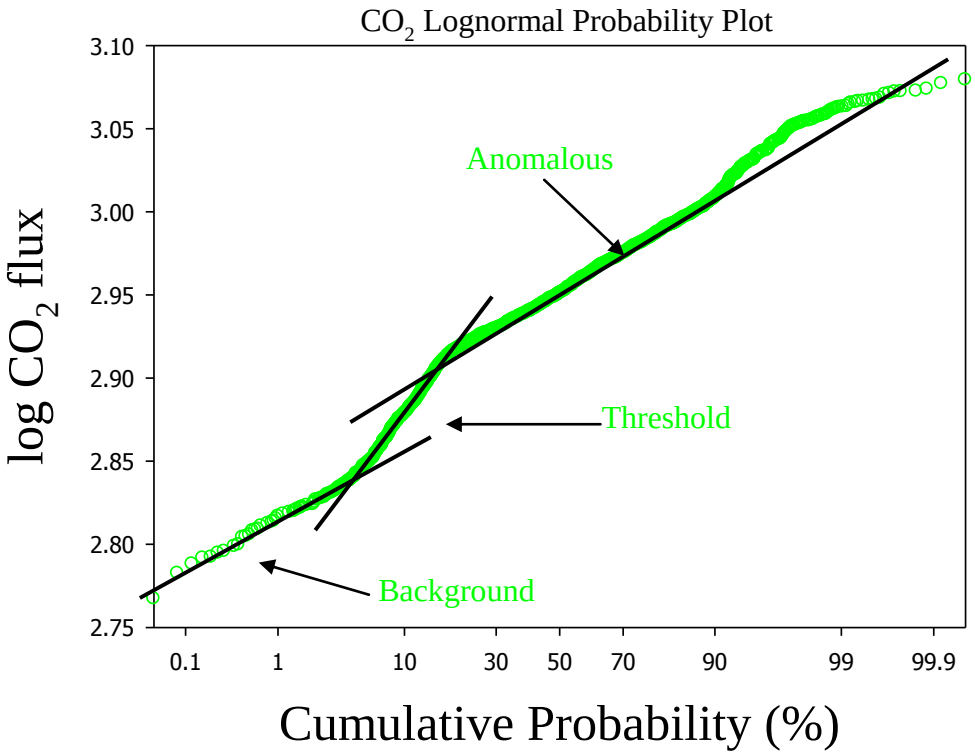

Figure 22 Lognormal probability plot of the CO_2 flux measurements from BLV site. The Ordinate axis shows the logarithm of the CO_2 flux value, while the horizontal axis has probability scale type. The higher group represents the 80% of all the measurements, while the lower group showing flux values below 692 $gm^{-2}d^{-1}$ represents about 7% of the measurements. The third group representing the 13% of the measurements shows threshold values between both populations.

The probability plot is able to separate the data set of the measurements in the range of the lower values from the higher one according to the linearity of the distribution within the plot.

Figure 22 shows three main data populations. The lower population represents about the 5% of all data set having the average value of 692 $gm^{-2}d^{-1}$ corresponding to the percentile of 1%. About the 80% of the measurements represents the highest population having the average value of 900 $gm^{-2}d^{-1}$ corresponding to the percentile of 75%.

The data distribution suggests that the time average of the CO_2 flux emitted from the BLV fumarolic field, at least throughout the observation period, is well represented by the average CO_2 flux value of the highest population. The third population of threshold between the highest and the lower ones can be recognized in the CO_2 flux data set and represents about all the remaining 19% of the measurements.

The comparison between the statistical-graphical data analysis and the time series suggests that the BLV fumarolic field showed fairly constant the typical value of the CO_2 fluxes since the second mid-July. The relative higher CO_2 flux has been reached after an increasing trend observed since the installation of the H_2-CO_2 system.

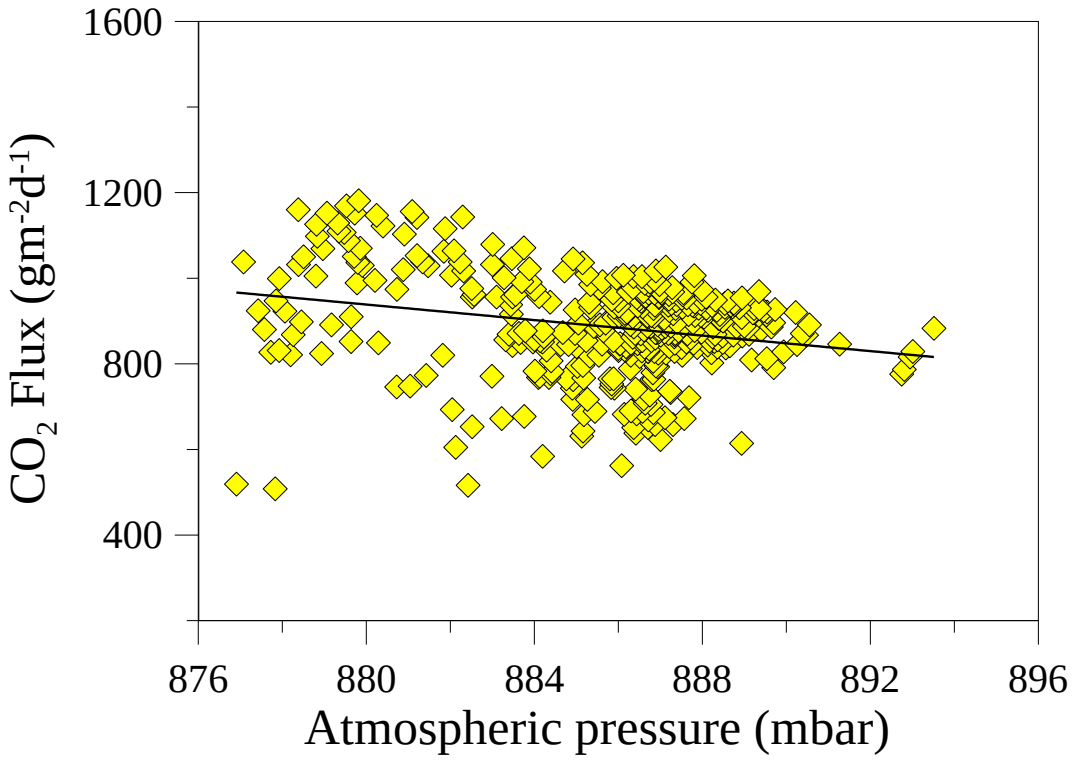

Figure 23 Correlation diagram between the CO_2 flux measurements and the atmospheric pressure.

In order to both evaluate and correct the interpretations of soil gas anomalies by the effects of the variations of the working conditions, the comparison between the CO_2 flux and the atmospheric pressure has been performed. A selection of the CO_2 flux measurements has been done according to the availability of the atmospheric pressure data and the correlation diagram between both parameters was shown in Figure 23

The CO_2 flux data have Pearson's coefficient r = -0.416 in comparison to the atmospheric pressure and low value of the coefficient of correlation (R^2 = 0.173) of the fitting line.

This distribution suggests that the variations of the CO_2 flux could be affected by interferences with the variations of the atmospheric pressure. Since both parameters shows fairly similar relationship, the large drops in the atmospheric pressure can produce pumping effect on the soil gases resulting in false anomalies in the time series of the CO_2 flux parameters. In the same way, the large increases of atmospheric pressure can hide the actual increases of the CO_2 flux emitted from the fumarolic field.

The CO_2 flux data hourly acquired by the H_2-CO_2 system have been processed according to the results obtained by the comparison with the atmospheric pressure and filtered from the interferences of working conditions in MatLab environment, using the Signal Processing tool (SPtool).

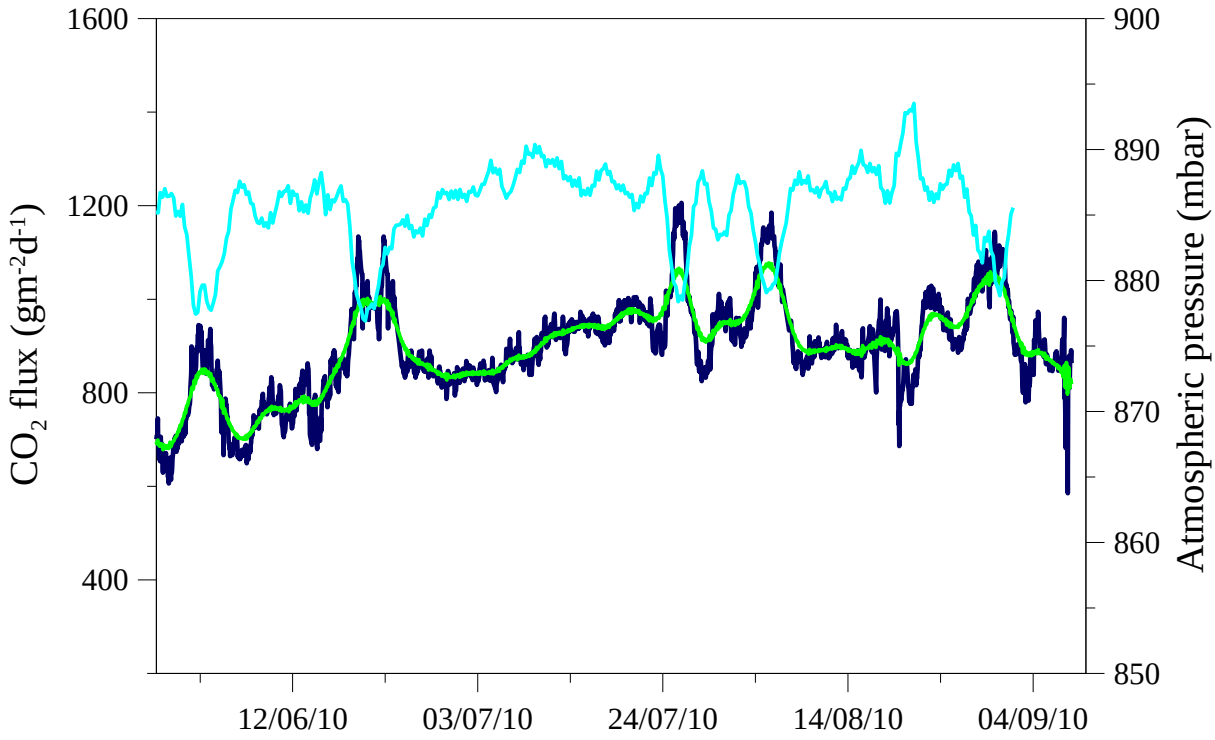

Figure 24 Time series of CO_2 fluxes (green line) and atmospheric pressure (light blue line).

The data processing has been done using both digital filters designed and applied also to the H_2 concentration unprocessed data (Bandstop direct form II filter structure, second order sections stable filter, IIR Butterworth designing method and Lowpass direct form II filter structure, first order section stable filter, IIR Butterworth designing method) in order to remove the variations having daily frequencies and the higher than 3 hours ones. The time series of the filtered CO_2 flux and the atmospheric pressure are reported in Figure 24.

As can be seen from the Figure 24, the largest atmospheric pressure variations have been in the order of 10 mbar. The temporal comparison between the CO_2 flux time series with the atmospheric pressure shows that the large increasing peaks affecting the trend, having the average amplitude of about 100 g m^{-2} d^{-1}, were synchronous with the larger atmospheric pressure drops.

Comparison between the monitored parameters and the volcanic activity

The selection of the measurements performed trough the probability plot allows a more detailed analysis of the data set aimed to compare the distribution of the H_2 concentration data according to the CO_2 flux ones. The H_2 data have been divided in background and anomalous populations and separately compared with the CO_2 flux. The Figure 25 shows the correlation diagram between the H_2 concentration and the CO_2 flux.

The H_2 background has negative Pearson's coefficient ($r = - 0.248$) and low coefficient of correlation ($R^2 = 0.062$), while the Pearson's coefficient and the coefficient of correlation for anomalous population is $r = 0.187$.

The distribution of the data set showed in Figure 25 suggests that two distinct behaviours can be identified from the comparison of the H_2 and the CO_2 signals. The H_2 concentration of the gas emitted from BLV fumarolic field are independent in comparison to the CO_2 flux. Otherwise, they can show reciprocal inverse relationship and the anomalous degassing periods can be characterized by variations of both parameters having opposite sign.

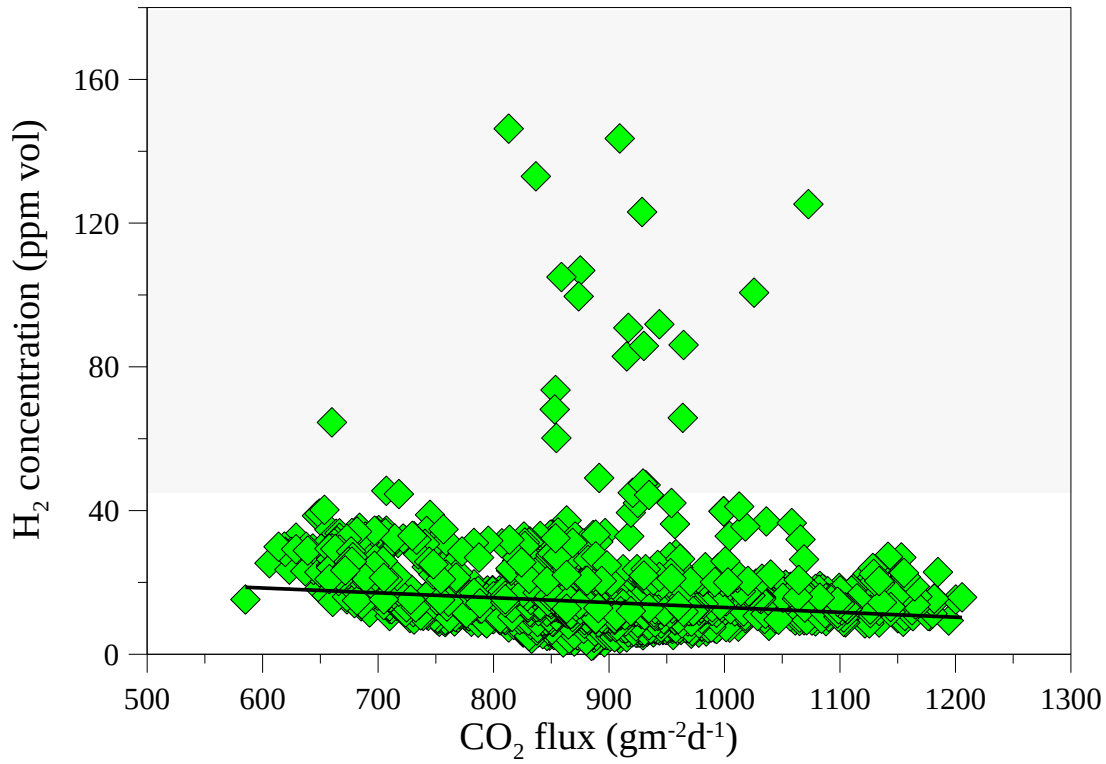

Figure 25 Correlation diagram between the H_2 concentration and the CO_2 flux measurements performed at BLV site. The whole dataset suggest low correlation between both parameters.

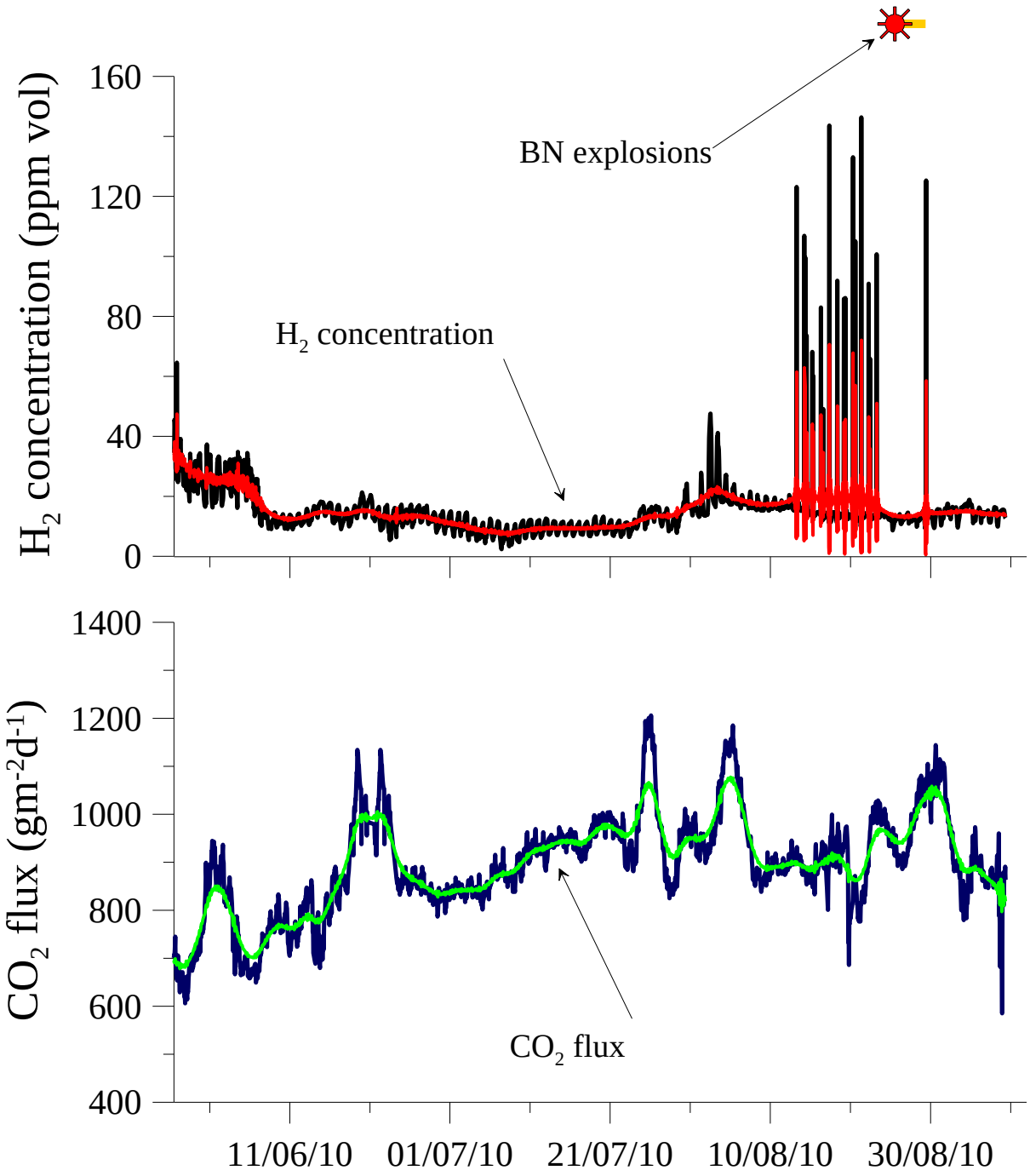

Figure 26 Time series of the H_2 concentration (red line) and CO_2 flux measurements (green line) performed at Belvedere site (Mount Etna volcano) and the main volcanic activity occurred since the 27 May 2010 until the 8 September 2010. The unprocessed data are reported on the background.

The main goal of the experience performed at Belvedere was the study of the relationships between the variations of both mass output and chemical composition of the gas emitted from the fumarolic field and the volcanic activity occurring on Mount Etna.

The figure 26 shows the time series of both the monitored parameters and the main volcanic activity recorded from the 27 May to the 8 September 2010. As can be seen from the figure,

the H_2 concentration within the gases emitted from the fumaroles showed decreasing trend since the first week of June. Throughout this period the H_2 concentration changed from more than 40 ppm vol. to about 10 ppm vol. fluctuating within the range of 20 ppm vol. with frequency of a few days. At the same time, the CO_2 flux increases from May to the end of July. Since the first weeks of June until the end of July, the H_2 concentration remained close to the average value of the background, slightly changing within a few ppm vol.

According to the reports issued by the INGV, during this period Mount Etna has been characterized by passive degassing activity, having variable rate between the different craters. Besides the pressurized gas emission persisting a few minutes occurred the 5 July 2010 from BN crater, the volcanic activity has been characterized by pulsating emissions of dense vapour, mainly from the pit crater of the base of SEC cone. The passive degassing activity continued by showing almost unchanged features until the end of the month.

The last day of July, both monitored parameters showed significant changes in their general trends. The H_2 doubled the background concentration from 10 ppm vol. to about 20 ppm vol. maintaining this higher background almost unchanged throughout all the following period. From the 13 August 2010, sharp differences have been recorded by the H_2 signal due to the sudden increases of the H_2 concentration in the gases released from the BLV fumarolic fields. Each H_2 concentration increase persisted a few hours producing the sudden variations of the H_2 signal. The increases are expressed by the peaks showed in the H_2 concentration time series (see Figure 26). Two following peaks are divided by a period of a few hours, during which background values of the H_2 concentration has been measured within the gas mixture. The peaks in the H_2 signal have been recorded with high frequency until the 23 August 2010. The last one occurred the 29 August 2010, after 6 days through which the H_2 goes back to the background concentration.

Interesting features have been observed also by the CO_2 flux. The enhancing trend recorded until the end of June stopped and the CO_2 flux persisted until mid-August, having constant average value of 800 $gm^{-2}d^{-1}$. A few days behind the change in the H_2 concentration of the 13 August, a renewed enhancing trend can be identified in the CO_2 fluxes. The Figure 26 shows that the maximum of the enhancing trend can be placed between the 27 and the 31 of August, after which the CO_2 fluxes showed a sudden decreasing trend. As reported before, the enhancing trend of the CO_2 flux was affected by two sharp peaks synchronous with two variations of atmospheric pressure at which they can be attributed.

Throughout the month of August 2010 Etna volcano showed increasing signs of unrest (i. e. deep-sealed explosions without emission of new eruptive products). Nevertheless, starting

from the last week of August 2010, explosive activity associated with ash emissions occurred at BN crater. The activity started the 13.09 h on 25 August producing a dark grey column rising about 1-2 km above the summit of Mount Etna. The column contained hot gases and fine-grained ashes having lithic nature in the large part with a fraction of fresh juvenile material. Further explosions, internal collapse and ash emissions occurred from the BN crater throughout the following days.

Geochemical and geophysical investigations (Aiuppa et al., 2010; Marchetti et al., 2009) have previously pointed out a geometrical connection between the Etna's central crater (Bocca Nuova and Voragine) and the South-East Crater, representing a geometrically secondary branch of the Etna's shallow conduit system. According to Marchetti et al. (2009) this geometrical connection involves a switching behaviour mainly controlled by the change of gas/magma flux rate within the shallow conduit system. In particular, the central craters represent the preferential pathway for usual degassing activity, while the increasing rate of gas or magma supply above a threshold activates the SE crater degassing (Marchetti et al., 2009). Aiuppa et al. (2010) integrated geochemical (CO_2/SO_2 ratio plume) and geophysical data (GPS, tremor source and long-period events) and evaluated between 1 and 2.8 km a.s.l. below the central craters the shallow magma storage before the SEC paroxysmal activity during 2007-2008. They recorded the decrease of CO_2/SO_2 ratio associated to the upward and eastward migration of source location of seismic tremor. These evidences indicated the magma migration from the storage zone below the central conduit toward the south-east crater a few hours or days before the SEC paroxysmal activities, according to the switching behaviour of the branched shallow conduit system activated by the structural control exerted from the eastern sector of Mount Etna (Aiuppa et al., 2010).

Further hints on the relationships between the degassing activity and the dynamics involving the shallow volcanic conduits system can be drawn from the chronological correlation of the H_2 peaks data and the explosive activity occurred at BN crater during the last week of August 2010 (data obtained from INGV surveillance weekly bulletins).

In detail, within the time series (Figure 26) can be identified eighteen H_2 anomalous peaks correlated in time with the eighteen mains explosions. Therefore, the time interval between the first H_2 peak and the explosion occurred the 25 august 2010 has been computed. Likewise, each following H_2 peaks has been linked with the subsequent explosions, obtaining a series of eighteen *delay* data.

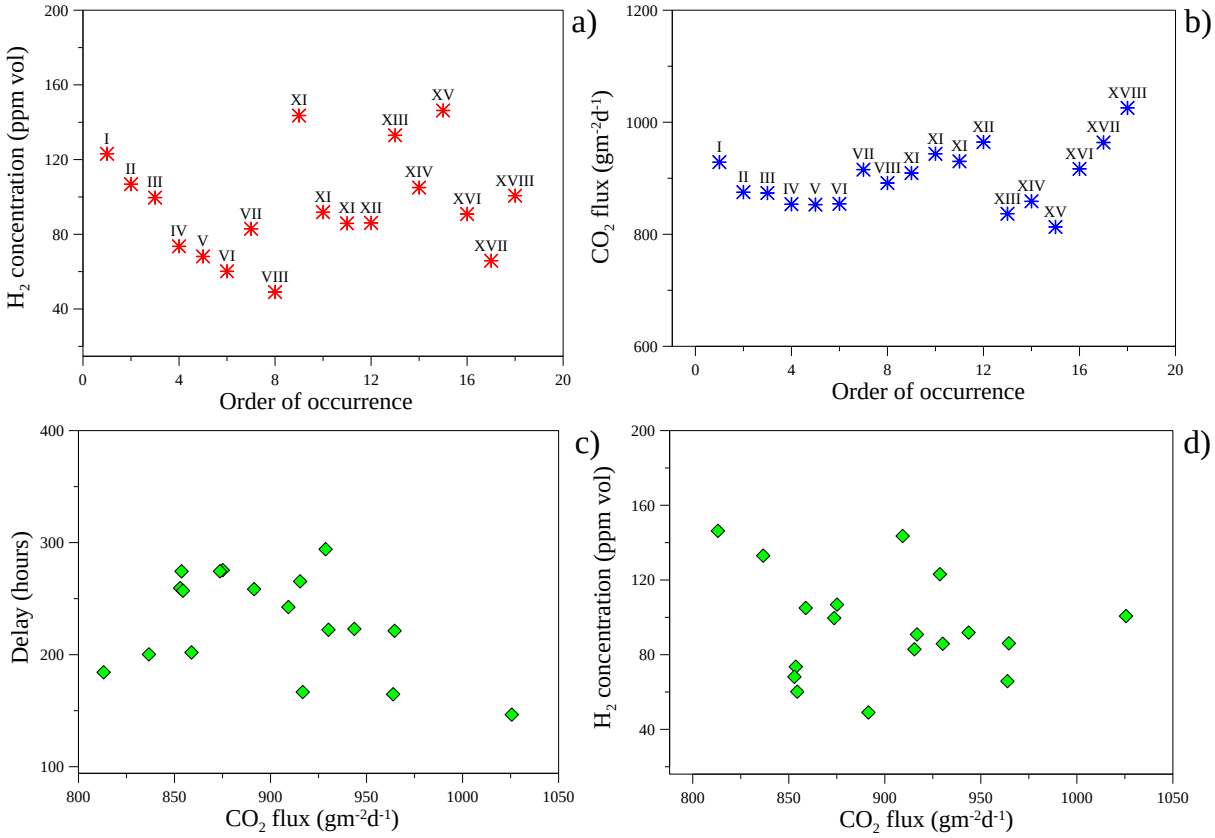

Figure 27 Relationships between the H_2 peaks data and the order of occurrence of the main explosions at BN crater. a) H_2 peak concentration. b) CO_2 flux synchronous to the H_2 peak. c) Dependence of the delay from CO_2 flux data. d) H_2 peak concentration in comparison to the CO_2 flux.

Figure 27-a shows the maximum H_2 concentration measured at the H_2 peaks without systematic temporal variations, while the Figure 27-b shows that the simultaneous CO_2 fluxes have been fairly steady at the average of 900 $gm^{-2}d^{-1}$, suggesting that the measured delays are fairly independent from the CO_2 flux (Figure 27-c).

Moreover, the peak values of H_2 concentration and the simultaneous CO_2 flux data shows the typical independence (Figure 27-d).

The most important outcome of this correlation consists on the average delay between the H_2 peaks and the explosive activity. Indeed, it has been computed the delay of 230 hours (standard deviation 49 hours), declining systematically from 294 to 147 from the first to the last explosive event (Figure 28).

Since the time interval between the H_2 anomalous release and the time-correlated explosive event may be somewhat revealing of the gas reservoir depth, the decreasing trend of the delay suggests a progressive decrease of the distance between the degassing source and the point of measurement.

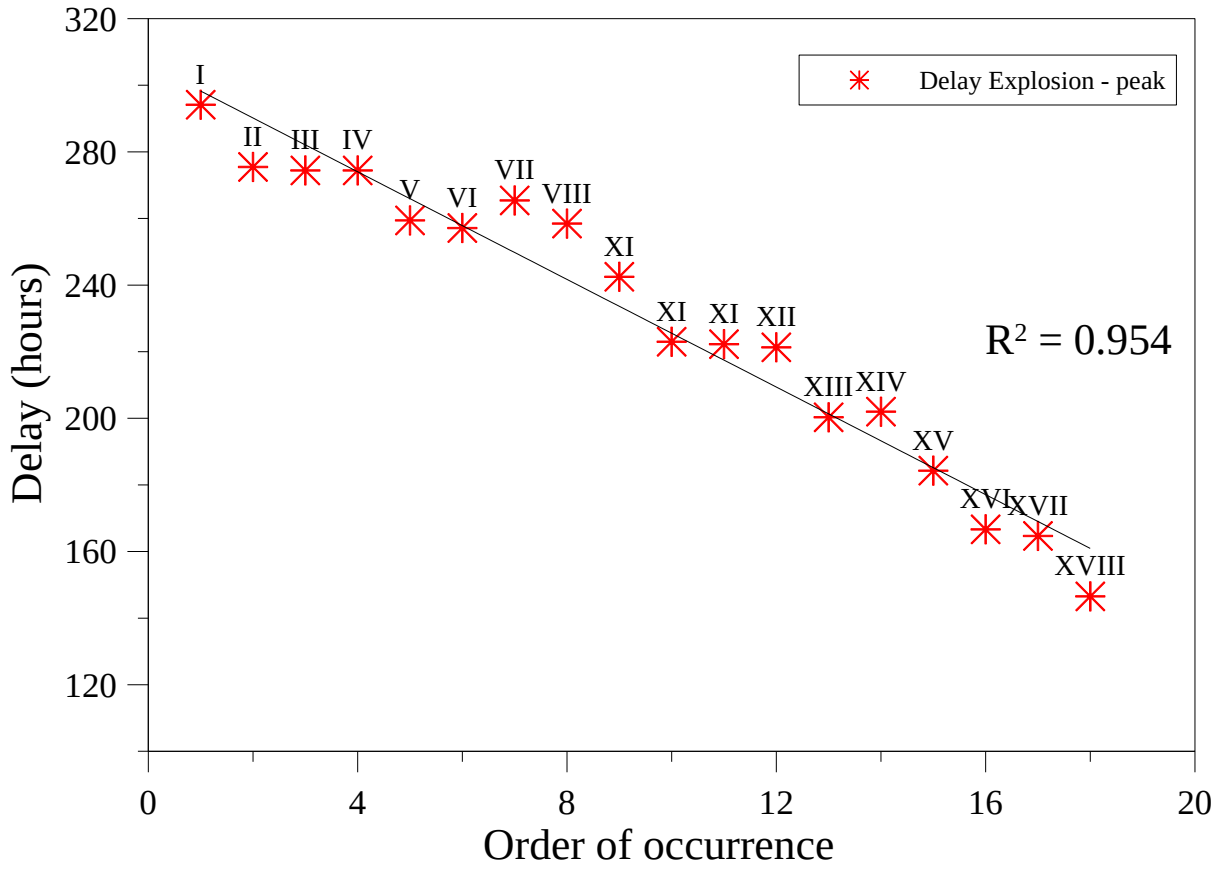

Figure 28 Delay between the main explosions and H_2 peaks reported according to chronological occurrence.

A greater number of H_2-CO_2 systems at the summit area of the volcano could provide more accurate indications on the effective uprising of fresh and relatively undegassed magma batch. Moreover, the independence of the delay from the CO_2 flux data represents further evidence that the impulsive H_2 peaks may result from impulsive H_2 releases from the magma batch upon its ascent toward the surface.

In summary, since the 27 May to the 8 September 2010 passive degassing and explosions from the summit crater associated to ash emissions have been observed at Mount Etna volcano. The passive degassing prevailed throughout the months of June and July by showing variable intensity, while the crater explosions occurred during the last weeks of August. Throughout these periods, sharp differences have been shown from the CO_2 flux and the H_2 concentration measurements. Until the end of July, the H_2 persisted with limited variations in the typical range of the H_2 concentration measured at BLV site. At the same time, the CO_2 flux showed slightly increasing trends persisting at higher relative values until mid-August.

A few days before the unrest occurred from the BN crater, a sharp change has been recorded in the H_2 signal due to several recurring changes of the H_2 concentration in the fumarolic

emissions. The magnitude of the H_2 concentration variations are an average one order of magnitude larger than the background value of the H_2 concentration typical of the BLV emissions. Through the same period, the CO_2 flux undergoes a sudden increase culminating between the 27 and the 31 August. After the last significant explosion occurred from BN (the 09:31 h on 29 August), the H_2 concentration showed the last larger variation (11:00 h on 29 August) and a sudden decreasing trend started in the CO_2 fluxes.

Continuous monitoring of H_2-CO_2 at Stromboli

An H_2-CO_2 system has been installed on Stromboli volcano from May 2009. An improvement of the sensing equipments has been made in order to monitor the H_2 concentration and the CO_2 flux from two different sampling points. The main goal of the continuous monitoring experience on Stromboli consists on the investigation of the relationships between the degassing from the fumarolic field of the top area and the typical volcanic activity.

In the following part of the chapter have been shown the results of the measurement performed from the 13 May 2009 to the 5 October 2010.

Stromboli background

Stromboli is the northernmost and recent island of the Aeolian archipelago (Italy) in the south eastern side of Tyrrhenian Sea. The island is the emerging part of a larger volcanic edifice reaching the elevation of 918 m a.s.l at Pizzo sopra la Fossa area from the base placed 2000 m b.s.l. The island of Stromboli was built through seven different phases (Paleostromboli -I, -II and -III, Scari, Vancori, Neostromboli and Recent Stromboli) characterized by long period of magma emissions leading to the growth of the stratovolcano, interrupted by lateral collapses affecting the western side of the volcanic cone.

The edifice is composed by different volcanic products exhibiting a variety of petrologic features ranging from early erupted calc-alkaline (c. 160 ka) to shoshonitic composition magmas (Landi et al., 2006; Francalanci et al., 2004; Francalanci et al., 1989; Hornig-Kjarsgaard et al., 1993).

The island of Stromboli is oriented along the regional NE-SW structural trend affecting the south eastern side of Tyrrhenian Sea and representing the eastern branch of the Aeolian-Tindari-Letoianni fault system (Ghisetti, 1979). Locally, the regional NE-SW fault system crossing the island represents an important discontinuity periodically injected from depth by the magma rising toward surface (Mattia et al., 2008).

Stromboli is worldwide one of the most active basaltic volcanoes exhibiting the typical persistent activity that remained without significant variations over the past 1400-1800 years (Rosi et al. 2000).

The recent activity of Stromboli takes place from three main vents open inside the crater terrace area placed at about 750 m a.s.l. within the Sciara del Fuoco, a horse-shoe depression resulting from large sector collapses affecting the northwestern flank of the volcano.

The typical persistent activity of Stromboli, for which the volcano is famous as "the lighthouse of the Mediterranean", consists of mild explosions sustained for a few seconds (4-30 s) occurring every 10-20 minutes.

The products of strombolian explosions range from ash-dominated, through molten lava fragments to the incandescent partly degassed crystal-rich scoriae and bombs thrown up to hundred meters above the crater area. As a rule, the products fall within the crater terrace, reaching unusually the "Pizzo Sopra la Fossa" area. Strombolian explosions are associated to active degassing (puffing) originated from high frequency gas bursts (1-2 s) and passive degassing from the crater area. It is worth to note that the routine strombolian activity is an average behavior, being highly variable on timescale of hours or days. A few examples of such typical strombolian activities attracting thousands people to climb on top of the volcano are shown in Figure 29.

a)

b)

c)

Figure 29 The typical activity of Stromboli volcano. a) Strombolian explosion from the north crater typically molten lava containing. b) Strombolian explosion ash-dominated from south crater. The "puffing" activity occurring at central crater.

The magma overflow from the active craters typically produces effusive activity involving the crater terrace as well as the upper part of the Sciara del Fuoco for a few hours or days. On a larger timescale, effusive eruptions have also occurred at Stromboli, producing lava flows onto the Sciara del Fuoco, fast moving toward the sea. Several lava effusions, on average every four years, occurred at Stromboli since the 1888 (Aiuppa et al., 2010) and the largest ones originated from the vents opened a few hundred meters below the craters area. During last decades two lava effusions occurred from the 28 December 2002 to the 22 July 2003 and from the 27 February to 2 April 2007. It is worth nothing that, several millions of cubic meter of lava were emitted during the effusive phase with a rate of mass flux higher than the rate sustaining routine activity (Landi et al., 2009).

The routine activity of Stromboli, as well as the effusive phases, can be interrupted by more energetic explosive events. Such more powerful blasts, occurring on average 0.5-3 times per years are usually called major explosions, throwing meter-sized ballistic blocks together with lapilli several hundred meters away from the crater area. The power and the unpredictability features make the major explosions among the most hazardous activities of Stromboli volcano, although they are less energetic than the paroxysms.

The paroxysms are the most powerful eruptive activity exhibited by Stromboli, having the potential of affecting the inhabited areas of the island. The higher magma discharge rate characterizing the paroxysms led to the formation of thermal convective plumes of gas and ash, which rise up to 10 km above the summit of the volcano (Ponte, 1919). Since the 1874 the frequency of paroxysm crises at Stromboli is of one event every 4-5 years (Barberi et al., 1993). The last two paroxysmal explosions at Stromboli were on 5 April 2003 and on 15 March 2007.

According to Aiuppa et al. (2010), paroxysms are impulsive events consisting of synchronous explosions from different craters associated with the emission of vertical jets of gas and pyroclasts, evolving in short-lived convective eruptive columns. Paroxysms are characterized by the simultaneous emission of two magma types having slight different bulk composition, but contrasting textures and composition of the glass matrix (Bertagnini et al., 2008; Francalanci et al., 2004; Landi et al., 2009; Metrich et al., 2001; Pichavant et al., 2009). The first magma type is the black crystal-rich scoriae (often indicated in literature as high-porfiricity magma, HP) representing the partly degassed shoshonitic basalt filling the shallower plumbing system of the volcano and sustaining the routine strombolian activity. The second type is a deeper (7-10 km of the source according to Métrich et al., 2010) volatile-rich crystal-poor magma type emitted only during the paroxysm (Rosi et al., 2000; Métrich et

al., 2001, Francalanci et al., 2004; Bertagnini et al., 2008) as highly vesicular yellowish pumice (also called golden pumice).

Among the typical activity, the CO_2 flux from the soil represents a common phenomenon recorded on Stromboli volcano. Large amounts of CO_2-dominated emissions have been noticed on Stromboli by several researchers (Carapezza et al., 2009; Cigolini et al., 2009; Carapezza and Federico, 2002; Finizola et al., 2003, Finizola et al., 2002; Capasso and Carapezza, 1994) along the NE-SW trending structure affecting the island. According to Carapezza and Federico (2000) about the 10% of the total CO_2 output from Stromboli were represented by the diffuse degassing from the soil of the upper part of the volcanic edifice.

Sampling site of the H_2-CO_2 permanent monitoring device

Since the 13 May 2009 a new prototype of the H_2-CO_2 system has been installed on the summit area of Stromboli volcano. The main development concerned the sensor equipments, consisting of the H_2 RewPower Fuel Cell-based sensor to measure the H_2 concentration, two Gascard II sensors (both having the range 0-100 vol. %) to measure simultaneously the CO_2 flux from two different sampling sites according to the dynamic concentration method and the STS ATM/T pressure transducer for measuring the atmospheric pressure. Since the 27 April 2010 the station has been equipped also with a thermo-resistor PT-100 to measure the case temperature.

Before the installation, a detailed survey of the soil gases has been performed on the summit area of Stromboli volcano leading to the identification of the place showing the best condition to arrange the sampling points of the H_2-CO_2 system. The survey has been performed close to the Pizzo sopra la Fossa area moving away some tens of meters from the summit area, along NW direction. Several potential appropriate sampling points have been recognized through the portable H_2 device RewPower fuel cell-based described in detail in the previous chapter and the Infra Red Gas Analyzer (IRGA) Gascard II-based portable spectrophotometer. Moreover, several dry gas samples have been collected from the more interesting points by inserting a probe up to 50 cm within the soil, stored within glass sample-holder and analyzed through laboratory gas-chromatographic techniques.

The sampling point of the H_2-CO_2 device has been chosen in agreement with the following criteria:

- from low to moderate CO_2 flux (hereafter named CO_2 L.F.)
- from moderate to high CO_2 flux (hereafter named CO_2 H.F.),
- from moderate to high H_2 concentration.

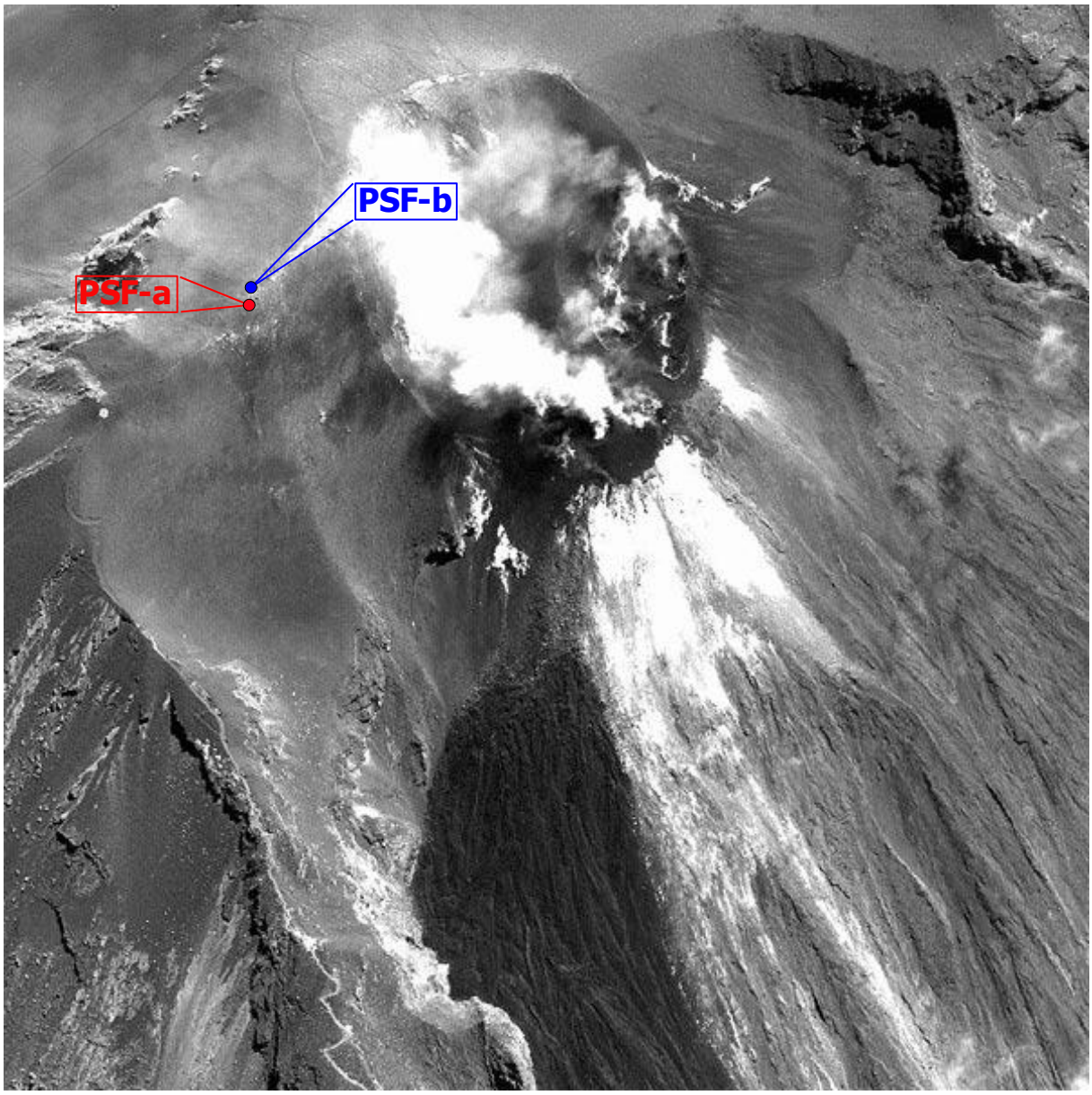

Figure 30 Nasa Aircraft image of the western flank of Stromboli. Both the sampling points are indicated.

The H.F. sampling site (hereafter PSF-a site) has been chosen close to the SC5 fumarole periodically monitored by the INGV-Pa staff (Figure 30).

Both the H_2 concentration and the CO_2 flux (H.F. and L.F.) have been measured from the May 13, 2009. The H_2-CO_2 device is today operating on Stromboli, while measurements reported here cover the period up to the October 5, 2010. The measurements are collected hourly, stored within the solid memory onboard the station and daily radio transmitted toward the INGV-Pa monitoring room.

Results and discussion II

The main goal of the field experiments carried out at Stromboli has been the investigation of the relationships between the variations of the degassing features from the fumarolic field close to the Pizzo sopra la Fossa area (PSF) and the time-changing persistent activity characterizing the volcano.

Data analysis has been performed by sorting both the CO_2 flux and H_2 concentration values between background and anomalous populations on the basis of cumulative probability plot (Sinclair, 1974). The variations of both parameters in the range of anomalous values have been compared with the volcanic activity variations occurring on Stromboli throughout the sixteen months of measurements. At the same time, the correlation analyses were performed to verify the relationships among the monitored parameters, the atmospheric and the working conditions.

Several periodic surveys have been performed at PSF site in order to collect a set of gas samples useful to check the correct operative conditions of the system and test the accuracy of the H_2 concentration measurements. The gases have been collected in glass sample-holders and analysed in laboratory through gas chromatographic techniques in order to identify their compositions. The results of the laboratory analysis are collected in Table 3

Table 3 Chemical analysis obtained through chromatographic techniques of the gas samples collected at PSF site fumarolic field during the surveys. The gas samples were collected through the same probe inserted into the soil and used to perform the measurement with the automatic H_2-CO_2 device and transported toward the INGV-Pa laboratory for the analysis. Each sample consists of ~ 20 cc of fumarolic gases collected with a syringe and inserted within the glass sample-holders.

Date	He (ppm vol.)	H_2 (ppm vol)	O_2 (vol %)	N_2 (vol %)	CO (ppm vol)	CH_4 (ppm vol)	CO_2 (vol %)
12/05/2009	7	301	5.27	21.47	3.9	1.7	72.77
16/06/2009	7	122	5.38	21.33	4.8	1.6	74.33
23/07/2009	7	81	5.41	21.16	4.6	1.5	72.82
27/08/2009	6	87	4.10	15.91	1.2	2.0	79.28
28/10/2009	6	94	4.07	16.19	2.2	1.9	79.84
19/01/2010	5	73	4.10	16.43	1.1	2.1	79.71
25/05/2010	5	97	5.73	22.54	10.7	1.8	71.54
13/07/2010	6	66	5.02	20.27	38.5	4.6	75.39
12/08/2010	5	83	5.70	22.76	12.0	2.6	70.48

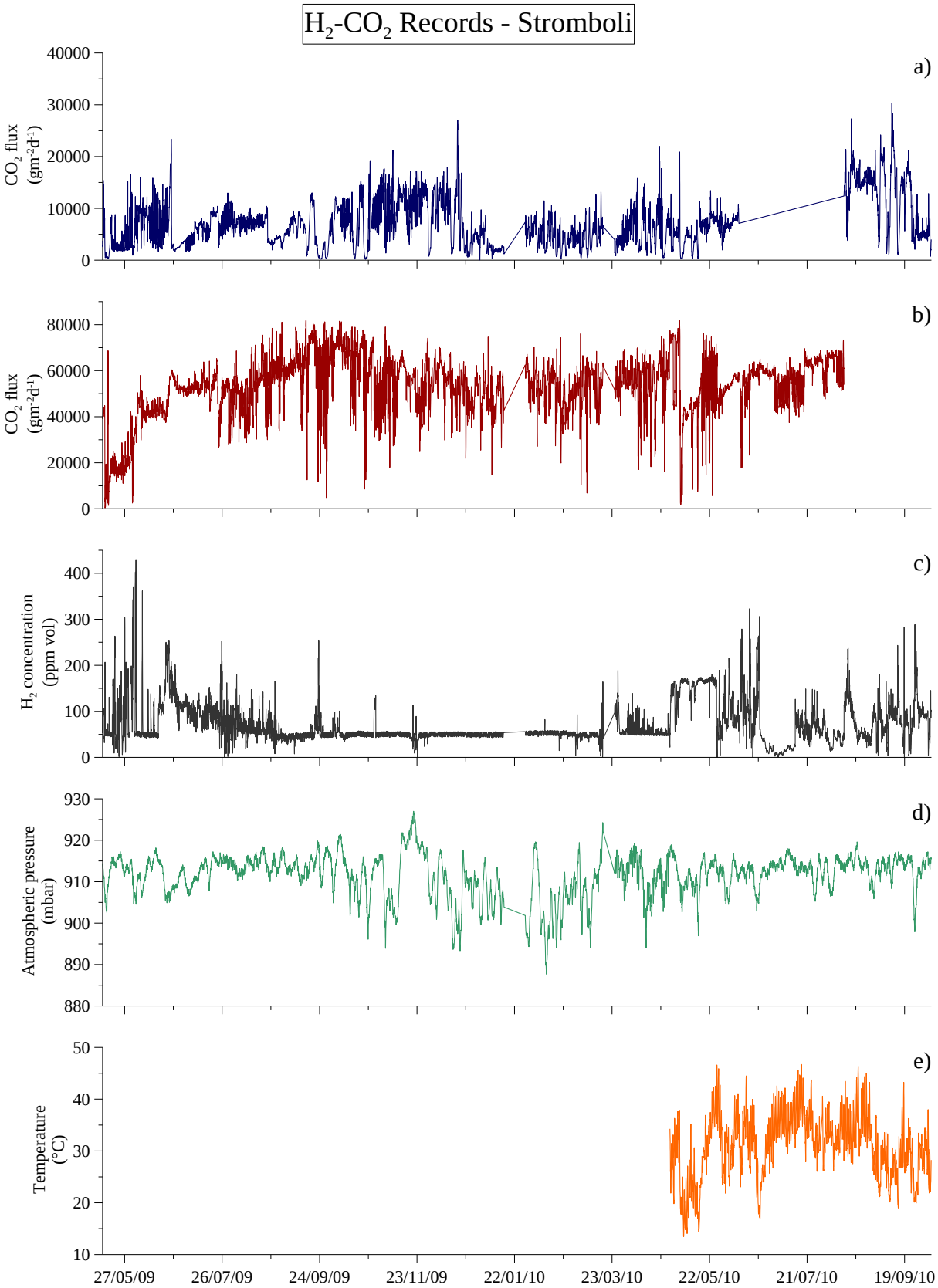

Figure 31 Time series of the measurements performed through the H_2-CO_2 permanent monitoring device at Pizzo sopra la Fossa (henceforth PSF) on Stromboli volcano. a) CO_2 low flux (L.F.) time series, b) CO_2 high flux (H.F.) time series c) H_2 concentration the time series; d) Atmospheric pressure time series, e) Case temperature time series. The data have been hourly acquired from the 13 May to the 5 October 2010.

The measurements performed through the H_2-CO_2 system have been used to investigate the time-changing features of both the chemical composition and the mass output from the fumarolic field of the Stromboli top area. All the measurements of CO_2 flux L.F., CO_2 flux H.F., H_2 concentration, atmospheric pressure and case temperature are shown in figure 31. The figure 31-e) shows the case temperature time series (T-Case) beginning from the 27 April 2010 when the H_2-CO_2 system has been further improved by the temperature sensor. The T-Case monitoring, together with the monitoring of the atmospheric pressure, allows better evaluating the effects of working conditions on the performances of the device. As can be seen from the figure 31-e), the temperature ranged from about 20°C to 45°C according to the average seasonal variations and heat output from the soil.

The time series of atmospheric pressure (Figure 31-d) shows that the main variations affecting the monitoring system are in the range of a few tens of mbar. Beside the direct interferences on the measurement with the H_2-CO_2 device, these variations may produce effects of barometric pumping on the soil gases, in agreement with the variations of the weather conditions. The changeable extent of such interferences can be dependent from the peculiarities of the different sampling site (permeability, exposure in comparison to the wind direction). As will be shown later in this chapter, the main features of these effects can be evaluated trough the correlation between the atmospheric pressure and both the H_2 concentration and CO_2 flux data.

H_2 concentration at Stromboli – PSF-a

Figure 32 shows in detail the time series of the H_2 concentration in the gases emitted from the PSF fumarolic field, measured since the 13 May 2009 to the 5 October 2010. The Figure shows that the H_2 concentration ranged between 0 and 428 ppm vol. reaching the maximum during the month of May 2009. Throughout the observation period, the average H_2 concentration has been 74 ppm vol. having the standard deviation of 45 ppm vol.

The most striking feature showed by the time series is the presence of several peaks sustained for short time interval during which the H_2 concentration increases above the average value mentioned before. These sudden variations have produced the typical saw-teeth trend of the continuous H_2 concentration measurements in the fumarolic emissions.

The red diamonds superimposed on the time series indicate the H_2 concentration measured by chromatographic techniques in the samples collected in the field (see Table 3). The agreement between both types of the measuring method represents a further validation of the good performance of the H_2-CO_2 system.

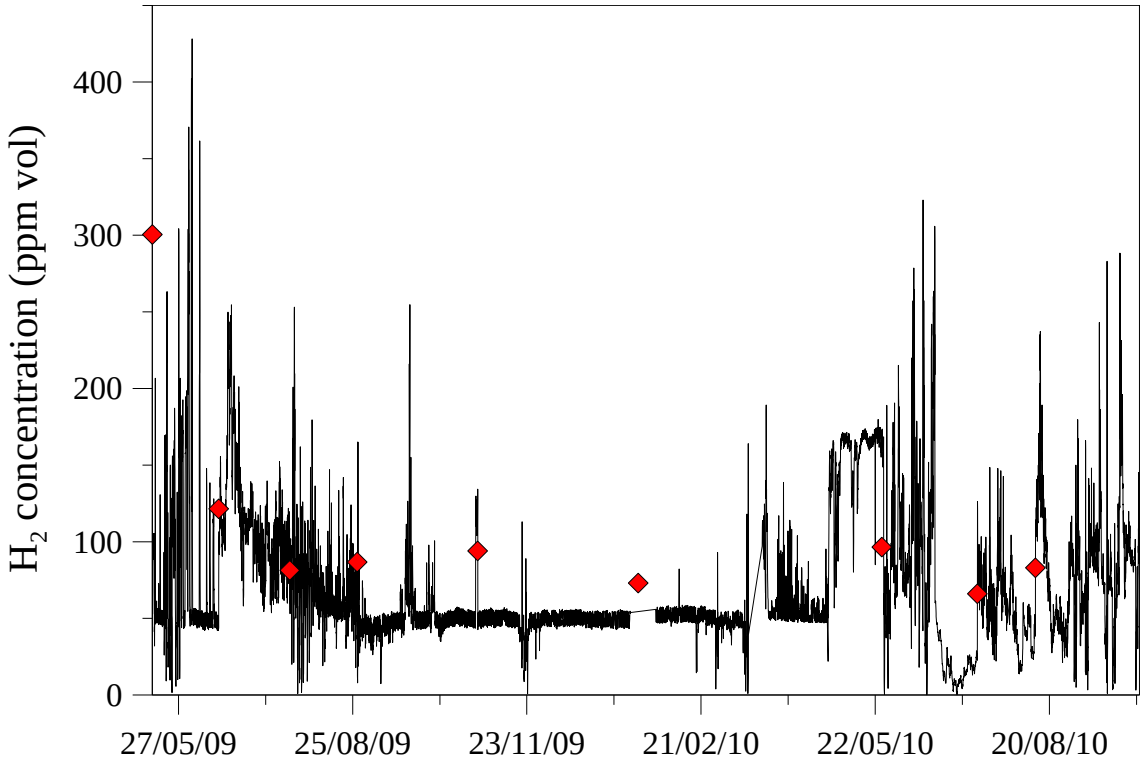

Figure 32 Time series of the H_2 concentration measurements performed at PSF site (Stromboli) from the 13 May 2009 to the 5 October 2010 with the permanent monitoring H_2-CO_2 device (black line). The red diamonds show the H_2 concentration measured by chromatographic analysis in the survey sample collected at PSF site. The time series shows the typical "sow teeth" trend produced by the sudden variation of the H_2 concentration within the mixture emitted from the soil.

It is worth noting that the average H_2 concentration measured in the survey samples (122 ppm vol.) agrees with the average value of the measurements performed by the H_2-CO_2 system (74 ppm vol.) in the limits of the respective standard deviations (69 ppm vol. and 45 ppm vol. respectively). The large number of data allows an improved statistical analysis and validation of the classification of the H_2 concentration measurements performed at PSF-a site through the probability plots (Sinclair, 1974). This statistical-graphical method has been widely used to differentiate the values of any data set having polymodal distribution between anomalous and background populations. In so doing, each population can be identified according to their appropriate density distribution, since each of them shows a straight line distribution in the plot (Figure 33).

The probability plot of H_2 data set shows four different populations having values above the detection limit of the sensor (~ 5 ppm vol.). The background population, representing the 51% of the data set, shows value ranging from 42 to 63 ppm vol. Moreover, the average concentration of the background population (equals to 52 ppm vol.) can be read on the 30 cumulative percentile of the probability axis.

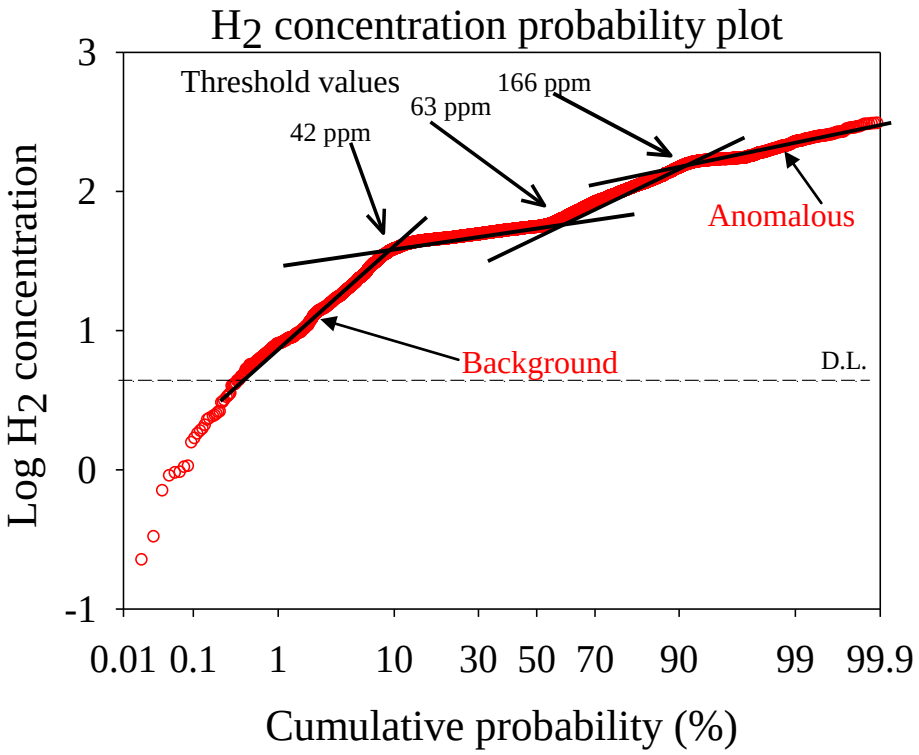

Figure 33 Lognormal probability plot of the H_2 concentration data set collected at PSF site. The ordinate axis reports the logarithm of the H_2 concentration, while the horizontal axis has probability scale type. Above the detection limit of the H_2 sensor (~ 5 ppm vol.), the H_2 concentration data have polymodal distribution. The anomalous population, having H_2 concentration values above 166 ppm vol., represents the 10% of all the measurements. The background population represents about the 51% of the data set shows value ranging from 42 to 63 ppm vol. The threshold population represents the 31% of the measurements. A further population of lowest H_2 concentration can be clearly identified below the 42 ppm vol. representing about the 8% of the data set, while the remaining 1% is represented by the measurements showing values below the detection limit of the H_2 sensor indicated with the acronym D.L. above the dashed black line. The arrows indicate the threshold values allowing the data classification described before.

The anomalous population represents the 10% of the data set having the H_2 concentration from 166 to the maximum of 428 ppm vol. The average value of the range of anomalous H_2 concentration is 316 ppm vol. corresponding to the 99 cumulative percentile of the data set.

The third population collects the measurements ranging between 63 and 166 ppm vol. representing the 31% of the data set. This "threshold" population has the average concentration of 100 ppm vol. corresponding to the 80 cumulative percentile.

The left over 8% of the data represents the concentration values ranging from the detection limit of the H_2 sensor (~ 5 ppm vol.) and the lower limit of the background population (42 ppm vol.) having the average concentration of 15 ppm vol. corresponding to the 6 cumulative percentile.

The comparison between the data classification obtained by the probability plot and the H_2 concentration time series (Figure 32) indicate that the gas emitted by PSF-a site showed long-lasting time periods characterized by steady H_2 background concentration, slightly changing with daily frequency within its typical narrow range (42 to 63 ppm vol.). These steady conditions have been interrupted by sudden increases of the H_2 concentration up to the anomalous values, often going back to the typical background within a few hours.

Moreover, a well defined decreasing trend, although interrupted by several increasing peaks, can be distinguished from the end of June 2009 to the end of August 2009 when "threshold" concentrations have been measured. The high frequency variations recorded seems to reflect the typical variability on hours or days timescale of Stromboli's activity.

In a quite similar mode to the increasing events, but with a lower frequency, the H_2 concentration in the emissions from PSF-a site showed sharp variations between the background and anomalous population, going to the background values already within a few hours.

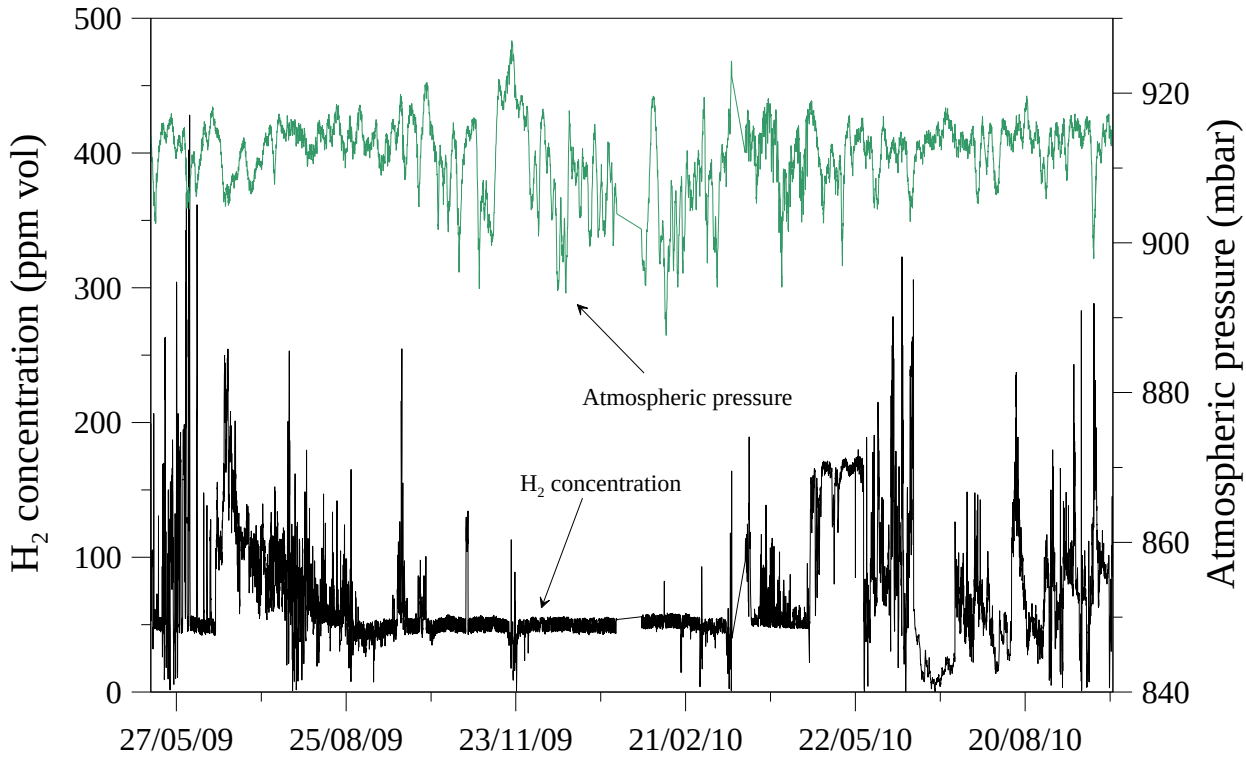

Figure 34 H_2 concentration (black line) and atmospheric pressure (green line) time series showing the temporal variations of both parameters. The larger variations of the atmospheric pressure are in the range of 30 mbar and being measured in a time interval without any variations of the H_2 concentration in the gas emitted from the PSF site.

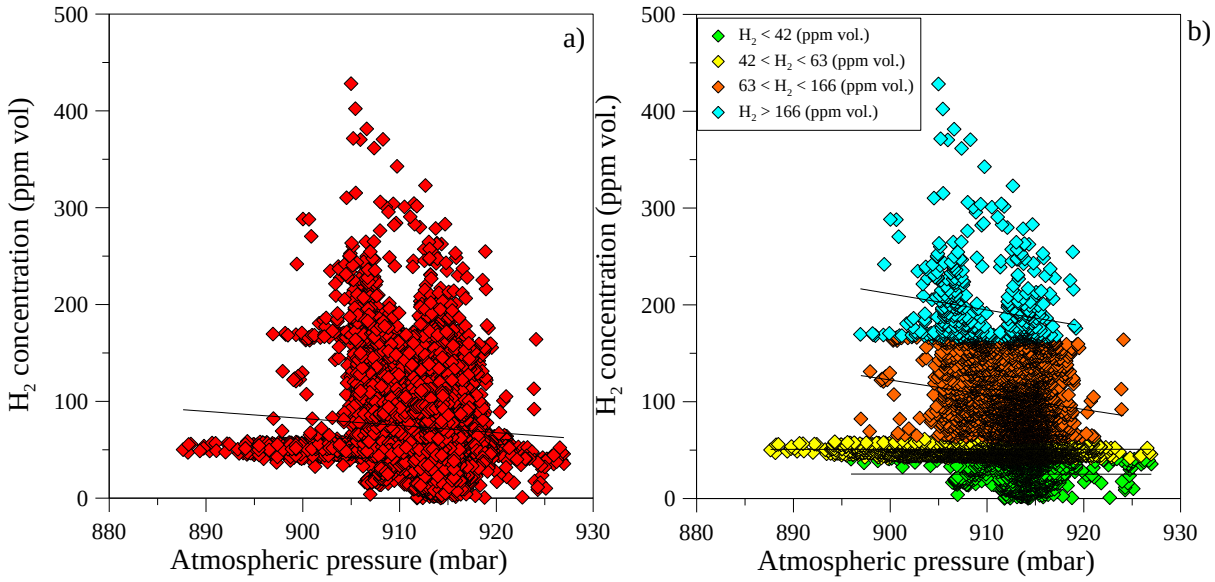

Figure 35 Correlation diagrams between the H_2 concentration and the atmospheric pressure values. a) All data set. b) H_2 concentration measurements classified by the probability plot. Green diamonds indicate the lowest population of H_2 concentration values, the yellow diamonds indicate the background population, orange diamonds indicate the threshold population and the light blue diamonds indicate the anomalous population.

The temporal variations of the H_2 measurements selected on the basis of the probability plot suggest that several changes, with high frequency, between background and anomalous values have been measured in the gas emitted from PSF site. The accurate interpretation of the soil gases anomalies needs to consider the effects produced by the meteorological conditions that may allow variable amounts of atmospheric air to enter the soils and affects the concentration of monitored gases. Figure 34 shows both the H_2 concentration and the atmospheric pressure time series recorded at PSF site without any noticeably correlation between the main variations of the H_2 concentration and the atmospheric pressure ones. Moreover, the absence of correlation between the variations of the H_2 concentration and the atmospheric pressure appears also from the correlation diagrams reported in figure 35.

CO_2 flux measured at Stromboli - PSF-b (L.F.)

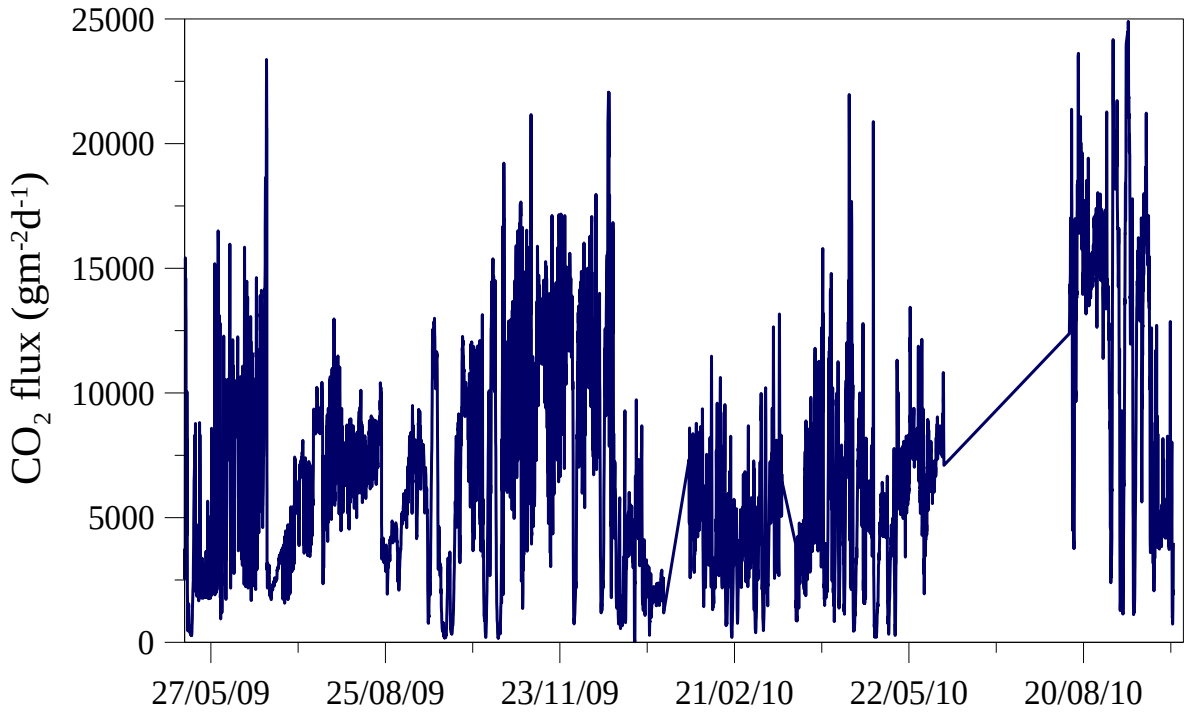

Figure 36 Time series showing the CO_2 flux measurement performed at PSF-a site (L.F.) from 13 May 2009 to 5 October 2010. The CO_2 flux values are given in g m^{-2} d^{-1}.

Figure 36 shows in detail the time series of CO_2 flux measured at PSF-b site (hereafter CO_2 L.F.) from 13 May 2010 to 5 October 2010. The average CO_2 flux value has been 6500 g m^{-2} d^{-1} (standard deviation 3679 $gm^{-2}d^{-1}$) ranging from 161 g $m^{-2}d^{-1}$ to of 27023 g $m^{-2}d^{-1}$.

The most striking features of CO_2 L.F. time series are the long-lasting increasing trend affected by sudden variations of the CO_2 flux.

Several well defined trends can be distinguished on the time series producing variations of the CO_2 flux larger than one order of magnitude from a few hundred up to thousands of $gm^{-2}d^{-1}$. The most evident trends are shown from May to June 2009, from July to August 2009, the large trend lasting from the month of September to December 2009 and from March to April 2010.

As has been shown for H_2 concentration measurements, a widely used tool for the classification of any data set having polymodal distribution is the probability plot (Sinclair, 1974).

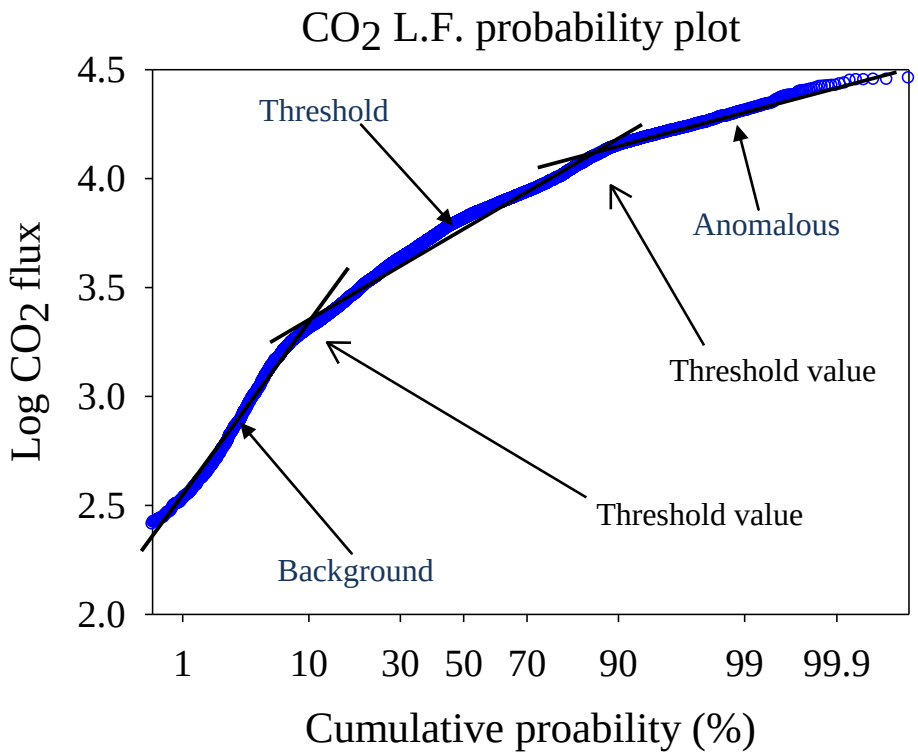

Figure 37 Lognormal probability plot of the CO_2 L.F. data set collected at PSF site. The ordinate axis reports the logarithm of the CO_2 flux value, while the horizontal axis has probability scale type. The highest values populations, showing CO_2 flux above 12590 $gm^{-2}d^{-1}$, represents the 10% of all the measurements. The lowest value population represents about the 10% of the data set showing CO_2 flux below 2230 $gm^{-2}d^{-1}$. The threshold population represents the 80% of the measurements. The arrows indicate the threshold values allowing the data classification described before.

The statistical validity of such analysis is enhanced by the large number of data. Three data populations of the CO_2 L.F. measurements can be distinguished through the probability plot (Figure 37). The lowest values population, representing the 10 % of all data set, shows CO_2 flux value below 2230 g m^{-2} d^{-1} (average of 630 g m^{-2} d^{-1} corresponding to the 5 cumulative percentile), while the highest population shows values above 12590 g m^{-2} d^{-1} representing the 10% of the data set. The average value of CO_2 flux of the highest population is 19950 g m^{-2} d^{-1} corresponding to the 99 cumulative percentile. It is worth nothing that only the 1% of the measurements show flux values above the mentioned average high flux.

The threshold population has intermediate CO_2 flux values representing the 80% of the data set showing the average flux value of 5620 g m^{-2} d^{-1} (52 cumulative percentile).

The comparison between the CO_2 flux measurements selected through the probability plot and the time series of CO_2 L.F. (Figure 36) suggests that the highest CO_2 emissions have been recorded during the periods between the month of October to December 2009, as well as the July-August 2009 and the March-May 2010.

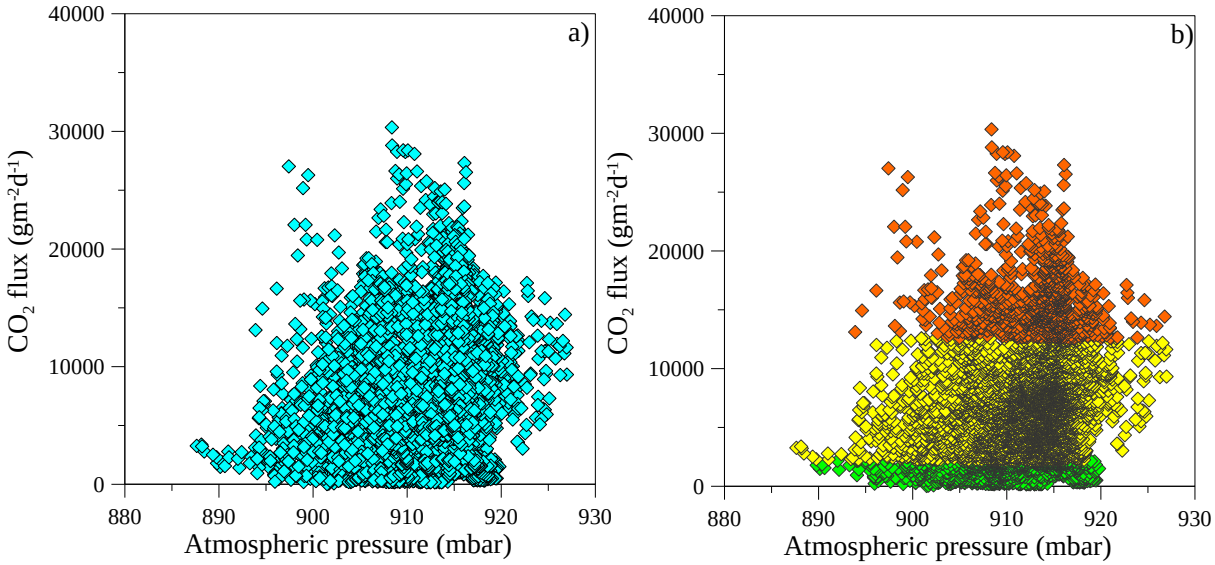

Figure 38 Correlation diagrams between the CO_2 L.F. and the atmospheric pressure values. a) All data set. b) Classified. The CO_2 flux measurements have been classified according to the probability plot. Green diamonds indicate the lowest population of CO_2 flux values, the yellow diamonds indicate the intermediate population and the orange diamonds indicate the anomalous population.

Moreover, well defined enhancing trend can be distinguished throughout these periods changing the CO_2 flux from the intermediate to the anomalous values. Since the threshold population represents the large part of the data set, the average value of 5620 $gm^{-2}d^{-1}$ can be considered a good approximation of the typical time average of the CO_2 flux emitted from the PSF-b site.

The comparison between the CO_2 flux and the atmospheric pressure (Figure 38) indicates that no correlation is evident between both the parameters.

CO_2 flux measured at Stromboli - PSF-a (H.F.)

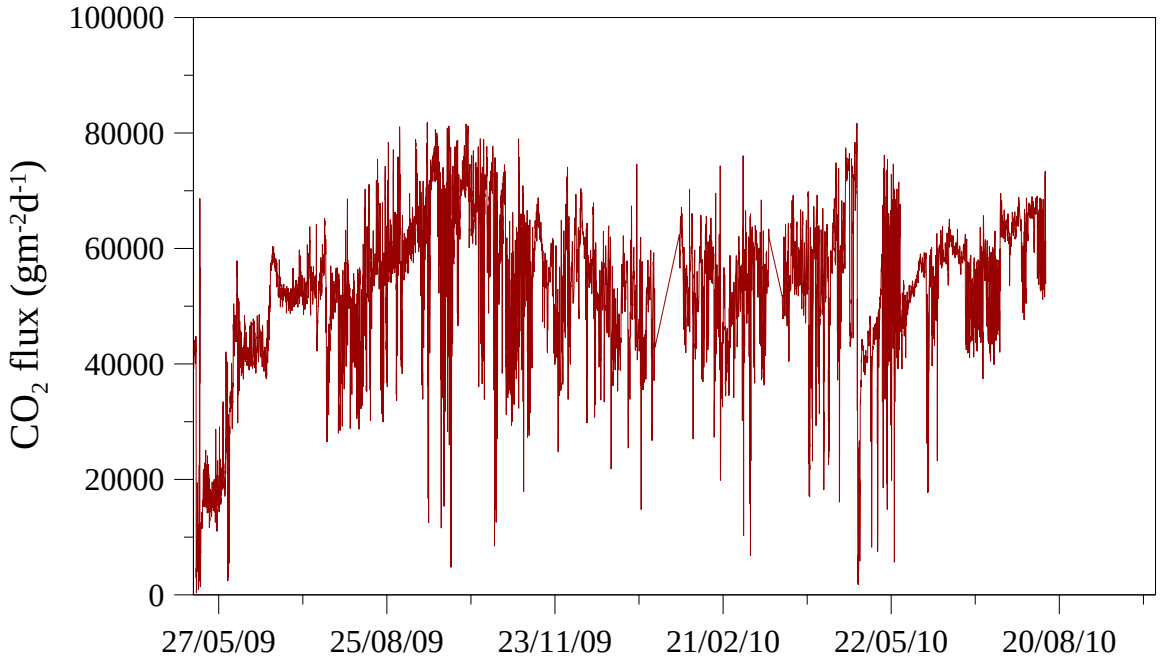

Figure 39 Time series showing the CO_2 flux measurement performed at PSF-a site (H.F.) from 13 May 2009 to 12 August 2010. The CO_2 flux values are given in g m^{-2} d^{-1}. Failure of the system occurred the 12 August 2010 prevented the following measurements of CO_2 H.F. at PSF-a site.

Figure 39 shows the time series of the CO_2 flux emitted from the PSF-a site, the same sampling point where the H_2 concentration has been concurrently measured. The average CO_2 flux recorded from the 13 May 2009 to 12 August 2010 has been 52670 $gm^{-2}d^{-1}$ (standard deviation 13245 $gm^{-2}d^{-1}$). It has been reached during the months of June 2009, after a noticeably increasing trend started at the end of the months of May 2009. Throughout the following period lasting until December 2009 the CO_2 H.F. flux has been higher than the average value, showing a well defined increasing trend from the month of July to September 2009. The measured CO_2 flux ranged between the minimum of 337 $gm^{-2}d^{-1}$ to the maximum of 81795 $gm^{-2}d^{-1}$ reached the mid-October 2009, while from the month of November 2009 to March 2010 the CO_2 flux changed around the time average of 51290 $gm^{-2}d^{-1}$. Since the month of May 2010 one of the larger increasing trends can be distinguished in the CO_2 H.F. time series. As shown before for CO_2 L.F., high frequency variations of the CO_2 flux have been recorded also at PSF-a site, suggesting a positive correlation between the high frequencies time-changing features of the gas emitted from the top area of Stromboli and the high frequency variations exhibited by the volcanic activity.

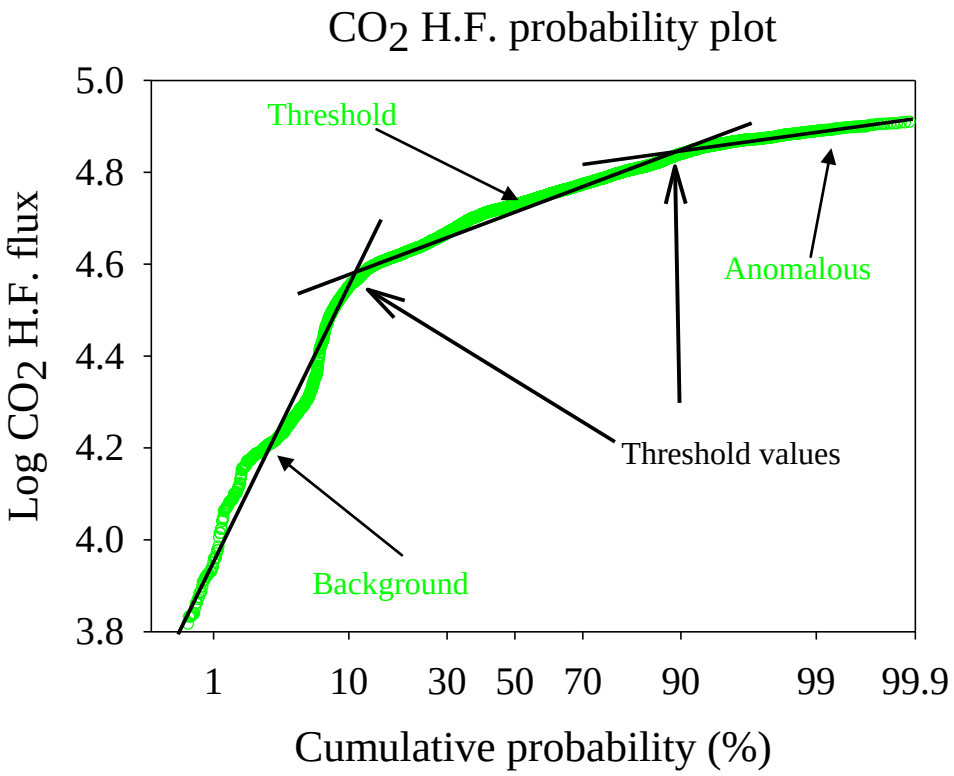

Figure 40 Lognormal probability plot of the CO_2 H.F. data set collected at PSF-a site. The logarithms of the CO_2 flux values are reported onto the ordinate axis, while the horizontal axis has probability scale type. Three main populations can be distinguished, the lowest one collecting the values below 38228 g m^{-2} d^{-1} representing about the 10% of the data set. The intermediate flux values represent the 82 % of the dataset having values ranging from 38228 $gm^{-2}d^{-1}$ to 69855 $gm^{-2}d^{-1}$ representing the threshold with the highest population (8% of the data set). The arrows indicate the threshold values dividing the three data populations.

The selection of the measurements has been done through the probability plot of the CO_2 flux emitted from the PSF-a site, aimed to sort the data between anomalous and background populations.

Three main data population can be identified within Figure 40. The highest population, collecting the anomalous flux values, corresponds to the 8% of the data set having the average CO_2 flux value of 74700 $gm^{-2}d^{-1}$ (99 cumulative percentile). The intermediate population has average CO_2 flux value of 57124 $gm^{-2}d^{-1}$ corresponding to the 58 cumulative percentile. This figure represents a good approximation of the time average of the CO_2 flux emitted from the PSF-a site, since the intermediate population corresponds to the large part of the data set (82%). The left over 8% of the measurements represents the lowest population having the flux value below 38228 $gm^{-2}d^{-1}$ and the average of 17600 $gm^{-2}d^{-1}$ corresponding to the 4 cumulative percentile.

The comparison between the data classification obtained from the probability plot (Figure 40) and the time series (Figure 39) indicates that highest CO_2 flux has been measured at PSF-a site from July to October 2009 and from the end of March throughout the month of April 2010. Between these periods the CO_2 flux remained within the intermediate range, changing around the time average figure reported before. Moreover, throughout the observation periods several peaks, on the timescale of a few hours or days, changed suddenly the CO_2 flux from intermediate to the highest values. According to several authors (Hinkle and Ryder, 1987; Hinkle, 1990; Hinkle 1994; Asher-Bolinder et al., 1990; Giammanco et al., 1995), the meteorological conditions can affect the gas transport process through the soils. Also the soil type (particle size distributions) can be accountable among the main factors affecting both the gas concentration and flux. In our case, the influences of the soil type have been neglected since the CO_2 flux measurements, as well as the H_2 concentration ones, refer to the same sampling point whose soil properties can be considered constant.

The comparison between the CO_2 H.F. and the atmospheric pressure parameter has been done for better understanding the variations of the CO_2 flux measured at PSF-a site and to correct the interpretation of the soil gas anomalies from the interferences produced by the variations of the weather conditions.

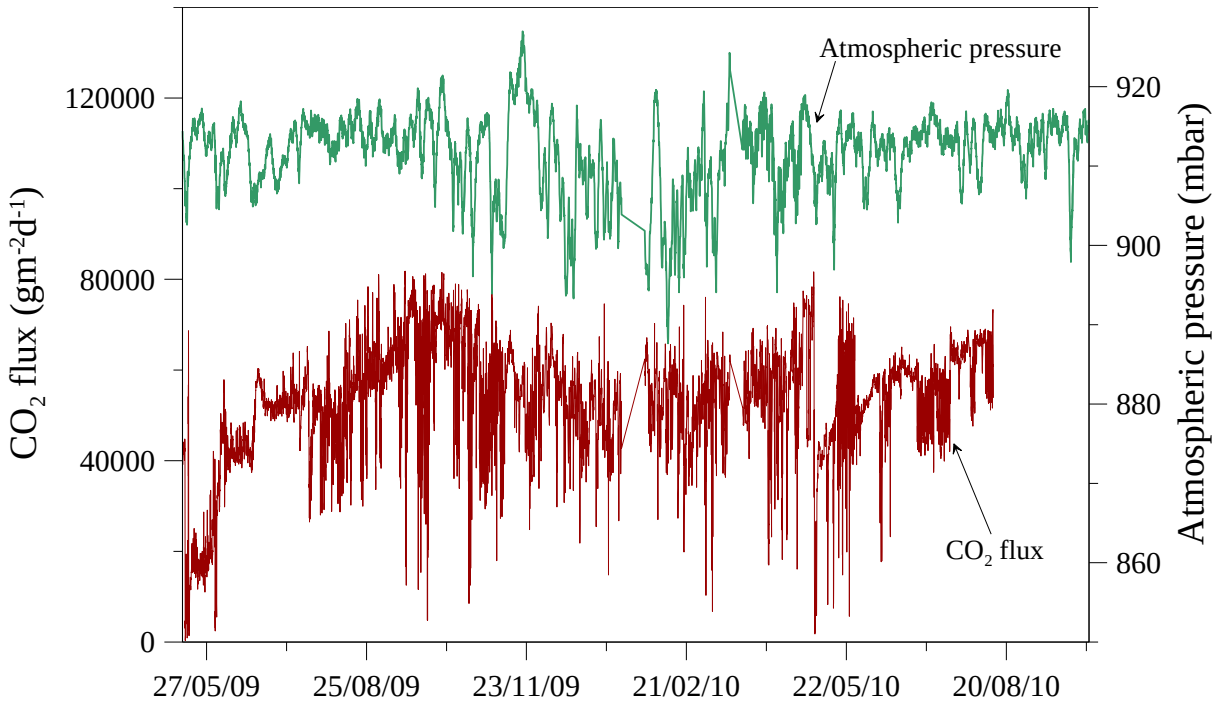

Figure 41 CO_2 H.F. flux (brown line) and atmospheric pressure (green line) time series showing the temporal variations of both parameters.

In so doing, the right interpretation of the CO_2 flux anomalies allows better investigating the relationships between the variations of the gas emissions from the fumarolic field of the top area of Stromboli and the volcanic activity. Figure 41 reports both CO_2 H.F. flux and atmospheric pressure time series. The figure shows that despite of largest variations in the atmospheric pressure, in the order of 30 mbar, recorded throughout the winter 2009, any noticeably influence have been observed onto the main trend of CO_2 flux.

Comparison between the monitored parameters

In order to better understand the changes of degassing features observed at PSF-a site, the measurements of H_2 concentration and CO_2 flux performed through the H_2-CO_2 system have been compared through the correlation diagram reported in Figure 42-a. The data display a wide spreading (R^2 = 0.045), suggesting that both parameters are largely independent.

More interesting features can be highlighted following the data set classification obtained through the probability plot (Figure 42-b). The H_2 concentration values in the range of intermediate and anomalous populations show inverse correlation (r = - 0.127) with CO_2 flux values ranging within both the typical and anomalous populations (dark yellow diamonds).

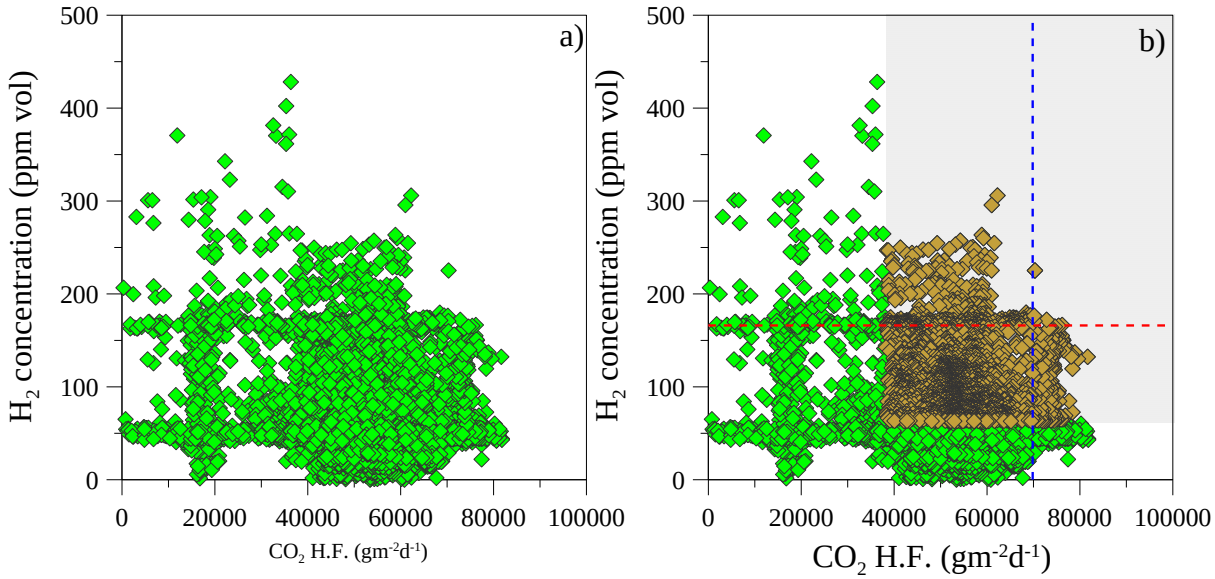

Figure 42 Correlation diagram between the CO_2 H.F. and the H_2 concentration measurements performed at PSF-a site. Green diamonds indicate the whole data set (a and b). Dark yellow diamonds indicate the H_2 concentration and CO_2 flux values of intermediate and anomalous populations. The red and blue dashed lines indicate the threshold values individuating the anomalous populations of H_2 concentration and CO_2 flux respectively.

Moreover, several times the H_2 concentrations has been measured in the range of intermediate or highest values, while the corresponding CO_2 flux values were in the range of background or the lowest populations. On the other hand, highest CO_2 flux values (on the right side of blue dashed line) are mainly associated with intermediate H_2 concentrations (on the right side of blue dashed line and below the red line). Nevertheless, one of the most distinctive features displayed in figure 42-b is the low data density that fall within the field defined by anomalous H_2 concentration and anomalous CO_2 flux (above the red dashed line and on the right of blue dashed line respectively), suggesting that anomalous H_2 releases have been hardly ever associated to simultaneous highest CO_2 emissions. According to the data distribution shown in Figure 42, the large independency of the H_2 concentrations in comparison to the CO_2 flux (CO_2 H.F.) suggests that large anomalies of the chemical composition of the gas emitted from PSF-a site may be uncorrelated to synchronous anomalous gas output from the fumarolic field.

The investigation of the relationships between the H_2 concentration and the CO_2 flux measurements allows better understanding the temporal variations of both the monitored parameters. In so doing, the significant changes of the degassing features of PSF-a site can be compared with the time-changing volcanic activity occurring at Stromboli.

In order to identify the significant changes of the degassing activity, both the H_2 concentration and CO_2 flux (H.F. and L.F.) measurements collected hourly by the H_2-CO_2 system have been processed and filtered from the interferences of the working conditions and the atmospheric pressure. The data processing has been done in MatLab environment using the Signal Processing tool (SPtool), dealing the unprocessed data time series as digital signals and distinguishing the frequency variations through the Fast Fourier Transform (FFT) analysis. The frequency bands identified in the H_2 concentration and CO_2 flux signals have been compared with the frequencies spectrum of atmospheric pressure parameter. Two distinct digital filter (Bandstop direct form II filter structure, sixth order sections stable filter, IIR Butterworth designing method and Lowpass direct form II filter structure, tenth order section stable filter, IIR Butterworth designing method) have been designed, tuned and applied to the unprocessed data in order to remove the variations having daily frequency and the variations having frequencies higher than 2 hours.

The processed data have been compared with the time-changing Stromboli's eruptive activity, focusing on both the routine activity and the sudden variations occurred throughout the period of observation, represented by major explosions.

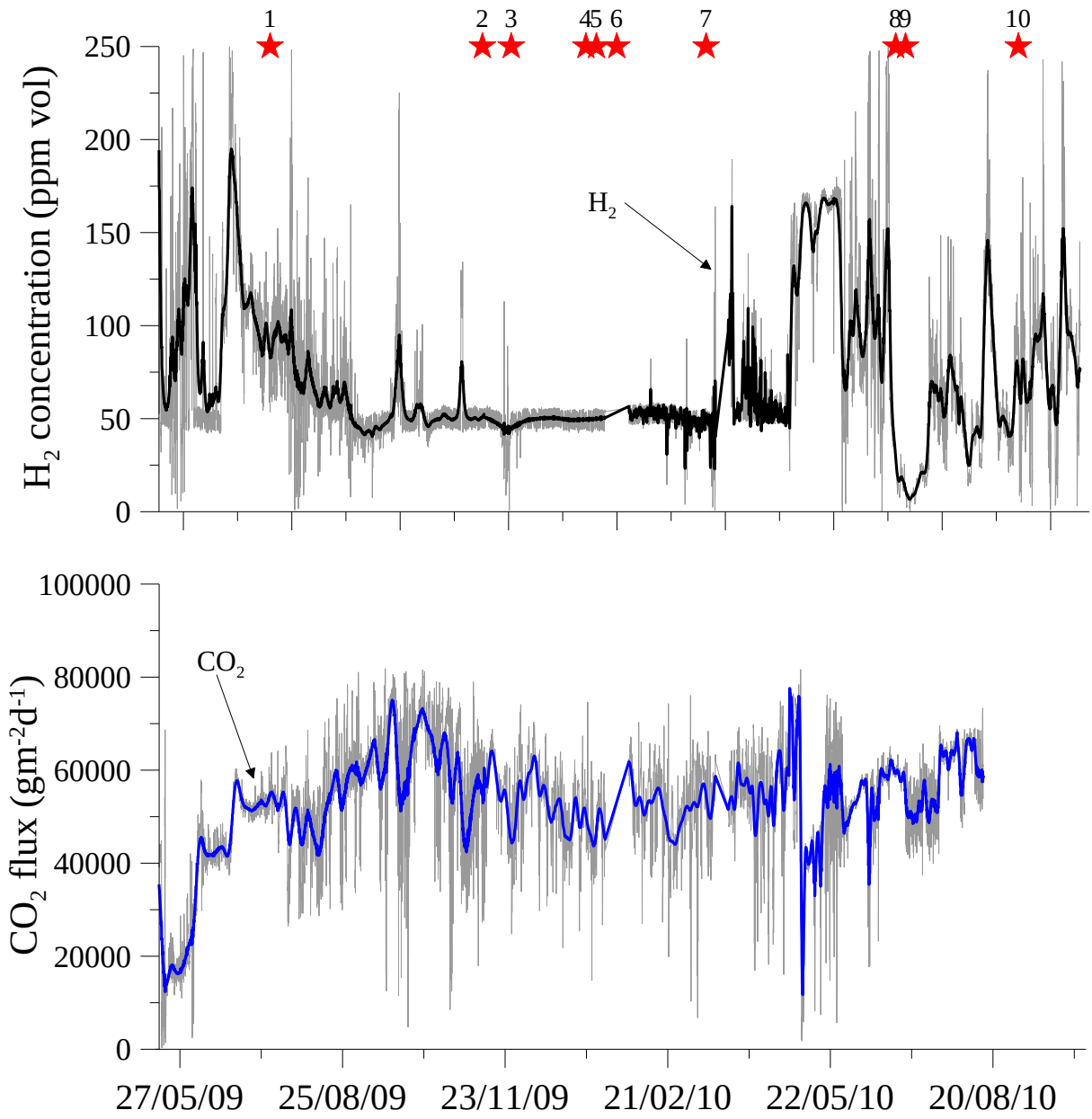

Figure 43 Time series of: a) H_2 concentration (Black line – filtered data); b) CO_2 H.F. (Blue line – filtered data). The major explosions occurred at Stromboli are also reported (red stars).

As reported before, major explosions are impulsive events stronger than the typical strombolian explosions, associated with the emission of vertical gas jets and pyroclasts (Barberi et al., 1993).

Besides the event of 5 May 2009, a few days before the installation of the H_2-CO_2 system at PSF site, throughout the sixteen months of H_2 concentration and CO_2 flux measurements occurred ten major explosions listed within Table 4, a figure larger than the average 0.5-3 events per years typical of Stromboli's activity.

Table 4 Major explosions (date and time) occurred on Stromboli volcano since the May 13, 2009 to the October 5, 2010. The events are indicated with red stars in Figure 41 and 42.

Event	Date	Time - GMT
1	July 14, 2009	20.09
2	November 8, 2009	12:28
3	November 24, 2009	11:20
4	January 4, 2010	19:12
5	January 10, 2010	14:48
6	January 21, 2010	20:45
7	March 12, 2010	07:57
8	June 25, 2010	06:02
9	June 30, 2010	16:33
10	September 1, 2010	04:02

As can be seen from Figure 43, at least seven on top to the ten major explosions [1 – 2 – 3 - (7) – 8 – 9 – 10 as listed in Table 4] were preceded by relative increases of H_2 concentration within the gas emitted from PSF site and coupled, or right away followed, by relative increases of CO_2 flux. The CO_2 flux increases have been also observed from PSF-b site (CO_2 L.F. time series), where the CO_2 flux showed large variations from the end of October to the end of December 2009 (Figure 44).

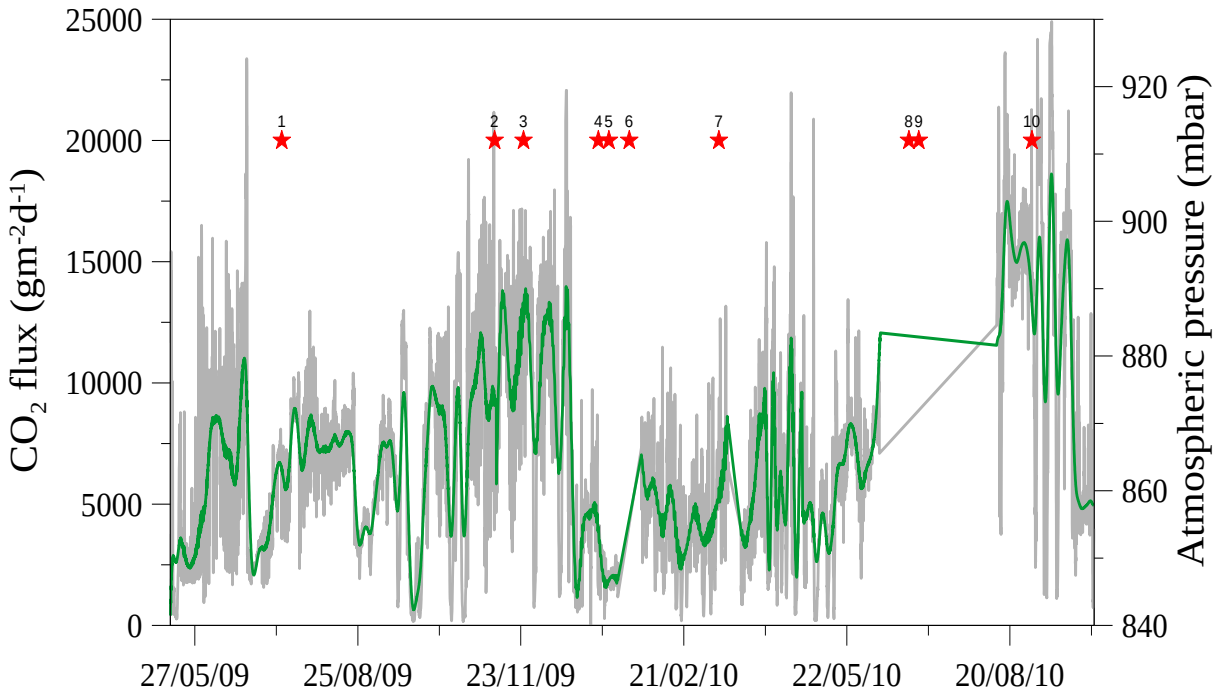

Figure 44 Time series of CO_2 L.F. (Green line – filtered data). The major explosions occurred at Stromboli since 13 May 2009 are also reported (Red stars).

The synchronous variations measured on both site, far away some meters tenths along NE-SW direction, suggests that the CO_2 flux increases has been a widespread phenomenon occurred onto the top area of Stromboli during a period of significant increases of volcanic activity.

Moreover the January 4 and January 10, 2010 events [4 – 5 in Table 4] were correlated with relative increases of CO_2 flux above the typical time average value measured at PSF-a site, although small-scaled in comparison to the previously ones. Before or during these events the measurement system did not recorded any significant variation of the H_2 concentration within the gas emitted from PSF-a site, while nothing can be said about the event occurred the January 21, 2010 due to the temporary failure of the H_2-CO_2 system.

The key features of the time series shown in Figure 43 and Figure 44 that must be explained for better understanding the relationships between the gas emission from PSF site and the volcanic activity are:

- the variations of both CO_2 flux and H_2 concentration associated to major explosions;
- the wide variations of H_2 concentration occurring during routine strombolian activity;
- the fundamentally steadiness of H_2 concentration between both large and narrow increases within the gas emitted from PSF site.

One of the most striking features of CO_2 is his low solubility in silicate melts, showing the attainment of CO_2 saturation at mantle to deep crustal level. On the other hand, large amount of H_2 can be produced through the water dissociation reaction at high temperature at relatively shallow depth (1-2 Km) where silicate melts attain water saturation. Petrological, geochemical and volcanological study (Aiuppa et al., 2010; Allard 2010; Métrich et al. 2010; Burton et al., 2007) support the evidences that exolved CO_2-rich gas bubbles coexist with LP magma at reservoir condition (7-10 km) on deepest Stromboli's plumbing system.

In order to understand the relationships between the degassing activity from PSF site and the volcanic activity, a remarkable feature is the occurrence of several peaks uncorrelated to major explosions. For this reason, the correct interpretation of our measurements requires the understanding of the relationships between the relative larger H_2 peaks and the variations of routine strombolian activity.

Although LP magma emission occurs only during the paroxysms together with the HP magmas (Bertagnini et al., 2008; Francalanci et al., 2004; Landi et al., 2009; Metrich et al., 2001; Pichavant et al., 2009), Stromboli's persistent activity behavior requires (Metrich et al., 2009; Aiuppa et al., 2010):

- continuous magma supply, with some rate, from the deepest volcano plumbing system (7-10 km of LP magma source) also during the routine strombolian activity;
- an effective process preventing the straight emission of LP magma and leading to the formation of the HP magma from the LP one.

Petrological, geochemical, and volcanological data (Bertagnini et al., 2008; Francalanci et al., 2004; Landi et al., 2009; Metrich et al., 2001; Pichavant et al., 2009; Burton et al., 2007; Metrich et al., 2009; Aiuppa et al., 2010) strongly indicated that a de-hydration (from H_2O = 2.5-3.5 wt% of LP magma to H_2O =1.5 wt% of HP magma according to Metrich et al., 2009) CO_2-mediated fluxing process (Spilliaert et al., 2006) coupled with extensive gas bubbles separation (Burton et al., 2007; Aiuppa et al., 2010) and large crystallization (Di Carlo et al., 2006) trigger the transition from LP to HP magma at depth between 2 and 4 Km within the shallow Stromboli's plumbing system.

According to the degassing model proposed for Stromboli volcano (Aiuppa et al., 2010), the shallow plumbing system is persistently supplied, through the gas-melt separation occurring in the LP storage zone, by CO_2-rich gas phase. Part of the CO_2 reaching the shallow zone moves toward the surface through the discontinuities of volcanic pile, sustaining the degassing activity from the fumarolic field of the top area.

The "excess degassing" (Shinohara, 2008) ordinary observed in the large part of basaltic volcanoes requires a convective system activated by the sinking of denser degassed magma and the consecutive uprising of the less dense volatile-rich magma. This overturning occurs with some rate depending on the relative ratio between volatile-poor and volatile-rich magma batches. In the Stromboli system, the change of the rate of magma supply to the shallow plumbing system implies the change of the ratio volatile-rich/volatile-poor magma suggesting that the increase of the CO_2 flux emitted from the fumarolic field of the Stromboli's top area may indicate the enhancement of volatile-rich magma supplied to the shallow volcano plumbing system.

The de-hydration of LP within the magma implies that more moles of molecular water are able to generate large amount of hydrogen according to the dissociation reaction of $H_2O_{(g)}$ at high temperature

$$H_2O_{(g)} \rightleftarrows H_{2(g)} + \frac{1}{2}O_{2(g)} \qquad [1]$$

implying that

$$f_{H_2} \propto \frac{f_{H_2O}}{f_{O_2}^{1/2}} \qquad [2]$$

Since the H_2 moves in silicate melts million times faster than O_2 (Carmichael et al 1974), the de-hydration process would be linked to the start of hydrogen front from depth within the volcano plumbing system, fast-moving toward the earth surface (Nuccio and Valenza, 1993). At the same time, the redox conditions of Stromboli's LP magma are well described by NNO buffer (fO_2 given for LP magmas range between NNO + 0.2 ÷ NNO + 1 according to Métrich et al., 2010; fO_2 ranging from NNO to NNO + 0.5 according to Di Carlo et al., 2006 and Pichavant et al., 2009). Regardless of the fixed redox state, the buffer properties within the silicate melts prevent large oxygen fugacity deviations from the conditions mentioned before, implying that the denominator of equation [2] is known and fairly constant. In this way, the fH_2 is rightly dependent from the water amount exolved from the silicate melt. The larger amount of hydrogen released from magma batch, due to the de-hydration of LP at shallower level, can move through the discontinuities of the edifice together with the CO_2-rich mixtures, reaching the top area of the volcano and sustaining the gas emission from the PSF site fumarolic field, where the gas are sampled. Steady-state continuous magma supply from depth, at a given rate, implies quite constant formation and next emission of hydrogen in accordance with the water dissociation reaction. As the result, the narrow range displayed by the background H_2 concentration can be explained through the steady-state conditions of magma supply from the deep to the shallow Stromboli's plumbing system.

The increase of the rate of magma supply to the shallow plumbing system involves increasing rate of LP de-hydration (also increasing amount of CO_2-rich gas phase is supplied from LP reservoir) enhancing the water availability within the system. As the result, the higher H_2 emissions corresponding to the large and intense peaks not associated to major explosions can be explained as an indicator of increasing amount volatile-rich magma supply to the shallow plumbing system synchronous to the routine strombolian activity. As mentioned before, routine activity is an average behaviour of Stromboli volcano, since the strombolian activity is highly time-changing in the period of days or hours. Indeed, an increasing rate of magma supply from depth can results in either the increases of the average number or the higher magnitude of strombolian explosions.

The data obtained through the continuous monitoring of H_2 concentration and CO_2 flux interpreted through the degassing model recently proposed for Stromboli volcano (Aiuppa et al., 2010) allowed understanding some interesting relationships between the time-changing features of the gas emitted from PSF fumarolic field and the Stromboli's routine eruptive activity.

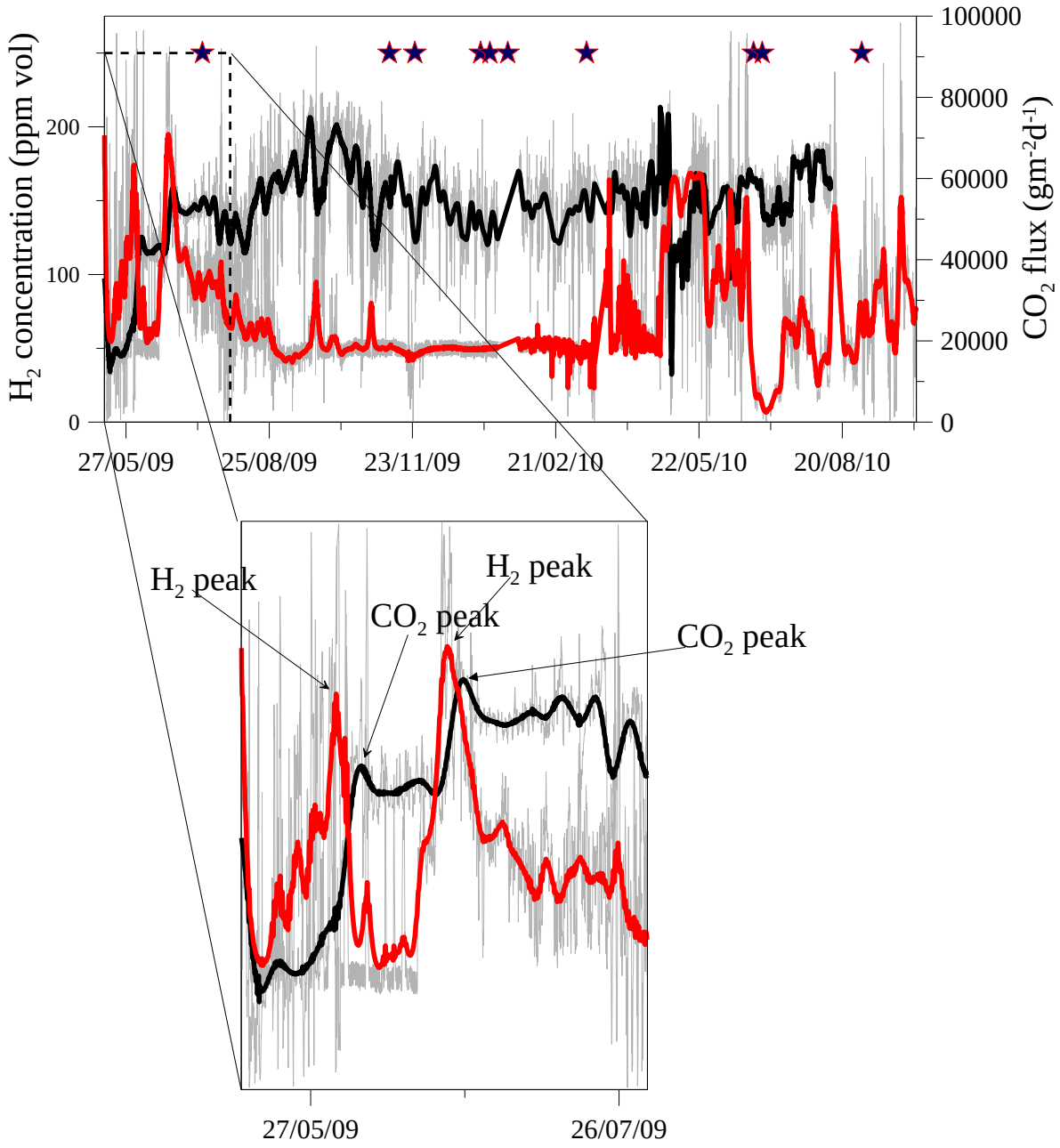

Figure 45 Time series of H_2 concentration and CO_2 flux measurements showing the time-changing features of both monitored geochemical signals. Within the box are highlighted two of the main H_2 concentration changes preceding the change of CO_2 flux from the fumarolic field of PSF-a site.

Nevertheless, the direct comparison of both parameters allows a more careful analysis of time-changing features of both geochemical signals monitored by the H_2-CO_2 system.

Figure 45 reports in the same graph the time series of H_2 concentration and CO_2 flux recorded at PSF-a site, showing that the large variations of CO_2 flux have been preceded systematically by large H_2 concentration variations.

Moreover, Figure 45 also shows in detail (see box) two of the asynchronous variations observed throughout the 16 month of continuous monitoring on Stromboli volcano, focusing

the delay between H_2 and CO_2 peaks. These peculiarities can explain the very low density of measurements in the field defined by anomalous H_2 concentration and anomalous CO_2 flux, representing one of the most distinctive features exhibited by the correlation diagram of both measurements (Figure 42). The delays between the H_2 concentration and CO_2 flux peaks ranges from several hours to days up to week and systematically the H_2 concentration peak precedes the CO_2 flux one.

The observed delays between the variations of both geochemical signals can reflect the different mobility between the H_2 and CO_2 species producing a sort of noticeably natural chromatographic effect onto the time series. Throughout the time series recorded at Stromboli, the delay time between the peaks of different species can be observed several times. Actually, these time-changing features of both geochemical signals have been recorded through the simultaneous monitoring of H_2 concentration and CO_2 flux also at Mount Etna volcano through the measurements performed at both Torre del Filosofo and Belvedere sites (see Figure 16 and Figure 27). The systematic nature of the asynchronous variations exhibited by the time series of the H_2 concentration and CO_2 flux measurements performed at Stromboli and Mount Etna volcanoes strongly suggests the independency of the typical delay from the specific sampling site as well as the more general independency from the specific monitored volcanic system.

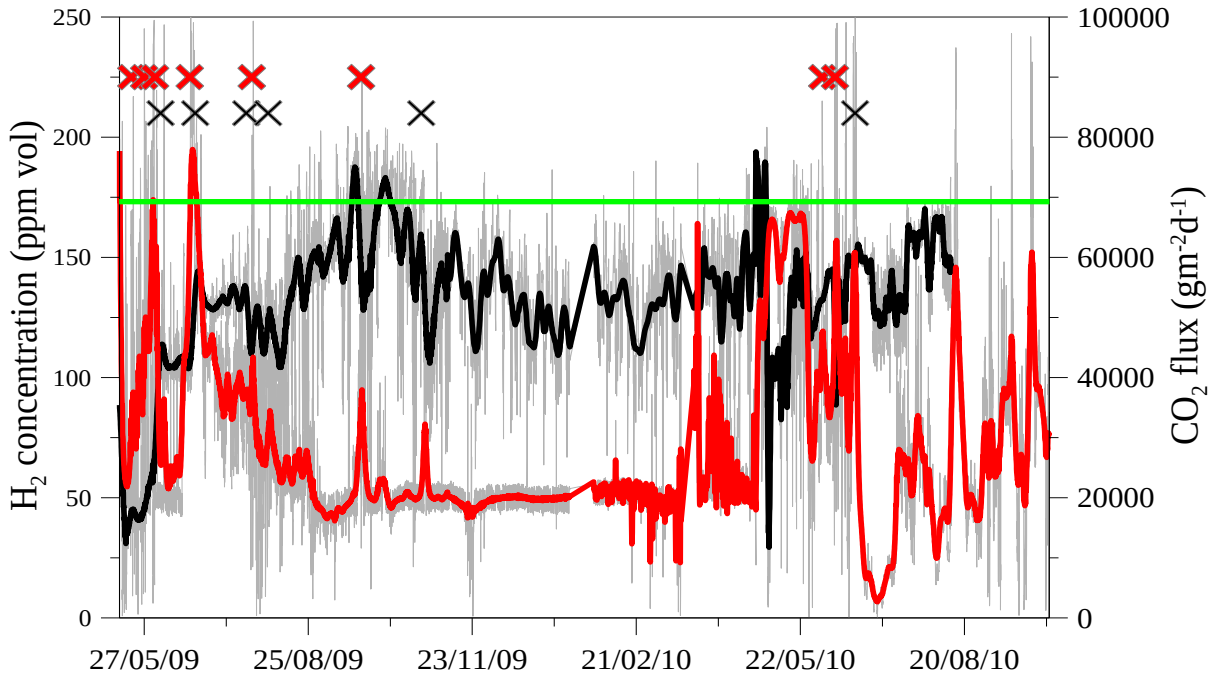

Figure 46 Time series of H_2 and CO_2. The green line indicates the threshold values of anomalous population for both geochemical signals. Red crosses and Green crosses indicate the selected H_2 and CO_2 anomalies respectively for computation the average depth of the gas reservoir (see text).

The data set analysis and the development of the theoretical model of the gas composition transients in porous media (see Chapter 4) allow evaluating the relationship between the delays of both CO_2 and H_2 perturbation and the depth of the gas reservoir supplying the emissions from the top area of Stromboli.

The probability plots showed that the H_2 anomalies were characterized by H_2 concentration above 160 ppm vol., while the CO_2 flux were anomalous above 70000 $gm^{-2}d^{-1}$. Therefore, the respective thresholds values enable selecting the periods of anomalous CO_2 flux following as many H_2 anomalies listed in table 5.

In the table are also listed two further periods throughout which the climax of CO_2 flux were just below the statistical threshold reported before, being clearly preceded by H_2 anomalies. The identification of these anomalies and the evaluation of their respective delays enable attempting the computation of the gas reservoir depth.

The relation

$$\delta \approx 3 \cdot v \cdot \Delta t \cdot \left(\frac{D_{H_2} + D_{CO_2}}{D_{H_2} - D_{CO_2}} \right) \qquad [3]$$

of the average delay (Δt) between CO_2 and H_2 anomalies and the depth of the gas reservoir (δ) is obtained settling together equations [31] (see Chapter 4) for both CO_2 and H_2 species.

The average delays between the identified anomalies are used with the threshold anomalous flux rate (v) to evaluate the average depths reported in table 5.

The results are a rough estimate of the level corresponding to the modeled upper surface of the gas reservoir from which the gas mixture containing both species begins to move through the porous medium. The values provided by the computation ranges between 2000 and 4400 meters, giving the average depth of 2900 meters (standard deviation 960) below the top of the volcanic pile.

Geochemical, volcanological, petrological and geophysical investigations (Aiuppa et al., 2010; Métrich et al., 2010; Bonaccorso et al., 2008) pointed out a magma storage zone between 2 and 4 km within the shallow plumbing system of Stromboli where CO_2-fluxing, released from the deepest magma source, triggers the transition from LP to HP magma, bringing about crystallization and water loss. The data reported in table 5 suggest that the depth estimated by using the delay between H_2 and CO_2 anomalies agree fairly well with the depth identified for the shallower magma storage zone of Stromboli.

Table 5 The identified CO_2 flux and the correlated H_2 concentration anomalies (Figure 44). The average depths are computed according to the threshold flux rate and the average delay between the anomalies.

H_2 anomalies	**CO_2 anomalies**	**Delay (days)**	**Computed depth (meters)**	**Average depth (meters)**
20.05.2009	05.06.2009	17	2500	2000
27.05.2009		10	1500	
02.06.2009	24.06.2009	22	3000	3000
21.06.2009	22.07.2009	30	4400	4400
25.07.2009	03.08.2009	8	1100	2600
23.09.2009	26.10.2009	28	4100	
03.06.2010	21.06.2010	18	2700	2150
10.06.2010		11	1600	

In this zone, CO_2 is supplied from below (Allard et al., 2010; Aiuppa et al., 2010; Métrich et al., 2010) and large amount of hydrogen can be produced by high temperature water dissociation reaction (Nuccio and Valenza, 1993). Therefore, we infer that the monitoring of degassing activity from the top area of the volcanic pile could provide information on the dynamics involving the shallower-intermediate plumbing system of Stromboli volcano.

In summary, since the 13 May 2009 the typical time-changing activity has been observed at Stromboli volcano. Throughout this period, the H_2-CO_2 system, installed on the top area of the volcano, allowed the simultaneous measurements of H_2 concentration and CO_2 flux from the PSF-a fumarolic field. At the same time, the CO_2 flux from the soil has been measured from PSF-b site, some tenths meters away along the direction NE-SW.

Beside the typical strombolian explosions occurring on average every 15 minutes, Stromboli activity showed ten major explosions and paroxysms throughout the period during which the H_2 concentration and CO_2 flux measurements have been performed. The description of the main variations of both monitored parameters through the degassing model recently proposed for Stromboli volcano (Aiuppa et al., 2010) allowed highlighting some relationships between the variations of the degassing activity from the fumarolic field of the top area of the volcano and the time-changing style of its eruptive activity.

Moreover, the simultaneous monitoring of different parameters such as the H_2 concentration and the CO_2 flux allows understanding the time-changing relationships between the variations of both gas species. Indeed, the most noticeable feature is the asynchronous variations of both parameters, with the H_2 concentration variations preceding the CO_2 one as the results of the different mobility of the chemicals. We believe that such a sort of chromatographic effect can

be explained through the very different diffusive features of the H_2 and CO_2 molecules. Indeed, although the advective flux is the more efficient process during the mass transport, the diffusive ones operates simultaneously towards the separation of the mixture in its own components, depending on the diffusive velocity of each gaseous species.

In the next chapter of this thesis the theoretical model based on the mass balance and advective-diffusive transport properties of fluid will be developed and discussed. The model represents a step forward the understanding of the transients of the chemical composition of the gases emitted from earth surface in volcanic and geothermal areas. The theoretical model proposed in this thesis can be used as a tool for understanding the delay between the variations of both monitored parameters as the result of the very different mobility of H_2 and CO_2 species.

Chapter 4
Theoretical model of the composition profile into the soils

Introduction

The continuous and high frequency monitoring of volcanic activity by measuring the variations of the chemical compositions of the gases emitted from the soils and low temperature fumaroles requires the study of the transport dynamics in a multiphase system.

A theoretical model has been developed in order to understand the relationships among the chemical composition of the surface gas emissions, the sub-surface gas flow regime, the transport parameters of the porous medium (porosity and tortuosity) and the depth of the gas reservoir.

In our scheme the soil has been considered as homogeneous semi-infinite porous medium, and the model includes the effects of both diffusive and advective transport processes. In the described conditions, the mass transport occurs according to a non-zero concentration gradient producing the diffusion flux, and a non-zero pressure gradient producing the advective component. In detail, our model describes the mass transfer process through the transient state produced by the perturbations of the flux variables within the system. The study of the transient fluid flow through the porous media may be used to improve the understanding of the relationships between the chemical variations measured through the permanent H_2-CO_2 monitoring system and the degassing process occurring in the Earth crust.

In this chapter we illustrate the theoretical model proposed in order to describe the transients of the chemical composition of the gas phase into the soils. The main part of the chapter focuses on both the formulation and the basic concepts used for the solution of the problem of the transient of the chemical composition into the porous media.

Finally, in order to check the reliability of the theoretical model and understand the limits of its validity, a set of dedicated laboratory tests has been performed. The results are compared with the model prediction and shown at the end of the chapter.

Basic concept of the gas flux

The chemical composition profile produced by the soil gases may be studied considering the transport processes through the porous medium.

The figure 1 shows a schematic view of the natural system described by our theoretical model. The soils are considered as a semi-infinite homogeneous porous medium of constant thickness.

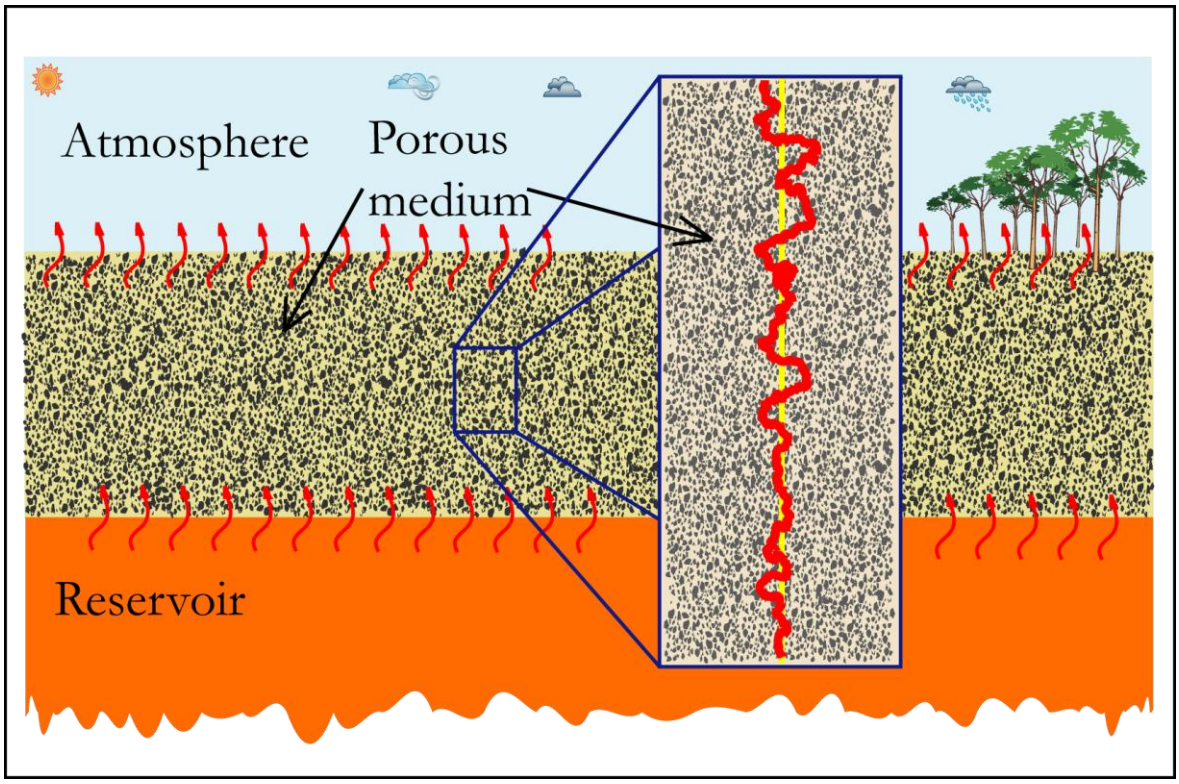

Figure 1 Schematic picture showing the natural system described by the theoretical model. The soils are considered as semi-infinite homogeneous porous medium of constant thickness. The upper surface limiting the porous medium represents the soil surface separating the Earth interior from the atmosphere, while the lower surface of the medium divides the soil from the gas reservoir representing the source of the perturbation of the chemical concentration profile. In the right box has been depicted the difference between the tortuous path of the gas during the transport into the soil (red line) and the right distance separating the reservoir from the surface (blue line).

The upper surface limiting the porous medium represents the soil surface dividing the Earth interior from the atmosphere. The lower surface divides the soil from the gas reservoir, representing the sources of the perturbations of the gas composition profile within medium.

The theoretical model proposed in this thesis analyses the temporal variation of the chemical composition profile within the soils produced simultaneously by the gas diffusion and advection. The first process is described by the first Fick's law

$$\varphi_{d(i)} = -D_i \nabla C_i \qquad [1]$$

where $\varphi_{d(i)}$ is the diffusive flux of the i^{th} component, ∇C_i is the chemical potential gradient and D_i is its diffusion coefficient.

Equation [1] describes the rate of mass transfer through the medium of unit cross section area. Gas flows along the direction of the negative concentration gradient measured normal to the surface through which the diffusion is taking place, being proportional to the size of the concentration gradient.

The soils can be depicted through the solid skeleton and the porous void. The solid particles of the porous media cause a barrier to the diffusion of the gases, making the diffusion volume smaller than the total volume of the medium.

The diffusion through the fluid filled pores of the impermeable porous solid media takes place only through the cramped and tortuous pores of the composite. Because the pores are not straight, the diffusion actually takes place over a longer distance than it would in a homogeneous material. Because the solid is impermeable, diffusion occurs over a smaller cross-sectional area than that available in a homogeneous material. The effects of longer pores and smaller areas are often lumped together in the definition of the bulk diffusion coefficient (or effective diffusion coefficient)

$$D = \frac{D_i \cdot p}{\tau} \qquad [2]$$

in which D_i is the molecular diffusion coefficient within the gas filling the pores, p is the void fraction and τ is the tortuosity, attempting to account for the longer distance traversed within the pores. Tortuosity usually ranges between two and six, averaging about three.

The second mechanism producing mass transport through the porous media is the advective flux, also called *effusive*, *convective* or *viscous flux*. This is expressed as follow

$$\varphi_a = C_i \cdot v_{ai} \qquad [3]$$

where C_i is the concentration of the i^{th} gas species and v_{ai} is the advective flux rate. The terms v_{ai} depends on gas viscosity μ, on the permeability of the medium k and on the pressure gradient ∇P

$$v_{a(i)} = -\frac{k}{\mu} \cdot \nabla P \qquad [4]$$

known in the literature as Darcy's law.

Equation [4] describes the transfer mass rate of a gas advecting through a medium of unit cross section area. Gas flows along the direction of the negative pressure gradient measured normal to the surface through which the advection is taking place and it is proportional to the size of the pressure gradient.

In a wide range of environmental conditions the mass transport is produced by the interactions between the two boundaries transport mechanisms. Since both the diffusion and the advection processes occur at the same time producing the gas movements, the most general equation describing gas flux through the porous media is the sum of the diffusive and advective components

$$J_i = \varphi_{d(i)} + \varphi_{a(i)} = -D\nabla C_i + C_i v_{a(i)} \qquad [5]$$

The integral method

The fluid flow problem describing the variations of the chemical composition profile within the soils is based on the solution of the equation of continuity, coupled with the advective-diffusive equation (equation [5]).

Usually, the exact or the approximate analytic solutions of the problems are useful in the engineering analysis, providing insights into the physical significance of various parameters affecting the problem of interest. The exact solution of the differential equation in a given region subject to specified boundary and initial conditions, satisfy the problem of the concentration profile at each point over the considered region. When exact analytic solutions are impossible or too difficult to obtain, or the resulting analytic solutions are too complicated for computational purposes, approximate analytic solutions provide a powerful alternative approach to handle such problems.

Among the numerous approximate analytic methods for solving the partial differential equations governing the engineering problems, the integral method has been widely used in the solution of various types of one-dimensional heat conduction problems, melting and solidification problems, and heat and momentum transfer problems for specified boundary conditions.

Wu and Pruess (2000) applied the integral method in the solution for transient fluid flow through a porous medium with pressure-dependent permeability. The application of the integral method to the problems of fluid flow in porous media gives a solution satisfied in average integral sense over the region subject to specified boundary and initial conditions. The results are approximate, but several solution obtained with this method, when compared with the exact solutions have confirmed that the accuracy is generally acceptable for many engineering applications.

The analysis with the integral method applied to the concentration profile problem in a semi-infinite porous medium, subject to some prescribed boundary and uniform initial conditions without gas production into the medium, has been performed according to the following steps:

- The differential equation of the concentration profile has been integrated over a phenomenological distance (δ_t), called *composition layer* in order to remove from the differential equation the derivative with respect to the space variable. The composition layer is defined as the distance beyond which, for practical purpose, there is no mass flow. Hence the initial composition profile within the porous medium remains unaffected beyond (δ_t). The resulting equation is called concentration integral equation.

- A polynomial function has been chosen for concentration profile over the *composition layer*. The coefficients in the polynomial were determined in terms of the composition layer thickness (δ_t), according to the boundary conditions. The accuracy of the solution depends on the degree of the polynomial function having no significant improvement over the fourth degree.
- When the concentration profile constructed is introduced into the concentration integral equation and the indicated operations are performed, an ordinary differential equation is obtained for the composition layer thickness (δ), being the time as independent variable. The solution of this differential equation subject to the appropriate initial condition gives the composition layer thickness (δ) according to the time variable.
- Once δ is available, the concentration profile C(z,t) is known according to time (t) and position (z) within the medium, and the mass flux at the surface is determined.

In the following will be described the theoretical model of the concentration profile of the i^{th} gas species in a semi-infinite medium $z \geq 0$ initially at a uniform concentration C_i. For times $t > 0$ the boundary surface is kept at constant concentration C_i.

Mathematical formulation

The fundamental equation of the one dimensional model proposed in this thesis is obtained coupling the advective-diffusion equation with the equation of continuity

$$\frac{\partial}{\partial z}\left(-D\frac{\partial C}{\partial z}+\nu C\right)=-\frac{\partial C}{\partial t} \qquad [6]$$

where z indicates the space variable, D is the bulk diffusion coefficient defined by the relation [2], C is the concentration, t is the time variable and (v) is the advective flux rate, kept constant.

The equation of continuity is verified for

$$z > 0 \quad \text{and} \quad t > 0$$

indicating that the mass variations in the independent time variable within the porous medium are produced by the spatial variation of the total gas flux.

The conditions that must be satisfied from the solution of the problem are

$$C = C_1 \quad \text{at} \quad z = 0,\ t > 0 \qquad [7]$$

where C_1 is the forced concentration of the specific gas species, while the third one states

$$C = C_i \quad \text{for } t = 0 \text{ in } z \geq 0 \qquad [8]$$

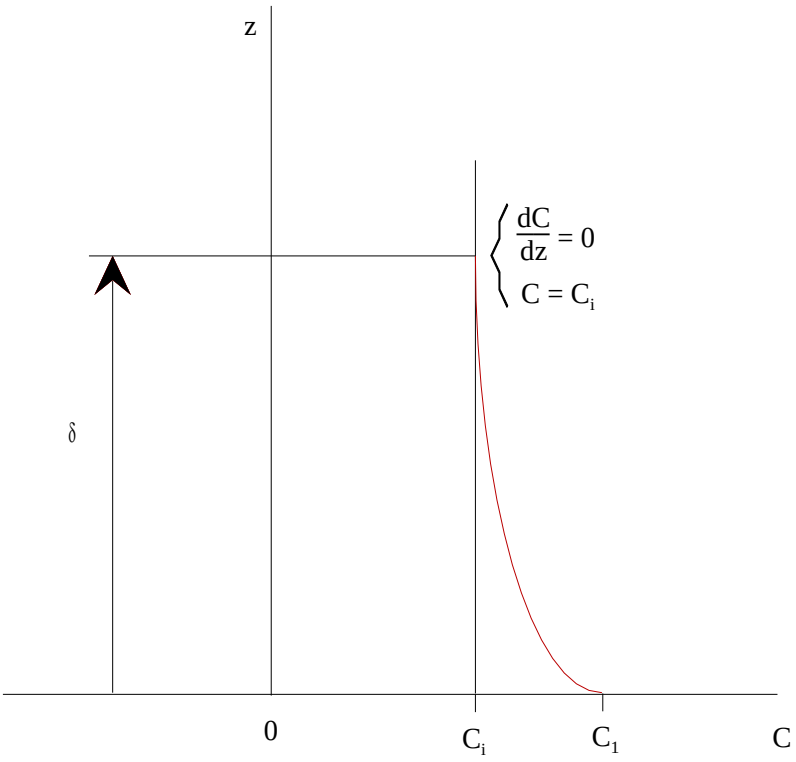

Figure 2 Schematic picture indicating the composition layer (δ) of the fluid flux problem described in this thesis. The composition layer (δ) is represented in the theoretical model by equations [12] and [13] reported also within the bracket in the figure. The red line indicates the concentration profile according to the perturbation of the concentration (C_1) imposed within the porous medium. The z axis indicates the gas flux direction.

where C_i is the initial concentration of the specific gas species within the pores of the medium.

The definition of the composition layer (δ) and the physical conditions described by the equation [7] and [8] are illustrated in the figure 2.

In order to obtain the concentration profile within the semi-infinite homogeneous porous medium, the basic steps mentioned above for the integral method are followed.

The solution of the fluid flux problem is obtained through the computation of the definite integral with respect to the space variable between z = 0 and z = δ of the equation [5]

$$\int_0^{\delta} \frac{\partial}{\partial z}\left(-D\frac{\partial C}{\partial z}+\nu C\right)dz = -\int_0^{\delta}\frac{\partial C}{\partial t}dz \qquad [9]$$

According to the Leibniz's rule for the differentiation of a definite integral whose limits are functions of the differential variables, the equation [9] becomes

$$-D\frac{\partial C}{\partial z}+\nu C\Big|_{\delta} - \left(-D\frac{\partial C}{\partial z}+\nu C\right)\Big|_0 = -\frac{\partial}{\partial t}\left(\int_0^{\delta} C dz - C\Big|_{\delta}\,\delta\right) \qquad [10]$$

where $C|_\delta$ indicates the concentration of the i^{th} gas species at the phenomenological distance δ. Moreover, the following boundary conditions were imposed.

$$-D\frac{\partial C}{\partial z} + \nu C = J \qquad \text{at} \qquad z = 0 \qquad [11]$$

By the definition of the composition layer, at the phenomenological distance (z = δ) the following boundary conditions are satisfied

$$\frac{\partial C}{\partial z} = 0 \qquad [12]$$

and

$$C = C_i \qquad [13]$$

Under the boundary conditions fixed above ([11], [12], [13]), equations [10] simplified as:

$$\nu C_i - J = -\frac{\partial}{\partial t}\left(\int_0^\delta C dz - C\big|_\delta \delta\right) \qquad [14]$$

In order to give an analytical solution of equation [14] a second order polynomial function is chosen to represent the concentration variation along the z axis:

$$C = a + bz + cz^2 \qquad [15]$$

in which the *a*, *b* and *c* coefficients are function of the time and were determined according to the boundary conditions at z = 0 and at the edge of the composition layer z = δ (the equations [11], [12] and [13]). The polynomial function that describes the concentration profile within the porous medium obtained by the substitution becomes

$$C = \frac{J\delta + 2DC_i}{\delta\nu + 2D} - 2\frac{J - \nu C_i}{(\nu\delta + 2D)}z + \frac{J - \nu C_i}{\delta(\nu\delta + 2D)}z^2 \qquad [16]$$

The detailed arithmetical procedure followed to obtain the coefficients of the polynomial function is completely reported in Appendix 4.

Introducing the equation of the concentration profile [16] within the concentration integral equation of the flux problem and performing the indicated computation, the following differential equation is obtained for δ

$$3 = \frac{\partial}{\partial t}\left[\frac{\delta^2}{(\nu\delta + 2D)}\right] \qquad [17]$$

subjects to

$$\delta = 0 \text{ for } t = 0 \qquad [18].$$

The solution of the [17] equations gives

$$\delta_1 = \frac{\sqrt{3}(\sqrt{t(8D + 3t\nu^2)} + \sqrt{3}t\nu)}{2} \qquad [19].$$

According to the equation [14], the concentration profile within the system has been determined by knowing δ. The solution reported above represents the concentration profile for the time lasted between the beginning of the compositional perturbation ($t = 0$) from the lower limit of the porous medium and the time t_δ at which the perturbation reached their upper surface computed according to:

$$t_\delta = \frac{\delta^2}{6D + 3\delta v} \quad [20].$$

The result find in equation [20] will be compared to the experimental measurement of the arrival time (hereafter also named "retention time") of the chemical perturbation as shown in the following.

Experimental study of the transient of chemical composition in the porous medium

In order to check the reliability of the developed model of the chemical composition transients and define the limits of its validity, a set of dedicated laboratory tests has been performed. The tests results allow investigating the relationships between the measurements performed with the continuous H_2-CO_2 experimental system and the degassing processes occurring beneath the earth surface.

The tests have been performed using a gas flux simulator showed in its main components in figure 3. The experimental apparatus is composed by a cylindrical PVC container 280 cm high (hereafter also indicated as FC) with circular cross section (about 50.3 cm^2 cross-sectional area) of 8 cm of diameter, filled of pyroclastic sand collected at the island of Vulcano (Aeolian archipelago). The permeability and the particle sizes features of the sand used to perform the laboratory tests were accurately determined and known.

Throughout each test, the gas flow has been produced from the base of the column using several laboratory gas standards of known chemical composition. The flux of the gas standard has set through a flowmeter placed just before the inlet, at the base of the FC and carefully maintained constant by the pressure gouges array (manometers) connected to the gas tank.

The flux simulator has been provided with several gas sensors to detect the different target species contained in the standard mixtures flowing through the column.

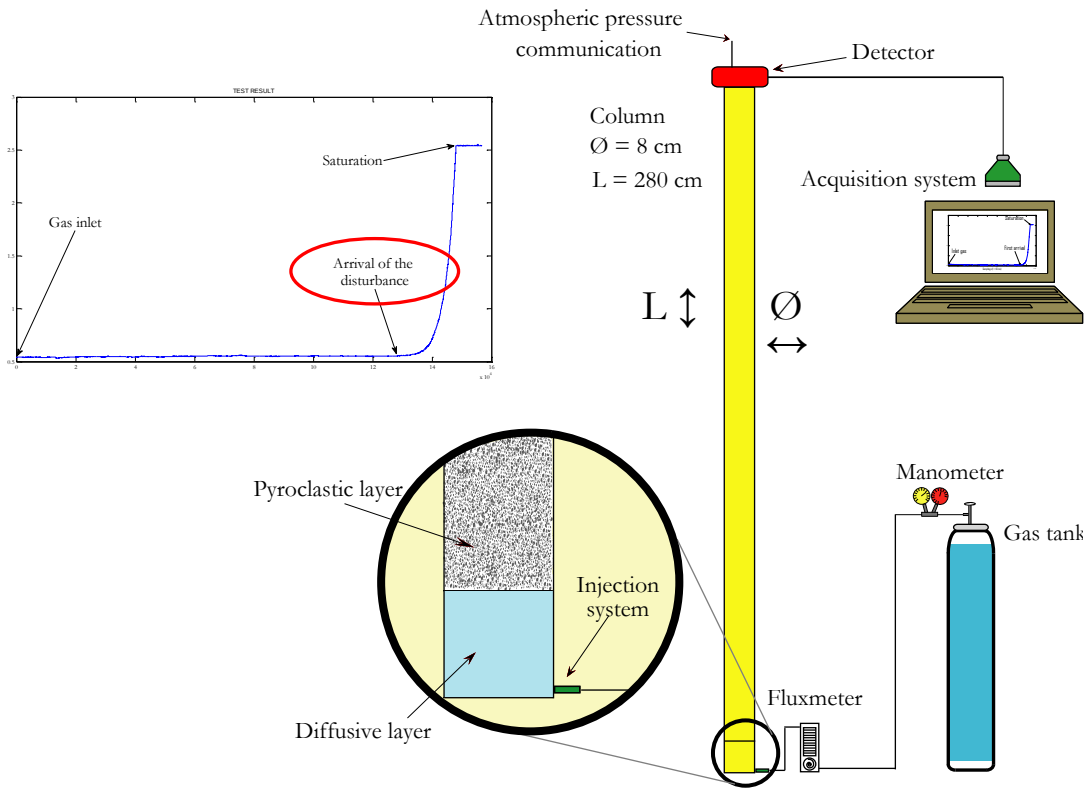

Figure 3 Experimental device used in the laboratory order to test the reliability of the theoretical model proposed to the interpretation of the transient in the chemical composition of the fluid emitted from the soil. The figure depicts the flux simulator made of a PVC tube of diameter 8 cm (cross section 50.2655 cm^2) and high (L) of 280 cm, the gas tank containing the laboratory gas standards, the summit box containing the detector array connected with the computer for the record and storing of the test. The signal of the sensor was acquired sampling at 10 Hz frequency.

The table 1 lists the target gas species investigated throughout the flow experiments and the main features of the sensors placed at the top surface of the column. The sensors are connected to an acquisition computer sampling the signal at 10 Hz. The test are recorded and stored to the data processing.

Table 1 The investigated gas species investigated during the experimental validation of the theoretical model. The table also contains the main features of the sensors placed at the top surface of the column.

Target gas species	Sensor
CO_2	Gascard II – range 0 -1 %
H_2	City Technology H_2 sensor – range 0-200 ppm vol.
He	Alcatel ASM 100 HDS

Among the chemical gaseous species used in the experiments, CO_2 and He are used as pure single component gas standard, which allow studying the relationship between the chemical composition transients and the flux properties operating within the system.

The test results have been compared with the computations made by the theoretical model that describes the transport of a single chemical component within the porous medium.

At the same time, the use of a single component gas standard allows computing the differences between the experimental results and the model predictions, neglecting the possible reciprocal influence of the different chemical species. It is worth nothing that the binary diffusion coefficients of each single gas species in air ($D_{X\text{-}Air}$) have been used for computation of the model retention time-flux velocity curve reported hereafter.

Several multicomponent mixtures, containing the typical gas species found in the volcanic emissions (He, H_2, O_2, N_2, CO, CH_4 and CO_2), are also used to perform the flux tests. The results of these tests allow checking the reliability of the model and understand the limits of its validity in the analysis of the chemical composition transients recorded by the continuous monitoring system of gas emitted from the earth surface.

The tests have been designed and performed with the aim to measure the time (t) of the variation of the gas species concentration at the top surface of the FC simulator produced by the sustained gas flux within the column. According to equation [20], the measured time ($t_{measured}$) represents the experimental time at which the composition layer (δ) defined by the equations [12] and [13] reaches the top surface of the FC.

In the following part of the chapter the time at which the composition layer reaches the top surface of the column will be defined as "*retention time*" of the considered chemical species (H_2 or CO_2) within the flux column, referring to the process of the movement of the gas species occurring within the chromatographic columns.

The figure 4 shows the typical record of the test of the retention time measurements. In the figure, the time zero corresponds to the beginning of the test, since the gas standard starts entering at the constant flux rate at the base of the FC. The figure shows that through the large part of the tests the signal of the sensor remains stable at the value corresponding to the initial concentration of the target species at the top surface of the column. The signal-time curve remains almost constant, showing slight variation produced by the sensor noise. Since the perturbation produced by the gas flux causes the change of the concentration profile, the sensor signal shows a sharp increase, changing the slope of the signal-time curve.

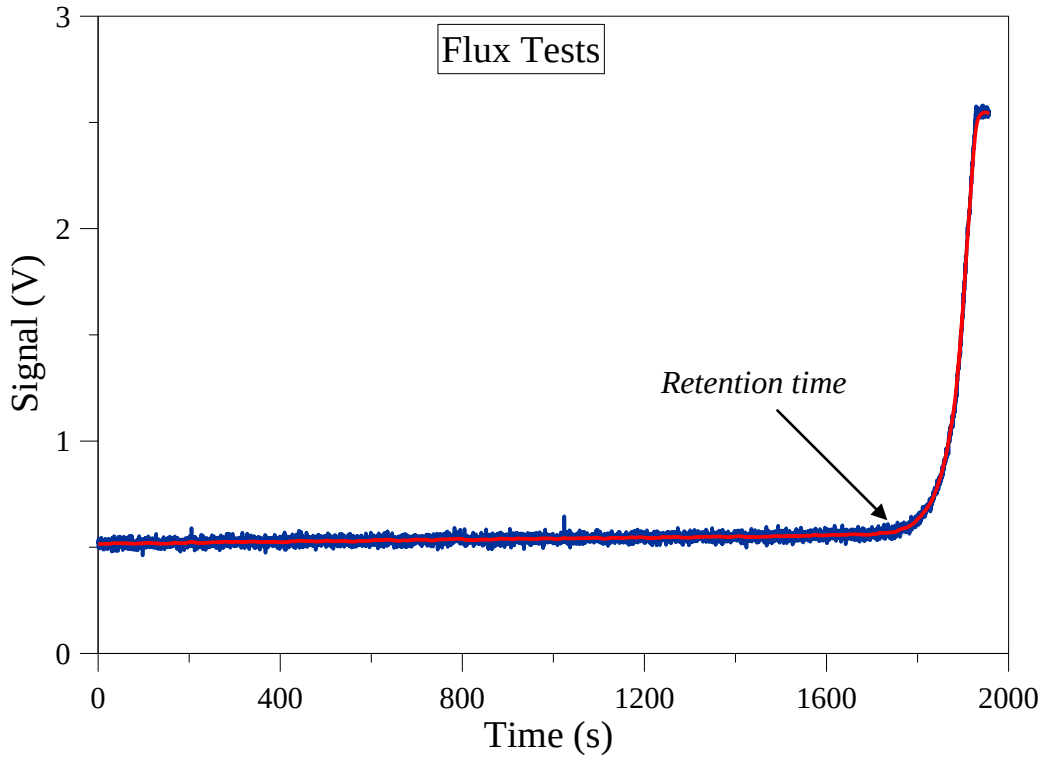

Figure 4 The record of the flux tests performed with the flux simulator. The record of a typical time measurement result shows that the signal of the detectors remains stable at the value corresponding to the initial concentration of the target species until the perturbation produced by the gas flux, set at the base of the column, produces the change of the concentration profile. The dashed vertical line indicates the time of the first change at the summit of the flux column of the concentration of the target gas species. The vertical axis contains the electric signal of the sensor (V), while the horizontal axis contains the time expressed in second. Time zero corresponds to the beginning of the tests when the gas standard start to enter the base of the column showed in figure 3.

The change of the slope of the curve, marked with the vertical dashed line in Figure 4, represents the *retention time* of the chemical species. Each test has been stopped a few minutes later the sharp change of the concentration measured by the sensors.

The tests have been performed at several gas flux values ranging from 10^{-3} to 10^{-1} $cm^3s^{-1}cm^{-2}$ well including the experimental flux interval typically measured in both low temperature fumaroles and soils of volcanic environments. Throughout the tests, the environmental pressure and the temperature conditions have been also controlled.

In order to purify the column from gas pollution, a cleaning procedure has been adopted before each retention time measurement by flushing with air for several minutes. The results of the experiments are showed and discussed in the following.

Laboratory flux test with pure CO_2

In order to study the chemical composition transients produced by the main components of the gas emitted from the soils of volcanic areas, several tests have been performed using pure CO_2 laboratory gas standard. All the tests have been performed in the same experimental conditions described above by changing the gas flux rate (v) within the range 0.004 - 0.11 $cm^3s^{-1}cm^{-2}$, covering the typical range of flux rate found in the soils of the volcanic environments.

In order to obtain accurate measurements of the retention times, the flux rate is a critical parameter of the flux experiments being carefully monitored through a system of flowmeters and pressure gauge (manometers). In detail, above the value of 0.06 $cm^3s^{-1}cm^{-2}$ the flux rate was set using the variable area flowmeter Ky Instrument (range 0 – 0.33 $cm^3s^{-1}cm^{-2}$) having an error of 0.0166 $cm^3s^{-1}cm^{-2}$. The flux rate below 0.06 $cm^3s^{-1}cm^{-2}$ was set most accurately using the Omega Engineering Inc. FMA-114 digital flowmeter (accuracy: 2% of full scale).

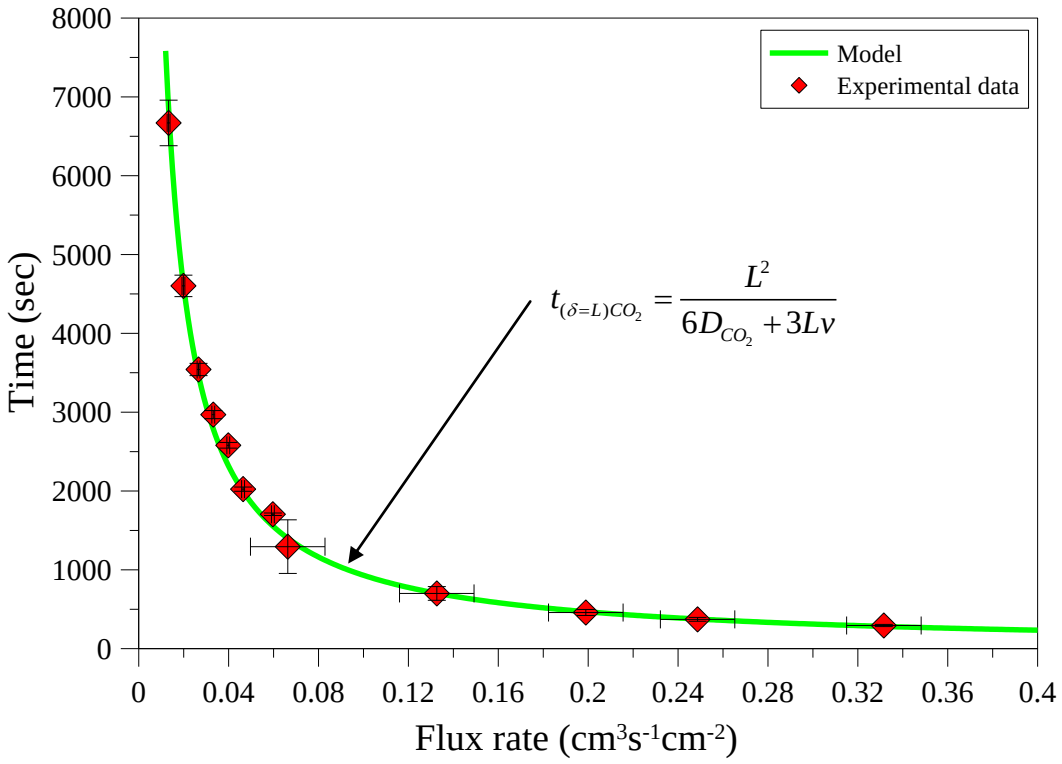

Figure 5 The test results obtained using pure CO_2 (99.99%) to produce the flux into the column. The horizontal axis contains the value of flux rate (v) expressed in $cm^3s^{-1}cm^{-2}$, while the vertical axis shows the corresponding time of the concentration change at the top surface of the column. Green line represents the curve computed according to the theoretical model. Brown diamonds show the retention times experimentally measured by the tests. Time error bar are computed taking into account only the error in the flux rate measurements.

Table 2 Time evaluated (t_{model}) and measured ($t_{measure}$) of the first change of the concentration of the CO_2 target species at the top surface of the flux column. The tests have been performed using pure CO_2 in the typical range of the gas flux velocity (v) found in volcanic areas.

Flux velocity (v) ($cm^3s^{-1}cm^{-2}$)	t_{model} (s)	$t_{measure}$ (s)	χ^2
0.013	6877	6886	0.007
0.020	4620	4602	0.050
0.027	3478	3465	0.047
0.033	2789	2785	0.094
0.040	2328	2301	0.569
0.046	1997	2022	0.449
0.060	1556	1564	0.069
0.066	1412	1310	0.090
0.133	709	705	0.002
0.199	474	461	0.124
0.249	381	377	0.017
0.332	281	290	0.398

The results of the test performed with pure CO_2 are reported in figure 5 showing the curve computed according to the model (green curve) and the retention times, corresponding to the variation of the CO_2 concentrations at the top surface of the column ($t_{measure}$).

The brown diamonds showed in figure 5 represent the retention times measured through the tests ($t_{measure}$) and the superimposed error bars have been computed taking into account only the casual error made in the flux rate measurements. They neglect several effects influencing the measurements of the actual variation of the concentration at the top surface of the column such as the gas losses through the walls of the cylindrical container, the temperature inside the column. Therefore, they represent the minimum errors made throughout the experimental measurements of the retention times.

In order to compare the reliability of the measurements with the computations of the model, the results of the tests performed with the pure CO_2 are reported in Table 2.

The comparison between the model and the experimental data may be performed through the function χ^2 defined as

$$\chi^2 = \frac{(t_{model} - t_{measure})^2}{\sigma^2} \qquad [31]$$

were t_{model} and $t_{measure}$ are the retention times of the target species computed by the model and the times measured by the experiments respectively, while σ represent the error in the time measurements. The agreement between the experimental measurements and theoretical data,

in the range of the experimental error, gives value of χ^2 computed for each test smaller than or equal to 1. The χ^2 computed for the CO_2 show values lesser than 1 for all the gas flux rates chosen to perform the tests.

The data reported in the table 2 as well as the figure 5 show the good agreement within the limits of experimental accuracy between the t_{model} and $t_{measure}$ for all the tests performed with pure CO_2, suggesting that the proposed theoretical model could be used to study the relationships between the chemical composition transients and the flux regime parameters.

Multicomponent mixture

Several tests have been performed using a multicomponent laboratory gas standard containing the typical gas species found in the soil emissions of volcanic areas. The test results have been compared with the model computations in order to check its reliability and discuss the deviations between experimental and theoretical data. The laboratory gas mixture contains He, H_2, O_2, N_2, CO, CH_4 and CO_2 each one having the concentrations specified in the Table 3. Hereafter this laboratory gas standard has been named MGM-mixture.

The MGM-tests were carried out in the same experimental conditions of the test performed with pure CO_2 and described above, choosing different flux rate in the range from 0.004 up to 0.11 $cm^3s^{-1}cm^{-2}$, according to the typical flux rate of the gases emitted from the soils and fumaroles of the volcanic areas. A crucial parameter of the tests was the flux velocity, since the reliability of the experimental measurements of retention times was largely dependent from the accuracy of the flux rate set up. The flux rate of the MGM has been set using a variable area flowmeter Ky Instrument for the tests performed above 0.199 $cm^3s^{-1}cm^{-2}$. The flux rates below 0.199 $m^3s^{-1}cm^{-2}$ were set up using a digital flowmeter Omega Engineering Inc FMA-114 having a specific flux gauge for the measurements of the CO_2 flux.

Table 3 Chemical composition of the Multicomponent Gas Mixture laboratory standard (MGM) used to tests the reliability of the model in the description of the transients of the chemical composition of the soils and low temperature fumarole gases

He (ppm vol)	**H_2 (ppm vol)**	**O_2 (% vol)**	**N_2 (% vol)**	**CO (ppm vol)**	**CH_4 (ppm vol)**	**CO_2 (% vol)**
462	909	20.5	78.1	919	964	1.1

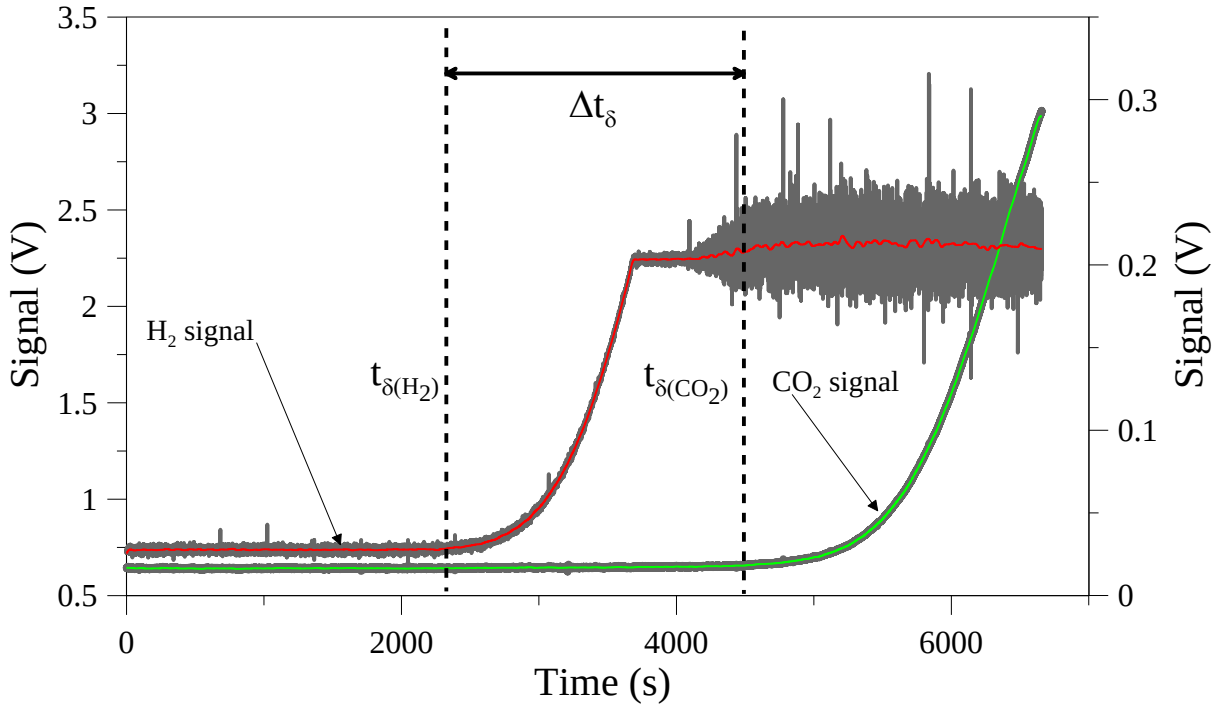

Figure 6 The record of a retention time – flux test performed with the MGM laboratory standard. The red line indicates the record of the City Technologies H_2 sensor, while the green curve indicates the record of the Gascard II CO_2 detector. H_2 and CO_2 species reached the top surface of the column after a distinct retention time indicated with vertical black dashed lines. The time difference between the retention times of both species has been defined "*delay*" time (Δt_δ) resulting from a sort of "chromatographic effect" occurring within the porous medium.

The use of the digital flowmeter to set the flux rate of the MGM within the column required a special calibration by a glass bubble flowmeter having a graduate scale with 1cc resolution in order to carefully measure the absolute flux rate.

During the tests performed using the MGM standard, the top surface of the flux simulator has been provided with both the electrochemical City Technology sensor and the Gascard II to detect simultaneously the variations of both H_2 and the CO_2 concentration respectively.

The typical record of the MGM-tests is reported in figure 6 showing that, neglecting the noise, both the sensors signal remains stable at the value of the starting concentration of the target gas species at the top surface of the column.

The time zero represents the beginning of the test, when the mixture starts entering the base of the column. The red line showed in Figure 6 represents the H_2 sensor signal showing a sharp change of the slope of the concentration-time curve according to the variation of the H_2 concentration profile, produced by the sustained gas flux set at the base of the column. The H_2 signal continues to increase as the H_2 concentration increases at the top surface of the column. At the same time, the CO_2 detector do not shows any variation, remaining steady at the initial

CO_2 concentration. After a *delay* respect to the change of the H_2 concentration, also the CO_2 detector shows the change of the slope of its own concentration-time curve, indicating the change of the CO_2 concentration profile within the column. After a few minutes later the change of the CO_2 concentration profile, the test has been stopped and the data are recorded in the computer acquisition system. The data processing of the record has been aimed to identify the retention times of both chemical species and compute their differences. In the following part of the chapter, the time difference between the retention time of the CO_2 and the H_2 species will be defined as "*delay*".

The very different diffusive features of the respective molecules can explain such a sort of chromatographic effect exhibited by the H_2 and CO_2 species. The chromatographic effect splits the chemical disturbance produced by the multicomponent mixture flowing within the column in concentration waves, each one moving according to the distinct movement capability of the gas species. According to the experimental data, the perturbation of the gas concentration profile within the FC begins when the MGM standard starts to enter from the base of the column. The chemical disturbance, described by the composition layer (δ), reaches the summit of the FC after a time inversely correlated to both the flux velocity (v) and the molecular diffusion coefficient (D_i) a quantity which Fick called "*the constant depending of the nature of the substances*".

The differences between the molecular diffusion coefficients of H_2 ($D^3_{(H_2\text{-Air})} = 0.627\ cm^2s^{-1}$) and CO_2 ($D_{(CO_2\text{-Air})} = 0.160\ cm^2s^{-1}$), produce the *delay* between the individual H_2 and CO_2 retention times. In agreement with the model computations, the change of the H_2 concentration at the top surface of the FC occurred before the CO_2 one.

According to the equation [20], the retention times of each one species is

$$t_\delta = \frac{\delta^2}{6D + 3\delta v} \qquad [20].$$

Therefore, from the theoretical standpoint, the delay between the change of the concentration profile of H_2 and CO_2 species is inversely proportional to the flux rate of the mixture (v) within the column and directly proportional to both the differences between the binary diffusion coefficients of the considered gas species and the length of the theoretical distance of the composition layer (δ), according to equation

[3] The values of diffusion coefficients reported within the text are the binary diffusion coefficient of the species given in the handbook of chemistry and physics T = 293.15 K and P = 101.325 KPa.

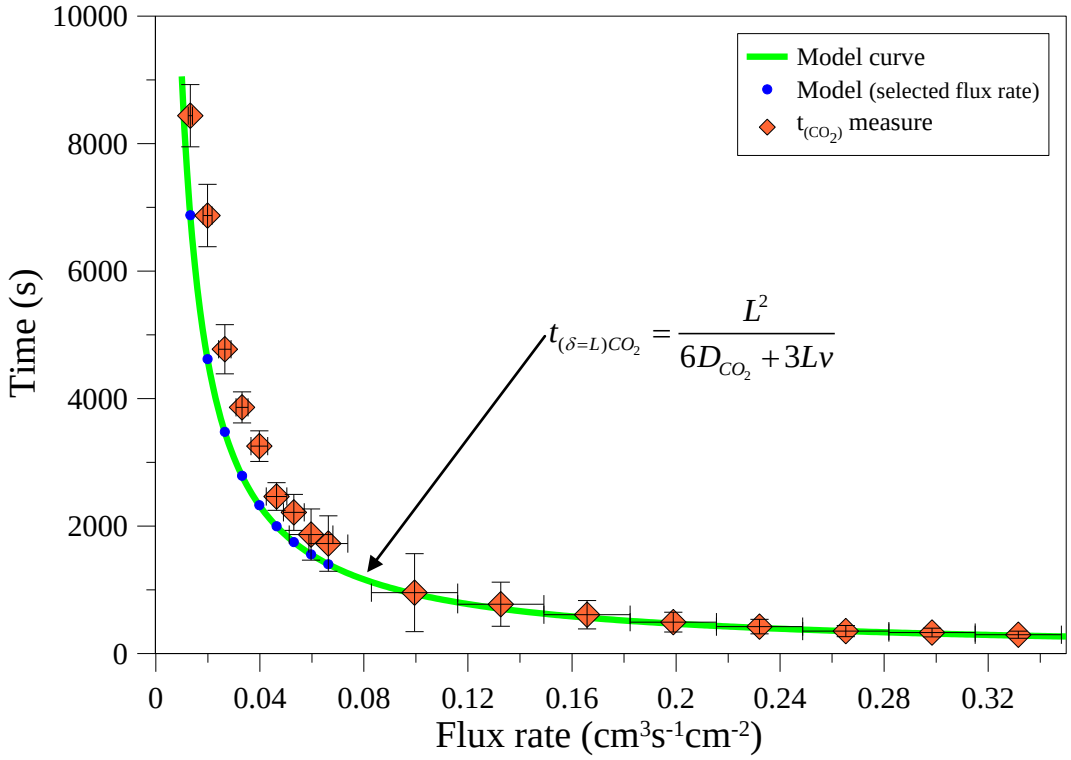

Figure 7 The test results for the CO_2 species obtained using MGM laboratory standard to produce the flux into the column. The horizontal axis shows the value of flux rate (v) expressed in $cm^3s^{-1}cm^{-2}$, while the vertical axis shows the time at which have been recorded the CO_2 concentration changes at the top surface of the flux column. Green line represents the curve computed according to the theoretical model. Orange diamonds show the retention times experimentally measured by the tests. Time error bar are computed taking into account only the error in the flux rate measurements.

$$\Delta t_\delta = t_{\delta(CO_2)} - t_{\delta(H_2)} = \frac{2}{3}\frac{(D_{H_2-air} - D_{CO_2-air})}{(2D_{H_2-air} + \delta v)(2D_{CO_2-air} + \delta v)}\delta^2 \quad [32]$$

The importance of the measurement of the delay between the retention times of both chemicals relies in its direct dependence from theoretical distance (δ) representing the depth of the chemical disturbance source pictured in figure 2 to the natural systems. Therefore, the measurements of the delay between two or more chemicals typical of the volcanic emissions could be usefully employed to further constraint the depth of the gas reservoir.

The retention times, experimentally measured through the tests performed with the MGM standard, are reported in Figure 7 and Figure 8 for CO_2 and H_2 species respectively according to the flux rate of the mixture.

The green line showed in Figure 7 represents the CO_2 retention times computed by equation [20] according to the flux rates of the mixture. The blue spots highlight the t_{model} computed for the tested flux rate, while the orange diamonds show the retention time ($t_{measure}$) obtained from the flux tests. The flux rate of the MGM standard has been set in the range from 10^{-3} to 10^{-1}

$cm^3s^{-1}cm^{-2}$, being values well within the typical range of the flux rate found in volcanic areas. As observed with the pure CO_2, when the flux velocities were set above 0.060 $cm^3s^{-1}cm^{-2}$ the times measured overlap the retention times predicted by the model within the experimental error. Accordingly, the χ^2 values of the CO_2 reported in Table 4 are lesser than 1, suggesting that the model computations agree with the experimental measurements.

The retention times measured setting the flux rate of the MGM standard below the 0.053 $cm^3s^{-1}cm^{-2}$ are systematically larger than the retention times computed by the model and the χ^2 value for the CO_2 χ^2 values reported in Table 4 are larger than 1.

According to the laboratory experiments reported in Figure 5, the larger differences between the experimental data and the model computations have been observed by reducing the flux rate of the MGM standard, since the relative importance of the advective process producing the flux within the column become comparable in its magnitude to the diffusive one, suggesting that the diffusion rate, depending from the chemical features of the mixture, strongly influences the retention times of each chemical species.

Table 4 Experimental data for both CO_2 and H_2 obtained from the flux experiments performed with the MGM laboratory standard. The retention times computed for both species have been reported. The χ^2 values have been computed according to equation [31].

Flux rate ($cm^3s^{-1}cm^{-2}$)	CO_2 t_{model} (s)	CO_2 $t_{measure}$ (s)	H_2 t_{model} (s)	H_2 $t_{measure}$ (s)	CO_2 χ^2	H_2 χ^2
0.332	281	295	280	290	0.063	0.029
0.298	312	330	312	324	0.066	0.035
0.265	351	353	350	328	0.000	0.066
0.232	402	423	400	401	0.036	0.000
0.199	468	493	466	447	0.026	0.016
0.166	562	610	559	557	0.047	0.000
0.133	702	774	697	623	0.043	0.046
0.099	935	955	927	764	0.001	0.071
0.066	1401	1726	1382	1249	0.559	0.093
0.060	1556	1867	1533	1354	0.602	0.198
0.053	1749	2215	1720	1455	2.728	0.885
0.046	1997	2465	1960	1595	4.623	2.808
0.040	2328	3254	2277	1792	14.926	4.086
0.033	2789	3862	2716	1943	19.359	10.034
0.027	3478	4774	3365	2375	11.299	6.601
0.020	4620	6872	4423	2920	21.181	9.427
0.013	6877	8438	6449	3514	10.230	36.178

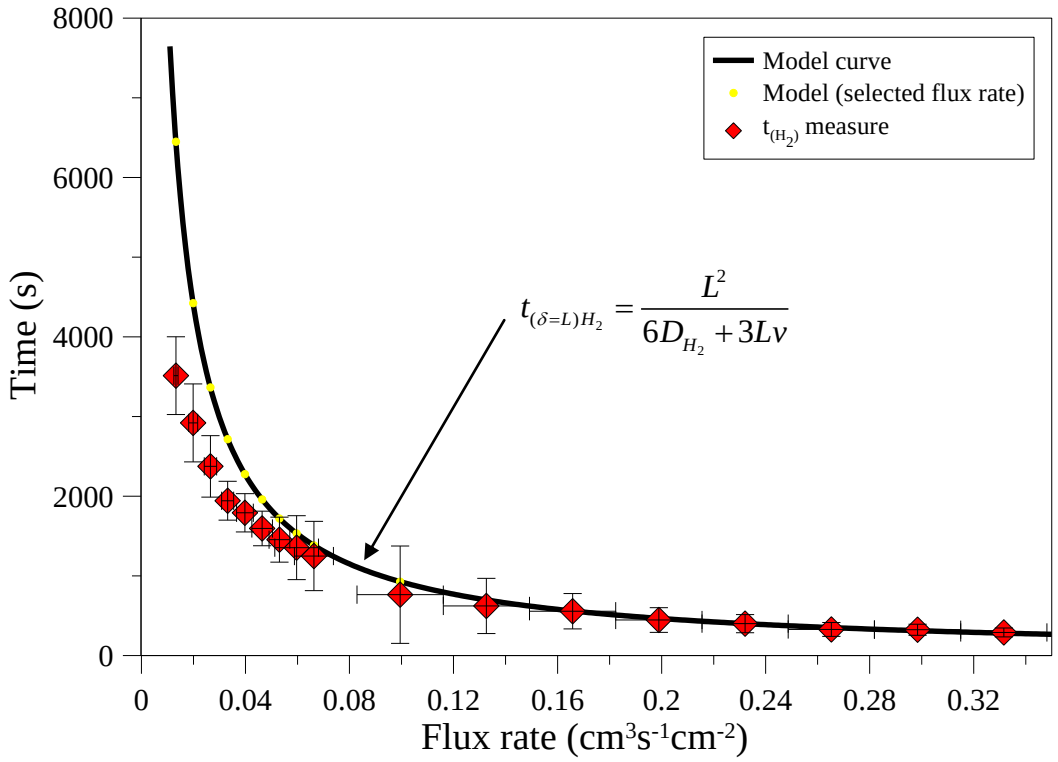

Figure 8 The test results for the H_2 species obtained using MGM laboratory standard to produce the flux into the column. The horizontal axis shows the value of flux rate (v) expressed in $cm^3s^{-1}cm^{-2}$, while the vertical axis shows the time at which have been recorded the CO_2 concentration changes at the top surface of the flux column. Black line represents the curve computed according to the theoretical model, while the red diamonds show the retention times experimentally measured by the tests. Time error bar are computed taking into account only the error in the flux rate measurements.

The test performed with the MGM standard allowed the simultaneous measurements of the retention times of the CO_2 and the H_2 species. In detail, red diamonds in Figure 8 indicate the retention times of the H_2 species according to the flux rate of the MGM standard within the column. The black line represents the curve of retention times of the H_2 computed by equation [20]. The yellow spots highlight the t_{model} computed for the tested flux rates. As be found from the measurement of the CO_2 retention times, the $t_{measured}$ overlap the model curve until the flux rate has been set above 0.053 $cm^3s^{-1}cm^{-2}$, while the experimental data leave from the model computation as the flux rate decrease.

The figure 8 shows that the largest differences between the experimental data and the theoretical model have been observed when the advective process became comparable in its magnitude to the diffusive one. The data of the retention times for the H_2 species within the flux column according to the flux rate have been reported in Table 4 with the proper χ^2 values. The retention times measured for tests performed setting the flux rate below 0.046 $cm^3s^{-1}cm^{-2}$

are systematically smaller than the model computations and the related χ^2 values are larger than 1.

As observed for the retention times of the CO_2, the largest difference between the experimental H_2 retention times and the model computations became larger for low flux rates, since the magnitude of the diffusive process became comparable to the advective one.

The tests results suggest that the diffusive features of the chemical species strongly affect the movement capability of the concentration wave within the flux column, also when the magnitude of the advective process is comparable to the diffusive one.

Summarising, the laboratory tests performed by the MGM standard to produce the flux within the simulator allowed measuring simultaneously the retention times of both H_2 and CO_2 species in the experimental condition closely to the typical composition range of the mixture emitted from the soils of volcanic areas. The results of the measurements indicate that the retention times of both species agree with the computed model curve within the limit of the experimental error since the flux rate of the gas has been set above 0.053 $cm^3s^{-1}cm^{-2}$. As the flux rate of the MGM standard decreases, the retention times of both CO_2 and H_2 species showed interesting difference in comparison to the model computations. In detail, setting the flux rate of the MGM standard below 0.053 $cm^3s^{-1}cm^{-2}$, the H_2 and CO_2 gas species showed different features each other, since the $t_{measure}$ for the CO_2 species are systematically larger than the t_{model}, while the $t_{measure}$ for the H_2 species are smaller than the t_{model}.

Moreover, further constraints on the retention times of the CO_2 species could be obtained by the comparison of the MGM-tests results, reported in Table 4, with the retention times measured with the pure CO_2, reported in Table 2. The comparison shows that, in the range of the lower flux rate investigated, the retention times for the CO_2 species measured through the tests performed with the MGM are larger than the $t_{measure}$ obtained using the pure CO_2, suggesting that compositional effects of the mixture could affect the retention times of the species making the MGM standard.

According to equation [20], the diffusive component of the flux process, described by the bulk diffusion coefficient, is generally smaller than the advective one, increasing their relative magnitude as the flux rate decreases. Since the difference between the measured retention times and the model computations became larger for low flux rate (v), the compositional effects must be taking into account in order to explain the difference between the experimental data and the model computations. As mentioned before, the binary diffusion coefficients of H_2 and CO_2 in air have been used in the computation of the retention time-flux rate curves reported in Figure 7 and Figure 8, as well as in the Figure 5 containing the tests

performed with pure CO_2. In the latter case, the diffusion coefficient of CO_2 represents the actual diffusivity of the CO_2 into the air filling the pore of the FC sands. In this case, the model computations are in agreement with the measured retention times. Instead, the binary diffusion coefficients do not represent exactly the actual diffusivity of both H_2 and CO_2 into FC using the MGM standard, since multicomponent effects develop among the species making the mixture. According to Cussler (1997), the multicomponent effects are larger when the mixture is concentred or contains interacting species. In general, these interactions can originate from chemical reaction, from electrostatic coupling or from major differences in molecular weights, as in the case of CO_2 and H_2. Several authors (Krishna and Wesseling, 1997) proposed different equations taking into account the multicomponent effects in the evaluation of the diffusion coefficients of the chemicals making the mixtures. The complexity of the computations needed to solve the multicomponent diffusion problem prevented in most cases the theoretical evaluation of the diffusion coefficient in system with more than three or four components.

In our case dealing with a system of several components, the compositional effects on the retention times of each single species are experimentally evaluated through a dedicated test series. The tests have been performed using several mixture obtained by dilution of MGM laboratory gas standard with pure CO_2. As a consequence, different mixtures with different CO_2 and the H_2 concentrations have been produced (Mixture 1, Mixture 2, Mixture 3, Mixture 4). The chemical compositions of these gas mixtures have been accurately determined by chromatographic analysis performed with the Perkin Elmer Clarus 500 having Shincarbon ST 100/120Mesh 3m x 1/8" OD column and listed in table 5.

Table 5 Chemical composition of the mixtures obtained from the dilution of the MGM laboratory standard with pure CO_2. The chemical compositions of the mixtures have been determined from chromatographic analysis with the Perkin Elmer Clarus 500 having Shincarbon ST 100/120Mesh 3m x 1/8" OD column.

Name	**He** (ppm vol)	**H_2** (ppm vol)	**O_2** (% vol)	**N_2** (% vol)	**CO** (ppm vol)	**CH_4** (ppm vol)	**CO_2** (% vol)
MGM Standard	462.7	909.2	20.5	78.07	919.9	964.5	1.1
Mixture 1	245	413	12.35	50.50	411	429	37.42
Mixture 2	194	317	7.46	29.91	334	352	62.72
Mixture 3	117	190	4.50	17.92	205	215	76.37
Mixture 4	64	134	0.19	8.09	146	162	91.94

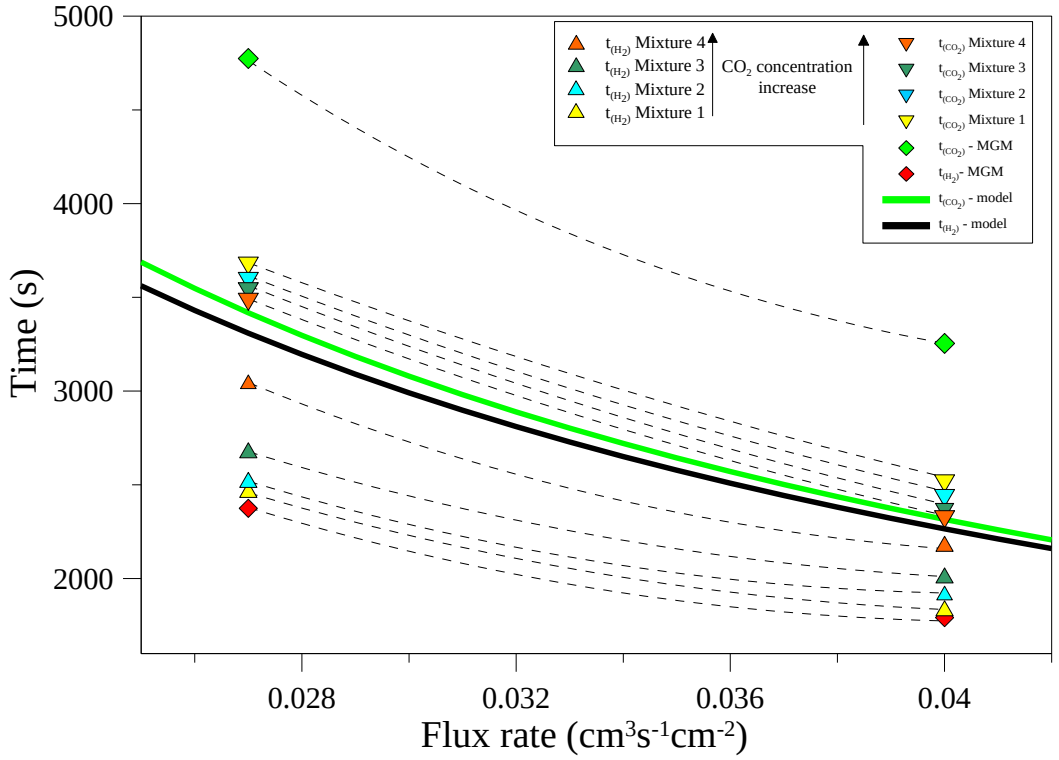

Figure 9 The test results for the CO_2 species obtained using MGM laboratory standard to produce the flux into the column. The horizontal axis shows the value of flux rate (v) expressed in $cm^3s^{-1}cm^{-2}$, while the vertical axis shows the time at which have been recorded the CO_2 concentration changes at the top surface of the flux column. Blue line represents the curve computed according to the theoretical model. Green diamonds show the retention times experimentally measured by the tests. Time error bar are computed taking into account only the error in the flux rate measurements. Black arrows indicate the increases of the CO_2 concentration within the mixture, having the MGM as the CO_2-poor extreme and the Mixture 4 as the CO_2-rich one. The red and green diamonds indicate the $t_{measure}$ obtained from the tests performed with the MGM standard. The yellow triangles indicate the retention times measured using the Mixture 1, blue triangles Mixture 2, green triangles Mixture 3 and orange triangle Mixture 4, the CO_2 concentration ranging from 1% vol. up to 92% vol. The triangles with the apex pointing up indicate the measured retention times for the H_2 species, while the apexes pointing down indicate the measured retention times for the CO_2

The tests have been performed setting the flux rate of the mixture to 0.027 $cm^3s^{-1}cm^{-2}$ and 0.04 $cm^3s^{-1}cm^{-2}$. The results of the tests are reported in Figure 9 showing the retention times of both the H_2 and CO_2 species according to the gas flux rate. The green and black curves represent the retention times predicted (t_{model}) for the CO_2 and the H_2 respectively. The red and green diamonds indicate the $t_{measure}$ obtained from the tests performed with the MGM standard, while the triangles indicate the tests performed with the four gas mixture. In detail, yellow triangles indicate the retention times measured using the Mixture 1, blue triangles Mixture 2, green triangles Mixture 3 and orange triangle Mixture 4, the CO_2 concentration ranging from 1% vol. up to 92% vol. Moreover, the triangles with the apex pointing up

indicate the measured retention times for H_2 species, while the apexes pointing down indicate the measured retention times for CO_2.

Figure 9 show that, keeping constant the flux rate, the retention times of both the CO_2 and the H_2 species change according to the chemical compositions of the mixture. The retention times measured for the CO_2 using the intermediate composition mixtures (Mixture 1- Mixture 4), changed between the model curve (as the lower extreme) and the retention times measured using the MGM, showing the largest differences in comparison to the model curve. It is worth noting that the MGM represents the CO_2-poor end-member of the compositional range investigated.

As observed for the retention times of the CO_2, the $t_{measure}$ of the H_2 species change according to the composition of the gas mixture. The largest difference between the model curve and the experimental data has been observed using the MGM, while the lower ones have been observed in the case of the Mixture 4.

The variations of the retention times setting the flux rate at 0.04 $cm^3s^{-1}cm^{-2}$ have the same features of the ones observed setting the flux rate at 0.027 $cm^3s^{-1}cm^{-2}$ suggesting that the relationship observed between the variation of the measured retention times and the variation of the chemical composition of the gas mixtures were independent from the flux rate investigated.

The retention times measured for both the CO_2 as well as the H_2 species using the starting mixtures having intermediate compositions (Mixture 1, Mixture 2, Mixture 3 and Mixture 4) allow the evaluation of the differences between the experimental data and the model computations. In Figure 10, the retention times of the CO_2 are reported according to the CO_2 concentration within the mixtures. The dashed lines indicate the retention times computed according to equation [20] for each flux rate set to perform the tests. The figure shows that the retention times measured by the MGM standard are larger than the retention times computed by the model. Moreover, the difference $t_{measured}$-t_{model} exceeds the experimental uncertainty.

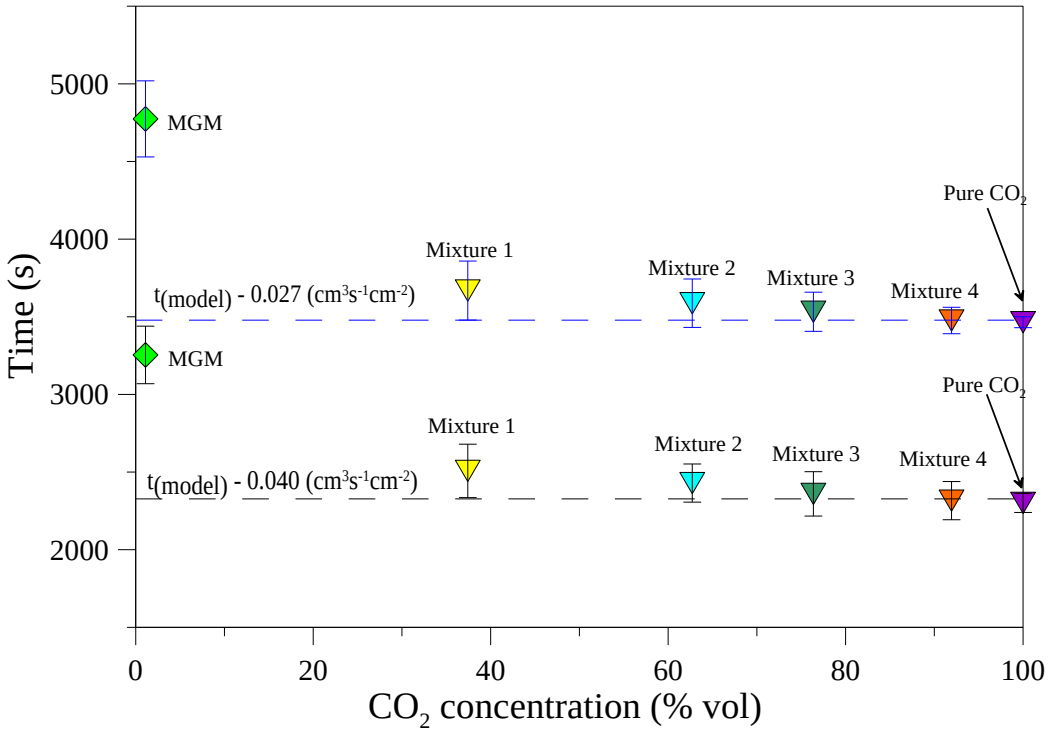

Figure 10 The retention time – composition relationship. The dashed lines indicate the CO_2 retention times according to equation [20] for both the flux rate investigated. The CO_2 retention times have been measured using the mixture of intermediate composition between MGM and pure CO_2 laboratory standards (Mixture 1, Mixture 2, Mixture 3 and Mixture 4). The retention time of the pure CO_2 are also reported. The error bars are computed according to the accuracy of the flux rate measurements.

According to the enhancement of the CO_2 concentration within the mixture, the retention times decrease approaching the model predictions since the CO_2 concentration in the mixture is larger than 40 vol %. The smallest difference between the experimental data and the model computation have been recorded when the pure CO_2 has been used to produce the gas flux within the column (see figure 3). The retention times measured setting the flux rate to 0.04 $cm^3s^{-1}cm^{-2}$ showed the same composition dependency observed setting the flux velocity to 0.027 $cm^3s^{-1}cm^{-2}$ suggesting that the relationships between the retention times and the composition of the starting mixture was independent form the flux rate within the column. It is worth nothing that, being produced by dilution of the MGM standard by pure CO_2, the mixture having the highest CO_2 concentration at the same time was the H_2-poor (Mixture 4).

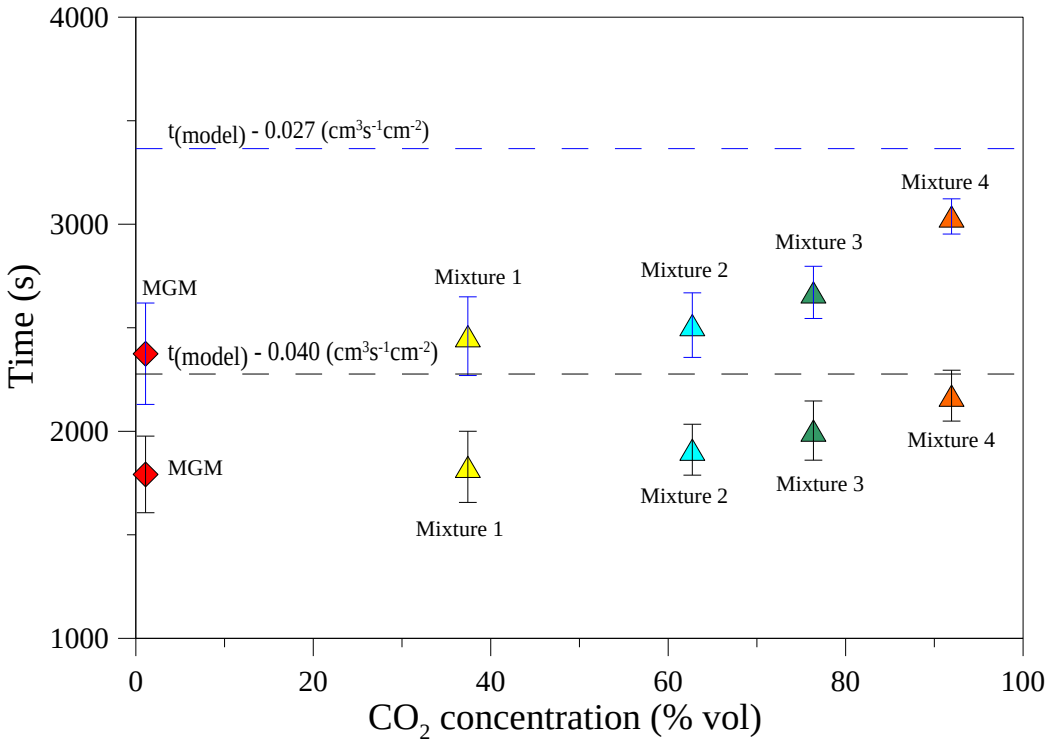

Figure 11 The retention time – composition relationship. The dashed lines indicate the H_2 retention times according to equation [20] for both the flux rate investigated. The H_2 retention times have been measured using the mixture of intermediate composition between MGM and pure CO_2 laboratory standards (Mixture 1, Mixture 2, Mixture 3 and Mixture 4). The error bars are computed according to the accuracy of the flux rate measurements.

The Figure 11 shows the retention times measured for the H_2 according to the CO_2 concentration within the starting mixture. The triangles indicate the experimental retention times measured with the mixture of intermediate composition obtained by dilution of MGM with pure CO_2 (Mixture 1, Mixture 2, Mixture 3 and Mixture 4). The chemical compositions of the intermediate mixture are reported in Table 5. The black and blue dashed lines indicate respectively the retention times of the H_2 species computed according to equation [20], setting the flux rate to 0.04 $cm^3s^{-1}cm^{-2}$ and 0.027$cm^3s^{-1}cm^{-2}$ respectively.

The Figure 11 shows that the retention time of the H_2 species increases according to the enhancement of the CO_2 concentration within the mixture. The predicted H_2 retention times agree with the H_2 experimental measurements since the CO_2 concentration within the mixture was above 90 vol %. at least in the case of the test performed setting the flux rate to 0.04 $cm^3s^{-1}cm^{-2}$. The variations of the retention times setting the flux rate at 0.04 $cm^3s^{-1}cm^{-2}$ have the same features of the ones observed setting the flux rate at 0.027 $cm^3s^{-1}cm^{-2}$, suggesting that the relationship observed between the variation of the measured retention times and the

variation of the chemical composition of the gas mixtures were independent from the flux rate investigated.

The retention times of the H_2 and CO_2 species measured through the laboratory experiments performed with pure CO_2, MGM standard and the mixtures of intermediate composition (Mixture 1, Mixture 2, Mixture 3 and Mixture 4) indicate that the theoretical model proposed in this thesis allow accounting the differences between the temporal variations of the CO_2 and H_2 concentrations in CO_2 rich gas emissions. In detail, the agreement between the model computations and the experimental data has been observed since the CO_2 concentration was above the 40 % vol. and the H_2 concentration below 100 ppm vol. These chemical features of the flowing mixtures are well within the typical compositional range of the gases emitted from the soils and the fumaroles of volcanic areas.

The comparison between the retention times of the CO_2 species measured by the tests performed using the MGM standard and the pure CO_2 suggest that compositional effects of the mixture could produce the observed differences between the experimental data and the model computations and their order of magnitude could be estimated by comparing the tests results.

The flux tests using pure hydrogen as single diffusing species have been prevented due to the hazards in the employment of high concentration hydrogen-containing mixtures. Since the He molecules have several physical features, as the atomic weight and the diffusion coefficient ($PA_{He} = 4$; $D_{He\text{-}Air} = 0.58$ cm^2s^{-1}), comparable to the features of the H_2 ones ($PM_{H_2} = 2$; $D_{H_2\text{-}Air} = 0.672$ cm^2s^{-1}), it has been used in order to evaluate the average size of the experimental retention times of the H_2 single species.

As reported in table 1, the portable mass spectrometer Alcatel ASM 100 HDS has been used to measure the variations of the He concentration at the top surface of the FC in order to measure the retention times according to the flux rate of the He within the column. The laboratory experiments were carried out setting the flux rate in the range 0.004 - 0.11 $cm^3s^{-1}cm^{-2}$, according to the typical flux velocity of the gases emitted from the soils of volcanic areas.

As mentioned before, a critical parameter of the tests was the gas flux rate, since the reliability of the experimental measurements was largely dependent from the accuracy of the flux rate set up. The set up of the He flux rate has been performed using the variable area flowmeter Ky Instrument for the tests performed above 0.199 $cm^3s^{-1}cm^{-2}$. The flux rate below 0.199 $m^3s^{-1}cm^{-2}$ were set up using a digital flowmeter Omega Engineering Inc FMA-114 requiring a calibration with a soap bubble flowmeter to carefully measure the He flux.

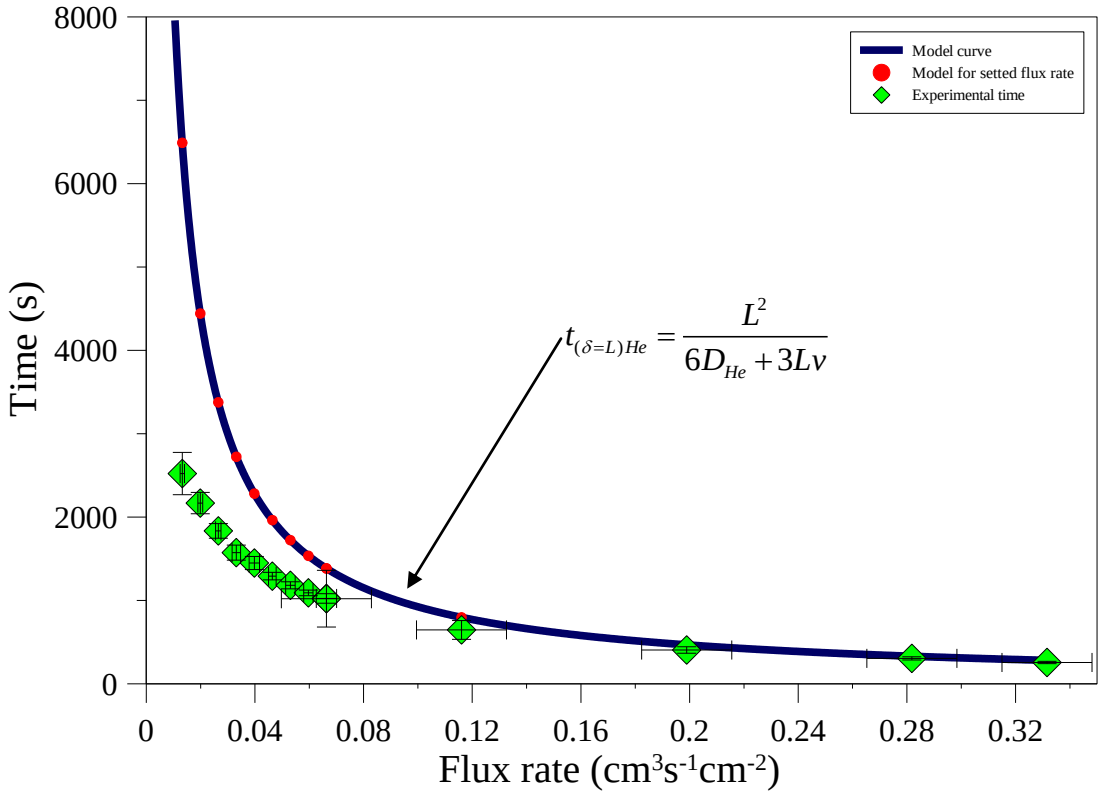

Figure 12 The results of the tests obtained using pure He (99.99%) to produce the gas flux into the column. The horizontal axis shows the value of flux velocity (v) expressed in $cm^3s^{-1}cm^{-2}$, while the vertical axis shows the corresponding first arrival time of the concentration change at the summit of the column. Blue line represents the curve obtained from the theoretical model. Green diamonds are the time of the first change of the concentration experimentally verified by the laboratory tests.

The results of the He-tests are shown within the Figure 12. The blue curve describes the He retention time computed according to equation [20] for each imposed flux rate. The red spots superimposed on the blue curve highlight the retention times (t_{model}) calculated according to the selected flux rate. The retention times measured experimentally ($t_{measure}$) are shown with the green diamonds. The error bars have been computed according to the accuracy of the He flux rate set up.

The accuracy of the model in the computation of the He retention times could be evaluated through the comparison of the data reported in Table 6. According to relation [31], the values of the χ^2 function smaller than 1 suggest that the measured retention times agree with the model computations when the flux rate was set above of 0.116 $cm^3s^{-1}cm^{-2}$ ($\chi^2<1$).

Table 6 Times evaluated (t_{model}) and measure ($t_{measure}$) of the change of the concentration of the He target species at the summit of the FC. The tests have been performed using pure He in the interval of flux rate (v) covering the typical range found in volcanic areas.

Flux velocity ($cm^3s^{-1}cm^{-2}$)	t_{model} (s)	$t_{measure}$ (s)	χ^2
0.013	6489	2522.2	244.904
0.020	4441	2167.8	314.369
0.027	3376	1834.6	306.760
0.033	2723	1573.4	161.742
0.040	2281	1449.2	112.121
0.046	1963	1292	222.073
0.053	1722	1181.4	163.268
0.060	1535	1091.2	172.011
0.066	1384	1024.2	0.953
0.116	796	1052	0.719
0.199	466	701	0.648
0.282	304	435.4	9.541E-05
0.332	280	304.7	0.105

The χ^2 values evaluated for the tests performed setting the flux rate below 0.060 $cm^3s^{-1}cm^{-2}$ are larger than 1 and the $t_{measure}$ are systematically smaller than the t_{model}, as can also be observed from Figure 12. The data reported in the Table 6 and pictured in Figure 12 suggest that the model well predicts the He retention times when the flux rate of the gas was higher than 0.066 $cm^3s^{-1}cm^{-2}$. The differences between the model computations and experimental data observed at lower flux rate increase as the diffusion process becomes the main transport process acting within the system.

Discussion

Laboratory experiments have been performed to check the reliability of the theoretical model describing the concentration transient of the gas species through the porous media and define the limits of its validity. The laboratory experiments allowed measuring the retention times according to equation [20].

The experimental data show that the retention times measured with pure CO_2 agree with the model predictions in the full range of the flux rates investigated. The observed differences using the MGM standard could be explained through compositional effects modifying the retention times of the species. Compositional effects reported in the literature as *solvent effect* (Dietz, 1996) are known to produces the shifting of the retention times in chromatographic applications.

Interesting differences have been observed between the retention times measured for the lighter gas species investigated (He and H_2) and the model predictions. The tests results showed that setting the flux rate below 0.066 $cm^3s^{-1}cm^{-2}$, both the He and H_2 retention times are systematically lower than the model predictions, while data agreement has been observed above the flux rate of 0.066 $cm^3s^{-1}cm^{-2}$ for all the species investigated.

According to equation [20], the role of the diffusion in the gas transport process becomes larger as the flux rate decreases. Since the larger deviation of the experimental data from the model computation have been observed in the range of the lower flux rate investigated, the diffusion process seems to be the main responsible of the higher mobility of both H_2 and He species. The experimental results suggest that the diffusion process play an important role in the transport of the gases within the porous media and the high diffusivity of the lighter species could explain the observed differences between the He and H_2 retention times and the model predictions. The data suggest that the high diffusivity sharply reduces the retention times of the lighter species in comparison to the model computation.

One of the main goals of this thesis has been the study of the *delay* between the variations of both the H_2 and CO_2 concentrations measured with the H_2-CO_2 experimental system in the gas emitted from volcanic areas. This purpose requires the accurate knowledge of the actual retention times of both gas species.

The relationships between the retention time of CO_2 and the chemical compositions of the mixtures suggest that the model well explain the transient of the CO_2 concentration in the CO_2-rich gas emissions. Therefore, the calculated CO_2 retention times well reproduce the observed one.

Differently from the CO_2, the experimental data indicate that the retention times of the H_2 species agree with the model predictions until the H_2 concentration was below 100 ppm vol. in CO_2-rich mixtures.

The deviations of the H_2 retention times from the model predictions must be exactly verified by performing flux tests with pure H_2. However, the diffusivities features of the He are comparable to the H_2 ones and the results of the tests carried out with pure He can be used to evaluate the deviations of the measured retention times for H_2 species from the model computations.

The differences between the He experimental results and the model predictions can be computed considering the ratio between the measured retention time ($t_{measure}$) and the corresponding values obtained by equation [20] (t_{model}).

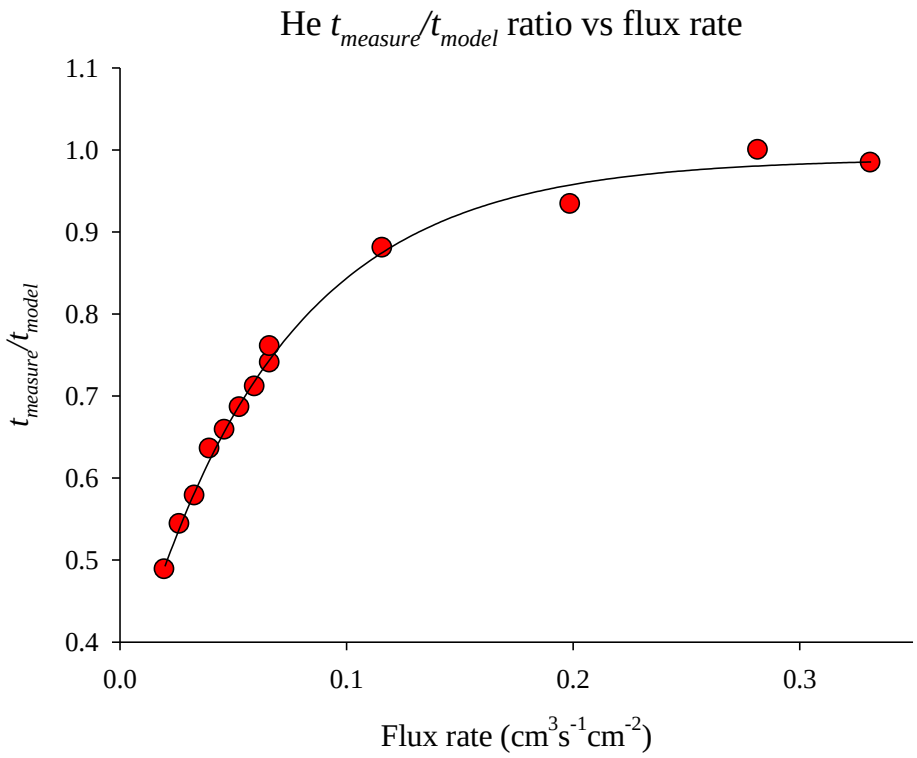

Figure 13 The relation between the $t_{measure}/t_{model}$ ratios according to the flux rate of the mixture. The fitting curve obtained from nonlinear regression is also showed ($R^2 = 0.995$).

The ratios are reported in Figure 13 showing that the $t_{measure}/t_{model}$ ratio increases according to the flux rate within the column. The Figure 13 also shows the fitting curve of the $t_{measure}/t_{model}$ ratios described by

$$(t_{measure}/t_{model}) = 0.3157 + 0.6739 \cdot (1\text{-}\exp(-15.2934 \cdot v)) \quad [33]$$

Since the diffusivity features of the He are comparable to the H_2 ones, the $t_{measure}/t_{model}$ ratio obtained from He experimental results could be revealing of the $t_{measure}/t_{model}$ ratio of the lighter species, including H_2. As mentioned before, the $t_{measure}/t_{model}$ ratio provides the size of the difference between the experimental data from the model prediction for each tested flux rate. Therefore, the fitting curve computed by equation [33] provides a measure of the deviations of the retention times of the lighter species from the model predictions according to the full range of the flux rate investigated.

The use of the $t_{measure}/t_{model}$ ratios obtained from the He tests, combined with the retention times predicted by the model for H_2 species, provides an experimental curve which represents the computed H_2 retention times according to the deviation of the lighter species from the model predictions. This curve can be computed multiplying the retention times predicted by equation [20] for the H_2 species to the $t_{measure}/t_{model}$ ratio computed by equation [33] according to the distinct flux rates (v).

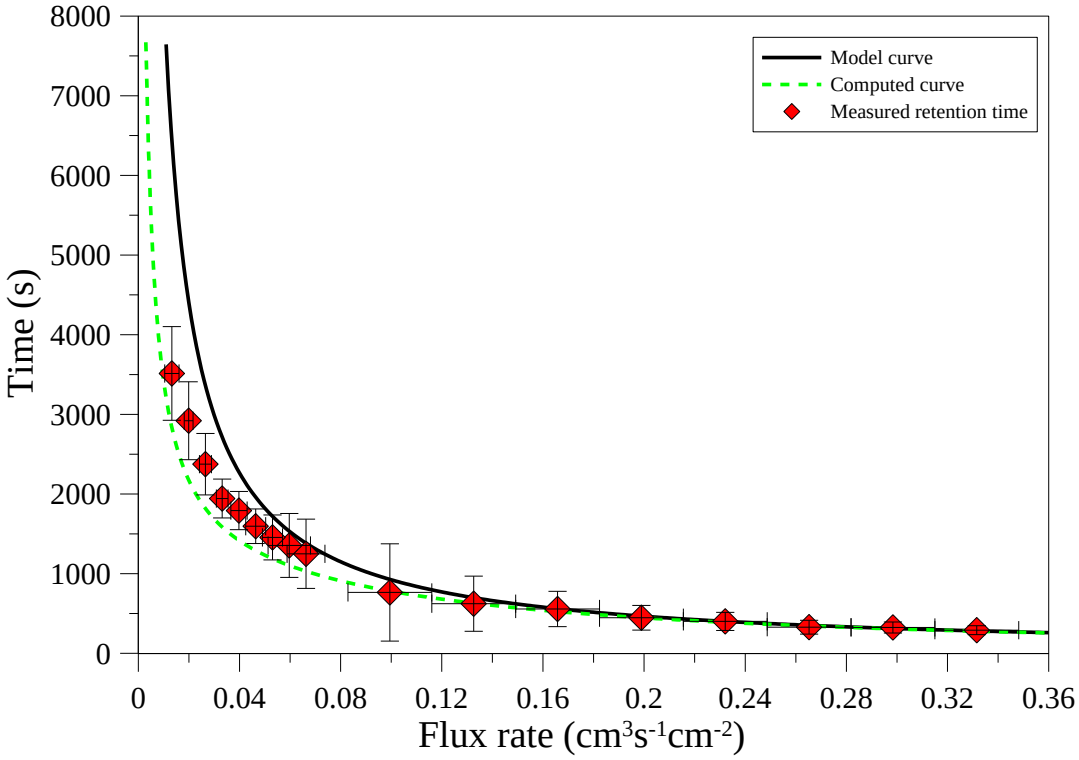

Figure 14 The test results for the H_2 species obtained using MGM laboratory standard to produce the flux into the column. Black line represents the curve computed according to equation [20], while the red diamonds show the retention times experimentally measured for H_2 species. The time error bars are computed taking into account the error made in the flux rate measurements. The green dashed curve represents the average H_2 retention times experimentally obtained according to the average deviation of the lighter species from the model predictions.

The green dashed line reported in Figure 14 shows the experimental relationship between the retention time and the flux rate for the H_2 species. The black curve has been computed according to equation [20] for H_2 species, while the red diamonds indicate the H_2 retention times experimentally measurement by the MGM-tests.

The figure 14 shows the agreement between both curves in the range of higher flux rates and the divergence as the flux rate decreases. As mentioned above, the experimental H_2 retention times agree with the model computations above the 0.066 $cm^3s^{-1}cm^{-2}$. Within the range of the flux rate below 0.060 $cm^3s^{-1}cm^{-2}$, the H_2 retention times measured by the MGM-tests move away from the theoretical curve (black curve) towards the experimental one (green dashed curve) suggesting that the retention times of the H_2 species, with the H_2 concentration of the mixture above 100 ppm vol., may be lower than the model predictions (an average about 25%). These wide differences in the retention times of the lighter gas species must be accounted in the computation of the delay between the concentration transients of different chemical species.

In comparison to both the theoretical model and the data acquired through the laboratory experiments, the variations of the chemical composition of the mixture released from the gas reservoir can be recorded with a *delay* between the concentration transients of each species making the mixture. A simple mechanism producing the delay can be briefly depicted as follow:

- The variation of the chemical composition of the mixture released from a gas reservoir produces a *composition wave* moving towards the surface through the porous medium.
- According to the diffusivity features of each single gas species, the composition wave splits in several *concentration waves* producing the transients of the concentration of each gas species making the mixture. This separation in concentration waves can be conceived like the separation process occurring within the chromatographic columns.
- Each *concentration waves* reaches the surface according to the proper retention time within the porous medium, depending on the distance between the reservoir and the surface (δ), the flux rate (*v*) and the effective diffusion of the considered species (D).
- The chromatographic separation of the mixture released from the reservoir in its own components will be recorded through the monitoring of the gas released from the surface through asynchronous variations of the concentration of different gas species.

Summarising, the theoretical model proposed in this thesis describes the chemical composition transients on the basis of the transport processes of a single gas species through semi-infinite porous media. The concentration integral equation has been obtained combining the equation of continuity with the advective-diffusion equation. The solution of the differential equation has been obtained applying the integral method to the flux problem, an approximate analytic method for the solution of the differential equations that has been successfully applied to the solution of the heat conduction (Ozisik, 1980; Mohamed 1993) as well as the fluid problem into the fractured rocks (Wu and Puess, 2000). The obtained solution shows mathematically that the retention time of the gas species within the porous medium is rightly dependent from the distance between the reservoir and the surface. At the same time it is inversely correlated to both the advective flux rate and the diffusion coefficient of the chemical species. Our model is formulated for single chemical species, each species of multicomponent systems following the proposed equation [20].

Our theoretical model has been experimentally checked through the simulation of the gas flux within the column filled with pyroclastic sand.

The test results showed that the experimental data obtained by using the CO_2 as a single component flowing within the column reproduce the model computations in the full range of the flux rate investigated.

Several tests have been done in order to check the reliability of the model in the prediction of the retention times of the typical gas species making the multicomponent mixtures emitted from fumaroles and soils of volcanic areas. The experimental results showed differences between the model computations and the retention times of the lighter gas species as the H_2 in multicomponent system. Moderate difference has been observed when the compositional effects of the mixtures flowing within the column produce sharp change of the diffusive features of the chemical species, because in our computation have been used the binary diffusion coefficients. A set of dedicated tests, aimed to check the relationships between the mixture composition and the retention times, indicated that the model agree with the experimental observations when the CO_2 is the main component of the mixture and the H_2 the minor one in terms of abundance. The compositional conditions described before agree with the typical chemical compositions of the gas emitted from fumaroles and soils of volcanic areas.

CONCLUSIONS

The relationships between the temporal variations of the chemical composition of volcanic gases emitted from soils and the dynamics occurring in underground magma has been investigated in this thesis.

In order to shed light these connections, a theoretical model has been formulated, developed and proposed as a tool explaining the asynchronous concentration transients for different gas species observed in the emission from crater areas of active volcanoes . The model, describing the chemical composition transients of the fumarolic gases as well as the soils gases of volcanic, geothermal and seismic areas, has been also experimentally validated. Moreover, a pioneer system for H_2 concentration (hydrogen fuel cell-based detector) and CO_2 flux measurements (Gascard II-based detector) has been designed, tested in laboratory and used for H_2 and CO_2 continuous monitoring on Mount Etna and Stromboli volcanoes.

The rigorous laboratory qualification procedure aimed to tune the RewPower Hydrogen Fuel Cell as H_2 detector indicated that the best setting conditions among resolution, response time and linearity of the signal output are obtained by using a 500 ohm resistor applied to the electric circuit of the sensor. The results of the qualification procedure indicated that the H_2 detector has sensitivity 0.2 mV per ppm vol. of H_2, resolution of ~10 ppm vol., accuracy of ± 5 ppm vol and response time below 300 seconds. The tests, repeated in different atmospheric pressure and room temperature conditions, indicated that the cross sensitivity effects made by variations of the working conditions are lesser than 10% of the H_2 concentration read by the sensor.

Several tests aimed to check the cross-sensitivities effects on the H_2 sensor, have been performed changing the H_2 dilution matrix as well as by using several reducing gas species typical of volcanic and geothermal emissions (CH_4, CO and H_2S besides H_2). The results achieved through these latter tests indicated that the largest cross sensitivity effects on H_2 concentration measurements have been produced by H_2S-containing mixtures, owing to the sulphur oxidation, that causes a four times larger sensitivity per equivalent concentration of H_2. The field-testing activity performed at Solfatara di Pozzuoli indicated that the use of H_2S chemical traps $Pb(CH_3COO)_2$-based effectively prevent in field applications the H_2S cross sensitivity effect verified by the laboratory experiments.

Beside the H_2S, the cross-sensitivity effects produced by changing the dilution matrix (N_2, O_2 and CO_2) as well as the other reducing species (CH_4, CO) typical of volcanic and geothermal emissions are smaller than 10% of the H_2 concentration measured by the sensor. The results of the rigorous laboratory tests supported the use of the RewPower Fuel Cell within the

system designed for H_2 monitoring in low temperature fumarolic emissions as well as in soil gases of volcanic, geothermal and seismically active areas.

The first preliminary investigations, made by using our H_2-CO_2 experimental system, have been performed at Torre del Filosofo, a fumarolic field placed close to the south-east crater of Mount Etna volcano, throughout the summer of 2008. Although the data set is too restricted to straight correlate the variations of the fumarolic degassing with the magmatic dynamics occurring within the Etna's feeding system, the changes of H_2 concentration and CO_2 flux are fairly well time-correlated with the main changes of Etna's 2008 eruptive activity. Moreover, the field experience performed at Torre del Filosofo can be considered fruitful also because H_2 and CO_2 anomalies were asynchronous, with delays ranging from a few hours to several days, providing the first field verification of this interesting behaviour exhibited by both the H_2 and CO_2 signals.

Since May 2010, the H_2-CO_2 system has been used to perform the measurements at Belvedere, a different fumarolic field sited close to the south-east crater cone of Mount Etna. The episodic variations of degassing activity observed at Belvedere showed some broad temporal correlations with the changes of volcanic activity occurred from the central craters of the volcano. Our results showed that throughout the monitoring period at Belvedere, the fumarolic degassing has been characterized by long-term steadiness value of H_2 signal at the typical background concentrations measured within the Belvedere fumarolic gases. Since the 13 August 2010, about two weeks before the Bocca Nuova unrest (25 August 2010), have been recorded several broad and sudden variations of H_2 concentration, larger than one size-order in comparison to the background. These variations are consistent with the increased amount of reduced species within the gaseous mixtures emitted from Belvedere fumarolic field, suggesting the more reducing conditions of the magmatic sources. Moreover, the persistent increasing trend of CO_2 flux observed from the end of May 2010 involves the increased contribution of deep-seated gases. This agreement between both parameters is consistent with the degassing of a relatively reduced and gas-richer magma batch, occurred since before the 25 August 2010 unrest from Bocca Nuova crater, whose effects have been recorded also from Belvedere fumarolic field.

The continuous monitoring of fumarolic degassing performed on Mount Etna volcano lets highlighting some characteristic features of the H_2 and CO_2 parameters. In particular, the main events of anomalous H_2 releases are characterized by a typical "pulsating", spike-like pattern within the time series, while the CO_2 flux increases are often characterized by long-term trend. Furthermore, it has been noted that the sharp CO_2 flux increase, culminated during the

unrest from Bocca Nuova crater, started the 21 August 2010, after the beginning of anomalous H_2 releases, providing further evidences that the typical sound between anomalous H_2 releases and CO_2 flux increases is the delay, ranging from a few hours to several days.

Since the comparison between the measurements performed in different volcanic system represents a step need forward the development of reliable tools to monitor the volcanic activity, the H_2-CO_2 system has been used to study the degassing activity also on Stromboli volcano.

The analysis of the data set obtained by the continuous monitoring performed on this volcano, made through the degassing model of Stromboli volcanic system, enabled better understanding the connections between the fumarolic degassing and its typical time-changing volcanic activity.

Synchronous CO_2 flux increases from both measurement site (PSF-a and PSF-b) have been recorded before or just after major explosion and paroxysmal activity. This evidence supported the inference that the increases of the gas contribution provided by the deep degassing source produced the increases of CO_2 amounts rising through the fractures of the volcano edifice and finally sustained large CO_2 emissions from the fumarolic field. These CO_2 flux increases, spatially extended to a larger part of the top area of the volcano, in comparison to the degassing surface actives throughout the typical strombolian activity, can be thought as the enlargement of the fumarolic degassing along SW direction.

Several persistent long-term increases of CO_2 flux mainly observed at PSF-a site (CO_2 H.F.) have been recorded throughout the routine strombolian activity, without noticeable synchronous CO_2 flux variations at PSF-b site. Geochemical, volcanological and geophysical studies indicated that the routine Stromboli's activity is sustained through continuous magma overturning triggered by the sink of degassed volatile-poor HP magma which in turn enables the ascent of less dense volatile-rich LP magma. The increased amount of gas released from the deep source of magma provides large amount of gas feeding the fumarolic degassing, suggesting that the long-term increases of CO_2 flux observed at PSF-a site may indicate the increased rate of volatile-rich magma or gas sustaining the routine strombolian explosions. The transition from LP volatile-rich to HP volatile-poor magma suggested that large amounts of H_2 can be released by water dissociation reaction at high temperature throughout the routine strombolian activity, producing the hydrogen front fast moving toward the surface.

Therefore, the change of the rate of magma and/or CO_2-rich gas supply from depth implies variable amounts of H_2 released through the dehydration process triggering the transition from LP to HP magma. In this framework, can be inferred that the steadiness H_2 background of

PSF-a emissions can reflect the typical H_2 concentration within the gas emitted in accordance with the routine average strombolian activity triggering the steady rate of magma/gas supply to the shallow plumbing system. On the other hand, the long-term H_2 increases affected by several spike-like variations can reflect the increased rate of magma supply to the volcano plumbing system, producing the period of high average activity as well as before or just after major explosions and paroxysmal activity. These conditions can persist until the rate of magma supply is sufficiently low that the magma ascents following open system conditions. Highest ascent rate, following closed system conditions, implies that the magma rises without water loss up to close the surface and the large part of water is emitted together with the magma as LP golden pumice.

Beside the evidence exhibited by the continuous monitoring on Mount Etna, the results of the data analysis obtained by the continuous monitoring performed on Stromboli provided further verification of the typical behaviour of both H_2 and CO_2 parameters. In particular:

- the pulsing features of H_2 releases evidenced by spike-like variations within the time series. In general, these variations are size-order larger than the diurnal change of H_2 concentration typically in the range of a few ppm vol.;
- the evidence that CO_2 flux variations occurred systematically behind the H_2 concentration one, with delays ranging from a few hours, to several days up to weeks.

The evidences that both fumarolic field of Mount Etna displayed systematically asynchronous variations of H_2 and CO_2 signals suggest the independency of this characteristic from specific site effects. Therefore, the continuous monitoring results obtained on both Mount Etna and Stromboli volcanoes strongly suggest that the asynchronous variations are independent from the specific monitored volcanic system, instead being a typical behaviour of the monitored parameters. These evidences drove the formulation of the theoretical model describing the chemical composition transients within the fumarolic gases according to both advective and diffusive transport processes of single gas species through the porous media. The mathematical solution of the model provided the time elapsing since the beginning of the chemical disturbance of the mixture filling the pores of the medium by the reservoir and its identification from the surface (named retention time). The development of the model provided that the retention times of each specific gas species had inverse correlation with both the advective flux rate and the diffusion coefficient, being directly correlated with the distance between the reservoir and the surface. Therefore, keeping constant the geometrical feature of the system (depth of the reservoir) and the flux properties of the medium (porosity and permeability), the delay between the transient affecting different species depends from its own

specific diffusivity. In other words, the solution of the model assess that although the advective flux is the most efficient process throughout the mass transport of multicomponent mixtures, the diffusive one operates simultaneously towards the separation of the gas mixture in its own components, in agreements with the diffusive velocity of the different gas species. This separation process made by the different diffusion properties can explain the chromatographic effect observed by the H_2 and CO_2 monitoring in field experiences.

As mentioned before, the model has been experimentally validated through laboratory flux tests investigating a range of flux rates larger than the typical one observed in fumarolic as well as diffuse degassing activity.

The results of the tests aimed to check experimentally the theoretical predictions provided the evidence that the retention times measured by using CO_2 as a single flux component reproduce the model computations in the full range of the gas flux rate investigated.

Beside the CO_2, the model has been checked to compare both predicted and measured retention times of the typical gas species making the multicomponent fumarolic mixtures as well as soil gases of volcanic and geothermal areas.

The experimental results displayed differences between the model computations and the measured retention times of the lighter gas species as the H_2 in multicomponent mixtures. Differences have been observed between model and experimental retention times when the compositional effects of the mixtures flowing within the column produce noticeable variations of the diffusive coefficients of the chemical species. Indeed, in the computation of the modelled retention times were used the binary diffusion coefficients. From experimental standpoint, the large difference between the binary and the multicomponent diffusion coefficients of the gas species occurs when the mixture contains different species with large difference in the molecular weight as in the case of H_2 and CO_2. The results of the tests aimed to check the relationships between the compositional effects of the mixtures and the retention times of the chemicals indicated that the model agree fairly well with the experimental observations when the CO_2 is the main component of the mixture and the H_2 the minor one in terms of abundance. In particular, the model predictions agree with the experimental results when the H_2 concentration within the multicomponent mixture is below 100 ppm vol. and the CO_2 concentration above the 40 vol %. This compositional range include fairly well the typical compositions of fumarolic gases as well as the composition of the soil gases emitted from volcanic, geothermal and seismic areas.

Acknowledgement

I wish to thank

- my Tutor Prof. Mariano Valenza;
- the Coordinator of the PhD course Prof Francesco Parello;
- my Co-tutor at the Palermo division of INGV Dr Marco Camarda;
- the Director Dr Sergio Gurrieri and all the staff of INGV-Pa;
- my Reviewers Dr Anthony Finizola and Prof. Dario Luzio;
- the staff of Dipartimento di Chimica e Fisica della Terra ed Applicazioni alle Georisorse ed ai Rischi Naturali (University of Palermo);
- my colleagues.

References

[1] Acocella V., Behncke B., Neri M., D'Amico S. (2003) *Link between major flank slip and 2002–2003 eruption of Mt. Etna (Italy).* Geophysical Research Letters vol. 30, pp. 121–124

[2] Acocella V., Neri M. (2003) *What makes flank eruptions? The 2001 Etna eruption and possible triggering mechanism.* Bulletin of Volcanology, N° 65, pp. 517-529

[3] Aiuppa A., Bertagnini A., Métrich N., Moretti R., Di Muro A., Liuzzo M., Tamburello G. (2010) *A model of degassing for Stromboli volcano.* Earth and Planetary Science Letters, vol. 295, pp. 195-204

[4] Aiuppa A., Burton M., Caltabiano T., Giudice G., Gurrieri S., Liuzzo M., Murè F., Salerno G. (2010) *Unusually large magmatic CO_2 gas emissions prior to a basaltic paroxysm.* Geophysical Research Letters, vol. 37

[5] Aiuppa A., Caleca A., Federico C., Gurrieri S., Valenza M. (2004) *Diffuse degassing of carbon dioxide at Somma-Vesuvius volcanic complex (Southern Italy) and its relation with regional tectonics.* Journal of Volcanology and Geothermal Research, vol. 133, pp. 55-79

[6] Aiuppa A., Cannata A., Cannavò F., Di Grazia G., Ferrari F., Giudice G., Gurrieri S., Liuzzo M., Mattia M., Montalto P., Patanè D., Puglisi G. (2010) *Patterns in the recent 2007-2008 activity of Mount Etna volcano investigated by integrated geophysical and geochemical observations.* Geochemistry Geophysics Geosystem, vol. 11, N° 9

[7] Aiuppa A., Federico C., Giudice G., Gurrieri S., Liuzzo M., Shinohara H., Favara R. and Valenza M. (2006) *Rates of carbon dioxide plume degassing from Mount Etna volcano.* Journal of Geophysical Research, vol. 111

[8] Aiuppa A., Federico C., Giudice G., Gurrieri S., Paonita A., Valenza M. (2004) *Plume chemistry provide insights into mechanisms of sulfur and halogen degassing in basaltic volcanoes.* Earth and Planetary Science Letters, N° 222, pp. 469-483

[9] Aiuppa A., Federico C., Paonita A., Pecoraino G., Valenza M. (2002) *S, Cl and F degassing as an indicator of volcanic dynamics: the 2001 eruption of Mount Etna.* Geophysical Research Letters, vol. 29, N° 11

[10] Aiuppa A., Inguaggiato S., McGonigle J. S. O'Dwyer M., Oppenheimer C., Padgett M. J., Rouwet D., Valenza M. (2005) *H_2S fluxes from Mt Etna, Stromboli and Vulcano (Italy) and implication for the sulfur budget at volcanoes.* Geochimica et Cosmochimica Acta, vol. 69, N° 7, pp. 1861-1871

[11] Aiuppa, A., Giudice G., Gurrieri S., Liuzzo M., Burton M., Caltabiano T., McGonigle A. J. S., Salerno G., Shinohara H., Valenza M. (2008) *Total volatile flux from Mount Etna.* Geophysical Research Letters, N° 35

[12] Aiuppa, A., Moretti R., Federico C., Giudice G., Gurrieri S., Liuzzo M., Papale P., Shinohara H., and Valenza M. (2007) *Forecasting Etna eruptions by real time observation of volcanic gas composition.* Geology, N° 35 -12, pp1115–1118

[13] Allard P. (2010) *A CO_2-rich gas triggering of explosive paroxysm at Stromboli basaltic volcano, Italy.* Journal of Volcanology and Geothermal Research, vol. 189, pp. 363-374

[14] Allard P., Behncke B., D'amico S., Neri M., Gambino S. (2006) *Mount Etna 1993-2005: Anatomy of an evolving eruptive cycle.* Earth-Science Reviews, N° 78, pp. 85-114

[15] Allard P., Burton M., Muré F. (2005) *Spectroscopic evidence for lava fountain driven by previously accumulated magmatic gas.* Nature, vol. 433, pp. 407-410

[16] Allard P., Carbonnelle J., Dajlevic D., Le Bronec J., Morel P., Robe M. C., Maurenas J. M., Faivre-Pierret R., Martin D., Sabroux J. C., Zettwoog P. (1991) *Eruptive and diffuse emissions of CO_2 from Mouut Etna.* Nature, vol. 351, pp. 387-391

[17] Alparone S., Andronico D., Giammanco S., Lodato L. (2004) *A multidisciplinary approach to detect active pathways for magma migration and eruption at Mt. Etna (Sicily, Italy) before the 2001 and 2002-2003 eruptions.* Journal of Volcanology and

Geothermal Research, vol. 136, pp. 121-140

[18] Andu´jar J. M. and Segura F. (2009) *Fuel cells: history and updating. A walk along two centuries.* Renewable and Sustainable Energy Reviews, vol. 13, pp. 2309-2322

[19] Asher-Bolinder S., Owen D.E., Schumann R.R., (1990) *Pedologic and climatic controls on Rn-222 concentration in soil gas, Denver,Colorado.* Geophysical Research Letters vol. 17, pp. 825-828

[20] Azzaro, R., Branca, S., Giammanco, S., Gurrieri, S., Rasà, R., Valenza, M. (1998). *New evidence for the form and extent of the Pernicana Fault System (Mt. Etna) from structural and soil–gas surveying.* Journal of Volcanology and Geothermal Research, vol. 84, pp. 143–152.

[21] Badalamenti B., Bruno N., Caltabiano T., Di Gangi F., Giammanco S., Salerno G. (2004) *Continuous soil CO_2 and discrete plume SO_2 measurements at Mt. Etna (Italy) during 1997-2000: a contribution to volcano monitoring.* Bulletin of Volcanology, vol. 66 - 1, pp. 80-89

[22] Badalamenti B., Capasso G., Carapezza M.L., D'Alessandro W., Di Gangi F., Di liberto I.S., Giammanco S., Gurrieri S., Nuccio P.M., Parello F., Valenza M. (1994) *Soil gas investigations during the 1991-1993 Etna eruption.* Acta Vulcanologica, vol. 4, pp. 135-141

[23] Badalamenti B., Di Gangi F., Gurrieri S., Valenza M. (1994) *Continuous monitoring (Temperature, CO_2 in soil gases and reducing capacity) (Vulcano).* Acta Vulcanologica, vol. 6, pp. 46-47

[24] Badalamenti B., Gurrieri S., Hauser S., Parello F., Valenza M., (1991) *Change in the soil CO_2 output at Vulcano during the summer 1998.* Acta Vulcanologica, vol.1, pp. 219-221

[25] Badalamenti B., Gurrieri S., Hauser S., Tonani F., Valenza M., (1984) *Considerazioni sulla concentrazione e sulla composizione isotopica della CO_2 presente nelle manifestazioni naturali e nell'atmosfera dell'isola di Vuolcano.* Società Italiana di

Mineralogia e Petrologia, vol. 39 - 2, pp. 367.

[26] Badalamenti B., Nuccio P. M., Valenza M. (1991) *Gas hazard on Vulcano Island. Nature*. vol. 350, pp. 26-27

[27] Badalamenti, B., Gurrieri, S, Hauser, S., Valenza, M., (1998) *Ground CO_2 output in the island of Vulcano during the period 1984–1988: gas hazard and volcanic activity surveillance implications.* Rendiconti Società Italiana Mineralogia Petrologia 43 pp. 893–899

[28] Bagnato E., Aiuppa A., Parello F., Calabrese S., D'Alessandro W., Mather T. A. McGonigle A. J. S. Pyle D. M., Wängberg I. (2007) *Degassing of gaseous (elemental and reactive) and particulate mercury from Mount Etna volcano (Southern Italy).* Atmospheric Environment, N° 41, pp. 7377-7388

[29] Barberi F. and Carapezza M. L. (1994) *Helium and CO_2 soil gas emission from Santorini (Greece).* Bulletin of Volcanology, vol. 56, No 5, pp. 335-342

[30] Barberi F., Rosi M:, Sodi A. (1993) *Volcanic hazard assessment at Stromboli based on review of historical data.* Acta Vulcanologica, vol. 3, pp. 173-187

[31] Baubron J. C., Allard P., Sabroux J. C., Tedesco D., Toutain J. P. (1991) *Soil gas emanations as precursory indicators of volcanic eruptions.* Journal of the Geological Society, London, vol. 148, pp. 571-576

[32] Baubron, J.C., Allard, P., Toutain, J.P. (1990) *Diffuse volcanic emissions of carbon dioxide from Vulcano island, Italy.* Nature 344, 51-53.

[33] Behncke, B., Neri, M., (2003). *Cycles and trends in the recent eruptive behaviour of Mount Etna (Italy).* Can. J. Earth Sci. 40, 1405–1411.

[34] Bellomo S., Aiuppa A., D'Alessandro W., Parello F. (2007) *Environmental impact of magmatic fluorine emission in the Mt. Etna area.* Journal of Volcanology and Geothermal Research, N° 165, pp. 87-101

[35] Bertagnini A., Métrich N., Francalanci L., Landi P., Tommasini S., Conticelli S. (2008) *Volcanology and Magma Geochemistry of the Present-day Activity: Constraints on the Feeding System.* In: "*Learning from Stromboli and its 2002–2003 Eruptive Crisis*", Calvari, S., Rosi, M., and Ripepe, M. (edts), American Geophysical Union – Geophysical Monograph volume.

[36] Bertami R., Buonasorte G., Ceccarelli A., Lombardi S., Pieri S., Scandiffio G. (1990) *Soil gases in geothermal prospecting: two case histories (Sabatini Volcanoes and Alban hills, Latium, central Italy).* Journal of Geophysical Research vol. 95, No. B13, pp. 475-481.

[37] Bonaccorso A., Gambino S., Guglielmino F., Mattia M., Puglisi G., Boschi E. (2008) *Stromboli 2007 eruption: deflation modelling to infer shallow-intermediate plumbing system.* Geophysical Research Letters, vol. 35

[38] Bonforte A., Bonaccorso A., Guglielmino F., Palano M., Puglisi G. (2008) *Feeding system and magma storage beneath Mt. Etna as revealed by recent inflation/deflation cycles.* Journal of Geophysical Research, vol. 113

[39] Borgia A., Ferrari L., Pasquare G. (1992) *Importance of gravitational spreading in the tectonic and volcanic evolution of Mount Etna.* Nature vol. 357, pp. 231– 235.

[40] Branca S., Coltelli M., Groppelli G. (2004) *Geological evolution of Etna volcano. In Mt. Etna volcano laboratory.* AGU Geophys. Monogr. vol. 143, pp. 49– 63

[41] Burton M., Allard P., Murè F., La Spina A. (2007) *Magmatic gas composition reveals the source depth of slug-driven Strombolian explosive activity.* Science, vol. 317, pp. 227-230

[42] Calvari, S., Coltelli, M., Neri, M., Pompilio, M., Scribano, V. (1994) *The 1991–93 Etna eruption: chronology and lava flow-field evolution.* Acta Vulcanologica N° 4, pp. 1–14

[43] Camarda M., Gurrieri S., Valenza M. (2006) *CO_2 flux measurements in volcanic areas using the dynamic concentration method: the influence of the soil permeability.*

Journal of Geophysical Research, vol. 111

[44] Camarda M., Gurrieri S., Valenza M. (2006) *In situ permeability measurements based on radial gas advection model: Relationship between soil permeability and diffuse CO_2 degassing in volcanic areas.* Pure and Applied Geophysics. vol. 163, N° 4, pp. 897-914

[45] Cannata A., Catania A., Alparone S., Gresta S. (2008) *Volcanic tremor at Mt. Etna: inferences on magma dynamics during effusive and explosive activity.* Journal of Volcanology and Geothermal Research, vol. 178, pp. 19-31

[46] Capasso G., Carapezza M. L. (1994) *A geochemical survey of Stromboli.* Acta Vulcanologica, vol. 6, pp. 52-53

[47] Carapezza M. L., Ricci T., Ranaldi M., Tarchini L. (2009) *Active degassing structures of Stromboli and variations in diffuse CO_2 output related to the volcanic activity.* Journal of Volcanology and Geothermal Research, vol. 182, pp. 231-245

[48] Carapezza M., Nuccio P. M., Valenza M. (1980) *Geochemical precursor of earthquakes: high pressure science and technology.* Edited by B. Vodar and Ph Marteau, Elsevier, New York

[49] Carapezza M., Nuccio P. M., Valenza M. (1983) *Geochemical surveillance of the Solfatara of Pozzuoli (Phlegraean Fielgs) during 1983.* Bulletin of Volcanology, vol. 47, N° 2, pp. 303-311

[50] Carapezza M.L., Federico C. (2000) *The contribution of fluid geochemistry to the volcano monitoring of Stromboli.* Journal of Volcanology and Geothermal Research vol. 95, pp. 227–245

[51] Carmichael I.S.E., Turner F. J., Verhoogen J. (1974) *Igneous petrology.* McGraw-Hill ed. New York

[52] Chiodini G., Cioni R., Guidi M., Raco B., Marini L. (1998) *Soil CO_2 flux measurements in volcanic and geothermal areas.* Applied Geochemistry, vol., 13, No

5, pp. 543-552

[53] Cigolini C., Poggi P., Ripepe M., Laiolo M., Ciamberlini C., Delle Donne D., Ulivieri G., Coppola D., Lacanna G., Marchetti E., Piscopo D., Genco R. (2009) *Radon survey and real-time monitoring at Stromboli volcano: influence of soil temperature, atmospheric pressure and tidal forces on 222Rn degassing.* Journal of Volcanology and Geothermal Research, vol. 184, pp. 381-388

[54] Ciotoli, G., Guerra, M., Lombardi, S., Vittori, E. (1998) *Soil gas survey for tracing seismogenic faults: a case-study in the Fucino basin (Central Italy).* Journal of Geophysical Research, vol. 103, pp. 23781-23794

[55] Cook B. (2002) *Introduction to fuel cell and hydrogen technology.* Engineering Science and Educational Journal, vol. 11, N° 6, pp. 205-216

[56] Crank J. (1975) *The Mathematics of Diffusion.* 2nd ed. Clarendon Press, London

[57] Cussler E. L. (1997) *Diffusion, mass transfer in fluid system.* 2nd ed. Cambridge University Press.

[58] D'Alessandro W., De Domenico R., Parello F., Valenza M. (1992). *Soil degassing in tectonically active areas of Mt. Etna.* Acta Vulcanologica, vol. 2

[59] De Gregorio, S., Diliberto, I.S., Giammanco, S., Gurrieri, S., Valenza, M., (2002) *Tectonic control over large-scale diffuse degassing in eastern Sicily (Italy).* Geofluids 2, pp. 273-284

[60] Di Carlo I., Pichavant M., Rotolo S. G:, Scaillet . (2006) *Experimental crystallization of high-K arc basalt: the golden pumice, Stromboli volcano (Italy).* Journal of Petrolgy, vol. 47, pp. 1317-1343

[61] Dietz E. A. (1996) *Shifting of gas chromatographic retention times due to solvent effects - A study using sulfur chemiluminescence detection.* J. High Resol. Chromatogr., vol. 19, pp. 485-491

[62] Diliberto I. S., Gurrieri S., Valenza M. (1996) *Diffuse CO_2 degassing from the ground.* Acta Vulcanologica, vol. 8, pp. 203-204

[63] Diliberto I. S., Gurrieri S., Valenza M. (2002) *Relationships between diffuse CO_2 emissions and volcanic activity on the island of Vulcano (Aeolian Islands, Italy) during the period 1984–1994.* Bulletin of Volcanology, vol. 64, pp. 219-228

[64] Finizola A., Sortino F., Lénat J-F., Aubert M., Ripepe M., Valenza M. (2003) *The summit hydrothermal system of Stromboli. New insights from self-potential, temperature, CO_2 and fumarolic fluid measurements, with structural and monitoring implications.* Bulletin of Volcanology, vol. 65, pp. 486-504

[65] Finizola A., Sortino F., Lénat J-F., Valenza M. (2002) *Fluid circulation at Stromboli volcano (Aeolian Island, Italy) from self-potential and CO_2 survey.* Journal of Volcanology and Geothermal Research, vol. 116, pp. 1-18

[66] Finlayson J. B. (1992) *A soil gas survey over Rotorua geothermal field, Rotorua, New Zeland.* Geothermics, vol. 21, No. 1/2, pp. 181-195

[67] Francalanci L., Manetti P., Peccerillo A. (1989) *Volcanological and magmatological evolution of Stromboli volcano (Aeolian islands) - The roles of fractional crystallization, magma mixing, crustal contamination and source heterogeneity.* Bulletin of Volcanology, vol. 51 - 5, pp. 355-378

[68] Francalanci L., Tommasini S., Conticelli S. (2004) *The volcanic activity of Stromboli in the 1906-1998 AD period: mineralogical, geochemical and isotope data relevant to the understanding of the plumbing system.* Journal of Volcanology and Geothermal Research, vol. 131 1-2, pp. 179-211

[69] Gerlach T. M. and Graeber E. J. (1985) *Volatile budget of Kilauea volcano.* Nature, vol. 313, pp. 273-277

[70] Gerlach T. M., Doukas M. P., McGee K. A., Kessler R. (2001) *Soil efflux and total emission rates of magmatic CO_2 at the Horseshoe Lake tree kill, Mammoth Mountain,*

California, 1995-1999. Chemical Geology, vol. 177, pp. 101-116

[71] Ghisetti F. (1979) *Relazione tra strutture e fasi trascorrenti e distensive lungo i sistemi Messina–Fiumefreddo, Tindari–Letojanni e Alia–Malvagna (Sicilia nord-orientale): uno studio microtettonico.* Geol. Romana vol. 11, pp. 35–42

[72] Giammanco S., Inguaggiato S., Valenza M., (1998) *Soil and fumarole gases of Mount Etna: geochemistry and relations with volcanic activity.* Journal of Volcanology and Geothermal Research, vol. 81, pp. 297-310

[73] Giammanco S., Gurrieri S., Principio E., Valenza M. (1996) *CO_2 fluxes from Mt. Etna soils.* Acta Vulcanologica, vol. 8, pp. 220-222

[74] Giammanco S., Gurrieri S., Valenza M. (1995) *Soil CO_2 degassing from the ground on mount Etna during 1992.* Acta Vulcanologica, vol. 6, pp. 7-9

[75] Giammanco S., Gurrieri S., Valenza M. (1995) *Soil CO_2 degassing on Mt Etna (sicily) during 1989-1993: discrimination between climatic and volcanic influences.* Bullettin of volcanology, vol. 57, pp. 52-60

[76] Giammanco S., Gurrieri S., Valenza M. (1999) *Geochemical investigations applied to active fault detection in a volcanic area: the North-East Rift on Mt. Etna (Sicily, Italy).* Geophysical Research Letters, vol. 26, pp. 2005-2008

[77] Giammanco S., Gurrieri S., Valenza M. (2000) *CO_2 flux from the soils of Mt. Etna.* Acta Vulcanologica, vol. 12, pp. 69-71

[78] Giammanco S., Gurrieri S., Valenza M. (2006) *Fault-controlled soil CO_2 degassing and shallow magma bodies: summit and lower East Rift of Kilauea volcano (Hawaii), 1997.* Pure and Applied Geophysics, No 163, pp. 853-867

[79] Giammanco, S., Gurrieri, S., Valenza, M. (1997) *Soil CO_2 degassing along tectonic structures of Mt. Etna Sicily: the Pernicana Fault.* Applied Geochemistry vol. 12, pp. 429-436

[80] Giggenbach,W.F. (1996) *Chemical composition of volcanic gases.* In: Scarpa, R., Tilling, R.I. (Eds.), *Monitoring and Mitigation of Volcanic Hazards.* Springer Verlag, Berlin-Heidelberg.

[81] Granieri D., Avino R., Chiodini G. (2009) *Carbon dioxide diffuse emission from the soil: ten years of observations at Vesuvio and Campi Flegrei (Pozzuoli), and linkages with volcanic activity.* Bulletin of Volcanology, vol. 72, No 1, pp. 103-118.

[82] Gregory R. G. And Durrance E. M. (1985) *Helium, carbon dioxide and oxygen soil gases: small-scale variations over fractured ground.* Journal of Geochemical Exploration, vol. 24, pp. 29-49.

[83] Gurrieri S. and Valenza M. (1988) *Gas trasport in natural porous mediums:a method for measuring CO_2 flows from the ground in volcanic and geothermal areas.* Rendiconti SIMP Carapezza M. Memorial Volume, vol. 43- 4, pp. 1151-1158

[84] Hernandez P., Pérez N., Salazar J., Sato M., Notsu K., Wakita H. (2000) *Soil gas CO_2, CH_4 and H_2 distribution in and around Las Cañadas caldera, Tenerife, Canary Islands, Spain.* Journal of Volcanology and Geothermal Research, vol. 103, pp. 425-438

[85] Hinkle M. E. (1990) *Tabulation of N_2, O_2, CO_2 and He concentrations in soil gases collected regularly for 13 months at a site on the summit of Kilauea volcano.* U.S. Geol. Surv. Open-File Rept. 90-66

[86] Hinkle M. E. (1994) *Environmental conditions affecting the concentration of He, CO_2, O_2 and N_2 in soil gases.* Applied Geochemistry, vol. 9, pp. 53-64

[87] Hinkle M. E. and Ryder J. L. (1987) *Meteorological variables and concentrations of helium, carbon dioxide, and oxygen in soil gases collected regularly at a single site for more than a year.* U.S. Geol. Surv. Open-File Rept. 87-449.

[88] Hornig-Kjarsgaard I., Keller J., Koberski U., Stadlbauer E., Francalanci L., Lenhart, R. (1993) *Geology, stratigraphy and volcanological evolution of the island of*

Stromboli, Aeolian arc, Italy. ActaVulcanologica vol. 3, pp. 21-68

[89] Irwin W. And Barnes I. (1980) *Tectonic relations of carbon dioxide discharges and earthquakes.* Journal of Geophysical Research, vol. 85, No B6, pp. 3115-3121

[90] Ito T., Nagamine K., Yamamoto K., Adachi M., Kawabe I. (1999) *Preseismic hydrogen gas anomalies caused by stress-corrosion process preceding earthquakes.* Geophysical Research Letters, vol. 26 (13),pp. 2009-2012

[91] Kameda J., Saruwatari K., Tanaka H. (2003) *H_2 generation in wet grinding of granite and single-crystal powders and implications for H_2 concentration on active faults.* Geophysical Research Letters, vol. 30, No 20, pp

[92] King C. (1980) *Episodic Radon changes in subsurface soil gas along active faults and possible relation to earthquakes.* Journal of Geophysical Research, vol. 85, No B6, pp. 3065-3078

[93] Kita I., Matsuo S., Wakita H. (1982) *H_2 generation by reaction between H_2O and crushed rock: An experimental study on H_2 degassing from the active fault zone.* Journal of Geophysical Research, vol. 87, pp. 789–795

[94] Klusman, R.W. (1993) *Soil gas and related methods for natural resource exploration.* Wiley, New York, pp. 1-483.

[95] Krishna R., Wesselingh J. A. (1997) *The Maxwell-Stefan approach to mass transfer.* Chemical Engineering Science, vol. 52, N° 6, pp. 861-911

[96] Landi P., Corsaro R. A.,Francalanci L., Civetta L., Miraglia L., Pompilio M., Tesoro R. (2009) *Magma dynamics during the 2007 Stromboli eruption (Aeolian Islands, Italy): mineralogical, geochemical and isotopic data.* Journal of Volcanology and Geothermal Research, vol. 182, pp. 255-268

[97] Landi P., Francalanci L., Pompilio M., Rosi M., Corsaro R.A., Petrone C.M., Nardini I., Miraglia L. (2006) *The December 2002-July 2003 effusive event at Stromboli volcano, Italy: an insight into the shallow plumbing system by petrochemical studies.*

Journal of Volcanology and Geothermal Research, vol. 155, pp. 263-284

[98] Marchetti E., Ripepe M., Ulivieri G., Caffo S., Privitera E. (2009) *Infrasonic evidences for branched conduit dynamics at Mt. Etna volcano, Italy.* Geophysical Research Letters, vol. 36

[99] Mattia M., Aloisi M., Di Grazia G., Gambino S., Palano M., Bruno V. (2008) *Geophysical investigations of the plumbing system of Stromboli volcano (Aeolian Islands, Italy).* Journal of Volcanology and Geothermal Research, vol. 176, pp. 529-540

[100] McCathy J. H. and Reimer G. M. (1985) *Advances in soil gas geochemical Exploration for natural resources: some current examples and practice.* Journal of Geophysical Research, vol. 91, No B12, pp. 327-338

[101] Mehta V. and Copper J. S. (2003) *Review and analysis of PEM fuel cell design and manufacturing.* Journal of Power Sources, vol. 114, N° 1, pp. 32-53

[102] Melián G. V., Galindo I., Pérez N. M., Hernández P. A., Fernández M., Ramírez C., Mora R., Alvarad G. E. (2007) *Diffuse emission of hydrogen from Poás volcano, Costa Rica, America Central.* Pure and Applied Geophysics, vol. 164, pp. 2465-2487

[103] Melián G. V., Galindo I., Salazar J., Hernández P. A., Fernández M., Ramírez C., Mora R., Alvarad G. E. (2002) *Hydrogen emission from Poás volcano, Costa Rica, America Central: a premonitory geochemical signature of volcanic unrest?* EOS. Transac. Am. Geophy. Union 83, F 1489

[104] Métrich N., Allard P., Spilliaert N., Andronico D., Burton M. (2004) *2001 flank eruption of the alkali- and volatile-rich primitive basalt responsible for Mount Etna's evolution in the last three decades.* Earth and Planetary Science Letters, N° 228, pp. 1-17

[105] Métrich N., Bertagnini A., Di Muro A. (2010) *Conditions of magma storage, degassingand ascent at Stromboli: new insights into the volcano plumbing system with*

inferences on the eruptive dynamics. Journal of Petrology, vol. 51 - 3, pp. 603-626

[106] Métrich N., Bertagnini A., Landi P. & Rosi M. (2001) *Crystallisation driven by decompression and water loss at Stromboli volcano (Aeolian Islands).* Journal of Petrology, vol. 42, pp. 1471-1490

[107] Mohamed F. A. (1993) *The energy-integral method: application to linear hyperbolic heat-conduction problems.* Applied Scientific Research, vol. 50, pp. 107-128

[108] Murru M., Montuori C., Wyss M., Privitera E. (1999) *The locations of magma chambers at Mt. Etna, Italy, mapped by b-values.* Geophysical Research Letters, vol. 26, N° 16, pp. 2553-2556

[109] Neri M., Acocella V., Behncke B., Maiolino V., Ursino A., Velardita R. (2005) *Contrasting triggering mechanisms of the 2001 and 2002-2003 eruptions of Mount Etna (Italy).* Journal of Volcanology and Geothermal Research, N° 144, pp. 235-255

[110] Nuccio P. M., Valenza M. (1993) *Magma degassing and geochemical detection of its ascent.* Water-Rock interaction, Arehart & Hulston eds., 1998 Balkema, Rotterdam

[111] Oskarsson N. (1984) *Monitoring of fumarole discharge during the 1975-1982 rifting in Krafla volcanic center, North Iceland.* Journal of Volcanology and Geothermal Research, No 22, pp. 97-121

[112] Ozisik M. N. (1984) *Heat Transfer.* McGraw-Hill, New York

[113] Patanè G., La Delfa S., Tanguy J-C. (2006) *Volcanism and mantle-crust evolution: the Etna case.* Earth and Planetary Science Letters, vol. 241, pp. 831-843

[114] Pecoraino G. and Giammanco S. (2005) *Geochemical characterization and temporal changes in parietal gas emissions at Mt. Etna (Italy) during the period July 2000 - July 2003.* Terrestrial Atmospheric and Oceanic Sciences, vol. 16 - 4, pp. 805-841

[115] Pichavant M., Di Carlo I., Le Gac Y., Rotolo S. G. & Scaillet B. (2009). *Experimental constraints on the deep magma feeding system at Stromboli volcano, Italy.* Journal of

Petrology, vol. 50, pp. 601-624

[116] Pisani L. (2008) *Multi-component gas mixture diffusion through porous media: A 1D analytical solution.* International Journal of Heat and Mass Transfer, vol. 51, pp. 650-660

[117] Ponte G. (1919) La catastrofica esplosione dello Stromboli. R. Accad. Naz. Lincei, 28, pp. 89-94

[118] Rosi M., Bertagnini A., Landi P. (2000) *Onset of the persistent activity at Stromboli Volcano (Italy).* Bulletin of Volcanology, vol. 62, pp. 294-300

[119] Sakthivel M. and Weppner W. (2006) *Development of a hydrogen sensor based on solid polymer electrolyte membranes.* Sensors and Actuators B-Chemical, vol. 113, N° 2, pp. 998-1004

[120] Salazar, J.M.L., Perez, N.M., Hernandez, P.A., Soriano, T., Barahona, F., Olmos, R., Cartagena, R., Lopez, D.L., Lima, R.N., Melian, G., (2002) *Precursory diffuse carbon dioxide degassing signature related to a 5.1 magnitude earthquake in El Salvador, Central America.* Earth Planet. Sci. Lett. 205 (1–2), 81–89.

[121] Satake H., Ohashi M., Hayashi Y., (1984) *Discharge of H_2 from atotsugawa and Ushikubi faults, Japan, and its relation to earthquakes.* Pure and Applied Geophysics, vol. 122, pp. 185-193

[122] Sato M. and McGee K. A. (1980) *Continuous monitoring of hydrogen on South flank of Mount St. Helens.* Geological Survey Professional Paper 1250 - The 1980 eruption of Mount St. Helens, Washington. In *The 1980 Eruption of Mount St. Helens, Washington* Ed. P. W. Lipman and D. R. Mullineaux

[123] Sato M., Sutton A. J., McGee K. A. (1984) *Anomalous hydrogen emissions from San Andreas Fault observed at the Cienega Winery, Central California.* Pure and Applied Geophisics, vol. 122, pp. 366-391

[124] Shinohara H. (2008) *Excess degassing from volcanoes and its role on eruptive and*

intrusive activity. Reviews of Geophysics, vol. 46, pp. 1-31

[125] Sinclair, A.J. (1974) *Selection of threshold values in geochemical data using probability graphs.* Journal of Geochemical Exploration, vol. 3 (2), pp. 129-149

[126] Spilliaert N., Allard P., Métrich N., Sobolev A. (2006) *Melt inclusion record of the conditions of ascent, degassing and extrusion of volatile-rich alkali basalt during the powerful 2002 flank eruption of Mount Etna (Italy).* Journal of Geophysical Research 111

[127] Stone C., Morrison A. E. (2002) *From curiosity to "power to change the world®".* Solid State Ionics, vol. 152 - 153, pp. 1-13

[128] Sugisaki R, Ido M, Takeda H, Isobe Y, Hayashi Y, Nakamura N, Satake H, Mizutani Y. (1983) *Origin of hydrogen and carbon dioxide in fault gases and its relation to fault activity.* J Geol 91, vol. 3, pp. 239-258

[129] Symonds R. B., Rose W. I., Bluth G. J. S., Gerlach T. M. (1994) *Volcanic-gas studies: Methods, results, and applications.* In *Volatiles in Magmas,* Vol. 30 (eds. M. R. Carroll and J. R. Holloway), pp. 1-66. Mineral. Soc. Am., Washington, DC.

[130] Tanguy J-C., Condomines M., Kieffer G. (1997) *Evolution of the Mount Etna magma: constraints on the present feeding system and eruptive mechanism.* Journal of Volcanology and Geothermal Research, vol. 75, pp. 221-250

[131] Valenza M. (1993) *Preliminary study on emanation of CO_2 from soils in some areas of Mount Etna (Sicily).* Acta Vulcanologica, vol. 3, pp. 189-194

[132] Valenza M. (1994) *Soil gas investigations during the 1991-1993 Etna eruption.* Acta Vulcanologica, vol. 4, pp. 135-141

[133] Viccaro M., Giacomoni P. P., Ferlito C., Cristofolini R. (2010) *Dynamics of magma supply at Mt. Etna volcano (Southern Italy) as revealed by textural and compositional features of plagioclase phenocryst.* Lithos, vol. 116, pp. 77-91

[134] Wakita H. (1996) *Geochemical challenge to earthquake prediction.* Proc. Natl. Acad. Sci., USA, pp. 3781-3786

[135] Wakita H., Nakamura Y., Kita I., Fujii N., Notsu K. (1980) *Hydrogen Release: New Indicator of Fault Activity.* Science, vol. 210, pp. 188-190

[136] Wu Y-S. and Pruess K. (2000) *Integral solutions for transient fluid flow through a porousmedium with pressure-dependent permeability.* International Journal of Rock Mechanics and Mining Sciences, vol. 37, pp. 51-61

APPENDIX 1

Historical development of the fuel cells

The fuel cells are a group of innovative devices employed for the diffuse production of the electric energy likewise the commercial batteries. Furthermore, the working principle is different and for the electric energy production they use a fuel likewise the power engines.

During the last century, the technology of the fuel cells has been improved with the goal of a commercial use for a diffuse electric energy production. From the pioneering experiment in the XIX century of Grove that developed the first "gas battery" (Cook, 2002) and those of Schönbein about the "fuel cell effect", the fuel cells were employed whether into unit power systems, in which take place the chemical reaction, or assembled into stakes where a numbers of the individual cells are modularly combined together in units with the desired output power.

It is during the thirties of the twenty century that Thomas F. Bacon developed the first ready to use fuel cell based on the hydrogen and oxygen reaction (Andu´jar and Segura, 2009) to produce an electric current. His studies were considered such as a milestone in the progression of the fuel cell technologies. The advance in the technology of the Bacon's fuel cells, in terms power density, allowed their use also in the Apollo Spacecraft missions, despite their high cost. Actually, for space applications the fuel cells showed several advantages. Among the most relevant ones, the fact that they produce much more energy per equivalent of unit weight compared to a battery power source and moreover the fuel cells are clean at the same time, given that the pure water is the product of the electrochemical reaction of hydrogen and oxygen.

The experiments performed by researchers and engineers were focused into the optimization of construction cost through the development of non-expensive electrodes, high conductivity membranes and high density power of the cell.

A strong impact on the fuel cell production technology has been provided in the second half part of the twenty century, by the availability of the PolyTeraFluoroEthylene (Teflon or PTFE) used as basic material to build aqueous electrolyte fuel cell. The main advantage of the Teflon membrane is the longer lifetime due to its chemical resistance, especially close to the acidic environment of the fuel cell electrodes.

During those decades, with the further progress made by the chemical division of the General Electric, the fuel cells were successful employed by NASA and McDonnell Aircraft the fuel cells employed during the Gemini space program.

However, for this device, the proton exchange properties of the membranes were still poor. In order to improve both the transport properties of the proton exchange membranes combined to the mechanical resistance ones, the major development was achieved in the sixty decade, thanks to the joint of General Electric and Dupont Company. The most important outcome of this research was the use of the perfluorosulfonic acid as proton exchange membrane. The product developed is known as Nafion® and used everywhere as solid polymeric electrolyte in the Proton Exchange Membrane Fuel Cells (PEMFC). This membrane was used for a widespread range of fuel cells for terrestrial applications.

The proton exchange membranes appear just at once one of the most promising technologies to overcome both the decrease of the availability of hydrocarbons as well the air pollution.

Nevertheless, a great limitation of the PEMFC was the relative large amount of platinum required as a catalyst on the electrodes. To overcome this limitation, the research was addressed on the reduction of the electrocatalyst amount of the membrane electrode assemblage (MEA). Several studies carried out by the Los Alamos National laboratory demonstrated that the reduction of the Platinum fraction of the electrode, is not affecting the current density and the output voltage, provided that the surface area of the electrocatalyst is wide enough (Stone and Morrison, 2002).

Due to these improvements, during last years it was recognized that the fuel cells could be made both smaller and cheaper enough to replace the conventional power supplies.

Several industries are working to develop the systems to use the hydrogen as energy vector for the energy produced by wind or sun. Recently, the OriginOil, Inc. announces the H_2 production from algae.

The PEM fuel cells are currently regarded as the possible energy-conversion device because their high efficiency, high cleaning device with low volume and weight compared to the conventional energy storage devices. Fuel cells are so promising that nowadays automotive companies were producing testing vehicles and developing special car models using the fuel cells instead of the combustion engines. Some of them are also looking for the development of the hydrogen distribution grid as well.

The distributed power generation is the strategy of both heat and electric energy production close to the customer, a combination known as “cogeneration”. Distributed power plant has several advantages over the centralized one, such as the high efficiency, the ability to quickly build up the power system in remote location or in developing nations as well without the need of an electrical grid, greatly reducing the cost of energy distribution. Moreover, in case of electrical production failure the excess of energy produced by distributed power plant could

be put into the grid resulting in an additional power supply. Both the ability to produce fuel cells stacks of required output associated to the possible storage of moderate hydrogen amount improve the strategy of the distributed power generation.

Several industries developed fuel cell systems providing both electricity and heat of the single families. However, they are able to supply almost the total electric and heat demand of a family housing in a modern-day home, reducing its dependence from the power distribution network.

In recent years, the industries involved in the fuel cell business developed fuel cell power supply for portable application such as laptop computer and mobile phone as well as for the replacement of hydrocarbon-engine power generator.

The main advantages of the fuel cell based portable power supply are due to the absence of moving part such as pumps or fans that makes quite silent their operation and the lighter and smaller volume in comparison to the usual battery power supply.

APPENDIX 2

Volcanic activity of the Mount Etna volcano since the end of 2006 eruption

In this section we summarize the volcanic activity displayed throughout the last years. The short summarization of the volcanic activity occurred at Mount Etna volcano since the end of the 2006 eruptive activity has been performed through the bulletins published on-line on the website of Catania division of the Istituto Nazionale di Geofisica e Vulcanologia (INGV-CT) *http: www.ct.ingv.it.*

The time period investigated has been divided in three main time intervals:

- The 2006-2008 period,
- The 2008-2009 eruption and
- The 2009-2010 period.

The 2006 - 2008 period

Since the end of the 2006 eruption, the volcanic activity developed mainly at the summit craters of the Etna volcano. The Bocca Nuova (BN) Crater and South-East Crater (SEC) have been the most active ones.

During this period, the first relevant eruptive event occurred the 29 March 2007 since a lava flow started from the BN crater and strombolian activity occurred at the SEC. While the BN crater subsequently showed passive degassing, the SEC remains fairly active until the end of May 2007 showing discontinuous eruptive activity mainly represented by strombolian explosions. The strombolian activity occurred remarkably the 11 April 2007, the 29 April 2007, the 7 April 2007 and the 23 May 2007 again at the SEC.

Since the end of May 2007 until the second half of august 2007, Etna volcano showed few weeks of passive degassing activity from the summit craters. Subsequently, the volcanic activity enhanced at the SEC through ash emissions and strombolian explosions. The activity climax was reached the 4 September 2007 when lava fountains were emitted from the eruptive fissure opened at the eastern base of the SEC. The high intensity eruptive activity lasted about 12 hours, showing fairly constant features during all the periods and producing lava fountains several hundred meters tall.

The eruptive strombolian activity occurred discontinuously at the SEC through all the autumn 2007 until the late winter 2008. During this period, the most remarkable strombolian activity events occurred the 9 and 10 January 2008 and started again the 7 February 2008 lasting for

the three next days. Since the 11 February 2008, Mount Etna volcano showed passive degassing from the summit craters persisting until the 21 April 2008 when strong and discontinuous explosive activity occurred again at the SEC. This eruptive event has been characterized by strombolian explosions progressively decreasing in intensity and frequency during the following days.

The 2008 - 2009 eruption

The largest volcanic event occurred during our observation period at Mount Etna volcano was the 2008-2009 eruption. In fact, the 2008-2009 eruption was preceded from the paroxistic event of the 10 May 2008 originating a lava flow from eruptive vent located at the base of the SEC, fast moving toward the Valle del Bove along ESE direction.

The 2008-2009 eruption started the 13 May with strombolian explosions, lava spatters and ash emissions occurring from the eruptive fracture opened the 4 September 2007 in the upper part of the Valle del Bove at about 2700 – 2900 meters a.s.l. having ENE-WSW direction. During the initial stages, the eruptive activity involved also the summit areas where ash emissions occurred from the pit-crater located at the base of the SEC.

Since the 14 May, a few hours later the beginning of the eruption, the eruptive scenario changed suddenly from explosive to effusive activity and two lava flows started to move along the eastern flank of the volcano edifice. One of them having high moving capability attains rapidly the 1200 m a.s.l. into the Valle del Bove, while the second attains the 1400 m a.s.l showing further moving incapability. A few days later, the eruptive activity underwent a sharply decrease reducing the magma emission rate from the eruptive fissure. As a result, the scarcely fed lava flows moved slowly, remaining contained in the upper part of the Valle del Bove. This eruptive scenario lasted a few weeks in a fairly constant way and until the first days of June the lava flows appeared moving back into the Valle del Bove.

Since the 8 June, Etna volcano showed a sudden renewal of the eruptive activity displaying strombolian explosions from the eruptive vent migrating 100 meters toward the summit area of the Valle del Bove. The enhancing magma emission rate allowed the lava flows attaining the 1400 m a.s.l. in a few hours from the beginning of the paroxistic activity, though showing incapability to moving further. The increase in the eruptive activity involved also the summit craters displaying high degassing mainly from the NEC and BN, while the SEC and VOR showed blocked floor and degassing from the fumaroles of the crater walls.

Figure A-1 The highest vent opened along the eruptive fracture activated during the 2008-2009 eruption. The picture was taken during the survey performed the 22 July 2008. On the background, is showed the northern rim of the Valle del Bove

During the month of June a copious degassing activity continued from the summit craters located mainly at the North-East Crater (NEC) and the BN crater. In the first time, the Voragine (VOR) and SEC showed weak degassing activity from the crater walls fumaroles, while since the 2 July 2008 a true plume formed at the SEC. Since then and through the few weeks later, the eruptive activity became generally discontinuous.

The frequency and intensity of the strombolian explosions occurring from the vents of the eruptive fracture decreased. As a consequence of the decreasing of the magma emission rate, the lava flows remained limited in the upper part of the Valle del Bove. Also the volcanic activity occurring at the summit craters seemed to go through a general declining phase, since the passive degassing occurred at NEC and BN, while the SEC showed only degassing from the crater rim fumaroles. The volcanic activity remained fairly constant through all the summer 2008 resulting a powerful attraction for thousands people climbing the volcano.

Already the end of August 2008, Etna volcano showed weak eruptive activity mainly focused along the highest part of the fracture activated since the 13 May. The decreasing magma emission rate allowed the formation of lava-tunnels a few hundred meters long. The short lava

flows moved from the vents located at the end of lava-tunnels and partly overlapping one another, making fun-shaped accumulation.

The eruptive activity remained fairly constant during the autumn and winter 2008, featured by low magma emission rate. Nevertheless, the sustained and progressive superimposing of the lava flows allowed the formation of a mega-tumulus greatly changing the morphology of the eastern slope of the volcano edifice. At the same time, the weak passive degassing occurred from the BN, while at SEC the degassing activity occurred from the crater rim fumaroles.

The 8 March 2009 the eruptive activity enhanced at the Etna volcano becoming mainly located in the summit areas. Strombolian explosions associated to ash emissions occurred at the highest vent located along the eruptive fracture opened the 13 May 2008 at 2700-2900 m a.s.l., while passive degassing occurred at the NEC and BN. Among the four summit craters, the SEC was the less active, showing only degassing activity from the crater rim fumaroles. The magma emission persists at the eruptive fracture of the eastern flank of the volcano and the vents at the end of the lava-tunnel fed short lava flows partly overlapping the ancient ones. Since the spring of 2009, the Etna volcano goes toward progressive decreasing phases of the volcanic activity until the 6 July 2009 when a slight degassing activity occurred from the eruptive vents located in the upper part of the eruptive fracture, characterizing the end of 2008-2009 eruption.

Summarizing, the 2008-2009 eruption of the Mount Etna volcano showed paroxistic events characterized by strombolian explosions and ash emissions occurring between persisting effusive phases.

Strombolian explosions, persisting a few hours, occurred mainly from the vents opened during the starting phase of the eruption at the eastern base of the SEC cone. Often the explosive activity emitting magma scoriae has been coupled with ash emissions.

During the effusive phases, the magma emission rate has been generally low with a few short events of high emission rate generating lava flows fast reaching the middle part of the volcano edifice (from 1400 to 1200 meters a.s.l.).

Most of the lava-field formed during the first weeks of the eruption, and the most recent lava flows progressively overlapped the ancient ones, allowing the formation of a fun-shaped mega-tumulus changing the morphology of the upper part of the Valle del Bove.

During all the 2008-2009 eruption, the volcanic activity occurred at the summit craters has been characterized by passive degassing mainly located at the BN and NEC, while the degassing activity at VOR and SEC occurred from the fumaroles of crater rims. It is also

being to note that the SEC showed wide range of activity variations, being the most active during the paroxistic phases.

The 2009-2010 period

Since the end of 2008 - 2009 eruption, the volcanic activity of the Etna volcano has been characterized mainly by passive degassing from the summit craters.

Throughout this period, the degassing activity showed appreciable variability among the four craters, since the NEC has been the most active one, while high intensity of degassing occurred discontinuously at the BN and the VOR. During the first weeks after the end of the 2008-2009 eruption, SEC showed degassing activity mainly located at the fumaroles of the crater rim. This weak degassing activity lasted throughout the summer and the autumn, while since the 6 November 2009 the INGV cameras recorded flashes produced by high temperature gas emissions from the pit-crater opened the 4 September 2007 at base of the SEC cone. The high temperature degassing activity continued during all the subsequent weeks, sometimes with blue-colored emissions, making fairly continuously white-hot the rim of meter-sized vent of the pit-crater. The degassing activity at the SEC pit-crater has been interrupted abruptly by the explosive sequence occurred the 8 April 2010. The explosive activity located at the SEC pit-crater was short-lasting; only 10 minutes long during which strongly energetic explosions made a dark ash-plume suddenly dispersed from the wind toward the eastern flank of the volcano edifice. This short-lasting explosive event sharply changed the morphology of the pit-crater becoming both widest and deepest with sub-vertical walls.

The degassing activity from the pit-crater became colder than observed since the 6 November 2009 and the flame produced by gaseous emission ends its flash. At the same time, the persistent passive degassing activity occurred from BN, VOR and NEC.

During the subsequent weeks the passive degassing activity at the summit craters represented the dominant features of the volcanic activity. The degassing occurred from all the four summit craters, displaying an appreciable variability mainly at the pit-crater of the SEC cone. About other craters, is to be noted that the 5 July 2010 a pressurized gas emission occurred from the BN crater. Since then, the degassing activity occurred at the BN from the floor of the crater and from the fumaroles of the walls. Similarly, the degassing activity occurred from the wall of the VOR, while most intense degassing activity occurred from the floor of the NEC.

Explosive activity occurred at BN crater during the last week of August 2010. The main event of the 25 August at 13.09, producing ash emission containing fresh products, has been associated to about other 20 events until the 29 August 2010. Before this sequence, the last eruptive activity involving the BN crater occurred the 12 January 2006.

APPENDIX 3

Definition of the parameters used for the data correlation

Pearson's coefficient (r)

The Pearson correlation coefficient is widely used as a measure of the correlation between two variables giving a value between -1 and +1 inclusive. Correlations equal to 1 or -1 correspond to data points lying exactly on a line, while value of 0 implies that there is no linear correlation between the variables.

The Pearson's correlation coefficient between the two variables x and y is defined as the covariance of the two variables divided by the product of their standard deviations

$$\rho_{x,y} = \frac{\operatorname{cov}(x,y)}{\sigma_x \sigma_y} = \frac{E[(x-\mu_x)(y-\mu_y)}{\sigma_x \sigma_y}$$

were ρ_x and ρ_y are the standard deviation of x and y variables respectively; $\rho_{x,y}$ gives the *population* correlation coefficient commonly represented by the greek letter ρ.

The sample correlation coefficient commonly denoted with the r is:

$$r = \frac{\sum_{i=1}^{n}(x_i - \bar{x})(y_i - \bar{y})}{\sqrt{\sum_{i=1}^{n}(x_i - \bar{x})^2}\sqrt{\sum_{i=1}^{n}(y_i - \bar{y})^2}}$$

Based on a sample of paired data (x_i, y_i), the sample Pearson correlation coefficient is

$$r = \frac{1}{n-1}\sum_{i=1}^{n}\left[\left(\frac{x_i - \bar{x}}{s_x}\right)\left(\frac{y_i - \bar{y}}{s_y}\right)\right]$$

where

$$n, \quad \bar{x}, \quad \frac{x_i - \bar{x}}{s_X} \quad \text{and} \quad s_x$$

are the number of data, the sample mean, the sample standard deviation and the standard score respectively. The last parameter is a dimensionless quantity representing the distance between the datum and the population mean in units of the standard deviation. The standard score has positive value when the datum is above the mean, negative when below.

Coefficient of correlation (R^2)

The coefficient of correlation, R^2 is used in the context of statistical models whose main purpose is the prediction of future outcomes on the basis of other related information. The R^2 coefficient represents the proportion of variability in the data set that is accounted for by the statistical model providing a measure of how well the future outcomes are likely to be predicted by the model.

In the case of linear regression, R^2 is the square of the sample correlation coefficient between the outcome and the values being used for prediction, changing between 0 and 1.

The most general definition of the coefficient of correlation is

$$R^2 \equiv 1 - \frac{SS_{err}}{SS_{tot}}$$

where (SS_{err}) is the residual sum of squares

$$SS_{err} = \sum_i (y_i - f_i)^2$$

and (SS_{tot}) is the total sum of square

$$SS_{tot} = \sum_i (y_i - \bar{y})^2$$

In the last equation, the term $\bar{y}$ is the mean of the observed data:

$$\bar{y} = \frac{1}{n} \sum_i^n y_i$$

where y_i is the observed value, having an associated modeled value f_i.

APPENDIX 4

Derivation of the coefficient of equation [15]

In order to obtain the expression of the *a*, *b* and *c* coefficients of the equation [15] ($C = a + bz + cz^2$) we use the boundary condition expressed in the theoretical model (Chapter 4) and summarised as follow:

$$-D\frac{\partial C}{\partial z} + \nu C = J \qquad \text{at } z = 0 \qquad [11]$$

$$\frac{\partial C}{\partial z} = 0 \qquad [12]$$

$$C = C_i \qquad [13]$$

For z = 0 and according to the equation [11] we have

$$C=a + bz + cz^2 \qquad \text{and} \qquad C = a$$

and

$$-Db + \nu a = J\ ;$$

Therefore

$$a = \frac{J + Db}{\nu} \qquad [21]$$

For $z = \delta$, according to the condition [12] we have

$$b + 2c\delta = 0$$

so that

$$b = -2c\delta \qquad [22]$$

Moreover, from [13] we have

$$C_i = a + b\delta + c\delta^2$$

so that

$$c = \frac{C_i - a - b\delta}{\delta^2} \qquad [23]$$

Substituting the equation [21] and [22] into the [23] we calculate the *c* term of the polynomial function

$$c = \frac{1}{\delta^2}\left[C_i - \frac{J + D(-2c\delta)}{\nu} - (-2c\delta)\delta\right]$$

from which we obtain that

$$c = \frac{J - \nu C_i}{\delta(\nu\delta + 2D)} \qquad [24]$$

Substituting the obtained expression [24] into the equation [22], we obtain

$$b = -2\left[\frac{J - \nu C_i}{(\nu\delta + 2D)}\right] \qquad [25]$$

To obtain the *a* term of the equation [15], we replace the equation [25] into the equation [21], so that

$$a = \frac{1}{\nu}\left[J + D\left(-2\frac{J - \nu C_i}{(\nu\delta + 2D)}\right)\right]$$

and

$$a = \frac{J\delta + 2DC_i}{\delta\nu + 2D} \qquad [26]$$

Summarizing,

$$a = \frac{J\delta + 2DC_i}{\delta\nu + 2D}; \qquad b = -2\left[\frac{J - \nu C_i}{(\nu\delta + 2D)}\right]; \qquad c = \frac{J - \nu C_i}{\delta(\nu\delta + 2D)}.$$

Therefore, the equation showing the relation between the concentration of the i^{th} species and the high inside the soil is

$$C = \frac{J\delta + 2DC_i}{\delta\nu + 2D} - 2\frac{J - \nu C_i}{(\nu\delta + 2D)}z + \frac{J - \nu C_i}{\delta(\nu\delta + 2D)}z^2. \qquad [16]$$

Replacing the equation [16] into the integral sign of the [10] equation, we obtain:

$$\int_0^\delta C dz = \int_0^\delta \left(\frac{J\delta + 2DC_i}{\delta\nu + 2D} - 2\frac{J - \nu C_i}{(\nu\delta + 2D)}z + \frac{J - \nu C_i}{\delta(\nu\delta + 2D)}z^2\right)dz$$

or

$$\int_0^\delta C dz = \frac{\delta\left[2C_i(3D + \nu\delta) + J\delta)\right]}{3(\nu\delta + 2D)}.$$

From the equation [10] we have

$$\nu C_i - J = -\frac{\partial}{\partial t}\left(\frac{\delta\left[2C_i(3D + \nu\delta) + J\delta)\right]}{3(\nu\delta + 2D)} - C\big|_\delta\,\delta\right) \qquad [27]$$

so that

$$\nu C_i - J = -\frac{\partial}{\partial t}\left[\frac{\delta^2(J - C_i\nu)}{3(\nu\delta + 2D)}\right]. \qquad [28]$$

Since *J*, *v* and C_i are constants, we can divide both [28] equation sides for $(\nu C_i - J)$ obtaining

$$3 = \frac{\partial}{\partial t}\left[\frac{\delta^2}{(\nu\delta + 2D)}\right] \qquad [29]$$

Solving equation [29] we obtain

$$\delta^2 - 6Dt - 3\delta\nu t = 0 \qquad [30]$$